

**EQUATORIAL SEA SURFACE TEMPERATURE
SEASONALITY IN THE MISSISSIPPIAN
(CARBONIFEROUS) DERIVED FROM
BRACHIOPOD SHELL CALCITE**

Thesis submitted for the degree of

Doctor of Philosophy

at the University of Leicester

By

Leah Sarah Polly Nolan

Department of Geology

July 2017

Abstract

The stable isotope composition ($\delta^{18}\text{O}$ and $\delta^{13}\text{C}$) of biogenic (low-magnesium) calcite is commonly used as a palaeoenvironment proxy. These proxies are used to help understand the palaeotropical environment in the Brigantian to help elucidate the timing of the onset of the Late Palaeozoic icehouse. However, to validate isotope data there needs to be an understanding of the environment in which the constituent organisms lived and the preservation of their calcitic shells must be assessed to ensure resultant data are reliable. This study focussed on shell beds at two localities on the Derbyshire carbonate platform that expose (Brigantian) age limestones deposited in open water, inner to mid-ramp settings. Palaeoecological analysis of the shell beds revealed a high dominance (but low diversity) of *Gigantoproductus* species (Brachiopoda). Specimens of this genus were collected from these localities and preservation analyses were conducted. This includes ultrastructure analyses via scanning electron, cathodoluminescence microscopy (SEM and CL), and measurement of trace element composition using laser ablation with inductively coupled plasma mass spectrometry (LA ICP-MS). Some species of *Gigantoproductus* have thick valves, allowing geochemical sampling to be conducted at high resolution across the growth lines of the shells. SEM and CL analyses commonly revealed fine ultrastructure detail preserved in the non-luminescent calcite of the prismatic shell layer. Specimens showing the best-preserved ultrastructure and dull or non-luminescence underwent analysis of trace element abundance (primarily Mn, Fe, Mg and Sr), before five were ultimately selected for $\delta^{18}\text{O}$ and $\delta^{13}\text{C}$ analysis. The range in $\delta^{18}\text{O}$ values suggest a $\sim 7^\circ\text{C}$ seasonal range in late Brigantian shallow sea water temperatures with average temperatures of $\sim 20^\circ\text{C}$ suggesting the onset of the Late Palaeozoic icehouse had begun prior to the latest Brigantian. Overall, this research shows the success of rapid colonisation mechanisms adopted by *Gigantoproductus* species at the study site, demonstrates the importance of a multi-phased preservation screening approach, highlights the heterogeneity in preservation of the biogenic shell material and contributes robust $\delta^{18}\text{O}$ data for equatorial Brigantian waters to the literature.

Acknowledgements

This PhD has most certainly been a rollercoaster ride that will continue to influence my perspective on life for many years to come. It has been a difficult yet positive experience and certainly would not have been possible without the support and guidance I received from many people.

This project was funded by the Natural Environment Research Council (NERC) and the British Geological Survey (BGS). Thank you to the University of Milano who allowed me to use their facilities for study and data collection and Natural England and Natural Stone Sales England who allowed and facilitated the collection of specimens and access to the study sites.

Personal thanks are given to the entirety of my supervisory team, Melanie Leng, Michael Stephenson and Vanessa Banks from the BGS, Lucia Angiolini and Flavio Jadoul from the University of Milano and Sarah Davies and Sarah Gabbott from the University of Leicester, all of whom contributed to my scientific development. Special thanks to Sarah Davies who not only provided scientific discussion and direction but also invaluable encouragement. Giovanna Della Porta from the University of Milano, must also be thanked for identifying foraminifera and helping develop my understanding of carbonate microfacies. Large parts of the geochemical analyses would not have been possible without the help of Simon Chenery from the BGS and being able to work alongside Simon also sparked a joy of method based analytical geochemistry. Hillary Slone (BGS) is also thanked for her the processing of stable isotope samples and Colin Cunningham (University of Leicester) who made the thin sections. I am also grateful to all who donated their time in the field, especially Roy Morris and John Etchell for their help with sample collection, and additional thanks to Vanessa Banks who is always generous in the time and effort she is willing to contribute to developing my skills as a field geologist and my capacities as a scientist.

I cannot end without thanking all of those friends and family members who supported me when I struggled, and celebrated when I succeeded. With thanks to Amy, Annika, Rob, Sarah, Laura, Tom and the residents of G87.

My final thanks go to my partner Howard Daley who never doubted my abilities, always encouraged me and certainly rode the rollercoaster with me and, of course, my parents who have always supported me, no matter what. Most of all, I cannot thank them enough for sparking my love of science; particularly geology with their excellent choice in holiday destinations!

Table of contents

Chapter 1:	Introduction	1
Chapter 2:	Sedimentary context and palaeoecology of <i>Gigantoproductus</i> shell beds in the Mississippian Eyam Limestone Formation, Derbyshire carbonate platform	6
2.1	Background.....	6
2.2	Stratigraphy and lithofacies.....	8
2.2.2	Study sites.....	13
2.3	Methodology.....	16
2.3.1	Facies	16
2.4	Palaeoecology	16
2.5	Results	17
2.5.1	Facies types: Ricklow Quarry	17
2.5.2	Facies Types: Once-a-Week Quarry	22
2.5.3	Palaeoecology: Ricklow Quarry	27
2.5.4	Palaeoecology: Once-a-Week Quarry	31
2.6	Discussion	32
2.6.1	Facies	33
2.6.1.1	Depositional environment and evolution at Ricklow Quarry	33
2.6.2	Palaeoecological interpretation of the <i>Gigantoproductus</i> Floatstone Facies	36
2.7	Summary.....	39
Chapter 3:	Assessing the preservation of species of <i>Gigantoproductus</i> using ultrastructure and cathodoluminescence analyses.....	42
3.1	Background.....	42

3.1.1	Shell Growth	44
3.2	Methods and materials.....	47
3.2.1	Specimen collection	47
3.2.2	Specimen preparation	47
3.2.3	Ultrastructure analyses methodology	48
3.2.4	Cathodoluminescence analysis method	49
3.3	Results	50
3.3.1	Ultrastructure analyses.....	50
3.3.2	Cathodoluminescence analysis	61
3.4	Discussion	67
3.5	Summary.....	71
Chapter 4:	Preservation assessment of <i>Gigantoproductus</i> species biogenic calcite using trace element and stable isotope analyses	74
4.1	Background.....	74
4.1.1	Understanding geochemical diagenetic alteration	75
4.1.2	Identifying geochemical diagenetic alteration	76
4.2	Materials and Methods	82
4.2.1	Preliminary sampling methodology	82
4.2.2	Modification of the methodologies	87
4.3	Results	92
4.3.1	Trace element analyses	93
4.3.2	Trace element analysis of non-shell and secondary/recrystallized calcite materials.....	96
4.3.3	Stable isotopes	98
4.3.4	Correlation of trace element and stable isotope data.....	101
4.4	Discussion	110

4.4.1	Comparing the geochemistry of shell and non-shell or recrystallized materials	110
4.4.2	Assigning geochemical parameters for identifying well preserved biogenic calcite.....	113
4.4.3	Using $\delta^{18}\text{O}$ and $\delta^{13}\text{C}$ to cross-check preservation	118
4.4.4	Modification of the dataset.....	122
4.4.5	Identification of diagenetic processes	124
4.5	Summary.....	129
Chapter 5:	Using high resolution $\delta^{18}\text{O}$ and $\delta^{13}\text{C}$ data from well-preserved species of <i>Gigantoproductus</i> brachiopods to help reconstruct palaeoenvironments of the Brigantian tropics.....	135
5.1	Background.....	135
5.1.1	Estimating $\delta^{18}\text{O}$ of seawater.....	142
5.2	Results	147
5.2.1	$\delta^{18}\text{O}$ and $\delta^{13}\text{C}$ data summary	147
5.2.2	Temperature calculations from $\delta^{18}\text{O}$ data.....	149
5.3	Discussion	153
5.3.1	Detrending the dataset.....	153
5.3.2	Evaluating calculated temperatures	155
5.3.3	Understanding $\delta^{13}\text{C}$ data	161
5.4	Summary.....	162
Chapter 6:	Conclusions and further work.....	164
6.1	Conclusions.....	164
6.2	Further work.....	167
Appendices.....		169
References.....		193

List of Figures

Figure 2-1 Chronostratigraphy of the British Mississippian.	8
Figure 2-2. Geology of the Derbyshire carbonate platform.	9
Figure 2-3 Photographs of the exposure at Ricklow Quarry.	14
Figure 2-4. Once-a-Week Quarry location.	15
Figure 2-5. Stratigraphic section at Ricklow Quarry with skeletal abundance and facies interpretations.	20
Figure 2-6. Thin section micrographs from the Ricklow Quarry section.	21
Figure 2-7. Stratigraphic section at Once-a-Week Quarry with skeletal abundance, and facies interpretations.	25
Figure 2-8. Thin section micrographs of the Once-a-Week Quarry section.	26
Figure 2-9. Schematic representation of Sections One and Two of the shell beds at Ricklow Quarry.	29
Figure 2-10. Illustration of the occurrence of individuals identified in the Ricklow Quarry sections.	30
Figure 2-11. Schematic representation of the <i>Gigantoproductus</i> shell bed alongside diversity.	32
Figure 3-1. Schematic diagram of a cross-section through the ventral valve of a <i>Gigantoproductus</i> species detailing the typical organisation of the shell layers.	45
Figure 3-2. A schematic cross section through the thickness of shell and the relationship of the outer epithelium cell migration with the secretion of the laminar secondary and prismatic tertiary layers (adapted from Williams, 2007).	46
Figure 3-3. SEM micrographs showing examples of the laminar secondary layer.	51
Figure 3-4. SEM micrographs showing examples of the prismatic tertiary layer.	53
Figure 3-5. SEM micrographs showing examples of structural shell features.	55
Figure 3-6 Location of the Derbyshire carbonate platform (DCP) within the UK	56
Figure 3-7. Transect through sample RCK 36 from the inner (bottom) towards the outer shell boundary (top) indicating changes in texture.	57
Figure 3-8 examples of partial dissolution and recrystallisation of the shell calcite.	59
Figure 3-9. Examples of poor fabric retentive specimens.	60

Figure 3-10. SEM micrograph examples of secondary mineralisation.	61
Figure 3-11. CL images of commonly observed features.	63
Figure 3-12. CL images depicting examples of luminescent features.....	65
Figure 3-13. CL image of common brightly luminescent shell features.	66
Figure 3-14. CL mosaic image of specimen OAW 105 showing a spectrum of luminescent features. Shell straight length (widest cross section) is 9 cm.	67
Figure 4-1 Additionally analysed materials analysed alongside specimen RCK 6bis using the preliminary sampling methodology.	83
Figure 4-2 Shell RCK 6bis growth lines and sampling technique for trace element analysis.	84
Figure 4-3. Comparing Mg concentrations through the XG shell transect at 100 μ m (top) and 200 μ m (bottom) spatial resolution.	89
Figure 4-4. Laser ablation craters in <i>Gigantoproductus</i> sample with 200 μ m spatial resolution.	90
Figure 4-5. The isotope sampling strategy.	91
Figure 4-6 shows the distribution of all raw Mg, Sr, Mn and Fe data with results from the Shapiro Wilks test (w) and the associated p value for this test (p).	98
Figure 4-7. Stable isotope values of all samples of all materials.....	101
Figure 4-8. Trace element cross plots for Fe, Mn, Sr and Mg of all shell and end-member data.....	102
Figure 4-9. Photograph and Mg, Sr concentrations of transect through the central, non-luminescent and generally fabric retentive <i>G. inflatus</i> specimen, OAW 03.....	105
Figure 4-10.Trace element and stable isotope data through the central, non-luminescent region shell region of <i>G. inflatus</i> , specimen RCK 33.	107
Figure 4-11. Trace element and stable isotope data from a transect through the central, non-luminescent of <i>G. inflatus</i> , specimen RCK 28.....	107
Figure 4-12. Trace element and stable isotope data for transect through the non-luminescent central shell region of <i>G. okensis</i> , specimen RCK 28bis.	108
Figure 4-13.Trace element and stable isotope data for transect through non-luminescent area of the shell ~1 cm from the anterior margin of <i>G. okensis</i> , specimen RCK 28bis, transect two (RCK 28bis_2).	108

Figure 4-14. Trace element and stable isotope data from a transect through the non-luminescent, central shell region of <i>Gigantoproductus</i> . sp. specimen XG.	109
Figure 4-15. Trace element and stable isotope data from a transect through the non-luminescent central shell region of <i>G. inflatus</i> , specimen OAW 03.	109
Figure 4-16. Principal component analysis (PCA) of all shell (green) and non-shell and recrystallized materials.	112
Figure 4-17.	115
Figure 4-18. Carbon and oxygen isotopes of shell specimens with diagenetic indicators highlighted.	120
Figure 4-19 presents the distribution of the $\delta^{18}\text{O}$ data from all well-preserved data points.	124
Figure 4-20 Comparisons of stable isotope data from Walkden and Williams (1991) and well-preserved data from this study.	127
Figure 4-21 flow diagram illustrating the screening process adopted to select specimens.	131
Figure 4-22. Trace element and stable isotope data for <i>G. inflatus</i> , specimen OAW 03 following preservation analyses.	132
Figure 5-1. Continental configuration during the Tournasian-Visean (Brigantian = latest Visean) with tropical, warm and cold temperate and arid climatic regions shown.	137
Figure 5-2 Demonstrated the variations in calculated temperature when using differing palaeotemperature equations.	140
Figure 5-3. Variations in global $\delta^{18}\text{O}$ values in modern oceans, taken from LeGrande and Schmidt (2006).	143
Figure 5-4 plots temperature against $\delta^{18}\text{O}$ showing the relationship between the two with different seawater $\delta^{18}\text{O}$ values when calculating temperature. Filled circles represent the standard dataset and the crosses the detrended. All data is plotted (including poorly preserved). Grey shaded boxes indicate data point that is either have a calculated temperature above brachiopod lethal limits (38oC) or $\delta^{18}\text{O}$ value that is considered poorly preserved (below -5.36‰).	151
Figure 5-5. Calculated temperatures through all specimen transects.	152
Figure 5-6. Seawater $\delta^{18}\text{O}$ trend after Jaffrés et al. (2007) with the reading of the Brigantian seawater $\delta^{18}\text{O}$ value shown by the red lines.	155

Figure 5-7. Modern sea surface temperature of global oceans (Descloitres, 2001) (data collected in May 2001).....158

List of Tables

Table 3-1. Sample identification number and species of those specimens that underwent ultrastructure and cathodoluminescence analyses.....	48
Table 4-1 Summary of published geochemical parameters of well-preserved biogenic calcite from both modern and fossil shells.	81
Table 4-2 Summary of analyses conducted.....	82
Table 4-3 Summary table of preliminary trace element analyses for specimen RCK 6bis.	93
Table 4-4. Summary table of trace element data for shell specimens in ppm.	94
Table 4-5. Summary of trace element data for end-member sample points. Minimum (Min), maximum (Max) and Average (Av) concentrations for Mg, Sr, Mn and Fe for end-member sample points.	97
Table 4-6. Summary table of stable isotope results collected from the ventral valve of <i>G.inflatus</i> , specimen RCK 6bis via the preliminary sampling technique.....	99
Table 4-7. Summary of all stable isotope data of transects through five specimens that run from the inner to the outer shell margin.....	99
Table 4-8. Summary of stable isotope data of non-shell and recrystallized materials..	100
Table 4-9. Correlation data calculated as Spearman’s rank correlation of key elements within all shell data (excluding RCK 6bis).	104
Table 4-10. Correlation data for all non-shell end-member data samples and recrystallized materials. Colour coding following that described for Table 4-9.....	105
Table 4-11 Shows the Minimum (min) Maximum (max) mean and standard deviations of the elements of interest within the well-preserved dataset for individual specimens.	123
Table 4-12 gives the minimum (min), maximum (max), range, mean and standard deviation (SD) of all of the well preserved data points across all specimens.....	123
Table 5-1. Seawater $\delta^{18}\text{O}$ values based on estimation for the salinity and evaporation effect of the Brigantian palaeoequatorial epicontinental seaways.	145
Table 5-2. Minimum (min) Maximum (max) data range and averages of $\delta^{13}\text{C}$ and $\delta^{18}\text{O}$ of all shell transects of well-preserved data points.	148

Table 5-3. Minimum (min) Maximum (max) data range and averages of and $\delta^{18}\text{O}$ of all shell transects of well-preserved data points after the data has been detrended (subtracted -3.65‰).....148

Table 5-4. Summary of calculated temperatures from the standard dataset. All temperatures are given as $^{\circ}\text{C}$ and are calculated using a seawater $\delta^{18}\text{O}$ value of $+1.5\text{‰}$ from equation $T (^{\circ}\text{C}) = 16.0 - 4.14 (\delta^{18}\text{O}_{\text{CaCO}_3} - \delta^{18}\text{O}_w) + 0.13 (\delta^{18}\text{O}_{\text{CaCO}_3} - \delta^{18}\text{O}_w)^2$150

Table 5-5. Summary of calculated temperatures from the detrended data values with a seawater $\delta^{18}\text{O}$ value of $+1.5\text{‰}$. All temperatures are given as $^{\circ}\text{C}$ from equation $T (^{\circ}\text{C}) = 16.0 - 4.14 (\delta^{18}\text{O}_{\text{CaCO}_3} - \delta^{18}\text{O}_w) + 0.13 (\delta^{18}\text{O}_{\text{CaCO}_3} - \delta^{18}\text{O}_w)^2$150

Chapter 1: Introduction

The Carboniferous Period was a time in Earth's history when dramatic climate change and continental reconfiguration occurred. During this period, the UK was located close to the palaeo-equator under a tropical climate (Boucot et al., 2014). The regional palaeogeography consisted of localised highs in Scotland, the Southern Uplands, and parts of central England and Wales, which formed areas of land that were surrounded by localised lows that formed basins, which during periods of high sea-level, were connected and formed an epicontinental sea way (Davies, 2008).

The Derbyshire carbonate platform is located in central UK. It was formed during the Tournaisian and Visean stages of the Mississippian, at the base and through to the middle of the Carboniferous period (Gradstein et al., 2012). The last phase of carbonate production on the platform occurred during the late Brigantian (late Visean), and is represented by the Eyam Limestone Formation (Gutteridge et al., 1987).

Preserved within the Eyam Limestone Formation are world-renowned deposits of gigantoproductid brachiopods, which are concavo-convex Productid brachiopods that lived during the Mississippian. *Gigantoproductus* are particularly abundant in Asbian and Brigantian age rocks (Late Visean) and can be found at many localities around the UK, in Europe, as well as in China and North America (Qiao and Shen, 2015; Ruban, 2015). Their rich abundance in such rocks is unique, and changes in their abundance through the middle and late Mississippian appear to coincide with a global climatic shift, with their extinction possibly linked to the cooling of tropical oceans (Qiao and Shen, 2015) during the postulated onset of the Late Palaeozoic Icehouse. Despite this suggested link between changing climate and changing habitats, little research has looked in detail at their preferred environment or ecology and little is known about the cause of their high abundance at specific localities.

The Asbian and Brigantian Stages are particularly interesting time intervals for palaeoclimate researchers, as it is proposed that glacio-eustatic sea level change occurred across the UK's epicontinental seaway (Wright and Vanstone, 2001), which is thought to represent the start of the Late Palaeozoic icehouse conditions. This icehouse

was the longest ice age and the only extended glacial period of the Phanerozoic (Montañez and Poulsen, 2013). It is argued that understanding the nature of this global icehouse can contribute to our understanding of current global warming trends during the modern ice age. Despite its potential importance, there is a lack of consensus on the absolute timing of the onset of the major glacial phase. Some authors (e.g, Barham et al., 2012) speculate that the onset occurred during the mid Brigantian while many think that this time represents the final warm, ice free, climatic period (Mii et al., 1999) and that the major glacial phase began at the Visean/Namurian boundary (Isbell et al., 2003).

Species of *Gigantoproductus* have been utilised by researchers as a palaeoclimate tool or a proxy for tropical Visean sea surface temperatures (e.g, Bruckschen et al., 1999; Mii et al., 1999; Mii et al., 2001) in order to better understand ocean temperatures and therefore climate during this major climate shift. Oxygen isotopes ($\delta^{18}\text{O}$) in biogenic carbonates have been used as a palaeothermometer since the relationship between temperature and the $\delta^{18}\text{O}$ of the water was shown empirically (Urey, 1947); a practical palaeothermometer scale was subsequently produced by (Epstein et al., 1953). Since this work, the $\delta^{18}\text{O}$ of many calcitic and aragonitic molluscs and brachiopods have been used as palaeotemperature proxies (see Immenhauser et al., (2016) for a comprehensive review). Brachiopods are one of the most commonly used organisms to reconstruct palaeotemperature since Lowenstam (1961) demonstrated that they precipitated their shells in equilibrium with ambient seawater and because of their global distribution and abundance within the geological record.

Species of *Gigantoproductus* are particularly good for such palaeoclimate research because they are composed of low-magnesium calcite (LMC), this means that they have <4 mol % of MgCO_3 (<9775 ppm) (Chave 1954). This is advantageous because LMC is thought to be the most resistant form of calcite to diagenetic alteration (Al-Aasm and Viezer, 1982). Additionally, this brachiopod genus contains the largest brachiopods ever-recorded (Muir-Wood and Cooper, 1960) and many species have thick shells allowing multiple isotopes samples to be taken from an individual. This has been capitalised on by some researchers (e.g, Angiolini et al., 2012) who sampled a single specimen within and across growth lines and therefore the sampling resolution represents specific growth events during the organisms' lifetime. Their results show geochemical variability across

the shell that reflect changes in environmental conditions during the organism's life; this is shown to occur in a cyclical pattern and was attributed to seasonal variation in temperature. The importance of this is that whilst most temperatures calculated from the $\delta^{18}\text{O}$ of biogenic calcite reflect average temperatures the method of sampling systematically across a shell has the potential to provide seasonal temperature ranges. By understanding more about the temperature range seen within an organisms life, rather than simply identifying an average temperature, a more comprehensive understanding of the seasonal environmental conditions they were exposed to may be gained. It may then be possible to understand climate processes on a larger scale, such as the influence of ocean circulation, localised rainfall or the influence of potential climatic processes, such as El Nina, on the palaeoenvironment (Tudhope et al., 2001).

$\delta^{18}\text{O}$ data from biogenic calcite has enormous potential in palaeoclimate studies, however as a precursor to studies of this type, preservation analyses, which are often time consuming and costly, are essential. It is essential to evaluate how representative the chemistry of the analysed material is compared to that of the seawater in which the shell grew and compared to any post depositional alteration by diagenetic fluids, which may have affected the geochemistry of the shell. Brand et al. (2011) state that "the best proxy is the one that has passed the most screening tests". Assessing the preservation allows the best preserved material to be selected for subsequent isotope studies, and therefore, increases the validity of the resultant data set. Although preservation analyses should be undertaken in all studies of this type (Brand et al., 2011; Immenhauser et al., 2016), it is particularly essential when the material is from deep geological time (such as the Carboniferous) (cf. Ullmann and Korte, 2015).

Several preservation assessment methods are available for calcite from shelly material, the most commonly used (and those used here) are:

1. An assessment of the shell ultrastructure, which looks at the detail of the structure in which the shell secretes its biogenic shell (ultrastructure) and assesses how much of the original, well-organised shell structure has been retained.
2. Cathodoluminescence analysis (CL), which gives an insight into the amount of Fe and Mn in calcite, which are usually post depositionally derived.

3. Trace element analyses, to quantify the concentrations of some key (not necessarily trace) elements that would be expected in pristine or diagenetic calcite.

This thesis is divided into four data chapters that address specific aims, but ultimately contributing to furthering the understanding of the suitability of *Gigantoproductus* species as a tool for high-resolution palaeoclimate studies and the insights the analysis of this material gives into the Brigantian palaeotropical climate.

Chapter 2: *Sedimentary context and palaeoecology of gigantoproductid shell beds in the Mississippian Eyam Limestone Formation, Derbyshire carbonate platform.*

This Chapter is published in the Proceedings of the Yorkshire Geological Society in July of this year (Nolan et al., 2017) as a standalone paper.

Aim/Research Questions:

1. What environments were the species of *Gigantoproductus* of the Eyam Limestone shell beds living in?
2. What were the colonisation mechanism(s) of these organisms and why are they so dominant?

Chapter 3: *Assessing the preservation of species of Gigantoproductus using ultrastructure and cathodoluminescence analyses.*

Aim/Research Questions:

1. Describe the *Gigantoproductus* ultrastructure.
2. Use ultrastructure and cathodoluminescence analyses to assess the preservation of collected specimens.

Chapter 4: *Preservation assessment of Gigantoproductus biogenic calcite using trace element and stable isotope analyses*

Aim/Research Questions:

1. Identify an optimal high-resolution sampling mechanism for identifying differential preservation via trace element analyses.
2. Assess the geochemical preservation of selected specimens and their suitability for use as a palaeotemperature proxy.

Chapter 5: *Using high-resolution $\delta^{18}\text{O}$ and $\delta^{13}\text{C}$ data from well-preserved species of *Gigantoproductus brachiopods* to help reconstruct palaeoenvironments of the Brigantian tropics.*

Aim/Research Questions:

1. Calculate sea surface temperatures for the Brigantian tropical epicontinental seaway from the $\delta^{18}\text{O}$ data from well-preserved specimens in order to help constrain the onset of the Palaeozoic icehouse.
2. Assess whether the variability seen in $\delta^{18}\text{O}$ data is recording seasonal variability.

The thesis is concluded in Chapter 6, which summarises the key findings of this research and suggests ideas for further work.

Chapter 2: Sedimentary context and palaeoecology of *Gigantoproductus* shell beds in the Mississippian Eyam Limestone Formation, Derbyshire carbonate platform

2.1 Background

During the Mississippian, species of *Gigantoproductus* brachiopods appeared within the geological record, diversified and subsequently declined (Qiao and Shen 2015). Evaluating their palaeoenvironmental setting and palaeoecology assists in elucidating the success of the genus and the relationship of these brachiopods with local environments. The Mississippian Eyam Limestone Formation of the Derbyshire carbonate platform, central England, UK (Figure 2-2), has been described by Aitkenhead and Chisholm (1982), Aitkenhead et al. (1985), and Gutteridge (1983, 1987, 1991, 1995, 2003). These authors commented on the association of species of *Gigantoproductus* brachiopods with mud mound deposits. The brachiopods are found in high abundance as shell beds at specific intervals within the Asbian-Brigantian Monsal Dale and Eyam Limestone formations (Aitkenhead et al., 1985). Little detailed work has been published on the palaeoecological significance of the gigantoproductid shell beds of the Derbyshire carbonate platform, and the link between their abundance and depositional environment.

The genus *Gigantoproductus* contains the largest brachiopod specimens ever-recorded (Muir-Wood and Cooper, 1960) and these most commonly occur in shell beds or lenses (Ferguson, 1978; Yao et al., 2016). *Gigantoproductus* species are distinguished by their large size, shallow corpus cavity, irregular ribbing and fluting, and the occurrence of dorsal brachial cones (Williams et al. 2007; Pattison, 1981). The morphology of the genus is seen to vary with population density and substrate (Ferguson, 1978). Four morphological sub-groups were identified by Pattison (1981), primarily based on shell curvature, ribbing and fluting, and ventral valve shell substance and thickness, which,

alongside other characteristics, are used as distinguishing features. Because *Gigantoproductus* were large, they presumably required a constant supply of oxygen and food, suggesting they would have thrived in shallow and agitated waters of normal salinity marine environments (Ferguson, 1978). Graham et al., (1995) suggested that the large size of *Gigantoproductus* species may be attributed to higher levels of atmospheric oxygen during the Carboniferous and their diversification has been linked to a warming climate in the late Visean (Brezinski and Kollar, 2012).

The Derbyshire carbonate platform formed on the eastern margin of the Laurasian landmass, 4° south of the equator (Scotese and McKerrow, 1990). *Gigantoproductus* species first appeared in the middle Visean, and reached their peak diversity and abundance in the late Visean (Figure 2-1) when they were distributed along shallow shelf environments around the Palaeotethys Ocean by the warm circum-Palaeotethys currents (Qiao and Shen, 2015). These brachiopods are also preserved in rocks from Eurasia and Nova Scotia (Qiao and Shen 2015), as well as in Serbia and Kazakhstan, that would have been located to the north of Palaeotethys (Ruban, 2015). Changes in the abundance of species of *Gigantoproductus* appear to have coincided with the palaeoclimatic shift from greenhouse to icehouse conditions in the Late Mississippian (Qiao and Shen, 2015). The extinction of the genus *Gigantoproductus* in the late Serpukhovian (Figure 2-1) may be linked to the cooling of tropical oceans and expansion of the Gondwana glaciation.

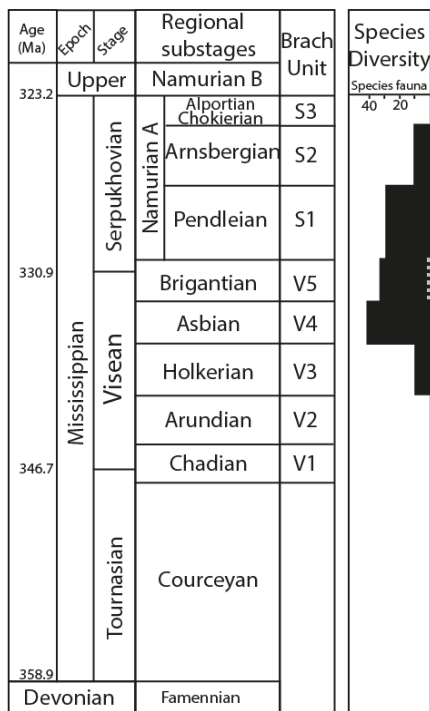


Figure 2-1 Chronostratigraphy of the British Mississippian. (Edited from Cohen et al., 2013; updated) with associated brachiopod units and *Gigantoproductus* species diversity (edited from Qiao and Shen, 2015, Figure 2-5).

The common association of *Gigantoproductus* in the Eyam Limestone Formation with localised mud mounds was noted by Aitkenhead and Chisholm (1982) and Gutteridge (1983). The significance of this association and exact location of gigantoproductids relative to the mud mound has been described by Nolan et al. (2017). The inactive mud mounds effectively generated a relict topography and influenced deposition. The nearby, overlying shell beds and lenses were studied at two key localities on the Derbyshire carbonate platform which are comparable in age, but have different geological settings relative to the mounds. Using field observations and thin section analysis, the sedimentary evolution of the Eyam Limestone Formation was investigated. Sedimentological analysis was combined with a palaeoecological study of the beds dominated by the genus *Gigantoproductus* that enables a better understanding of their strategy of rapid colonisation and the success of this genus on the Derbyshire carbonate platform.

2.2 Stratigraphy and lithofacies

Sedimentation across the Derbyshire carbonate platform began in the late Tournasian as sea level rose and a marine transgression flooded the Lower Palaeozoic basement

(Aitkenhead and Chisholm, 1982). The platform formed around a basement high that comprised three half-grabens (Smith et al., 1985). It is divided into two provinces (Figure 2-2D): the on-shelf province was characterised by shallow water deposition and the off-shelf province represented a deeper water setting (Aitkenhead et al., 1985). The Peak Limestone Group of the Derbyshire carbonate platform (on-shelf province) consists mainly of marine carbonate facies interbedded with marine shales and minor volcanic deposits (Aitkenhead et al., 1985). The oldest formation in the Peak Limestone Group, the Woo Dale Limestone Formation, was deposited during the Chadian to Holkerian (Schofield and Adams, 1985). Dolostones and limestones at the base of the formation pass upward into coarse-grained limestone with planar cross-bedding and lenticular-irregular bedforms (Aitkenhead et al., 1985; Schofield and Adams, 1985, 1986). These on-shelf limestones are overlain by the younger, predominantly Holkerian, finer-grained peritidal deposits, that are capped by restricted lagoonal limestones (Aitkenhead et al., 1985).

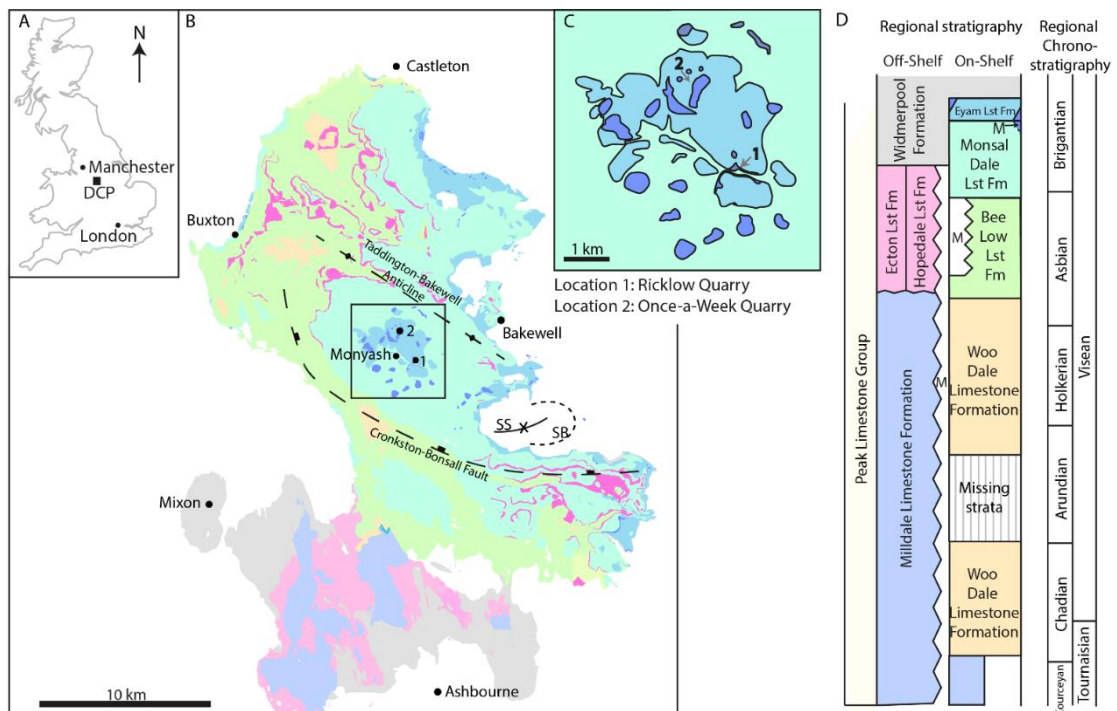


Figure 2-2. Geology of the Derbyshire carbonate platform.

a) The location of the Derbyshire carbonate platform (DCP) within mainland Britain. b) Outline of the platform with outcrop of Mississippian formations, modified from Aitkenhead et al. (1985, figure 3-3) c) Main Eyam Limestone Formation outcrop in the centre of the platform (highlight box). Study sites (1) Ricklow Quarry and (2) Once-a-Week Quarry are numbered. d) Derbyshire carbonate platform stratigraphy of the Peak Limestone Group: on-shelf (right) and off-shelf (left) provinces with regional chronostratigraphy

(modified from Waters et al., 2009, figure 2-4). Key: Lst Fm = Limestone Formation; M = carbonate mud-mounds; SB = Stanton Basin with eastern margin marked with the dashed line along with the Taddington-Bakewell Anticline and the Cronkston-Bonsall Fault; SS = Stanton syncline.

Shelf limestones of the Asbian and Brigantian sub-stages are characterised as regressive cyclic sequences (Bridges, 1982; Walkden, 1987). Characteristically, the Bee Low Limestone Formation comprises thickly-bedded, fine- to medium-grained calcarenites. Scattered crinoid debris are common, with other biota, including corals, brachiopods, foraminiferans and ostracods, also present (Aitkenhead et al., 1985). The overlying Monsal Dale Limestone Formation comprises two main facies: upper, heavily bioturbated, thickly-bedded packstone to wackestone; and skeletal grainstone (Cox et al., 1977). Fossiliferous beds are common (Aitkenhead et al., 1985), as are localised carbonate mud mounds (Gutteridge, 1995). The formation is laterally variable, with common surfaces preserving features that indicate subaerial exposure which pass laterally into thinly bedded, finer grained limestones without subaerially exposed surfaces. These lateral changes occur over short distances and are interpreted as the transition from shallow to deeper water deposition (Aitkenhead et al., 1985).

The Eyam Limestone Formation caps the Monsal Dale Limestone Formation and comprises thinly bedded, cherty, bioclastic limestone with fossiliferous beds of brachiopods, corals and crinoids, a few dark mudstone intercalations and localised mud mounds along with their associated facies. In the centre of the platform (around Monyash; Figure 2-1b) the formation was deposited on an easterly dipping intraplatform carbonate ramp that passed laterally into the Stanton intraplatform basin (Figure 2-1b) and which probably formed due to the localised subsidence of the basement (Gutteridge, 1987). To the south of the carbonate platform massive carbonate mud mounds (described below) overlay these beds, whereas in the central and northern parts they occur at the base of the formation (Aitkenhead and Chisholm, 1982). Mud mounds with evidence of a significant period of subaerial exposure prior to deposition of the overlying beds (Aitkenhead et al., 1985; Gutteridge, 1991b) led Gutteridge (1995) to propose a revision of the boundary between the Monsal Dale Limestone and the Eyam Limestone formations. This revised boundary has not been formally adopted; however, evidence indicating subaerial exposure of mound facies was observed at one of the study sites in

this study and was used as the formation boundary herein. The fossiliferous beds, rich in gigantoproductid brachiopods, were identified by Gutteridge (1983) as the fossil packstone sub-facies of an irregularly bedded bioclastic facies.

The mounds present within both the Monsal Dale and Eyam Limestone formations are the Type 3 build-ups (crinoid-brachiopod-fenestrate bryozoan) described by Bridges et al. (1995). They are, therefore, not Waulsortian type mounds which were described in Dove Dale at the platform edge by Bridges and Chapman (1988). The mud mound facies occurs in the on-shelf settings of the Derbyshire carbonate platform within the shelf interior, at the platform margins and in the shallow to middle section of the intraplatform ramp (Gutteridge, 1995). Three facies related to the mud mounds were recognised by Gutteridge (1995): bryozoan wackestone/mudstone (mound core facies); bioclast intraclast wackestone/packstone (mound-flank facies); and crinoidal grainstone (intermound facies). The mound cores are crossed by fractures that show evidence of formation at different stages of lithification and indicate that surface microbial binding probably stabilised the mud mound. The mounds pass laterally and vertically into intermound facies dominated by crinoid fragments derived from crinoid 'thickets' around the mounds. The mud mounds in the study area developed on the shallow part of the intraplatform ramp (Gutteridge, 1995) and their geometry was controlled by water depth. Towards the east, and into deeper water, the mud mounds increase in thickness, but become more laterally restricted. The present-day dip of exposed bedding reflects that of the original flank slopes of the mud mound at progressive growth stages. Concentrations of brachiopods hosted in scour features occur on the sides of the mud mounds (Gutteridge, 1990), but these are distinct from the brachiopod shell beds discussed within this paper, which are observed onlapping or overlying the mounds. It is most likely that the relationship of the whole-fossil packstone beds with the mud mounds resulted from the local palaeogeography with the mound topography enabling shallow lagoons to form around the mound as sea level continued to rise after the period of subaerial exposure (Gutteridge, 1983).

The Eyam Limestone Formation is the uppermost carbonate formation of the Peak Limestone Group and is overlain by the Longstone Mudstone Formation indicating a switch to deeper water deposition (Aitkenhead et al., 1985). The platform was eventually

buried by southerly prograding fluvio-deltaic systems that were deposited as water depths subsequently shallowed during the Serpukhovian and Bashkirian (Guion and Fielding, 1988).

2.2.1.1 Diagenetic history

Burial of the platform was associated with a number of diagenetic processes that include microbial micritisation, dissolution (including pressure solution), cementation, neomorphism (the process of replacement and recrystallisation in carbonate rock where there may be mineralogical changes (Folk 1965)) and compaction tending towards a reduction in porosity. More specifically, Walkden and Williams (1991) identified multiple (up to 5) phases of cementation within the Asbian and Brigantian limestones on the platform. Shallow burial occurred in the lower Namurian and resulted in calcite cementation driven by the presence of meteoric waters (Walkden and Williams, 1991). Following this, burial diagenesis occurred resulting in further calcite cementation. As greater depths of burial were reached Mississippi-Valley-Type mineralisation occurred as over pressurised fluids in the adjacent basins were driven into the platform giving rise to fracturing (Hollis and Walkden, 2002) and dolomitisation (Aitkenhead et al., 1985; Schofield and Adams, 1985), non-economic hydrocarbons (Ewbank et al., 1993) and economic deposits (Ixer and Vaughan, 1993) of fluorite and galena mineralisation, barite and calcite gangue and minor sphalerite mineralisation (Hollis, 1998).

The mud mounds remained largely unaffected by these phases of fluid flow, which may be a consequence of early cementation precluding penetration by mineralizing fluids or the intrashelf structural setting, which was more distal to the fluid flow paths (Bridges and Chapman, 1988). As the occurrence of shell beds dominated by species of *Gigantoproductus* are commonly associated with the mud mounds (Aitkenhead and Chisholm, 1982; Gutteridge, 1983), they often appear to gain protection from some diagenetic processes. Additionally, Angiolini et al. (2012) identified a range of diagenetic signals across a single *Gigantoproductus okensis*, suggesting that differing regions of the shell have undergone different types of alteration, while some areas appear well-preserved. This may be accounted for by the shape and size of the organisms, which allows some areas of the shell to be sheltered from some localised diagenetic processes.

2.2.2 Study sites

Two sites, Ricklow Quarry and Once-a-Week Quarry, were selected for detailed study (Figure 2-1). Ricklow Quarry (Figure 2-3) (53.192210N, 1.754669W) is approximately 1.5 km east-southeast from the village of Monyash, on the northern side of Lathkill Dale. Once-a-Week Quarry (Figure 2-4) (53.209364N, 1.765823W) is 1.75 km north-northeast of Monyash. Ricklow Quarry is disused, but was quarried for building and decorative stone used in the local area. Limestone from Once-a-Week Quarry is used for the same purposes and the site is currently undergoing a new phase of excavation.

Both localities expose sections of the Eyam Limestone Formation. Ricklow Quarry exposes the base of the formation and its contact with the underlying Monsal Dale Limestone Formation (Figure 2-5). At Ricklow Quarry two shell beds are exposed. The first bed is located at the top of a large exposed section, has a minimum thickness of 2.2 m and is the subject of this study. A second bed, 1.3 m thick and containing common *Gigantoproductus*, lies stratigraphically ~8 m higher and on the opposite side (south-west) of Lathkill Dale, approximately 80 m to the west. This bed, however, is poorly exposed and, because a detailed study was not possible, it is not discussed within this paper. At Once-a-Week Quarry, a 1 m thick shell bed is exposed at the top of the section and a second, less prominent, 20 cm-thick shell bed also occurs *ca.* 6.4 m from the base of the quarry (Figure 2-6). A third bed is visible on the quarry floor, but as only a bedding plane view; there is a small exposure in the centre of the quarry.

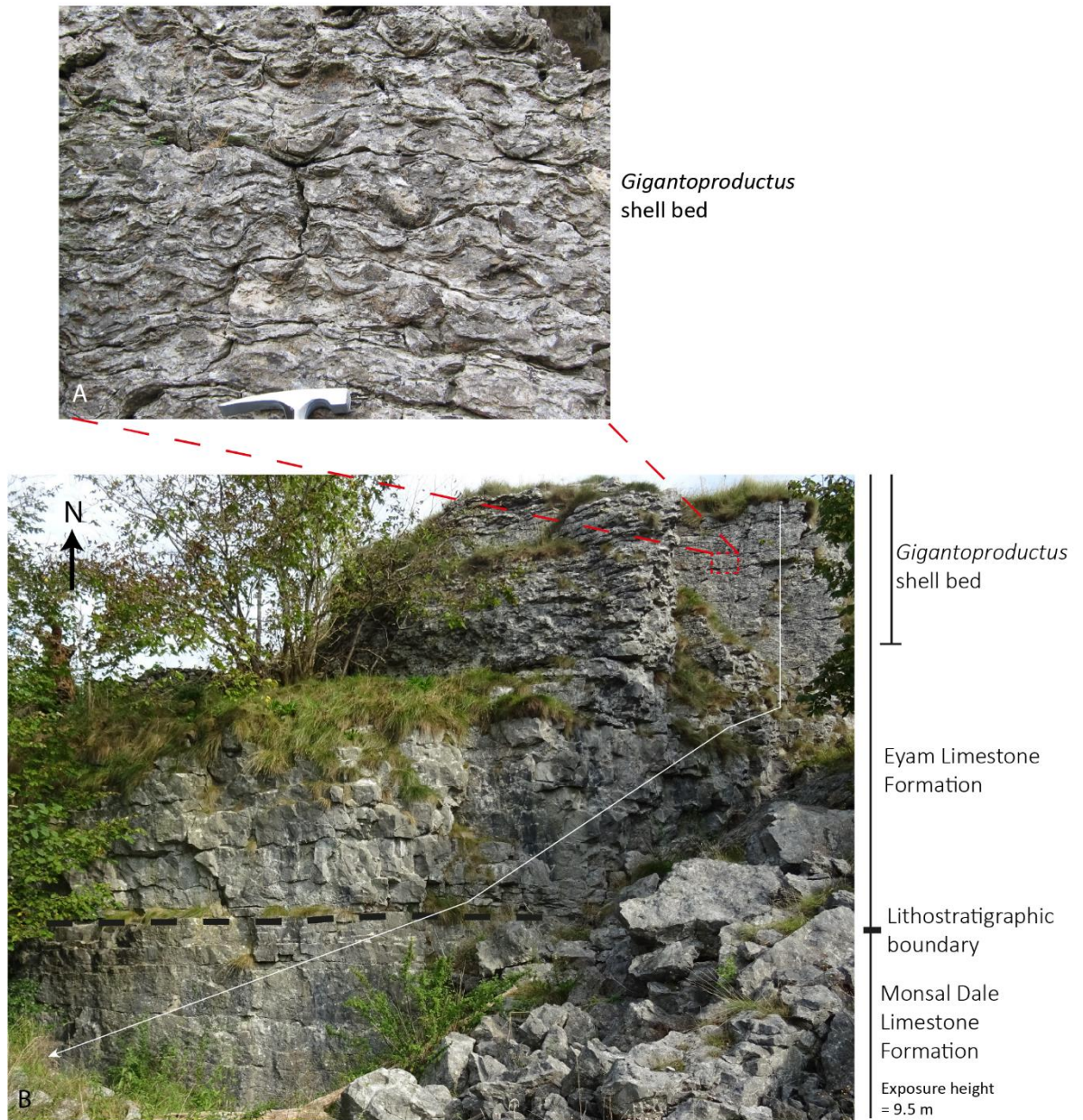


Figure 2-3 Photographs of the exposure at Ricklow Quarry.

a) A detail of a vertical section through the gigantoproductid shell bed with rock hammer for scale. b) The disused quarry face. The boundary between the Monsal Dale Limestone and the Eyam Limestone formations, and the gigantoproductid shell bed highlighted. The logged section (Figure 2-5) is represented by the white line but the most westerly sampling site is not shown.

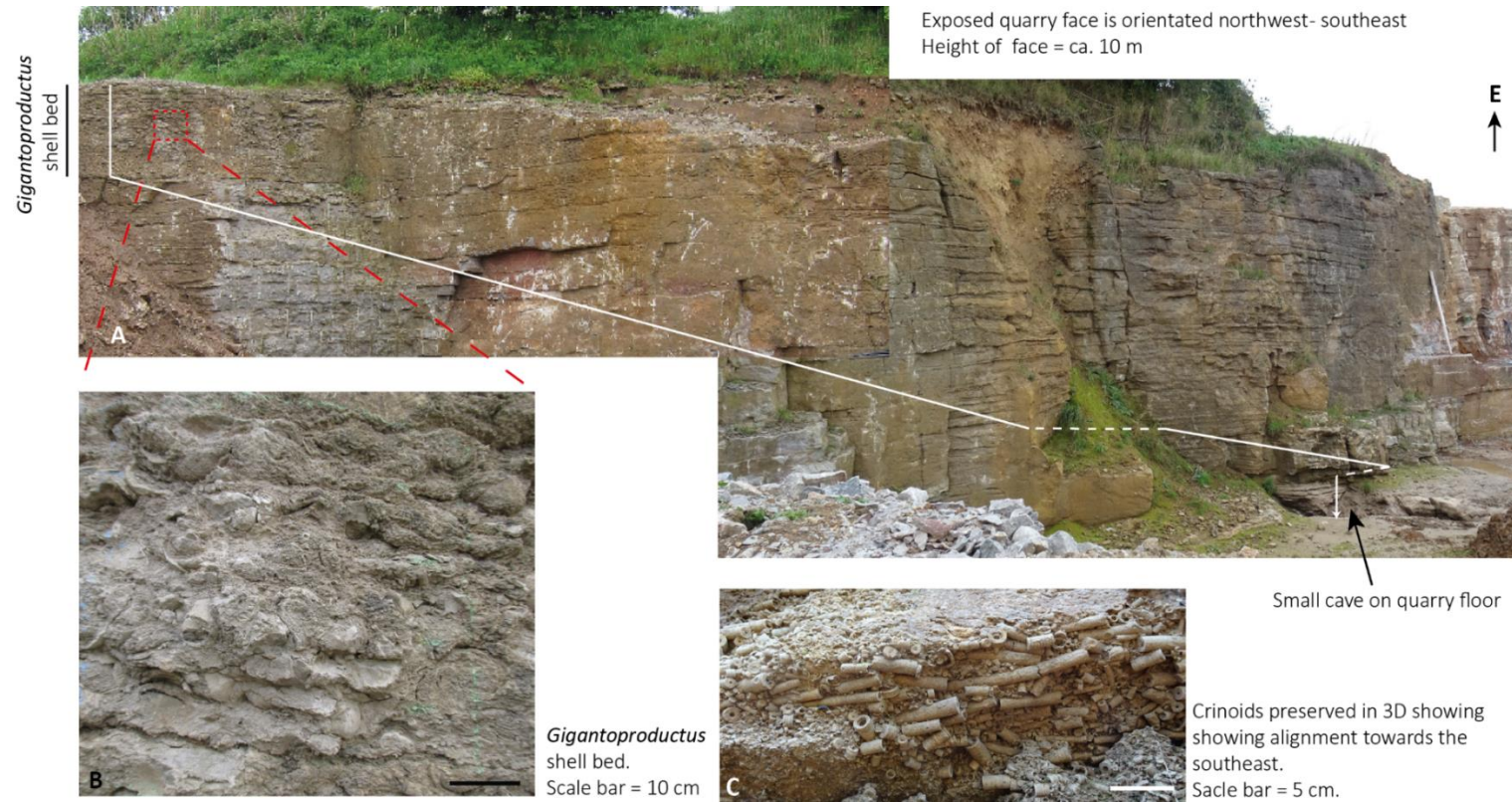


Figure 2-4. Once-a-Week Quarry location.

a) The extent of the logged quarry face (Figure 2-6) is represented by the white line. The base of the section was exposed and logged in a small dissolution feature as shown. To access the full section, the log was measured moving systematically to the NW across the quarry face. To the SE beyond the white marker pole, renewed quarrying has exposed more of the section. b) A detail of a vertical section through the gigantoproductid shell bed. c) A three-dimensional view of crinoid stems predominantly aligned NW-SE.

2.3 Methodology

2.3.1 Facies

Sedimentary logs were used as a sampling framework at both study sites. Macroscale field observations made at outcrop were supplemented by petrographic analysis and facies descriptions of thin sections from these samples. The Ricklow Quarry logged section was measured from the base of the exposure on the far west side of the northern wall of the quarry and progressed laterally 18 m east, with a total thickness of 9.5 m measured. Forty-three samples were taken through the logged section and thirty-nine thin sections were made. At Once-a-Week Quarry, a 10 m thick section was measured from a small dissolution feature in the centre of the quarry floor up through the south-west quarry wall and ten samples were collected for thin section analysis. Carbonate texture classifications are based on the Dunham (1962) and Embry and Klovan (1971) systems. The skeletal components and relative abundances were estimated visually as percentages of thin section area in every thin section and identified by Dr Giovanna Della Porta (University of Milano). Images of all thin sections are provided in Appendix A.

2.4 Palaeoecology

Palaeoecological assessments were conducted on the main gigantoproductid-rich shell beds at each location. The palaeoecological analysis involved detailed observations from selected one-metre square vertical sections in the quarry faces. Two sections from the north quarry face at Ricklow Quarry were analysed and both were located at the same stratigraphic level within the shell bed. One section was located broadly in the centre of the exposed quarry wall and the second was located ~5 m east of the first. Due to challenges with accessing a vertical quarry face, a single section was analysed at Once-a-Week Quarry.

At both study sites, all one-metre square vertical sections were divided into 10 cm divisions from the base of the section to its top, and the macrofossils within each interval were counted and classified. Brachiopod specimens were classified to species level where possible. For each fossil specimen the orientation (life or other position) was recorded, as well as whether oblique or transverse sections were present. For brachiopod specimens, the umbo orientation was noted. Where packing of the fauna was particularly

close, and where fossils overlapped two areas, divisions were amalgamated to form one 20 cm division. Identification to species level was not always possible, especially where the specimens were surrounded by matrix. Where individuals were obscured by the matrix, gigantoproductids were classified as thin- or thick-shelled species following the groups recognized by Pattison (1981).

Each division was classified as either a life assemblage or a neighbourhood assemblage based on the percentage of individuals in their original life position (Brenchley and Harper, 1998). Where more than 70% of the organisms were in original life position, the division was classified as a life assemblage; where this was less than 70%, the division was classified as a neighbourhood assemblage.

Diversity indices were calculated using the Shannon-Wiener and Margalef diversity calculations using PAST software (Hammer et al., 2001). For these calculations, *Gigantoproductus* species were grouped as thin- or thick-shelled to allow inclusion of all individuals. The Margalef index is based on the richness (this is the total number of species in a community), whereas the Shannon-Wiener index measures diversity based on the combination of richness and evenness (i.e., how evenly individuals are distributed among the different species in a community). Therefore, in this study, the Shannon-Wiener index is used as the preferred value as it is a more appropriate measure of the dominance of the *Gigantoproductus* genus, which is the ultimate aim of these calculations in this instance. Qualitative comments on biovolume are provided. Original data consisting of counted individuals and percentage calculations are provided in Appendix B.

2.5 Results

2.5.1 Facies types: Ricklow Quarry

Seven main facies are identified based on texture, and skeletal and non-skeletal carbonate components.

Skeletal packstone.

This facies (Figure 2-6a) occurs only in the basal ~1.6 m of the section (Figure 2-5), with beds with thickness between 25 and 45 cm, and containing clotted peloidal micrite wackestone intraclasts with common crinoids and bryozoans (mostly fenestrate and

fistuliporids). Typically, the facies is characterised by sparse ostracods and brachiopods, and rare foraminiferans, calcispheres and monoaxone sponge spicules. Echinoids are very rare in the lowermost sample, but common from 1.25 m where they co-occur with ungdarellid red algae. At 1 m from the base of the section the facies is a crinoidal packstone; brachiopods become common and detrital structureless micrite matrix is present.

Coral boundstone.

This facies (Figure 2-6b) occurs locally at 1.5 m and 7.75 m above the base of the section forming lens-shaped beds with a maximum thickness of *ca.* 15 cm. At 1.5 m, sparse echinoderms, ostracods and bryozoans are present with rare brachiopods, calcispheres and sponge spicules within intraclasts. Between rugose corals, patches of clotted peloidal micrite and of skeletal wackestone occur followed by blocky sparite cement. The thin (*ca.* 12 cm) lens of this facies at 7.75 m is surrounded by skeletal packstone with sparse brachiopods and foraminiferans.

Skeletal wackestone.

This facies (Figure 2-6c) occurs locally, *ca.* 1.7 m above the base of the section, and is defined by the absence of molluscs, red algae and coral, whilst all other skeletal components are sparse (brachiopods, bryozoans, foraminifera, ostracods and echinoderms) or rare (debris of green palaeoberesellid algae, sponge spicules, calcispheres and trilobites). Parts of the micritic matrix has a clotted peloidal character and evidence of burrowing. Vuggy and biomoldic dissolution porosity is present, and possible rhizoliths are observed.

Molluscan wackestone.

This facies (Figure 2-6d) characterises the interval between 2.4 m and 4.1 m above the base of the succession with abundant gastropods and bivalves. Foraminifera are identified in all samples from this facies in this interval; where they are common, at 3.25 m and at 4.1 m, the assemblage is dominated by *Bradyina* and endothyrids. Other biota include common to rare ostracods, rare/sparse brachiopods, sparse calcispheres with detrital micrite and sparse peloids present in all samples. Locally this facies has a floatstone texture and shows evidence of bioturbation.

Crinoid grainstone – rudstone.

This facies (Figure 2-6e) occurs 1.85-2.45 m above the base of the section as a lenticular unit with a sharp erosional base. This facies is underlain by the molluscan wackestone and appears to have a transitional boundary with the overlying molluscan wackestone (Figure 2-5). Cross-bedding is observed where the bed reaches its maximum thickness of 55 cm. The facies is characterised by abundant crinoid ossicles with common brachiopods and bryozoans (Figure 2-7). Other biota include ostracods and very rare foraminiferans (endothyrids, archaediscids, *Earlandia vulgaris*, *Pseudoendothyra*, *Tetrataxis* and *Omphalotis*). Micrite matrix includes sparse peloids and clotted peloidal micritic intraclasts. A range of cements are observed, including pendant vadose, equant blocky sparite and a syntaxial cement surrounding echinoderms. Dissolution vugs, root casts, iron oxides and micritic envelopes are also present. Some brachiopods show microborings and silicification.

Skeletal wackestone – packstone.

This facies (Figure 2-6F) typically contains sparse crinoids and ostracods. Brachiopods vary in abundance. Foraminifera show an initial decrease in abundance relative to the underlying facies and are typically rare to sparse. The benthic foraminifera assemblage contains endothyrids, *Tuberitina*, *Earlandia vulgaris*, palaeotextularids, rare *Tetrataxis* and *Bradyina*.

Where this facies first occurs at 4.1 m, gastropods are common and red algae fragments, such as *Fasciella* and ungdarellid debris, occur as rare to sparse components in all samples; some specimens have been silicified. Sparse echinoids and rare crinoids occur at the base of this facies. Bioturbation, peloids, faecal pellets, phosphate and pyrite are present in some samples.

Gigantoproductus floatstone facies.

This facies (Figure 2-6G, H) is characterised by its localised floatstone horizons, within a bioclastic skeletal packstone to wackestone matrix that contains detrital micrite, and rare peloids and faecal pellets. At the base of this facies there are several thin muddy horizons that can be traced along the exposure. Species of *Gigantoproductus* brachiopods are abundant. Sparse foraminifera and crinoids, and sparse to rare paleoberesellid and ungdarellid algae are present in all samples. The foraminiferan assemblage comprises

several *Omphalotis* and *Endothyra*, alongside *Pseudoendothyra/Eostafella*, *Tuberitina*, *Tetrataxis*, *Bradyina*, paleotextularids and *Earlandia*.

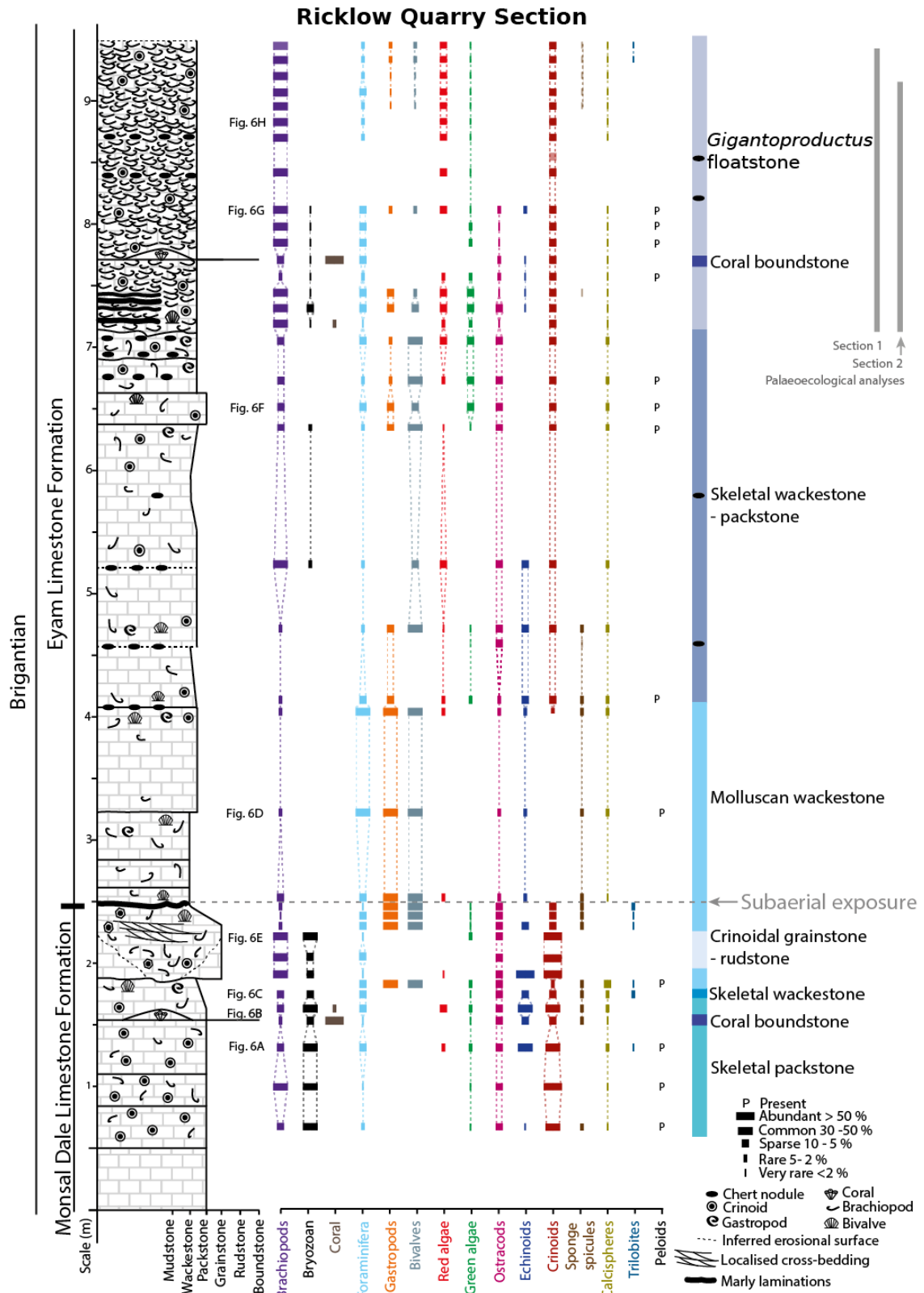


Figure 2-5. Stratigraphic section at Ricklow Quarry with skeletal abundance and facies interpretations.

Relative abundances of skeletal components within thin sections of samples are represented. Section One and Section Two refer to the locations of the palaeoecological studies (Figure 2-9 & 2-10). Figure numbers relating to the stratigraphic position of thin section micrographs in Figure 2-6 are labelled

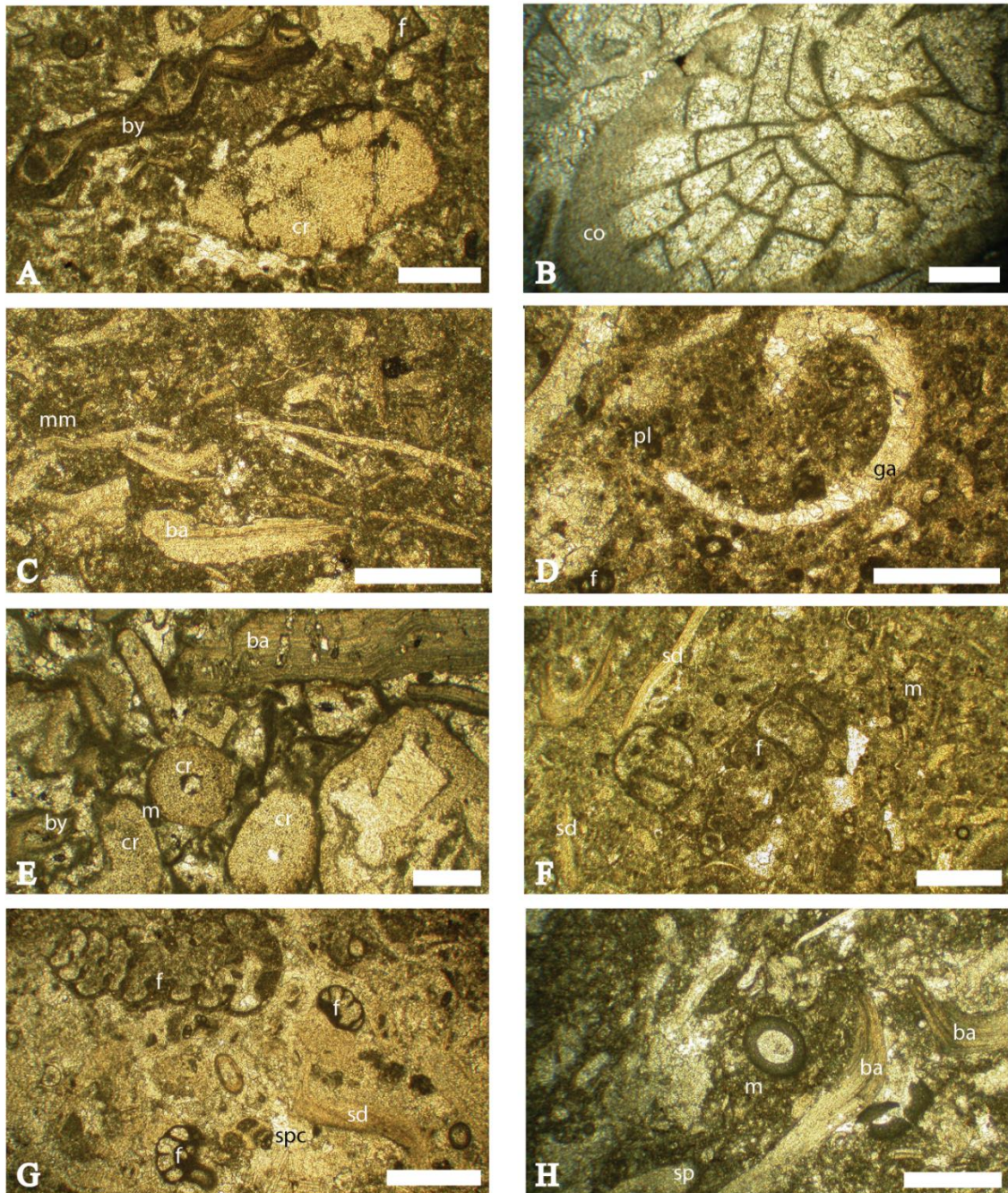


Figure 2-6. Thin section micrographs from the Ricklow Quarry section.

All scale bars are 0.5 mm. A) Skeletal packstone with preserved fenestellid bryozoan (by), *Tetrataxis* foraminiferan (f), crinoid ossicle (cr) (sample 1a, taken at height ca. 1.25 m from the base of the section is). B) Rugose coral boundstone showing a large section of a well-preserved coral (co) (sample 2a at ca. 1.55 m). C) Skeletal wackestone facies showing brachiopod fragments (ba) and a micritic matrix (mm) (sample 2c at ca. 1.75 m). D) Molluscan wackestone facies with gastropod moulds (ga), skeletal fragments,

foraminifera (f) and peloids (pl) within the matrix (sample 2d at ca. 3.20 m). E) The upper part of the crinoidal grainstone – rudstone dominated by crinoid debris, some with a micritic (m) envelope (sample 2i at ca. 2.25 m). F) Skeletal wackestone – packstone comprising highly fragmented shell debris (sd), including some foraminiferans (f, paleotextularid) (sample 5d at ca. 6.5 m). (G, H) *Gigantoproductus* floatstone with well-preserved foraminiferan (f, in G) there are paleotextularid at the top right and various endothyrid fragments; in (H) there is *Earlandia vulgaris* and brachiopod (ba) fragments surrounded by micrite (m) and some sparry calcite (spc). (G), sample 7h taken from ca. 8.75 and (H) and, sample 7m taken from ca. 8.1 m. All thin sections currently archived at the University of Leicester.

2.5.2 Facies Types: Once-a-Week Quarry

Four facies are recognised through the quarry section (Figure 2-7). Crinoids and bryozoans are common to abundant in every thin section collected from the Once-a-Week Quarry section. The orientations of the long axes of the crinoid stems are typically between 160° – 115° with some orientated perpendicular to the general trend. Intraclasts are commonly observed and are predominantly millimetre-sized and composed of wackestone with clotted peloidal and leiolitic micrite associated with sponge spicules. Typically, the facies at this locality comprise undulating 10 – 30 cm thin beds with normal grading of crinoids debris where they are abundant.

Skeletal packstone-wackestone with micritic intraclasts.

This facies (Figure 2-8A, B) is characterised by dominant packstone to wackestone with locally floatstone to rudstone or grainstone texture. It contains rare phosphate grains, pyrite and millimetre-sized wackestone intraclasts in blocky sparite cement. The fossil assemblage typically comprises common crinoids and bryozoans. The foraminifera are rare to very rare, but the assemblage commonly comprises *Tetrataxis*, *Tuberitina*, *Earlandia*, endothyrids, archaeodiscids and palaeotextularids.

A calcareous muddy horizon at 5.4 m separates two variants of the facies. The lower part of the facies is characterised by brachiopods, bryozoans, rare to very rare foraminifera and gastropods, sparse red algae, rare green palaeoberesellid algae, sparse ostracods and common crinoids. The facies overlying this muddy horizon is finer grained, lacking gastropods and algae with brachiopods becoming very rare. This facies also occurs at the top of the quarry section (9.75 m) where, at the macroscale, a 7 cm-thick graded bed of crinoid ossicles is noted. Here it is locally developed as a rudstone with common brachiopods, crinoids and bryozoans, with blocky sparite cement.

Crinoidal packstone-grainstone.

This facies (Figure 2-8C, D) occurs between 1.3 m to 4.75 m above the base of the section and is also recognised in a thin section of a 10 cm bed at 8.6 m. It is inferred to be present between 6.45 m to 9.25 m, based on the macroscale features, including the presence of lenticular bedding from 6.45 m to the bed sampled for the thin section. At the macroscale, semi-articulated crinoid stems are associated. The facies is characterised by the presence of peloids and abundant crinoids, many of which contain microborings (Figure 2-8C, D). Syntaxial calcite and blocky sparite cements occur at some horizons and phosphate grains are present throughout, with the exception of the sample at 8.6 m.

The fossil assemblage varies, but brachiopods, bryozoans, foraminiferans and ostracods are always present. The foraminiferan assemblage of this facies comprises mostly archaeodiscids, *Tetrataxis* and *Howchinia* alongside endothyrids, *Valvulinella* and *Earlandia vulgaris*. Calcspheres occur within all thin sections, except one sample at 3.1 m.

Skeletal intraclastic grainstone.

This facies (Figure 2-8E) occurs only once, at 4.75 m, within the section. It is characterised by its abundance of skeletal fragments and presence of wackestone intraclasts that are typically millimetres in size, and contain skeletal grains and peloids. The fossil assemblage comprises common crinoids, bryozoans (fenestellids, fistuliporids and ramose), sparse brachiopods and rare foraminifera.

Gigantoproductus skeletal grainstone.

This facies (Figure 2-8F) is characterised by abundant brachiopods, dominated by species of *Gigantoproductus*, and common crinoids within a fine- to coarse-grained bioclastic debris matrix. The texture is variable: locally, grainstone with coarse- to fine-grained skeletal fragments is intercalated with patches of packstone – wackestone and rudstone textures. Syntaxial cement around crinoids is present, possibly with micrite between gigantoproductids. Millimetre-sized intraclasts of detrital and clotted peloidal micrite are present within all samples.

A 20 cm-thick bed of this facies occurs 6.3 m above the base of the section. It contains sparse to rare foraminifera (endothyrids, *Tetrataxis*, *Tuberitina*, palaeotextularids,

Earlandia vulgaris, *Howchinia*), sparse ostracods, rare calcispheres and sponge spicules that are associated with clotted peloidal micrite. The horizon also contains wackestone – packstone textures. A second example of this facies occurs at 9.5 m where locally it has a rudstone texture and is rich in crinoids. Here the foraminiferans are very rare (though endothyrids and *Earlandia vulgaris* are identified) and bryozoans are typically fenestellids.

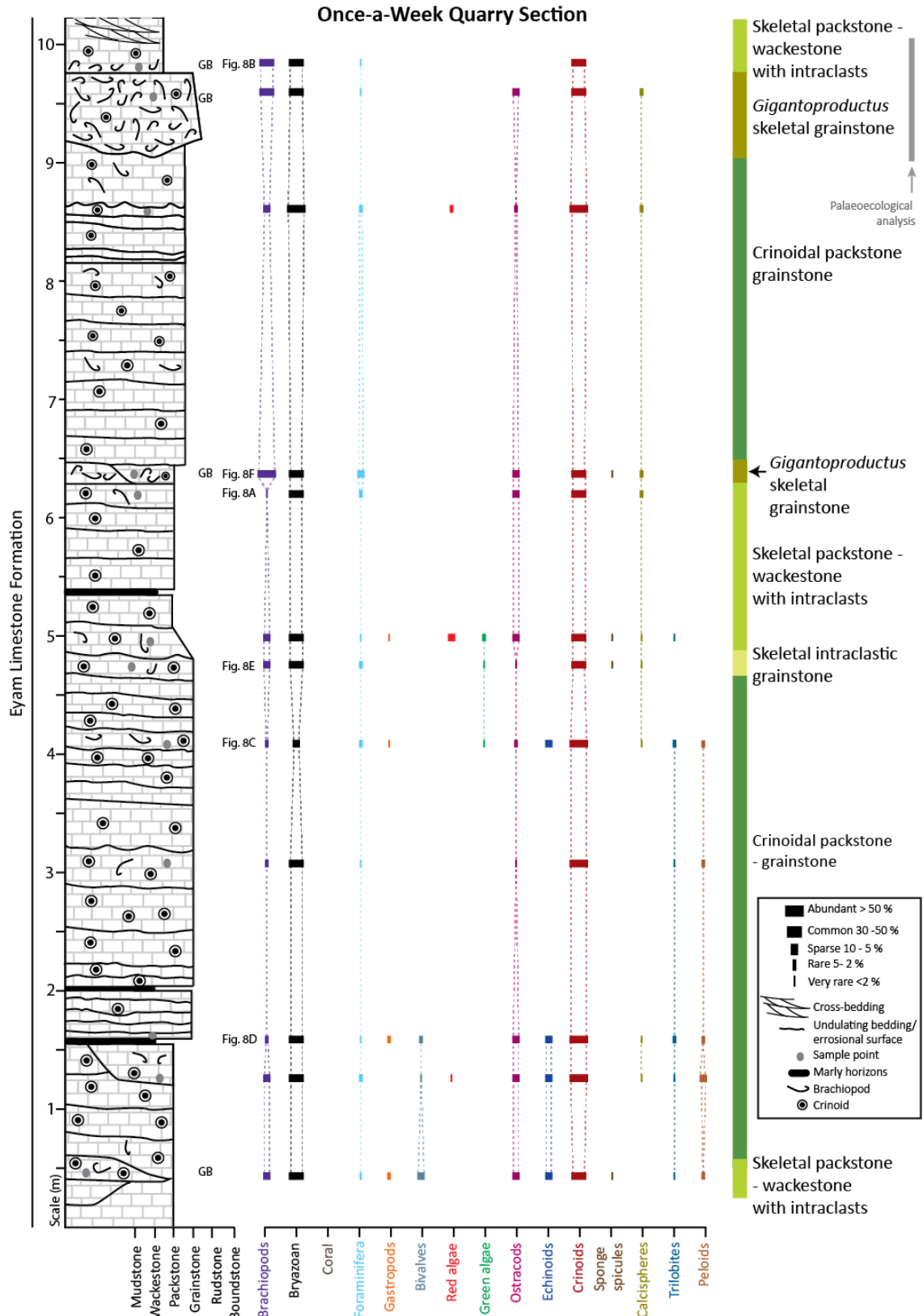


Figure 2-7. Stratigraphic section at Once-a-Week Quarry with skeletal abundance, and facies interpretations.

Relative abundances of skeletal components within thin sections of samples are represented. Section One refers to the location of the palaeoecological studies (Figure 2-11). Beds are normally graded where

crinoids are abundant or very abundant. Figure numbers relating to the stratigraphic position of thin section micrographs in Figure 2-8 are labelled. Beds (GB) with whole (not fragmented) *Gigantoproductus* that are visible in the exposure are located on the section. Undulating bedding represents areas where localised reworking has also occurred and commonly is eroded along these planes.

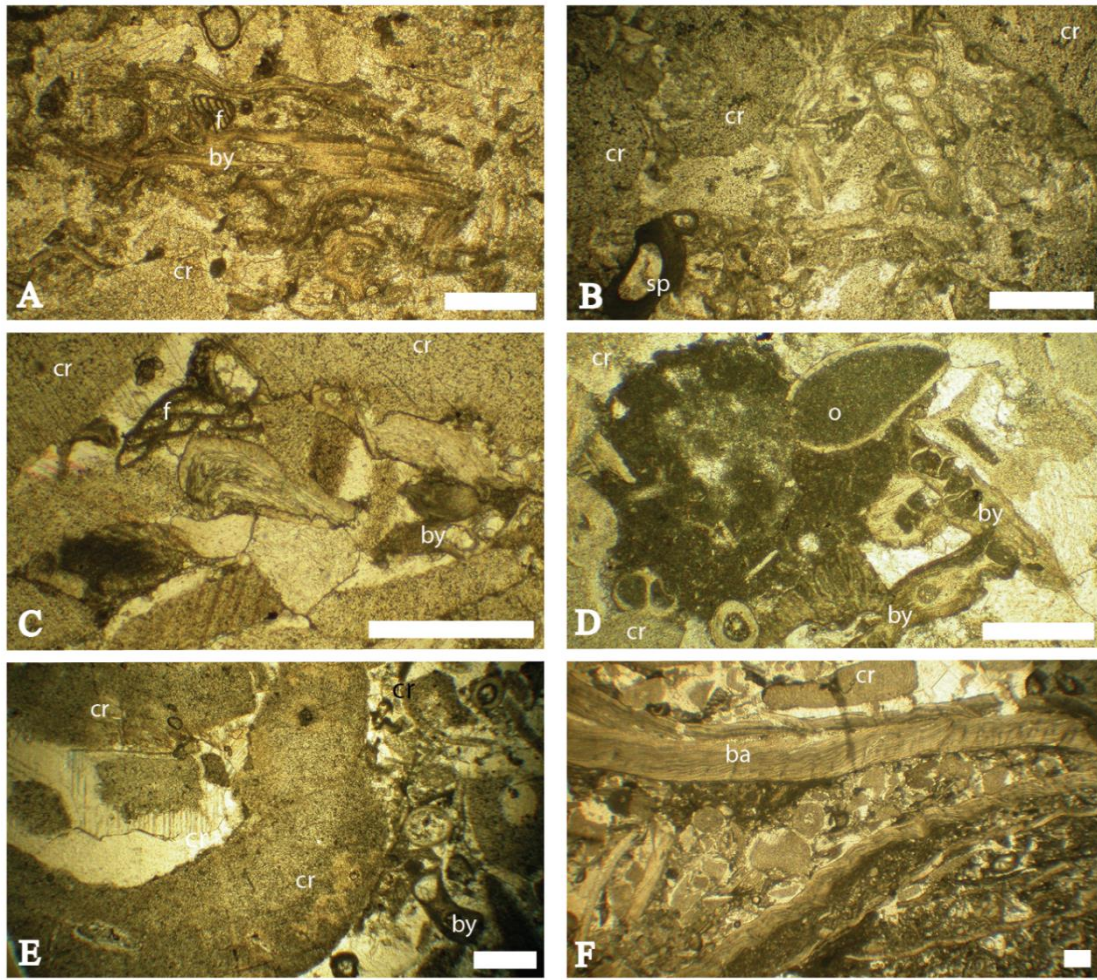


Figure 2-8. Thin section micrographs of the Once-a-Week Quarry section.

All scale bars are 0.5 mm. A) Skeletal packstone – wackestone with intraclasts from the central part of the section showing packing and dominant bryozoans (by) and crinoids (cr) with *Tetrataxis* foraminifer (f) (sample 7 at ca. 6.25 m). B) Skeletal packstone – wackestone with intraclasts from the top of the section showing strong compaction of brachiopod spines (sp), bryozoan and crinoid fragments (sample 11i at ca. 9.75 m). C) Crinoidal packstone – grainstone with fenestellid bryozoan, crinoids and foraminifera (sample 4 taken ca. 4.1 m from the base of the section). D) A micrite-rich intraclast within the crinoidal packstone – grainstone containing ostracods (o) and fenestellid bryozoan (by), and surrounded by crinoid ossicles which have undergone compaction (sample 2 at ca. 1.6 m). E) The skeletal intraclastic grainstone dominated by crinoid debris, and other skeletal debris (sample 5 at ca. 4.75 m). F) *Gigantoproductus* packstone – wackestone, showing heterogeneity at thin section scale (sample 8 at ca. 6.4 m). Sample

numbers are assigned to hand specimen samples and corresponding thin sections are currently archived at the University of Leicester.

2.5.3 Palaeoecology: Ricklow Quarry

At Ricklow Quarry, brachiopod-rich deposits are found as lenses 1 to 3 m-thick and tens of metres wide. Four species of *Gigantoproductus* are identified in the two analysed sections of the first bed (Figures 2-9, 2-10): *G. aff. expansus* (Sarytcheva, 1928), *G. gaylensis* (Pattison, 1981), *G. inflatus* (Sarytcheva, 1928) and *G. okensis* (Sarytcheva, 1928). In addition to gigantoproductids, other brachiopods (including species of *Latiproductus* sp., other productids, chonetids and spiriferids), solitary and colonial corals, and a single gastropod specimen are present. In both sections, three to 17 individuals are present within each 10 cm division and the gigantoproductids are predominantly orientated with their umbo pointing north. At Ricklow Quarry 72 % of the identified fauna were found in their original, convex-down life position.

The diversity indices through Sections One and Two (Figure 2-9) are < 1.37 for Shannon and < 1.86 for Margalef and both sections have similar averages, Section One has averages of 0.81 and 0.88 for Shannon and Margalef respectively, and Section Two has averages of 0.85 and 0.80. In Section One, the Shannon diversity index and the Margalef index follow the same broad trends. The highest diversity index is encountered in a life assemblage identified near the base of the section (Figure 2-9) and diversity indices decrease over the next three divisions into a neighbourhood assemblage. Between 70 – 160 cm, the diversity index fluctuates between 0.5 and 1.37; six of the highest diversity indices are associated with neighbourhood assemblages and three are within life assemblages for both calculated diversity indices (Figure 2-8). Several of the neighbourhood assemblages in Section One contain other productids, chonetids, spiriferids and species of *Latiproductus* alongside species of *Gigantoproductus* (Figure 2-10). The presence of these other brachiopod species increases diversity indices within these divisions. Similarly, in the life assemblages with the highest diversities, combinations of other productids, *Latiproductus* sp., chonetids and spiriferids are present.

In Section Two, both methods generate similar diversity indices. There is a subtle overall decrease in diversity over the lower 1.5 m, with a higher, but variable diversity at the top

despite a reduced sampling area. Two of the highest diversity indices are associated with neighbourhood assemblages and two are within life assemblages (Figure 2-9). Section Two differs from Section One in that other productids represent a significant component of the individuals present in all but three divisions (Figure 2-9). The lower diversity indices associated with the neighbourhood assemblages in Section Two, compared to Section One, reflects the dominance of *Gigantoproductus* species and other productids (*Latiproductus* sp., chonetid and spiriferid brachiopods are absent in all but one neighbourhood assemblage). In most of Section Two, the Shannon diversity index is the same as or marginally higher than the Margalef index because the presence of productids reduces dominance of *Gigantoproductus* species (Figures 2-9, 2-10). At 160 cm, however, only a few individuals of thin- and thick-shelled *Gigantoproductus* spp. occur in a division and this produces a higher Margalef diversity index relative to the Shannon diversity index (Figure 2-10).

Divisions are characterised by life and neighbourhood assemblages, and changes in the diversity cannot be correlated between the two sections (Figure 2-9). Differences in the gigantoproductid species and other brachiopod species are also observed in both sections; for example, the productids are far more abundant in Section Two compared to Section One. Thick and thin-shelled *Gigantoproductus* species are present within both sections at Ricklow Quarry. Thick-shelled forms dominate; thin-shelled *Gigantoproductus* species represent only 31.7% of Section One and 22% of Section Two. A small proportion (<5.5%) of shells in both sections are orientated such that a thick or thin shell cannot be determined. Bryozoans, corals and gastropods are observed, but form a minor component in both sections. Additionally, where a 100 cm width of the bed is visible (0 – 130 cm in Section One and 0 – 150 cm in Section Two), the average number of individuals present within each 10 cm interval is 10 and 12 for Section One and Two, respectively (where 100 cm width of the bed is exposed), indicating that Section Two is more densely populated.

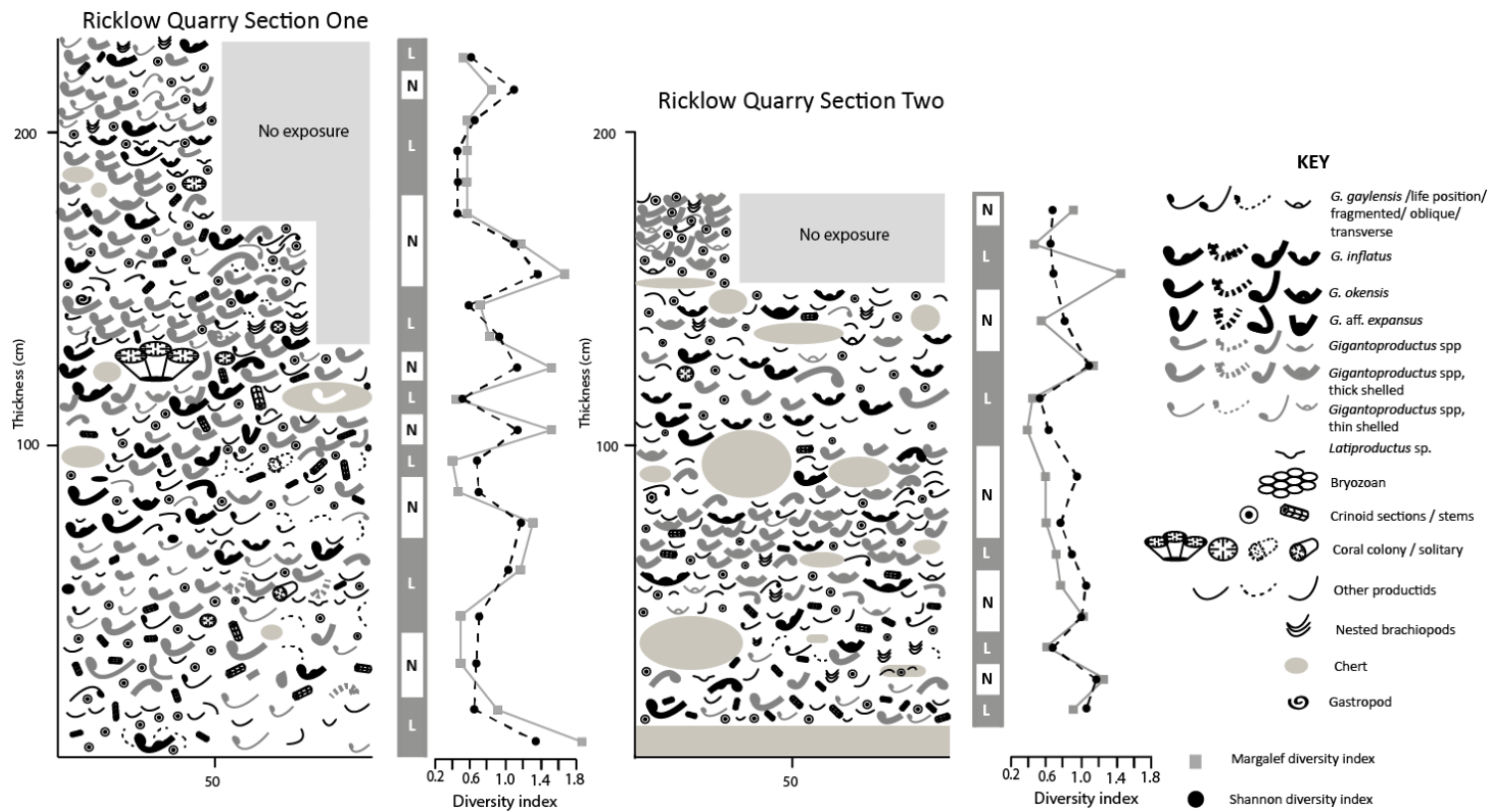


Figure 2-9. Schematic representation of Sections One and Two of the shell beds at Ricklow Quarry.

The base of these sections represents the base of the *Gigantoproductus* shell bed. Each shell represents an identified individual and is drawn in the observed orientation. Crinoids are represented as abundance and whether ossicles or stems are present. Individuals are drawn to scale where measurements are known. Classification as life (L) or neighbourhood (N) assemblages is illustrated, and Shannon and Margalef diversity indices shown.

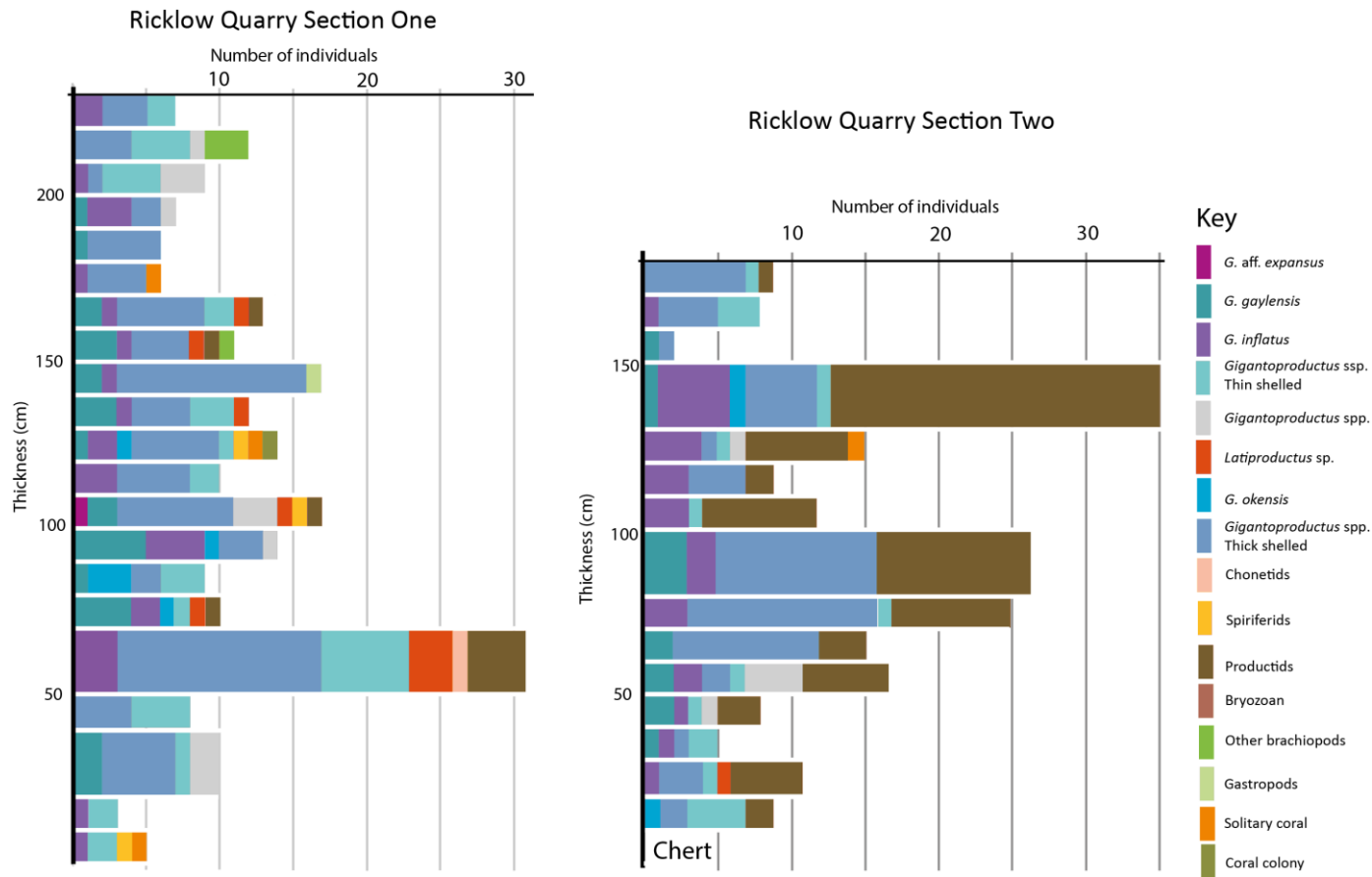


Figure 2-10. Illustration of the occurrence of individuals identified in the Ricklow Quarry sections.

The key represents the bar size for an individual and each bar represents a 10 cm interval. Where bars are double thickness, two 10 cm intervals have been amalgamated due to close packing of brachiopods.

2.5.4 Palaeoecology: Once-a-Week Quarry

At Once-a-Week Quarry three *Gigantoproductus* species are identified. *Gigantoproductus inflatus* (Sarytcheva) and *G. okensis* (Sarytcheva, 1928) are present, as they were at Ricklow Quarry. *Gigantoproductus elongatus* (Pattison, 1981) is present at Once-a-Week Quarry, but this species was not identified at Ricklow Quarry. Two species found at Ricklow Quarry, *G. aff. expansus* (Sarytcheva) and *G. gaylensis* (Pattison), were not observed at Once-a-Week Quarry. *Latiproductus*, other productids, spiriferids and one bryozoan colony are also found. Only thick-shelled gigantoproductids are present and dominate the biota in the section. Examining the orientation of the fauna, 37% were found in their original life position and brachiopod umbos had no preferred orientation.

The metre square section represents several neighbourhood assemblages (Figure 2-11). Peak diversity (1.07 for Shannon and 1.4 Margalef) is reached at 40-50 cm in the section where *Latiproductus* sp., spiriferid brachiopods and a bryozoan colony are present. The average Shannon diversity index is 0.42 (0.5 for the Margalef diversity index) is lower than the average calculated at Ricklow Quarry, although it should be noted that this lower average is based on only six points. Diversity indices were not calculated where only thick-shelled forms (*G. elongatus*, *G. okensis* and *G. inflatus*) are present. On average eight individuals were identified within each 10 cm division (Figure 2-11), thus demonstrating that this section is less densely populated than both Ricklow Quarry sections.

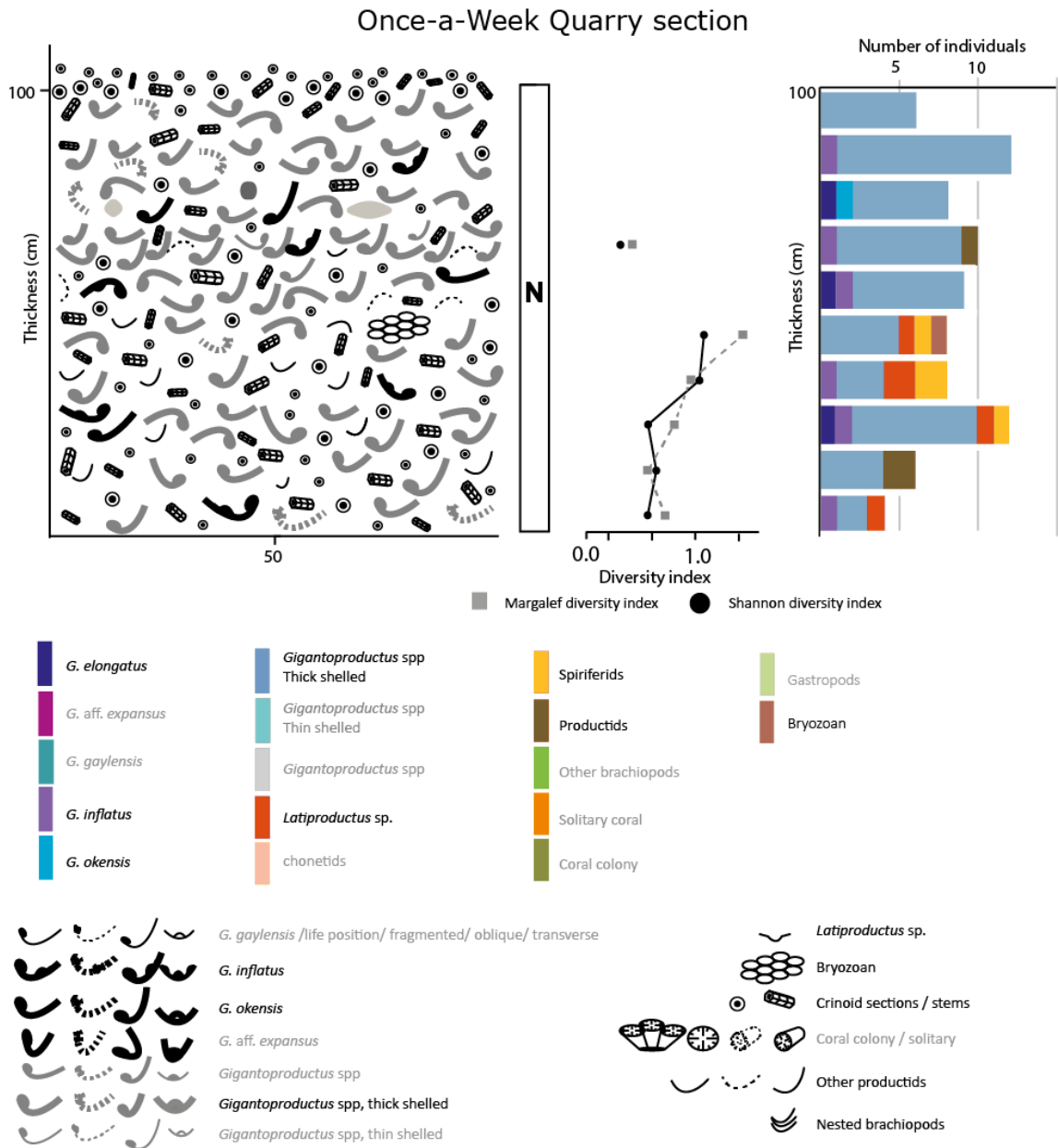


Figure 2-11. Schematic representation of the *Gigantoproductus* shell bed alongside diversity. Note that only neighbourhood (N) assemblages are present. Grey words on key indicate fauna that were not observed at Once-a-Week Quarry to aid comparison with the fauna found at Ricklow Quarry (Figure 2.9, 2.10).

2.6 Discussion

2.6.1 Facies

2.6.1.1 Depositional environment and evolution at Ricklow Quarry

The seven facies are grouped into three main facies associations that are related to their depositional environments: the mound-flank facies; the inner to middle ramp facies; and the mid ramp facies associations. The skeletal assemblage identified indicates generally subtidal open marine waters, mostly of normal salinity, but with possible variations.

The skeletal packstone facies at the base of the section represents a mound-flank facies association. The abundance of bryozoan and crinoid debris reflects their existence fringing the mud mound which lies directly adjacent to the Ricklow Quarry section (Gutteridge, 1995). The clotted peloidal micrite and wackestone intraclasts that are present here may be reworked from the adjacent mounds into the flanks. However, as these types of intraclasts are also found in other horizons, they may also be an *in situ* clotted micrite precipitation. A localised occurrence of a coral boundstone and skeletal wackestone facies is interbedded with the skeletal packstone facies. The *in situ* corals indicate a moderate energy, muddy depositional environment, just below the fair weather wave base (Copper, 1988). The skeletal wackestone facies also forms part of the mound-flanks as its micrite content indicates deposition below the wave base. The interbedding of the skeletal packstones, wackestones and coral boundstones reflects the lateral accretion of the mud mound (Gutteridge, 1995), and represents a transitional phase as the mound flank facies association transitions into the inner to middle ramp facies.

Overlying this transition zone is the inner to middle ramp facies association. This comprises three associations, the molluscan wackestone, the crinoidal grainstone-rudstone and the skeletal wackestone – packstone facies. During the deposition of these sediments, the adjacent mud mound was stable, but no longer active, partially lithified and therefore no longer contributing debris to the surrounding area (Gutteridge, 1995). This is reflected in the decrease of crinoid ossicles and bryozoan debris present within the molluscan wackestone and skeletal wackestone facies. Within this facies association occurs the lenticular unit at *ca.* 2 m, characterised by the crinoid grainstone – rudstone facies. This bed has an erosional base that suggests a channel morphology and the dimensions are within the range of tidal channels seen in Florida (Grinnell, 1974);

however, no other evidence of tidal influence is observed. The highly micritised grainstone facies described within the shoal facies by Gawthorpe and Gutteridge (1990) are very similar to the crinoidal grainstone – rudstone facies identified at Ricklow Quarry; however, the dimensions are different and the Ricklow Quarry unit is three orders of magnitude smaller than the shoals described by Gawthorpe and Gutteridge (1990). Furthermore, the facies described by these authors occur in the north-eastern margin of the platform with a very different structural (and therefore environmental) setting than the intraplatform ramp within which the sediments at Ricklow Quarry were deposited. This bed at Ricklow Quarry is interpreted as a depositional bar. The subtle grading towards the top of the Ricklow unit, which is then overlain by the molluscan wackestone, suggests the current velocity was decreasing as the bar was abandoned. These beds are more likely formed by current effects; their formation and size was restricted due to the lowering of sea level that occurred during their deposition prior to the Monsal Dale Limestone - Eyam Limestone formations boundary. Additionally, the effects of currents or tides may have been amplified within this region due to a potential funnelling effect caused by the geometry of the intraplatform ramp aiding the formation of such shoals in environments, which may otherwise not be suitable.

The recessive boundary observed at 2.5 m (Figure 2-5) represents a subaerial exposure surface confirmed by the presence of meteoric diagenetic features, including pendant vadose cement, secondary vuggy and biomoldic dissolution porosity, and uncommon root casts and iron oxides, as observed between 1.6 m and 2.35 m. This subaerial exposure, described by Adams (1980), Aitkenhead et al. (1985) and Gutteridge (1991b), represents the Monsal Dale – Eyam Limestone formations boundary proposed by Gutteridge (1995).

Following subaerial exposure, the ramp was re-established and sedimentation of the molluscan wackestone facies resumed. This deposit at the start of the Eyam Limestone Formation likely represents restricted environments, including the development of 'lagoon'-like environments within the inner to middle ramp depositional environment (Gutteridge, 1983), which developed due to the interaction of the low sea level (post-emergence) and the relict topography of the now inactive (though still present) mud mounds. It is noted that the sediments exposed at Ricklow Quarry lie directly to the east

of a mud mound at this locality and, therefore, is on the 'open' side of the mound, which potentially limited the formation of 'lagoon'-like environments. However, the morphology of this mound is not fully understood, with outcrops of mound facies to the south, west and north of the quarry itself (Figure 2-1c). This suggests that the mound geometry was more complex during the time of deposition than is currently visible in outcrop. This is likely to have complicated the interplay of sea level rise with the mound geometry, therefore allowing the formation of restricted 'lagoon'-like environments.

As the ramp evolved further, the skeletal wackestone-packstone facies was deposited above the molluscan wackestone. This textural change, from wackestone to packstone, suggests a change to more open marine conditions. This switch can also be inferred by the increase in occurrence of red ungdarellid algae and green paleoberesllid algae debris, and the end of the dominance of molluscs, alongside increasing energy.

The muddy carbonate horizons at the base of the *Gigantoproductus* floatstone facies suggest relatively low energy conditions during the initial gigantoproductid colonisation. The transition into deposition of the middle ramp facies association also includes a localised horizon of the coral boundstone facies. Deposition occurred below the active wave base with some mud present within the water column; this is indicated by the presence of the micrite rich floatstone lithofacies and the interbedding of a second occurrence of the coral boundstone facies. A continuation of open (less restricted) conditions is indicated by the presence of both green and red algal debris within several horizons, which are likely to have undergone some transportation. Brachiopods and echinoderms present within this facies indicate that normal salinity marine conditions were present throughout (Fürsich, 1993; Kammer and Ausich, 2006).

2.6.1.2 Depositional environment and evolution at Once-a-Week Quarry.

The skeletal packstone with intraclasts, the crinoidal packstone-grainstone and skeletal packstone wackestone, present from the base of the section to 6.25 m, are collectively interpreted as an inner ramp facies association. The presence of semi-articulated crinoid stems suggests that either energy levels were sufficiently low to avoid disarticulation or that sedimentation rates were high (Baumiller and Ausich, 1992; Ausich et al., 1979; Cain, 1968). A high sedimentation rate would also explain the absence of corals and their scarcity at the locality in general (only one example of a coral is seen in the quarry face).

Alternations between the skeletal packstone-wackestone with intraclasts and the crinoidal packstone-grainstone, associated with an increase in size of the crinoid ossicles, suggest changes from lower to higher energy conditions, respectively. The quantity of micrite, and the abundance and size of fragmented skeletal fragments, is also used to infer changes in energy and the amount of reworking.

The sparse to rare brachiopods noted in the facies and at outcrop are not in their life position, and the fragmentation suggests some reworking. However, the macrofossil assemblage identified is assumed to be representative of the *in situ* community because significant transport distances between habitats are unlikely (Lane, 1973; Macdonald, 1976). The very rare to sparse red and green algae suggests that water depth may have varied (Madi et al., 1996), but all algae present are debris and are likely to have undergone some transportation. Therefore, they cannot be used as direct or reliable indicators of water depth.

The *Gigantoproductus* skeletal grainstone appears at 6.25 m, where the coarse-grained, sand-sized skeletal fragments indicate high levels of reworking and increased energy levels relative to the underlying facies. The *Gigantoproductus* skeletal grainstone also occurs at 9.25 – 9.75 m, separated from the lower bed by the crinoidal packstone and wackestone. At the top of the section, size grading of crinoid ossicles indicates turbulent current allowed significant sorting during deposition of the skeletal packstone - wackestone with intraclasts. The presence of coarse-grained, sand-sized skeletal fragments and the relative absence of mud in the Once-a-Week Quarry section suggest a higher energy, inner ramp setting in comparison to the conditions for the *Gigantoproductus* shell bed at Ricklow Quarry. The orientation of crinoid stems indicates a roughly south-easterly palaeoflow as elongate stems preferentially align perpendicular and occasionally roll parallel with the direction of flow (Gutteridge, 1983). The consistent orientation of crinoids through the section indicates that flow patterns were steady through the deposition of these strata.

2.6.2 Palaeoecological interpretation of the *Gigantoproductus* Floatstone Facies

Gigantoproductus were suited for living in high-energy environments (Ferguson, 1978; Harper and Jeffrey, 1996) where currents ensured a constant supply of sufficient oxygen and food passing over them. The consistent brachiopod orientation in the

Gigantoproductus shell bed analysed at Ricklow Quarry, with umbos oriented pointing north, suggests currents were constant. As *Gigantoproductus* species tend to align with the umbo facing the current (Ferguson, 1978; Shino and Suzuki, 2011), it is inferred that the currents were flowing in a southerly direction.

This palaeoflow direction appears to be different to that inferred by Gutteridge (1983), who suggested there were east to west palaeocurrents on the platform during the deposition of the Eyam Limestone Formation. The mud mounds at the top of Monsal Dale Limestone Formation, one of which is exposed at Ricklow Quarry, were partially eroded during subaerial exposure (Aitkenhead and Chisholm, 1982; Gutteridge, 1991b) and produced a relict topography on the sea floor during the subsequent transgression that re-established the inner to middle ramp facies of the Eyam Limestone Formation. Renewed deposition of inner to middle ramp facies began around the inactive mud mounds (Gutteridge, 1991b). Continued sedimentation partially buried and smoothed the topography, providing a suitable habitat for the gigantoproductids, which sheltered at the side of the mound (in this case the eastern side). It is likely, therefore, that the relict topography of the mud mound influenced local current flow. It generated localised flows that were diverted around the mounds leading to north-south oriented brachiopods at the Ricklow location. The currents produced by the presence of a relict topography around the mud mounds would have also transported the larvae that colonised the sheltered margins of the pre-existing mud mound.

Although species of *Gigantoproductus* thrived in high-energy environments, quieter conditions were required to enable brachiopod larvae to settle and establish a gigantoproductid community. The mud-rich horizons present at the base of the *Gigantoproductus* shell bed at Ricklow Quarry suggest low energy conditions preceded the major phase of *Gigantoproductus* species colonisation. The brachiopods at Ricklow Quarry occur within a micrite matrix because the large shell size allowed them to baffle mud and fine bioclasts. Their size may have provided localised areas of shelter from currents for other nearby individuals and larvae once the community is established.

The diversity indices, and their averages, throughout the three sampled sections at Ricklow (2) and Once-a-Week (1) quarries are comparable to those recorded and interpreted by Angiolini (2007) as representing low diversity palaeocommunities. The

indices at Ricklow and Once-a-Week quarries would be even lower if a qualitative estimation of the biovolume, rather than only the number of individuals were considered, because the large size of *Gigantoproductus* species meant that this genus dominated the communities. The Margalef index value underestimates the true diversity due to reduced sample size (Gamito, 2010), whereas the Shannon-Wiener index reflects more clearly the dominance of *Gigantoproductus* species. Low diversities may reflect an absence of heterogeneities in the environment, particularly in the substrate and/or a high level of environmental disturbance and/or resources availability.

At Ricklow Quarry, the variation between low (<1) to moderate (considered as values >1) richness of the macrofauna, rather than a systemic change from basal low diversities to high diversities upwards, suggests the early stages of ecosystem development are not recorded. There is no evidence for an ecological transition into a climax community. In the topmost 1 m of Section One at Ricklow Quarry, Shannon-Wiener diversity values of 0.45-0.65 over four consecutive divisions may reflect an intermediate point in the ecological succession between the early and mature stages, as already observed in other Palaeozoic brachiopod-bearing successions (e.g. Angiolini, 2007; Angiolini et al., 2003). Therefore, the palaeocommunity dominated by *Gigantoproductus* species was rapidly established, but did not evolve towards a climax. The absence of a climax phase may be due to a combination of environmental disturbance and high resources. At Ricklow Quarry rapid colonisation probably lead to a taphonomic feedback where the large brachiopod species changed the environment and the nature of the substrate itself, thereby sustaining further rapid colonization by conspecific individuals, and the rich and diverse microbiota seen within the *Gigantoproductus* shell bed (e.g. Ferguson, 1978).

The generally low diversity indices calculated from the Once-a-Week Quarry section through the *Gigantoproductus* shell bed, compared to values at Ricklow Quarry, may reflect transport and winnowing of the biota at the former location. The general absence of thin-shelled varieties at Once-a-Week Quarry may also reflect that the environment was suited to specifically adapted organisms, including thick-shelled species of *Gigantoproductus*, bryozoans and crinoids.

The presence of *G. elongatus* at Once-a-Week Quarry infers that these assemblages are slightly younger than the first *Gigantoproductus* bed at Ricklow Quarry. This is because

G. elongatus appears slightly later than *G. inflatus*, *G. okensis* and *G. gaylensis* (Pattison, 1981). The second *Gigantoproductus* bed at Ricklow Quarry, although poorly exposed, also contains *G. elongatus*, confirming these stratigraphic relationships. No mud mound is observed at Once-a-Week Quarry; however, geological maps indicate one large and several smaller mud mounds within its vicinity. Original field slips indicate that geologists who mapped the region observed crinoid-rich facies that they interpreted to be derived from mound flanks (Chisholm, 1971 - 1972). The interpretation of the depositional environment places Once-a-Week Quarry in shallower water than that at Ricklow Quarry. This is consistent with the geographical location of Once-a-Week Quarry relative to the geometry of the carbonate ramp, despite the two localities not being time equivalent.

The facies observed beneath the first *Gigantoproductus* shell bed at Once-a-Week Quarry suggests lower energy conditions prior to its development. However, the absence of thin shelled gigantoproductids, such as *G. gaylensis*, the random shell and umbo orientations, a much lower percentage of brachiopods in their original life position and presence only of neighbourhood assemblages all indicate higher energy conditions, and a shallower setting on the ramp, at Once-a-Week Quarry compared to Ricklow Quarry. This is consistent with the observation that there are reduced numbers of individuals at Once-a-Week Quarry suggesting larvae had more difficulty settling here. The decline in diversity near the top of Once-a-Week Quarry, where only gigantoproductids are present, and the association with a 7 cm-thick, normally-graded, coarse-grained crinoidal bed, with no gigantoproductids, indicates that currents may have exceeded the threshold (30-38 cm/s) for moving/tiling of adult *Gigantoproductus* species, experimentally obtained by Ferguson (1978).

2.7 Summary

Both studied localities, Ricklow and Once-a-Week quarries within the Eyam Limestone Formation, represent inner to middle ramp settings, characterised by diverse facies with varied skeletal assemblages. Detailed analyses of the *Gigantoproductus* shell beds present at both quarries show that there are differences that relate to their local setting and environment. Despite these differences, shell bed occurrence is preceded by a

period of decreased energy. At Ricklow Quarry, several mudstone layers occur directly at the base of the *Gigantoproductus* shell bed. In contrast, at Once-a-Week Quarry, skeletal packstone-wackestone with intraclast facies underlie the first occurrence of the *Gigantoproductus* floatstone and the *Gigantoproductus* skeletal grainstone. These intervals of low energy allowed the deposition of fine-grained sediment and, potentially, time for the brachiopod larval stages to settle.

At Ricklow Quarry, the palaeoecological study of two sections within the 2.2 m thick *Gigantoproductus* floatstone facies revealed life and neighbourhood assemblages, with 72% of brachiopods in life position. These assemblages, and the observed variations in diversity indices, could not be correlated between two sections analysed at the same stratigraphic height, indicating highly localised variations across the original community. A low-moderate diversity in both of the Ricklow Quarry sections indicates a rapidly established palaeocommunity that did not reach a stable climax. Once the community was established, the large shell size of *Gigantoproductus* and the dominance of these thick-shelled forms enabled baffling of mud and fine bioclasts, and may also have provided localised shelter for other nearby individuals and larvae. This provided a positive feedback, encouraging further colonisation. In contrast, although similarly low diversity indices are seen at Once-a-Week Quarry, a palaeoecological study shows the *Gigantoproductus* skeletal grainstone was exclusively composed of neighbourhood assemblages, with only 37% of brachiopods in life position and having no preferred orientation. Although they do not represent life assemblages, the brachiopods are not thought to have been transported far from where they were living and the absence of thin-shelled productids suggested that higher energy conditions on the inner ramp were likely.

At Ricklow Quarry, the relict mud mound topography is interpreted to have provided shelter on its lee (east) side that enabled species of *Gigantoproductus*, including those with thin shells, to rapidly and successfully colonise these areas. Where orientations of brachiopods could be measured, a south-directed palaeoflow is indicated at this locality, which contrasts to the easterly palaeoflow inferred by Gutteridge (1983). This suggests that the relict topography of the mud mounds (of the Monsal Dale Limestone Formation) locally influenced currents and provided a potential mechanism for the transportation of

larvae during deposition of the Eyam Limestone Formation. No mud mound is present in the exposed sections at Once-a-Week Quarry. This, coupled with the low percentage of brachiopods in life position in the assemblages, may explain the contrast in character and palaeoecology between the *Gigantoproductus* shell beds here when compared to Ricklow Quarry.

The success of this genus on this part of the Derbyshire carbonate platform appears to be related to the location of inactive mud mounds. At Ricklow Quarry, the genus *Gigantoproductus* was able to rapidly establish a significant and stable community in the shelter of the relict mud mound. In contrast, at Once-a-Week Quarry, such shelter is absent, resulting in smaller communities of lower diversity, with evidence of some reworking and the establishment of only thick-shelled brachiopods. Overall, the evidence suggests that on the intrashelf part of the Derbyshire carbonate platform, species of *Gigantoproductus* were commonly associated with mud mounds in inner to middle ramp settings. However, they did not actively contribute to mound development and colonised the substrate following mud mound demise.

Overall, although these organisms benefited from the shelter of the inactive mud-mounds, their habitat appears to have been connected to open waters and was of normal salinity. The significance of this is that further palaeoenvironmental work can now be conducted in the knowledge that data collected from these organisms that may relate to environment, such as stable isotope data, which may then be used as a palaeothermometer, is informative of open shallow water of normal salinity.

Chapter 3: Assessing the preservation of species of *Gigantoproductus* using ultrastructure and cathodoluminescence analyses

3.1 Background

Various types of preservation analyses are an essential part of palaeoclimate studies because shells need to be pristine to ensure any isotope data can be reliably interpreted (Brand et al., 2011). If material is either not screened for preservation, or is seen to be poorly preserved, then its isotope composition should not be used as a palaeoclimate proxy as it may have been altered by diagenetic overprinting.

All brachiopods secrete their shells in an ordered and structured way, which results in a recognisable microfabric, referred to as the shell ultrastructure (Williams et al., 2007). For many brachiopod genera, both extant and extinct, their ultrastructure is well documented, is often well understood, (Garbelli, 2010; MacKinnon and Williams, 1974; Williams, 2007; Williams and Wright, 1970) and can be readily identified via Scanning Electron Microscopy (SEM). The identification of fine ultrastructure detail is commonly used as a preservation assessment tool (e.g. Angiolini et al., 2007; Angiolini et al., 2012; Azmy et al., 2011; Brand et al., 2003a; Garbelli et al., 2012; Grossman et al., 1993b; Mii and Grossman, 1994; Mii et al., 1999) alongside other observational methods, particularly cathodoluminescence (CL).

Productid brachiopods are extinct and there are no direct modern analogues to which *Gigantoproductus* species can be directly compared, however, some aspects of their ultrastructure are comparable to other modern brachiopods having a three layered shell structure (Parkinson et al., 2005), such as the terebratulid *Liothyrella neozelanica* and *Gryphus vitreus*,. However, the fabric of the secondary layer is very different, being

fibrous in the extant taxa, but laminar in the productids (Williams et al., 2007; Garbelli et al., 2012). While some studies have only focused on preservation (Garbelli et al., 2012), there are others that have also examined shell ultrastructure of Palaeozoic brachiopods as part of a preservation assessment prior to stable isotope analyses (Angiolini et al., 2012; Armendáriz et al., 2008; Mii et al., 1999; Mii and Grossman, 1994; Mii et al., 2001). These authors commented on the fabric structure in relation to preservation as indicated by how much detailed structure is observed and whether there is any evidence of dissolution or recrystallisation that are indicative of diagenetic alteration. There are however, no detailed studies, which outline the key features of a well preserved or pristine species of *Gigantoproductus* ultrastructure, including fine detail features that, when observed, are indicative of good preservation and can be helpful with preservation assessment. Observing the ultrastructure is a valid screening mechanism for sample selection, as it enables materials that have undergone dissolution, secondary mineralisation and/or recrystallisation to be identified and excluded from further analyses; however, this method alone is not robust enough to identify all poorly-preserved material as ultrastructure may appear well preserved if diagenesis occurs without the disrupting the crystal structure (Garbelli et al., 2012; Zachara et al., 1991). Hence, it is essential to use a range of screening methods including Cathodoluminescence (CL) and trace element analyses.

Cathodoluminescence analysis is commonly conducted on shell specimens alongside ultrastructure analyses to provide a further test of preservation. The luminescent properties of well-preserved and poorly-preserved (or diagenetically altered) brachiopod biogenic calcite are different (Barbin and Gaspard, 1995; Tomasovych and Farkas, 2005; Veizer et al., 1997; Walkden and Berry, 1984). In carbonate materials, luminescence is caused by distortion of the crystal lattice. This can occur due to various reasons including differing element proportions, imperfections in the crystal structure or crystals containing impurities (Boggs and Krinsley, 2006). Within carbonate materials, luminescence is thought to be mainly controlled by impurities. More specifically, it is largely influenced by the ratio of Mn^{2+} (acting as an activator) to Fe^{2+} (acting as a luminescence quencher) (Boggs and Krinsley, 2006). The significance is that Mn and Fe concentrations within biogenic calcite are commonly used as an indicator of preservation

(Azmy et al., 2011; Brand et al., 2003; Brand and Veizer, 1980; Swart, 2015) as biogenic calcite typically contains very low levels of Mn and variable contents of Fe (Azmy et al., 2011), especially when compared to the surrounding matrix and cement of the host rock. Therefore, the luminescent properties of shell material can be an indicator of trace element composition and, thus, is a proxy for chemical preservation.

By using both CL and ultrastructure as primary screening mechanisms, a general assessment of preservation can be made of each specimen, meaning specimens that are poorly preserved, based on these criteria, can be excluded from subsequent more expensive and time-consuming trace element analyses. This also allows cross-examination of material and methods, making the selection of well-preserved calcite for further analyses more reliable.

The aims of this chapter are to provide a comprehensive account of detailed shell structure and organisation of the pristine shell fabrics, including fine detailed structures that can then be used as an example of well-preserved *Gigantoproductus* species shell fabric, and assess preservation of each specimen based on the presence or lack of ultrastructure features and luminescent properties.

3.1.1 Shell Growth

Understanding the shell growth mechanisms helps establish whether features that are not commonly seen within the shell ultrastructure are natural or diagenetic. Additionally, as trace element and isotope data have been collected at high resolution, it is important to understand the growth mechanisms in order to know the relationship of time/age of samples across the shell and across samples (see chapter 4 for more details of sampling strategies).

All living brachiopods have an organic periostracum layer (Schmahl et al., 2012; Williams et al., 1997a), however being organic, it is rarely preserved in the fossil record. Underneath the periostracum, a microgranular primary layer should be present (Schmahl et al., 2012), which however is rarely preserved in fossil shells; the (preserved) outer shell layer typically comprises the secondary laminar or fibrous layer, followed by a prismatic tertiary layer (Schmahl et al., 2012; Williams, 1997). Both of these layers are present in all specimens collected for this study and have been observed in species of

Gigantoproductus in previous studies (Angiolini et al., 2012; Garbelli et al., 2012; Mii et al., 2001a).

In species of *Gigantoproductus*, the secondary layer consists of individual, elongate, closely packed calcite laminae, which would have been surrounded by organic protein sheets that are not preserved (Figure 3-1). The prismatic tertiary shell layer consists of elongate interlocking calcite columns, which has very little organic matrix.

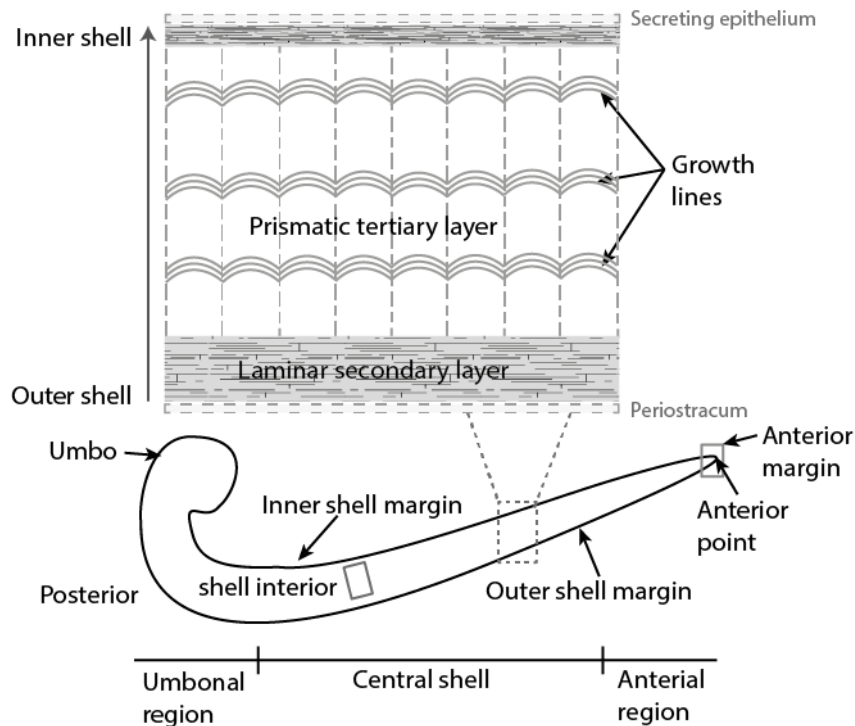


Figure 3-1. Schematic diagram of a cross-section through the ventral valve of a *Gigantoproductus* species detailing the typical organisation of the shell layers.

The laminar secondary layer is present at the outer shell margin and may occur intercalated to the tertiary layer. The outer shell would have been enclosed by the primary layer and by periostracum and the inner shell margin by the outer epithelium cells from which the shell itself is secreted however, these features are not preserved in these fossil specimens. Terminology of the labelled sections of the specimen illustrated in this figure has been adapted from the brachiopod anatomical descriptions in Williams et al. (2007).

In modern calcitic brachiopods the biomineralised shell is secreted by the organism throughout its life. Shell secretion and growth of *Gigantoproductus* species would most likely have been slow, but the rate and mode of calcite secretion changes through the organisms' life (Rudwick, 1959). During growth, secretion of the shell occurs from the

outer epithelium cells, which form a thin layer on the inner shell surface (figure 3-2) (Williams, 1997). As the shell grows, it lengthens and the anterior point migrates away from the umbo, which is the origin of growth. The epithelium cells at the anterior point migrate as the shell lengthens (and more cells are produced), when the cells are migrating, they secrete the laminar secondary shell layer. When an epithelium cell stops migrating, the mode of secretion from the cell changes and so does its physiology meaning this causes the cell to stop secreting organic material. This combination of the cell no longer migrating and it no longer producing organic material results in the secretion of the prismatic tertiary shell layer and an increase in the valve thickness (Williams, 2007). The type of calcitic fabric secreted may therefore be determined by a range of factors, for instance environmental, influencing the cell physiology (Garbelli et al., 2012) that ultimately determine whether or not the cell is migrating.

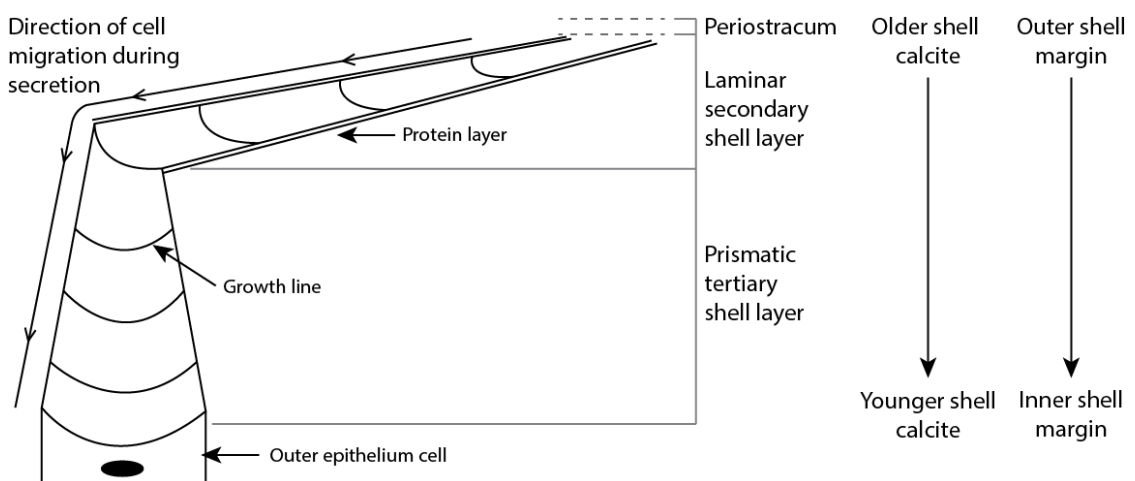


Figure 3-2. A schematic cross section through the thickness of shell and the relationship of the outer epithelium cell migration with the secretion of the laminar secondary and prismatic tertiary layers (adapted from Williams, 2007).

Additional to these features, both the secondary and tertiary shell layers may also contain growth lines. Growth lines are thought to represent a reduced growth rate, or even a temporary cease in shell secretion (Hiller, 1988). This results in a 'line' or an interval across the shell within which the fabric is microgranular. When growth rates return to normal, the standard fabric (either the laminar or prismatic) continues to be secreted.

3.2 Methods and materials

3.2.1 Specimen collection

Specimens of *Gigantoproductus* species were collected from shell beds present at Ricklow Quarry and Once-a-Week Quarry (Chapter 2). More than 250 specimens belonging to several different species were collected for the purpose of this study (these are housed at the University of Milan and University of Leicester). Several articulated specimens of *G. gaylensis* were collected from Ricklow Quarry; however, the ventral valve thickness for this species is too thin and therefore these specimens were not suitable for this study. All other species are relatively thick shelled and therefore suitable for this study. Multiple specimens were moulds or casts, or were not complete enough (i.e. without a complete ventral valve) and therefore were discarded. Additionally, some did not have sufficiently thick ventral valves (ca. <5 mm) despite being thick shelled species, or were seen to be heavily silicified and therefore did not undergo any analyses.

3.2.2 Specimen preparation

Specimens were sectioned longitudinally from the umbo to the anterior margin exposing a section through the shell interior. 26 specimens of three different *Gigantoproductus* species that appeared to be well-preserved were subject to further processing. The collection locality, species and specimen number of the 26 utilised specimens are outlined in Table 1.

An acetate peel was made of one of the surface of the sample that was exposed during sectioning and was used as a location reference for the ultrastructure and CL analyses. A thin section was then made of one side of the original sliced surface and was used for cathodoluminescence analyses while the counter surface was cut longitudinally a second time to produce a flat 'slice' which underwent ultrastructure analysis. Of the 26 specimens, sections were made from 24 of the specimens, two shells (OAW 212 and OAW 233) were seen to be heavily silicified once sectioned and were therefore disregarded.

After ultrastructure and CL analyses the best shells were analysed for trace element composition, along with spot analyses on poorly preserved material and end-member material (Chapter 4).

When discussing the preservation of the specimens in the following section, each shell length is divided into regions; the umbonal region, the central shell region and the region towards the anterior margin. The shell thickness is also divided into three regions; the outer shell margin, the inner shell and the inner shell margin (Figure 3-1).

Sample identification	Species	Sample identification	Species
OAW 51	<i>G. inflatus</i>	OAW 03	<i>G. inflatus</i>
OAW 50	<i>G. inflatus</i>	OAW 05	<i>G. inflatus</i>
RCK 35	<i>G. inflatus</i>	RCK 28bis	<i>G. okensis</i>
RCK 33	<i>G. inflatus</i>	OAW 08	<i>G. inflatus</i>
RCK 28	<i>G. inflatus</i>	OAW 102	<i>G. elongatus</i>
OAW 02	<i>G. elongatus</i>	RCK 100	<i>G. okensis</i>
RCK 6	<i>G. inflatus</i>	OAW 104	<i>G. inflatus</i>
RCK 6bis	<i>G. inflatus</i>	OAW 105	<i>G. inflatus</i>
RCK 41	<i>G. inflatus</i>	OAW 23	<i>G. elongatus</i>
XG	<i>Unknown</i>	OAW 27	<i>G. elongatus</i>
RCK 36	<i>G. okensis</i>	OAW 211	<i>G. elongatus</i>

Table 3-1. Sample identification number and species of those specimens that underwent ultrastructure and cathodoluminescence analyses.

Sample names: 'OAW' identify those specimens collected from Once-a-Week Quarry, and 'RCK' those collected from Ricklow Quarry. All samples consist of at least a ventral valve where analyses are focused. Many specimens also contain a dorsal valve. Where to dorsal valve is imaged or discussed this is highlighted.

3.2.3 Ultrastructure analyses methodology

After sectioning, the shell slices were polished using 500 µm and then 100 µm silica carbide grit. One half of each of the sectioned specimens underwent analysis using the Scanning Electron Microscopy (SEM) at the University of Milan (Cambridge S-360 within lanthanum hexaboride (LaB6) cathodes). An acetate peel to be used as a reference was made of the other half before being set aside. Samples were imaged at both high magnification (e.g. X 900) in order to assess the detailed structures of the shell fabric, and low magnification (e.g. X 70) in order to assess the organisation and distribution of the laminar and prismatic layers.

The ultrastructure of the ventral valve is described here, because this valve is generally the thickest, with better displayed growth lines, and most commonly used in palaeoclimate studies. The ultrastructure of the dorsal valves was only briefly examined.

The assessment of ultrastructure preservation is based on previously published images and descriptions of brachiopod ultrastructure. Although the ultrastructure of species of

Gigantoproductus has not been described in detail, many of the ultrastructure features are similar to other brachiopods within the order Productida (e.g. Garbelli, 2010). By comparing the ultrastructure of the samples being analysed with previously published examples of well-preserved ancient fossilised specimens and comparable species of extant brachiopods, a qualitative assessment of the preservation of the shell ultrastructure was made. All SEM images along with individual descriptions of the ultrastructure preservation combined with a description of the CL properties of each individual shell are provided in Appendix C.

3.2.4 Cathodoluminescence analysis method

Thin sections were made of the sectioned shell surfaces and were used for CL analyses at the University of Milan. A cathodoluminescence luminoscope (CL) (Nuclide mod ELM2B) mounted on a Letz Ortolux II microscope was used for this procedure (10 KV voltage and between 3-6 mA current). Specimens were placed inside a chamber that was under vacuum and images of the thin section were taken on a Nikon Coolpix 4500 digital camera with an exposure time of 1 second for the majority of images, and 2 seconds for some. Images were taken both under CL and under plane-polarised light (PPL) and/or cross-polarised light (XPL) to allow comparison of the shell details when viewed in different conditions. Many images were taken and systematically overlapped, allowing the images to be stitched together, using Photoshop software, to produce larger images of the shells under CL and PPL light (all images are given in Appendix D). This enables the identification and comparison of luminescent and non-luminescent areas within individual specimens and helps characterise areas of the shell with different luminescent features. In all cases, the entirety of the specimen was observed and analysed; however, given time constraints, in many cases, images were only taken of areas of the shell that are important for understanding the luminescent properties of the specimen.

Garbelli et al. (2012) quantified luminescence of shell layers by using Photoshop software to find the proportion of black to primary colours within an area or fabric and calculating a percentage of luminescence. This is difficult within these large *Gigantoproductus* species because the luminescent properties are highly variable within a single fabric and area of the shell. Areas are therefore qualitatively described whilst also considering the parameters assigned by Garbelli et al. (2012). Luminescence within this study is described

as followed; brightly luminescent (BL), moderately luminescent (ML), dully luminescent (DL), or non-luminescent (NL) however, it is noted that the boundaries of these classification are not clear-cut. Further explanation is given where required. It should be noted that as this method is qualitative, some observations are often subjective.

3.3 Results

3.3.1 Ultrastructure analyses

3.3.1.1 The laminar secondary layer

In all specimens, the laminar secondary layer is present at the outer shell margin as a continuous layer running along the length of the shell from the umbo to the anterior margin of the ventral valve. The thickness of this layer varies both within and between specimens but can be up to several millimetres thick. Typically, the thickness of this layer is greatest towards the umbo and gradually thins towards the anterior margin. In many specimens, the umbonal region is comprised of the laminar secondary layer and it is frequently very thick (e.g. in specimen OAW 105), (Figure 3-3). Some specimens also have intercalations between the secondary and tertiary layers, with occasionally the laminar secondary layer occurring at the inner shell margin (Figure 3.4A). The fabric of this inner layer is the same as is seen in other shell areas, but the thickness of this band varies within and between specimens. Generally, this band of the laminar fabric at the inner shell margin is thinner than that at the outer shell margin. The secondary laminar layer can also occur within the shell interior, though this is not common. Where this does occur, a thin layer of the laminar secondary layer is present *within* the prismatic tertiary layer. In these instances, the organism has switched from secreting the tertiary layer, to the secondary and then back to the tertiary again.

At low magnification (e.g. X 100) the parallel packing of the laminae can be observed (Figure 3-3A and B). These laminae are aligned in an orientation that is sub-parallel to the outer shell margin. At this magnification, individual laminae may not be easily identified, as these specimens are sectioned longitudinally and the laminae commonly extend *ca.* 90° to the shells longitudinal axis, the length of the individual laminae cannot be measured. At high magnification (e.g. X 750), where laminae are well preserved, individual blades forming the laminae can be easily identified (Figure 3-3C) and micro-

porosity (caused by the decay of the surrounding organic material) can be seen between them (Figure 3-3D). Individual laminae of the analysed specimens have an average thickness of c.a. 0.9 μm . This thickness appears to be consistent in all parts of the shell despite the differing thicknesses of the laminar layer as a whole. No clear differences in laminae thickness was observed among species.

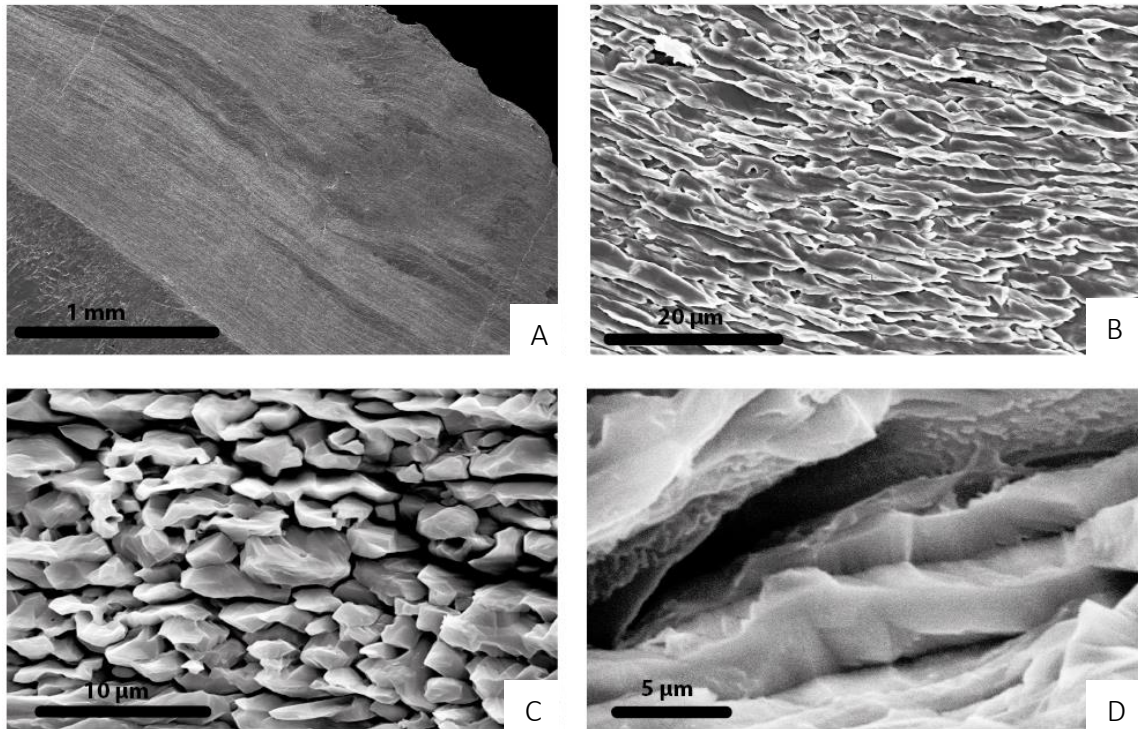


Figure 3-3. SEM micrographs showing examples of the laminar secondary layer.

a) Sub-parallel packing of the laminae within the laminar secondary layer of specimen OAW 105. b) Detailed image of the alignment of laminae within specimen OAW 105. c) Termination and thickness of laminae composed of aligned blades within specimen OAW 27. d) Details the 3-dimensional nature of the porosity between the lamina within specimen OAW 211.

In high magnification images, details of the transition from the secondary to the tertiary layer can be seen. These images show how individual lamina of the secondary layer gradually thicken as the cell slows and stops migrating before the laminae becomes a single prism of the tertiary shell layer (Figure 3-5E). This occurs at every instance where the fabric transitions from the laminar secondary to the prismatic tertiary layer, as it is caused by a change in the mode of secretion via the mantle and a stop in mantle migration.

3.3.1.2 The prismatic tertiary layer

The prismatic tertiary layer of the species of *Gigantoproductus* makes up the majority of the shell thickness in all specimens and thus is the dominant fabric. In large specimens, although individual prisms cannot be identified with a hand lens, their elongate nature often can. This layer is always present within the central shell region and often at the inner shell and anterior shell regions (Figure 3-1).

Typically, the prismatic tertiary layer is several times thicker than the laminar secondary layer and its thickness varies relative to the shell region. The prismatic tertiary layer for example generally becomes gradually thicker progressing away from the umbonal region while the thickness of the secondary laminar layer is greatest within the umbonal region and thins progressing away from the umbo. At the anterior margin, however, where the whole shell thickness has decreased, the thickness of the prismatic tertiary layer also thins but remains typically thicker than the laminar secondary layer.

Prisms are secreted orthogonal to the outer shell margin. They are tightly packed but separated by interlocking crystal boundaries (Figure 3-4A, B and D) with no regular porosity or organic material between individual prisms. The angle of sectioning of these specimens does not allow the nature of the three-dimensional 'stacking' of prisms on top of each other to be fully observed, but the boundaries between individual prisms are regularly seen and are well defined in many specimens. Individual crystals are typically elongate, except in specimens where strong packing of the crystals occurs during competitive growth, in which cases their shape may be irregular (Figure 3-4C).

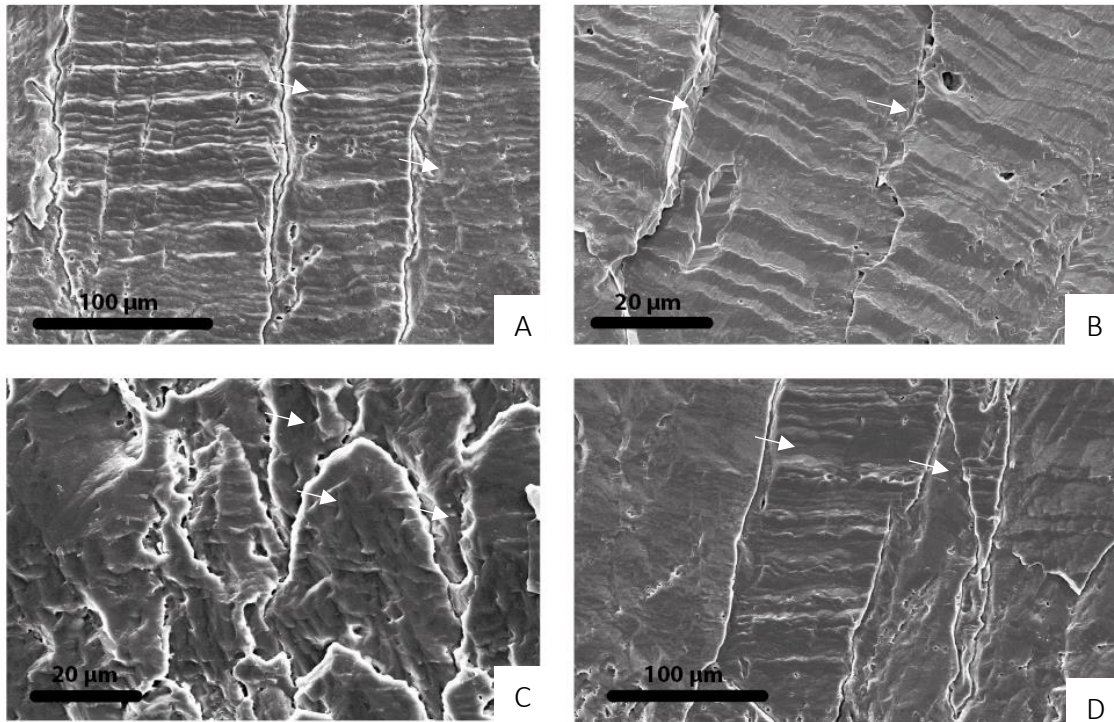


Figure 3-4. SEM micrographs showing examples of the prismatic tertiary layer.

A), specimen RCK 6 and B), specimen OAW 211, show the interlocking character of the prismatic layer and stepped growth patterns that cross several prisms. C) Illustration of the irregular form of packed prisms with stepped growth patterns within specimen RCK 6. D) Highlighting how stepped growth patterns cannot always be traced along adjacent prisms within specimen RCK 41. Crystal boundaries are indicated with white arrows.

Micro-scale ‘stepped’ growth patterns are present on the surface of many calcite prisms and are regularly seen at high magnification (e.g. X 380). These occur as semi-regular three-dimensional ridges aligned perpendicular to the prisms’ direction of growth. They are often unevenly spaced, but are typically spaced between 0.17 and 25.3 μm with an average spacing of 6.03 μm (Figure 3-4). In many specimens, the ridges formed by the stepped growth patterns are seen to cross multiple prisms although this is not always the case and adjacent prisms are sometimes seen with differing stepped patterns. Additionally, this feature is not identified on all prisms and is not seen regularly within all specimens.

3.3.1.3 Structural features

Although the general ultrastructure of the defined shell layers is consistent across specimens there are some structural features that occur, within which the ultrastructure

is different. An example of this is given by pseudopunctae; these are primary features of the shell structure that occur within the laminar secondary layer. They are produced by the rapid thickening of the secondary laminar layer (Williams et al., 2007), which causes asymmetrical deflection of laminae that is easily observed via SEM (Figure 3-5). The orientation of the deflected laminae can change by more than 90° and, they are characterized by an inner core of granular calcite, called taleola (Figure 3-5B, C and D) (Williams et al., 2007). No pseudopunctae have been observed within the umbonal region and they are most commonly present within the laminar secondary layer at the inner and outer shell margins within the central and anterior shell region.

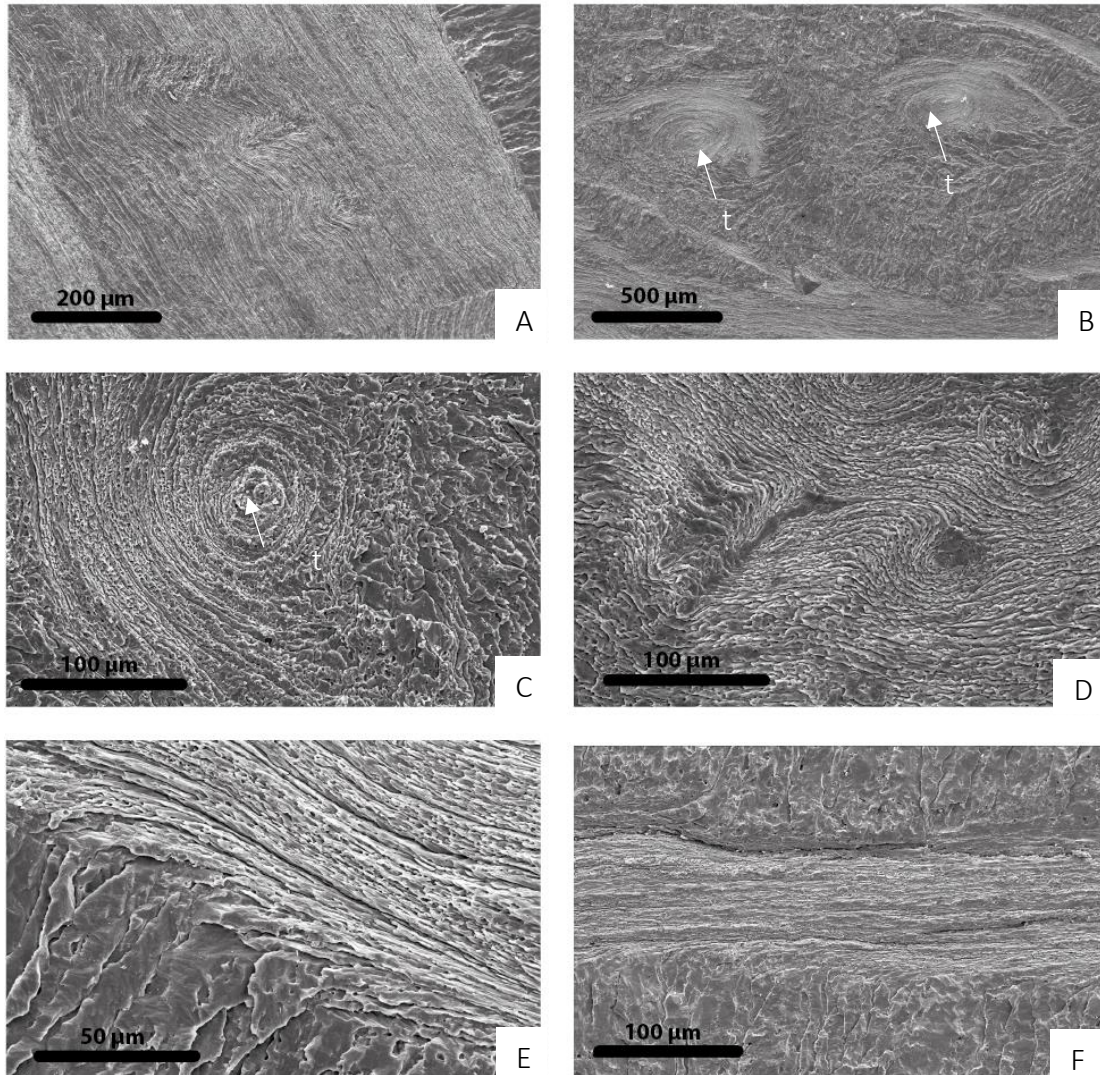


Figure 3-5. SEM micrographs showing examples of structural shell features.

A) Multiple asymmetrical deflections of laminae forming pseudopunctae near the outer shell margin within specimen OAW 03. B) Pseudopunctae with taleolae (t) in the secondary layer surrounded by tertiary prisms within specimen RCK 33, highlighting the three-dimensional nature of the stacked cones of the pseudopunctae. C) A taleola formed within a pseudopunctae of shell RCK 33. D) Asymmetrical deflection of laminae within specimen RCK 6. E) Transition of a single lamina into a single prism with the prismatic layer of specimen RCK 28. F) Shows the abrupt termination of prism growth before the growth of secondary lamina (2°). The transition from the laminar secondary layer into the prismatic tertiary layer is gradual, not abrupt, as a single lamina transitions into a single prism. This image is of specimen OAW 05.

Growth lines that can be traced along significant lengths of the shell (from near the umbonal region to the anterior margin) running sub parallel to the outer and inner shell margins are regularly observed. They have an average thickness of 0.4 mm and often contain some microporosity. They are easily recognised within the tertiary shell layer

where there is a pause in the prism structure, crossing several prisms, after which the prism formation generally continues (Figure 3-6A). Differentiating between a thin laminar secondary layer and growth lines within the tertiary shell layer can be difficult, as the structure within growth lines have a microgranular texture that may be similar to that of the secondary shell layer. However, the two can be distinguished by their marginally different structures, as growth lines have a more irregular internal structure than the laminae within the secondary shell layer (Figure 3-6C).

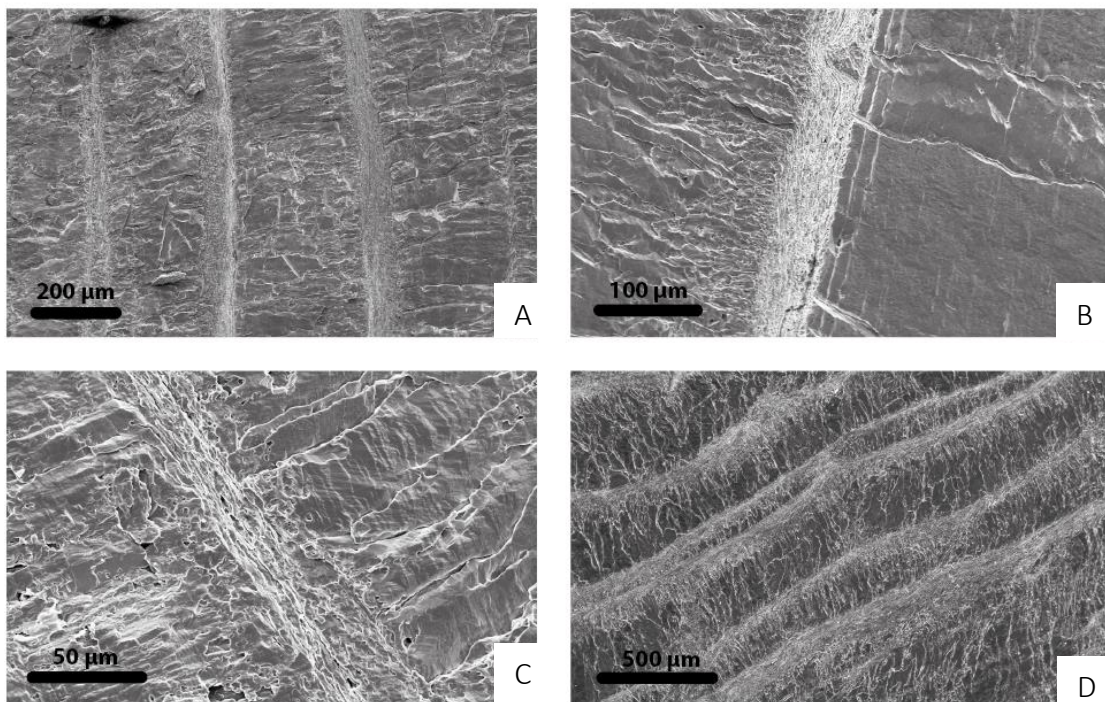


Figure 3-6. SEM micrographs showing examples of growth lines.

A) several bands of the laminar secondary layer intercalated in the prismatic tertiary layer within specimen RCK 100. B) and C) growth lines with disordered calcite granules within, crosscutting the prismatic tertiary layer within specimen OAW 105. D) several bands of the laminar secondary layer intercalated in the prismatic tertiary layer within specimen XG, with sharp boundaries where the fabric transitions from the tertiary to the secondary layer, but gradual transition from the secondary to the tertiary.

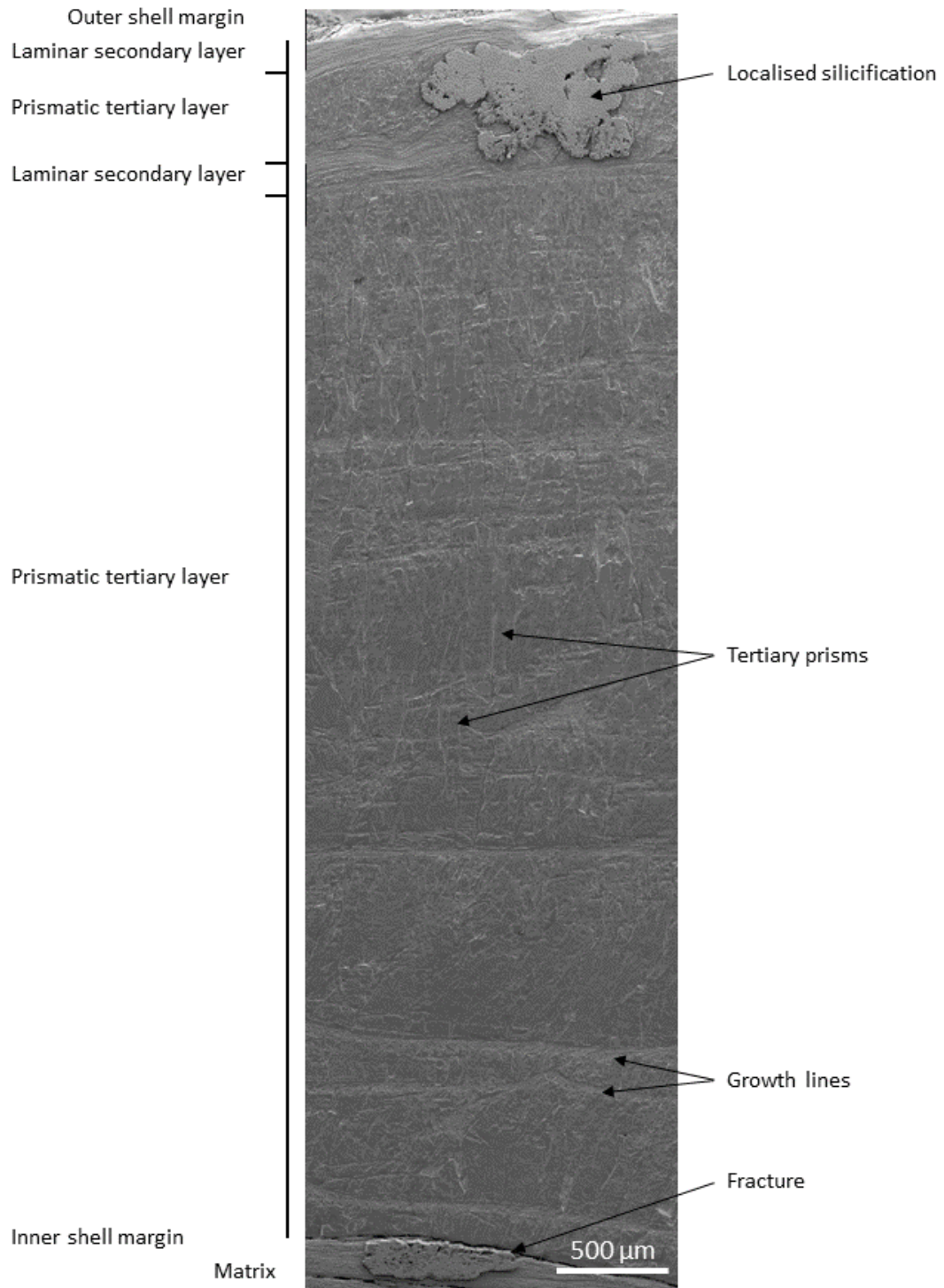


Figure 3-7. Transect through sample RCK 36 from the inner (bottom) towards the outer shell boundary (top) indicating changes in texture.

The outer shell margin remains intact with a thin layer of the laminar secondary layer present. The passage between the underlying tertiary layer is transitional with intercalations of the two layers. There is a large patch of localised silicification overprinting the original shell texture (both tertiary and secondary layers). The prismatic layers appear well preserved with some individual prisms identified at this magnification (X 70).

3.3.1.4 Additional observations

Although large areas of many specimens show detailed ultrastructure, it is regularly observed that areas of specimen's ultrastructure are distorted or disturbed, such as amalgamation of shell fabrics, recrystallisation, and silicification. Silicification is a secondary mineralization process whereby the original shell calcite is replaced by silica changing the mineralogy and crystallography of the calcite shell therefore no original geochemistry or ultrastructure is retained. Recrystallisation is the dissolution of the shell calcite and then the recrystallisation of the same material meaning the mineralogy remains the same, the material is still calcite, however its crystallography has changed and therefore also its microstructure. The secondary growth of calcite crystals is seen to mimic the form of the biogenic calcite that lies below, or forms crystals, which crosscut and disrupt the shell fabric. Overprinting of fabrics via recrystallisation during diagenesis is a common occurrence, however within the specimens analysed herein it is rarely observed. When it does occur, it is expected that this calcite will resemble a poorly ordered crystal growth similar to that of the bulk rock. However, this occurs when the shell material has been fully recrystallized whereas many specimens that show evidence of recrystallisation within this study appear to have undergone partial recrystallisation wherein the shell calcite has changed enough that it no longer shows the clearly ordered and organised structure of the well-preserved shell calcite however, it has retained some of its original form. In these cases, it is assumed that the shell has undergone partial dissolution and partial recrystallisation (Figure 3-8).

Within several specimens there are areas of the shell where detailed ultrastructure features, such as stepped growth or individual lamina, cannot be recognised, but would originally have been present. For example, the fabric may be recognised as the laminar secondary layer due to identification of an elongate form fabric, however, at high magnification individual laminae are seen to be amalgamated (Figure 3-9). Commonly, where amalgamation has occurred, the boundaries of tertiary prisms cannot be distinguished and details of the transition between the laminar and prismatic layers cannot be seen. Additionally, although rare, some specimens have areas of shell that do not resemble the original shell fabric as it has undergone dissolution followed by reprecipitation.

Silicification produces microcrystals that obliterate the shell fabric and may protrude out of the sectioned surface of the shell (Figure 3-10A, B and C). Silicification most commonly occurs at the outer shell margin, but also is frequently seen along growth lines within the prismatic tertiary layer; is rarely seen overprinting the tertiary prisms themselves.

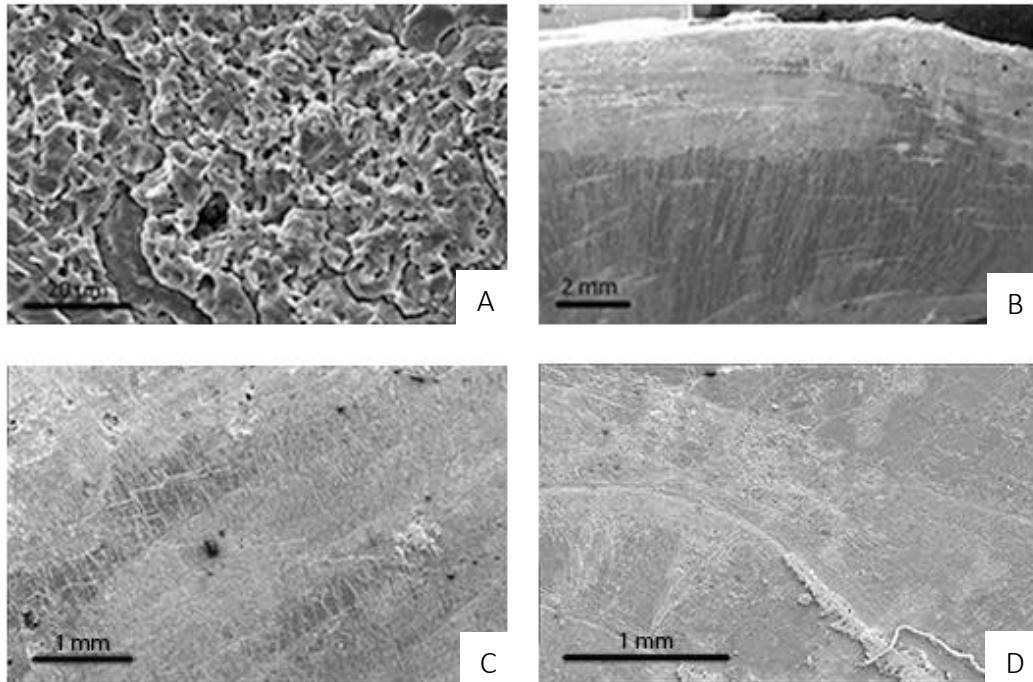


Figure 3-8 examples of partial dissolution and recrystallisation of the shell calcite.

Image A) shows an area of shell calcite which has not retained the original shell fabric however, can still be identified as shell calcite as it shows some crystal order indicating that it has undergone some alteration such as partial dissolution and recrystallisation but it does not appear to be pervasive. Images C) D) and E) show shell calcite that has undergone some partial dissolution and recrystallisation next to shell material that is fabric retentive demonstrating how the two materials can be distinguished.

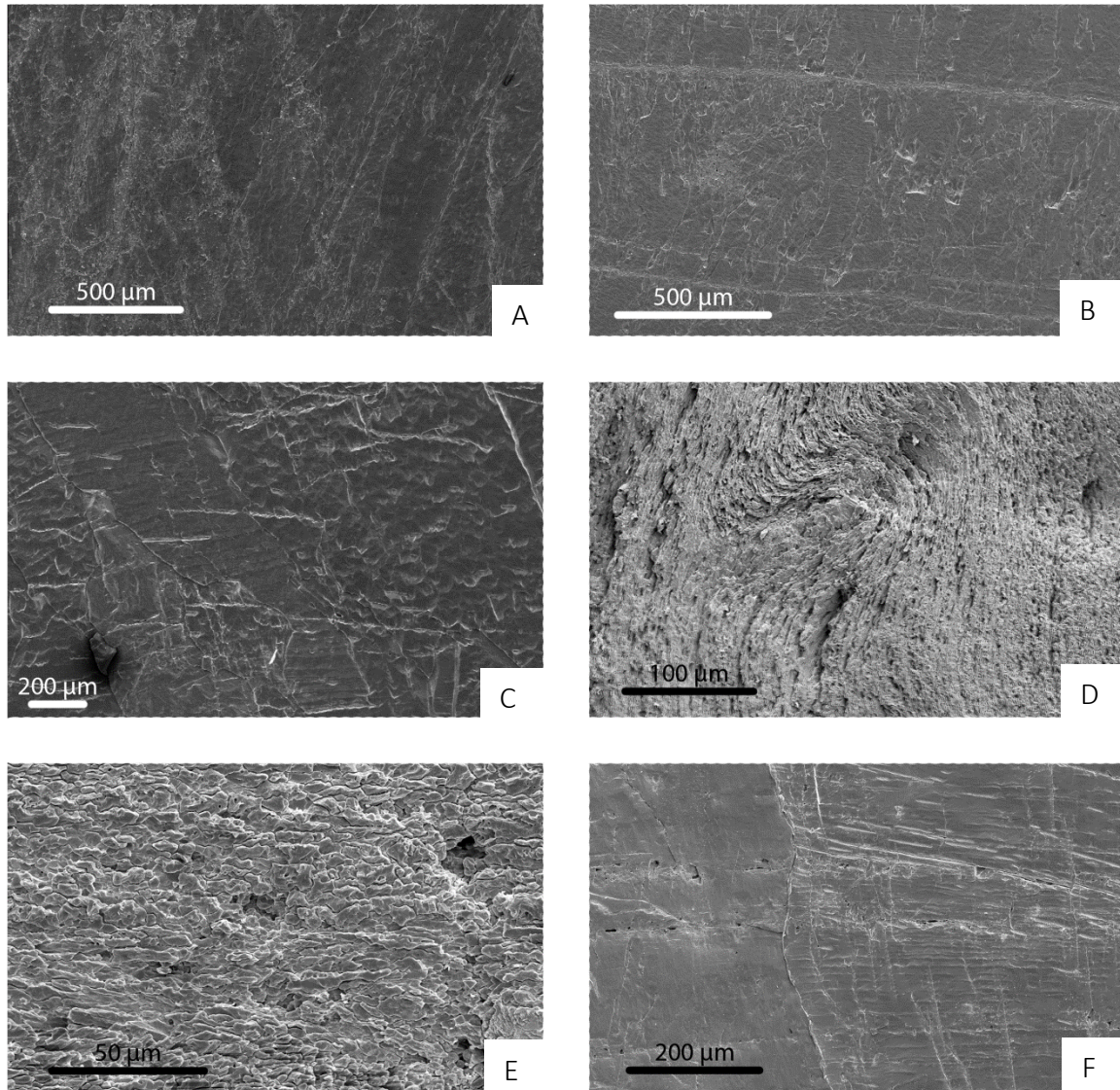


Figure 3-9. Examples of poor fabric retentive specimens.

Images A) and B) show the prismatic tertiary layer where the outline of individual prisms is not visible and areas with amalgamated fabric. Image C) shows the prismatic tertiary layer with stepped growth on only well-defined prisms (central) and poorly defined on adjacent prisms. Image D) shows the laminar secondary layer with some individual laminae visible. In many areas, they are poorly defined and have been amalgamated. Image E) shows amalgamation of lamina of the secondary shell layer. Image F) shows two calcite prisms of the tertiary shell layer; the one on the left shows no stepped growth patterns whereas that on the right does.

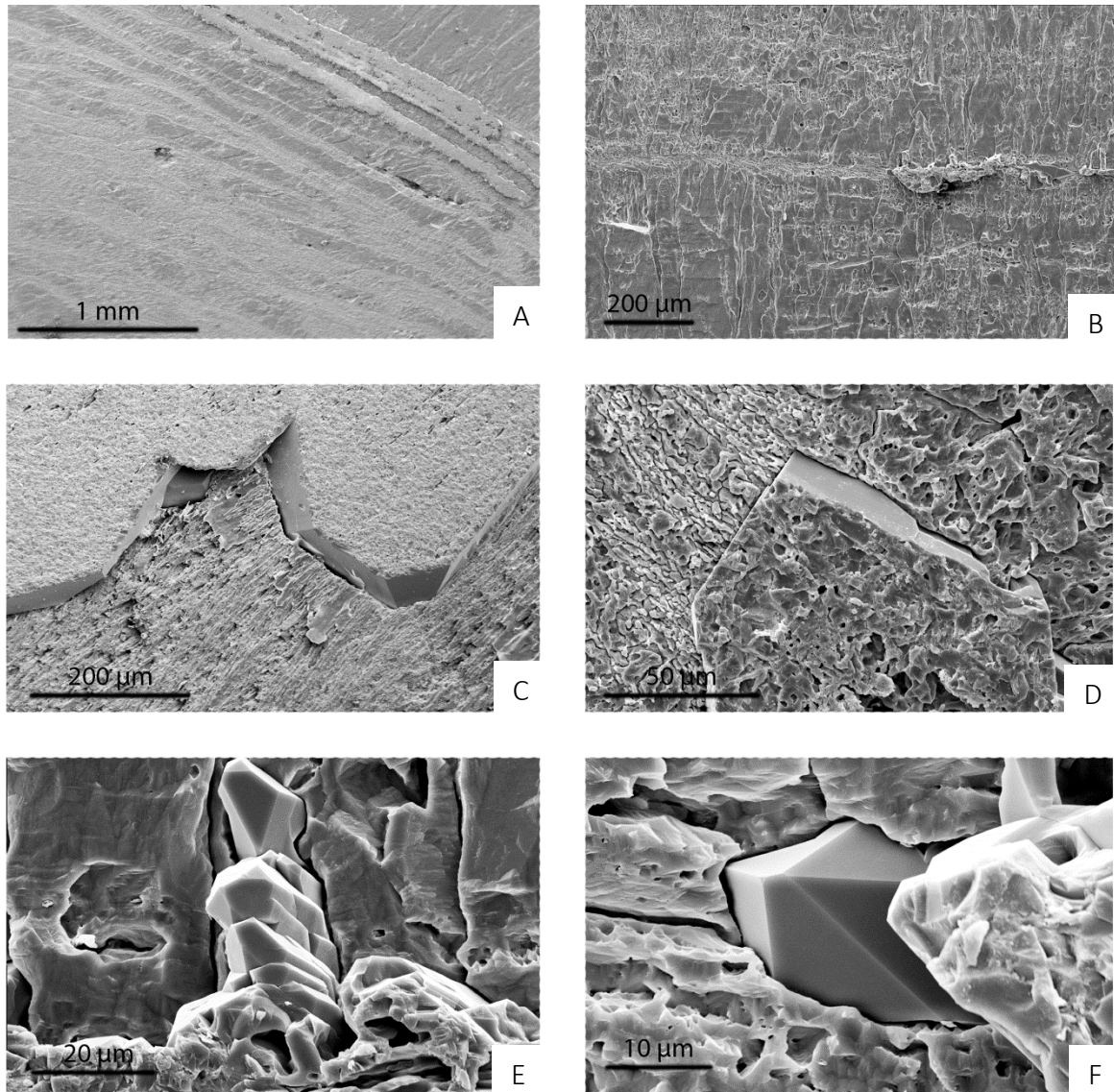


Figure 3-10. SEM micrograph examples of secondary mineralisation.

Images A) of specimen OAW 03 and B) of specimen OAW 05 show localised silicification occurring along growth lines. Images C) of specimen OAW 08 and D) of specimen OAW 50 show the growth of quartz microcrystals cross cutting through the laminae of the secondary layer. Images E) and F), both of specimen OAW 27 show quartz microcrystals at high magnification.

3.3.2 Cathodoluminescence analysis

A large spectrum of luminescent properties are observed over the specimens, ranging from non-luminescent to brightly-luminescent specimens, and including many samples with heterogeneous luminescence. Frequently, the laminar secondary layer and the prismatic tertiary layer can be differentiated by their luminescent properties and the umbonal shell region and anterior margin show different luminescent properties than the central shell region.

Non-luminescent calcite appears black or dark grey and, although it can occur in all parts of the shell, it is most frequently seen within the prismatic tertiary layer within the shell interior (Figure 3-10). This dull-luminescent calcite often contains flecks of moderately luminescent orange calcite and brightly or moderately luminescent growth lines. In many cases, the 'flecked' nature of the calcite is not persistent and the overall luminescence of this area of the shell remains low (Figure 3-10A and B). However, these flecks can be large, frequent and brightly luminescent; in these instances, the overall luminescence of the material may be compromised. Where flecks are persistent, they are commonly aligned, either parallel or perpendicular to the shell margins.

Growth lines within both shell layers are readily identified during CL analysis as they typically appear as thin, brightly luminescent lines, which run sub parallel to the outer or inner shell margins, and can commonly be traced along long lengths of the shell (Figure 3-10B and F). Growth lines within the laminar layer are typically more closely spaced and, although both are often bright, those in the laminar layer appears brighter than those in the prismatic tertiary layer.

At the outer shell margin, a thin strip (typically 1 – 3 mm) of brightly luminescent shell calcite is frequently seen and is usually composed of the laminar secondary layer (Figure 3-11A and F). Where this occurs, the shell interior commonly remains dull luminescent and the boundary between the two materials is often sharp. In the cases where this boundary between the luminescent laminar secondary layer and the non-luminescent prismatic tertiary layer is diffuse, (showing a gradual transition between the two areas of differing luminescent properties) the inner shell, is generally more moderately or poorly luminescent. Similar patterns occur at the inner shell margin; however, here a luminescent band is less common as the laminar secondary layer is not always present. It is typically less common towards the anterior margin where typically the laminar secondary layer is thinner or is not present.

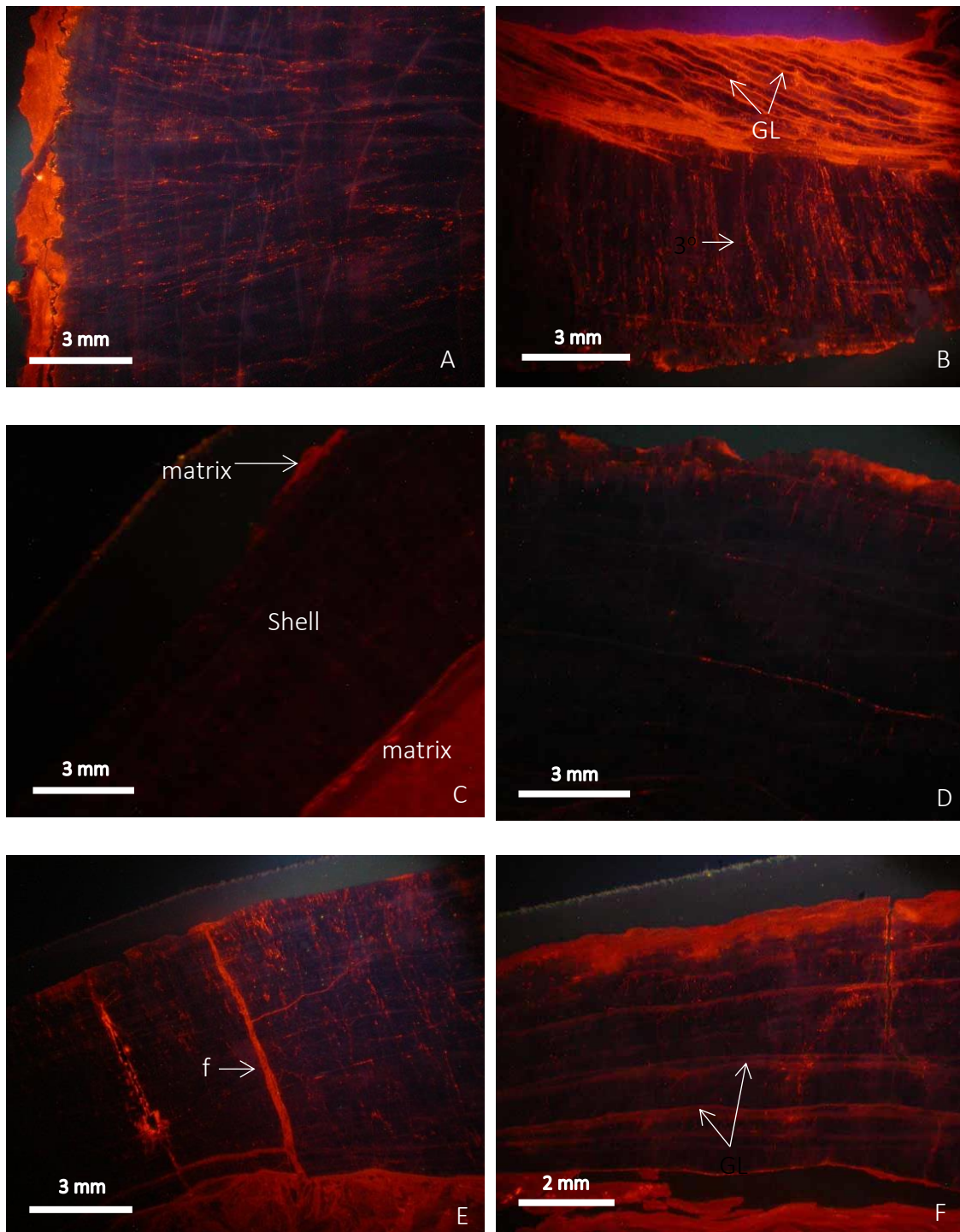


Figure 3-11. CL images of commonly observed features.

Image A) shows locally brightly luminescent outer shell margin and the shell interior, which remains largely non-luminescent within specimen RCK 36 (exposure time for this image is 2 seconds). Image B) shows the brightly luminescent growth lines at the interior shell margin with the material between growth lines remaining dull - non-luminescent in specimen OAW 03 (exposure time for this image is 1 second). Image C) shows a section through a valve of specimen RCK 41 that is non-luminescent (exposure time for this image is 1 second). Image D) shows the non-luminescent shell interior with small patches of localised brightly luminescent shell calcite in specimen RCK 28bis (exposure time for this image is 1 second). Image

E) shows the non-luminescent shell interior with brightly luminescent fractures in specimen RCK 35 (exposure time for this image is 2 seconds). Image F) shows brightly luminescent outer shell margin and moderately luminescent growth lines passing through the non – dully luminescent tertiary shell layer also within specimen RCK 100 (exposure time for this image is 1 second). All scale bars are approximations.

Where fractures occur, they are commonly infilled with brightly luminescent orange calcite, and frequently cross cut dully-luminescent shell calcite of the laminar and the prismatic layers (Figure 3-11B, C). In most instances, the shell calcite either side of fracture remains dully luminescent, and thus, is not influenced by the nearby fracture. However, in some specimens a ‘halo’ of more brightly luminescent calcite is present around the fracture within the shell calcite (Figure 3-12B). In some specimens, several fractures occur within a small area of the shell (Figure 3-11C). Within these specimens, although fractures may cross-cut dully luminescent shell calcite, the overall luminescence of the calcite within this area is compromised and is subsequently classified as moderately or brightly luminescent. This is because, in these instances, it becomes difficult to avoid these fractures during sampling for further analysis.

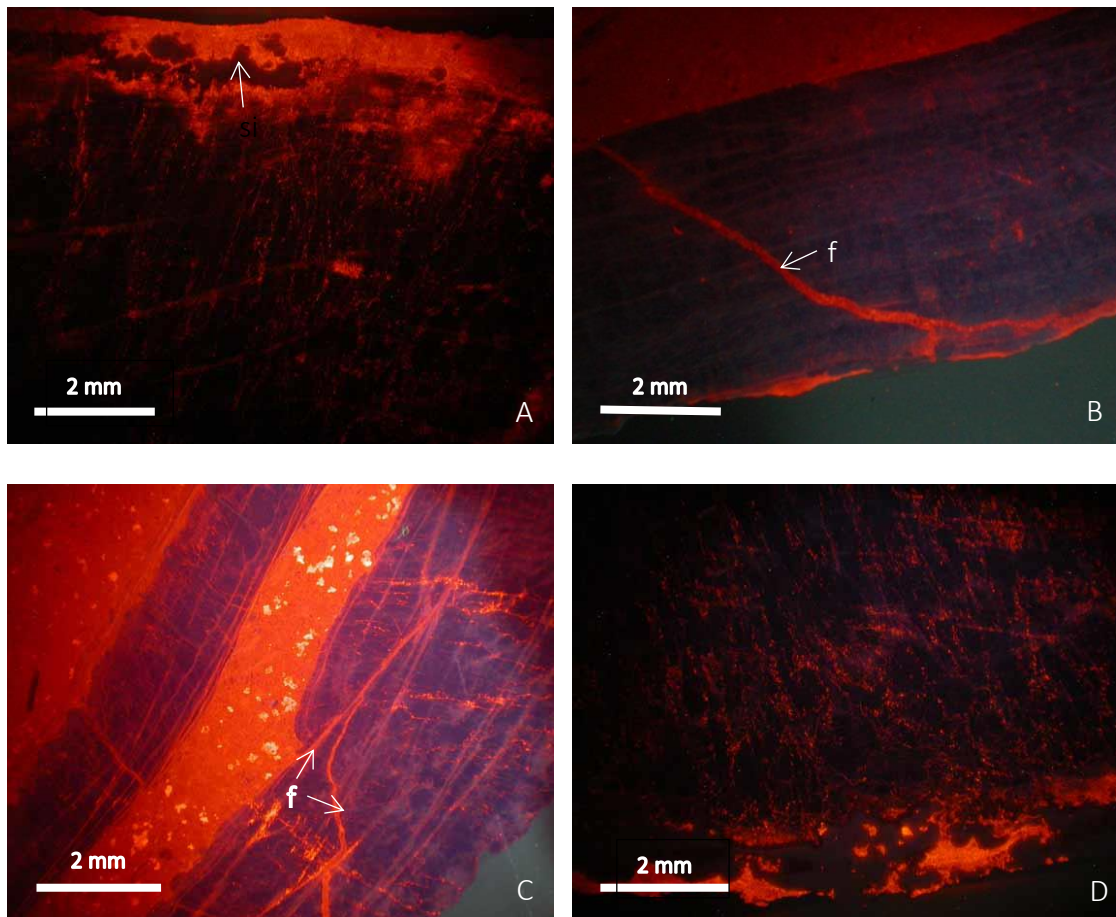


Figure 3-12. CL images depicting examples of luminescent features.

Image A) shows a brightly luminescent outer shell margin, which penetrates part way into the inner shell with isolated patches of localised silicification (which are not luminescent). The inner shell also shows some luminescent flecks. This image is of specimen OAW 03 (exposure time for this image is 1 second). Images B) and C) show dull to non-luminescent shell with fractures infilled with diagenetic calcite, which is brightly luminescent in specimen RCK 28bis (the exposure time for these images is 2 seconds). Image D) shows a dull luminescent shell with frequent flecks of brightly luminescent calcite within specimen OAW 03 (the exposure time for this image is 1 second). All scale bars are approximations.

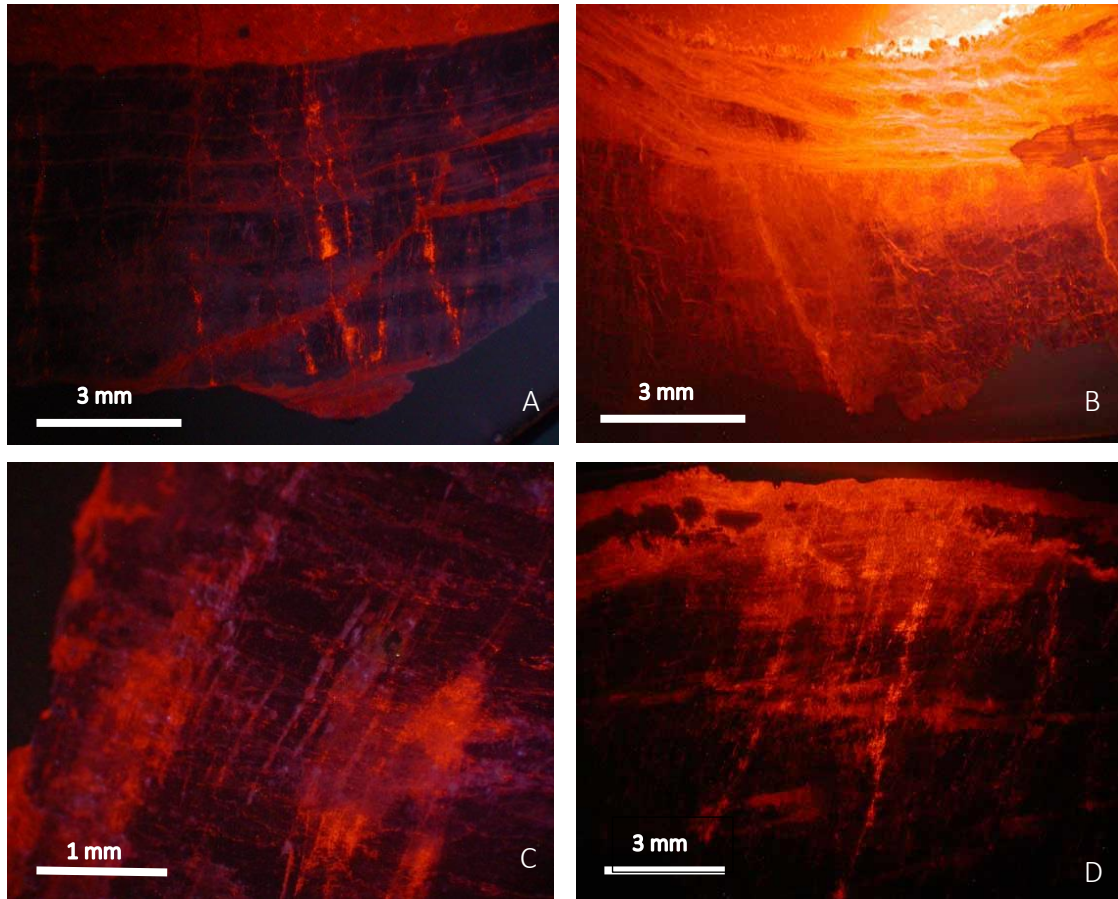


Figure 3-13. CL image of common brightly luminescent shell features.

A) Luminescent fracture cross cutting RCK6bis. B) Bright luminescence of the inner shell margin of specimen OAW 105 and localised silicification (not luminescent). C) Luminescent and non-luminescent areas of specimen OAW 02, which do not appear to be controlled by fabric. D) Bright luminescence at the outer margin of specimen OAW 08, which is also present in localised areas within the shell interior. All scale bars are approximations and all exposure times for these images are 1 second.

Identifying if dissolution and recrystallisation has occurred via CL analyses is difficult as crystal structure and form is often not visible. However, given that ultrastructure analyses identified that this form of alteration most commonly occurs at the shell margins, it is expected that this is the cause of the bright luminescence commonly seen at the shell margins. Partial dissolution (and possible partial-recrystallisation) is also likely the cause of the luminescence seen within the shell interior of some specimens, such as those illustrated in Figure 3-13 C) and D).

Commonly, many of the features described may occur within one specimen with different areas dominated by different luminescent properties. It is common for the umbonal region and the anterior margin of a specimen to be brightly luminescent, whilst

the central shell section remains moderately or even dully luminescent. An example is shown in Figure 3-14 where CL analysis of a specimen demonstrates that it can be divided into several sections (three sections in this example) based on their differing luminescent characteristics.

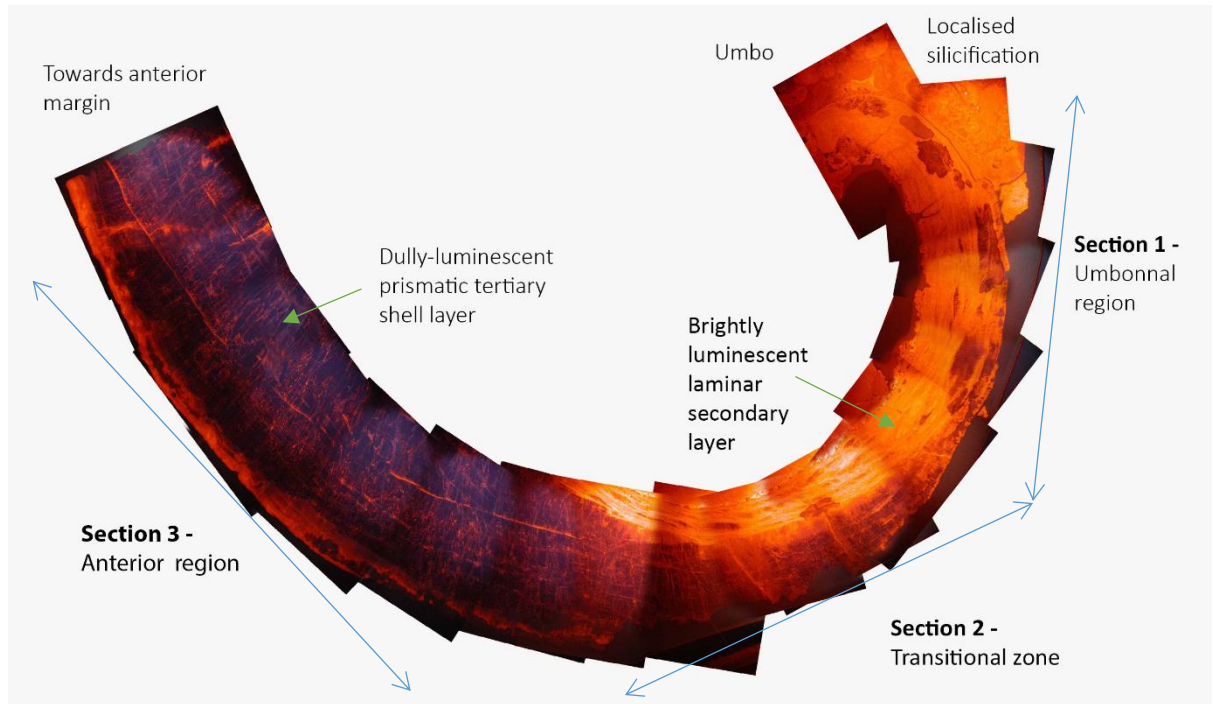


Figure 3-14. CL mosaic image of specimen OAW 105 showing a spectrum of luminescent features. Shell straight length (widest cross section) is 9 cm.

3.4 Discussion

The results presented demonstrate that within the ultrastructure of species of *Gigantoproductus*, the laminar secondary layer consistently occurs at the outer shell margin followed by a thick prismatic tertiary layer, as expected. However, there is variation within the thickness of these layers, the details preserved and the state of preservation and the occurrence of other structural features such as the presence of pseudopunctae and the thickness and frequency of growth lines. Following this, cathodoluminescence analyses illustrate the range of preservation occurring across multiple specimens and helps differentiate between shell fabrics as well as, potentially highlight structural and diagenetic features within the shell calcite.

Productida are known to produce a laminar secondary layer with a thickness that is generally up to 1 mm as previously identified by Garbelli et al. (2012). In some taxa the

thickness can largely exceed this. Some species of *Gigantoproductus* have a considerably thicker shell than that observed in other brachiopods, including other productids, made of a thicker secondary and tertiary layers. Irrespective of the thickness of the laminar layer, the prismatic layer is generally thicker than the laminar layer. The *G. aff. okensis* species analysed by (Angiolini et al., 2012) has a thick shell, as do the gigantoproductid species analysed in this study., *G. aff. okensis* has been shown to have a life span of up to 20 years, which is likely a large contribution to their extreme shell thickness. It is possible that the tertiary shell layer dominates the shell thickness because it does not contain organic matter, and therefore less energy is required to produce this fabric, which is more sustainable over long life spans. Additionally, as these organisms have a small body cavity in comparison to their overall size (Ferguson, 1978), and therefore presumably also a small lophophore, it may have been necessary for them to preserve energy for other biological processes, giving more reason to favour a thicker tertiary shell layer over a secondary shell layer rich in organic material.

Within the secondary shell layer individual lamina are commonly observed at high magnification. Similarly, within the prismatic layer stepped growth lines of the prism surfaces and the edge of individual prisms occur. Growth lines and their internal structure are also commonly seen. The identification of these detailed features suggests that some parts of the gigantoproductid shell may have remained well preserved in an unaltered form. Where diagenetic alteration of biogenic calcite has occurred, it is expected that the material would show poor original ultrastructure preservation (i.e. detailed features cannot be identified) and that the material shows moderate or bright luminescence. This is because alteration causes the shell fabric to undergo some form of distortion during the incorporation of diagenetic elements (such as Mn and Fe) into crystal lattices (Boggs and Kinsley, 2006).

The laminar secondary layer occurs at the outer shell margin in all specimens, within most it is commonly brightly luminescent, retains few detailed fabrics and often is seen to be overprinted by silicification. These features are indicative of diagenetic alteration. Modern brachiopods can show weak luminescence at the outer shell margin whilst the shell interior remains non-luminescent (Barbin and Gaspard, 1995), which is thought to be due to the interaction of the outer shell margin with the sediment in which specimens

are found (Barbin and Gaspard, 1995). In *Gigantoproductus* species the luminescence is coupled with other features indicative of alteration, such as poor fabric retention and overprinting by secondary mineralisation, so it is more likely that the cause of this luminescence at the outer shell margin in these fossil specimens is not caused by interaction of the shell with the sediment, but is more likely caused by diagenetic alteration. In areas of the shell where the laminar secondary layer occurs but is not at the outer shell margin it can appear brightly luminescent but can also be fabric retentive.

Barbin and Gaspard (1995) illustrated how the rate of growth affects the luminescent properties of biogenic calcite resulting in different luminescent properties within the laminar and prismatic layers. However, similarly to the laminar secondary layer, some growth lines are overprinted by silicification whilst the surrounding prismatic layer remains fabric retentive. Garbelli et al. (2012) demonstrated that the preservation of brachiopod low-magnesium biogenic calcite (in this instance of various Rhynchonelliformea, including species of *Gigantoproductus*) is influenced by taxonomy, host rock lithology and shell microstructure. Within the current study, as specimens were collected from only two shell beds, the effect of host rock lithology cannot be precisely assessed. However, differences in preservation, identified after ultrastructure and CL, between the two collection localities are noted, with specimens collected from Ricklow Quarry being more commonly better preserved. This is likely due to the difference in the host rock permeability and porosity (Garbelli et al., 2012) given that the specimens from Ricklow Quarry are collected from a floatstone with a high mud content while those from Once-a-Week Quarry are collected from a coarse bioclastic grainstone (Chapter 2). Influences of taxonomy result, in part, from differences in ultrastructure of the secondary shell layer, which acts as a protective layer at the shell margins to the internal prismatic calcite. Garbelli et al. (2012) suggested that a laminar secondary layer is less protective than a fibrous secondary layer because of differences in their organic content, which later results in a laminar layer having a higher microporosity and permeability. However, this effect is mitigated by the thick-shelled nature of the gigantoproductid shell. Additionally, these porous layers may help limit the alteration by 'containing' the diagenetic fluids to these areas (Angiolini et al., 2012). It is possible that this effect also accounts for the increased luminescence of growth lines within both shell layers as these typically have an

increased microporosity. Some prism boundaries show small amounts of micro-porosity, which may be attributable to decomposition of the organic membranes between prisms or by later fracturing.

In some specimens, the interval of production of the tertiary layer was interrupted by the production of more of the laminar secondary layer (before returning to the tertiary prismatic layer). The reasoning for this switch in the mode of secretion is unknown. It is speculated that it is related to the influence of surrounding environmental factors on the organism. These bands of the laminar fabric are similar to growth lines that are thought to be caused by environmental factors, a decrease in growth rate caused perhaps by the reduction in temperature and nutrient supply (Hiller, 1988). It is speculated here, that the similar changes in fabric and therefore changes in growth rate are due to similar processes, but extreme enough to cause a temporary halt in shell secretion rather than merely a change in the growth rate as is the speculated cause of growth lines.

Stepped growth patterns, which are observed on the surface of many prisms here, are rarely reported within the literature (Garbelli et al., 2012), and their origin is currently unknown. It is not clear if they would have been originally present on all prisms within all specimens. However, as adjacent prisms are secreted at the same time and rate, it is expected that they would contain the same growth features. Meaning, if one prism shows detailed stepped growth patterns, adjacent prisms would be expected to as well. If they are absent on those which are adjacent, it is suspected that they have been removed during diagenesis. However, it remains unclear why diagenetic alteration would preferentially occur within particular or individual prisms within the tertiary shell layer as comparatively there are no instances where CL analyses shows one prism with no luminescence and an adjacent prism with bright luminescence. Therefore, the lack of stepped growth line is not used to presume poor preservation but, their presence may be used as an indicator of good preservation.

Generally, ultrastructure and cathodoluminescence analyses agree when identifying areas of diagenetic alteration, though there are exceptions. The alignment of the flecked brightly luminescent calcite within the prismatic tertiary layer suggests that they are following lines of weakness within the shell. These may be minor stress fractures that could be present given that some specimens (e.g. RCK 6bis) have larger visible fractures

through the ventral valve, or they may be highlighting prism boundaries. These features are regularly identified via CL analyses, however, minor stress fractures are not evident during ultrastructure analysis and in such specimens prism boundaries do not appear to be structurally different than those within specimens or areas of the shell where aligned flecked luminescent does not occur. Typically, when a specimen has undergone silicification or amalgamation of shell fabrics it is concentrated at the outer shell margin within the laminar secondary layer. This is frequently identified using both ultrastructure and cathodoluminescence. It may be possible for calcite to preserve its ultrastructure having undergone some chemical alteration (Garbelli et al., 2012). In these instances, the ultrastructure may appear intact whilst the shell appears luminescent. It is unknown if diagenetic contamination disrupts the shell ultrastructure but if not, this could account for areas of shell that are fabric retentive but are luminescent. Similarly, if the Fe concentration is increased during diagenesis relative to the Mn concentration then an area of shell that has undergone diagenesis may appear non-luminescent.

3.5 Summary

This study shows how the most pristine areas of ultrastructure of ancient biogenic calcite can be identified from highly detailed features (such as individual laminae of the laminar secondary layer or stepped-growth prisms of the tertiary layer) being preserved. From this a detailed account of the ultrastructure of *Gigantoproductus* species that can then be used as a benchmark for well-preserved specimens has been established:

1. The thick prismatic layer of species of *Gigantoproductus* and the regular stepped growth lines on the surface of these prisms is the genus's distinctive ultrastructure feature. This is significant as the prismatic tertiary layer is thought to be the most resistant shell layer to diagenetic alteration (Grossman et al., 1993) due its low porosity. Therefore, in future studies that utilise this genus, the identification of stepped growth lines on the surface of prisms can be used as a feature of well-preserved material.
2. The absence of detailed ultrastructure features should not be used as an indication of poor preservation unless they are coupled with bright CL luminescence, or if there is evidence that detailed ultrastructure has been

removed via dissolution and recrystallisation or has been overprinted by secondary mineralisation. However, if further analyses are to be conducted the selection of specimens with detailed ultrastructure are best prioritised.

3. Checking the detailed structures (such as growth lines and transition from the laminar to the tertiary layer), rather than just the general preservation of the prismatic tertiary layer as a whole, may prove key in many studies that use ultrastructure as a means of assessing preservation. This is because the thick shell of species of *Gigantoproductus* makes it difficult to assess the ultrastructure of the entire shell length or thickness in detail. Once detailed features have been observed, CL analyses can then be conducted on the entire shell or key areas to demonstrate the likely extent of this suspected good preservation.
4. Results herein indicate that it is best to focus analyses on the inner central shell region as these areas are generally better preserved and contain a thicker tertiary shell layer.

Use of CL analysis as an assessment of preservation has limitations because the luminescent properties are primarily controlled by elemental ratios of two diagenetic elements (Mn and Fe) as opposed to their absolute abundances (Boggs and Krinsley, 2006). Additionally, the early phases of diagenetic cements of the Derbyshire carbonate platform appear non or dully luminescent (Walkden and Williams, 1991). However, because SEM analysis is typically conducted at very high magnifications, assessing the ultrastructure of the entire shell in high detail is difficult. This means that the heterogeneous nature of the shell is often overlooked during ultrastructure analysis highlighting the importance of the use of CL analysis, which can image larger areas of the shell, alongside SEM imaging and thus indicating the necessity of adopting a phased screening approach.

The thick shell of the gigantoproductids was advantageous in this study as it meant that the outer shell margin, which is commonly not fabric retentive and is brightly luminescent, could be avoided while the inner tertiary prismatic layer, which may remain fabric retentive and poorly luminescent, could still be used. This is also true when considering the length of the shell, as the umbonal and anterior regions are often brightly luminescent, these areas could be avoided while the often fabric retentive and non

or dullly luminescent central shell region could still be utilised. Avoiding growth lines through the prismatic layer is difficult as they are fine and not visible under standard microscopy. Where possible, thick brightly luminescent growth lines should be avoided in geochemical sampling, however, if they are not visible during CL it is arguable that there is no need to avoid them, and in any case, it is not possible without great difficulty.

The heterogeneity of ultrastructure preservation and luminescent properties within a shell highlights the need for specimens to be assessed individually when considering which should be used for further analyses. Full descriptions of the ultrastructure and luminescent properties of all individuals are provided in Appendix E: Description of ultrastructure analyses identified specimens where detailed features are preserved, and descriptions of the luminescent properties of each specimen identifies areas within a specimen with a transect (from the inner to the outer shell margin) of sufficiently thick, non-luminescent shell calcite that may be considered suitable for trace element analyses. From these descriptions, 15 specimens were selected for further preservation analyses such as trace element analyses, which are outline and discussed in Chapter 4.

Chapter 4: Preservation assessment of *Gigantoproductus* species biogenic calcite using trace element and stable isotope analyses

4.1 Background

The term diagenesis refers to the geological processes that affect sediments after deposition and before metamorphism occurs. Diagenetic processes that may occur in carbonate rocks include cementation, compaction, microbial micritisation, neomorphism, dissolution and dolomitization. These processes can occur in the marine, meteoric or burial realms and can result in a large variety of physical and chemical properties within the limestone. Chapter 2 (section 2.2.1.1) explains that some of these processes (microbial micritisation, dissolution, cementation, neomorphism, dolomitization and compaction) have occurred on the Derbyshire carbonate platform and features associated with cementation, compaction and micritisation are observed in the thin sections analysed within Chapter 2.

Whilst Chapter 2 focuses on identifying physical changes (ultrastructure and CL analyses) and touches on potential areas of geochemical alteration (CL) of the shell calcite, this chapter focuses on identifying samples and data points along shell transects where the original geochemical signature of the *Gigantoproductus* shells has been altered through diagenesis as is typically conducted in studies of this type (e.g. Brand and Veizer 1980, 1981, Veizer 1983 and many others). Ultimately, these altered specimens can be excluded from further analyses. By excluding materials that have undergone alteration through diagenesis the reliability of subsequent data collected, that may be used as a palaeoenvironmental proxy, is increased (Brand et al., 2011). Therefore, the aim of this study is not to understand the diagenetic history of the specimens or the Eyam Limestone Formations, but is to use this pre-existing science to distinguish between primary and

secondary geochemistry to assess the preservation of biogenically precipitated materials.

Complications arise when considering that trace elements such as Mg and Sr are naturally incorporated into brachiopod biogenic low magnesium calcite via substitution of Ca^{2+} , adsorption onto the outer surface of the crystals, they may occur within primary fluid inclusions (McIntire, 1963), or they may be included in the shell as mineral phases during growth and thus can be a primary feature (Popp et al., 1986). Therefore, it is not as simple as recognising their presence, but it is important to understand the diagenetic processes and environments that these specimens have been subject to in order to identify whether trace elements are depleted or enriched compared to what may be expected in primary biogenic calcite.

4.1.1 Understanding geochemical diagenetic alteration

Substitution of Ca^{2+} for other compatible cations can also occur within diagenesis. This commonly occurs if the material undergoes partial or complete dissolution and recrystallisation. When this occurs, the concentration of the trace element within the newly recrystallized material can be predicted based on the understanding of trace element distribution coefficient.

A distribution coefficient refers to the ratio of an element between two phases, which, in the case of carbonate diagenesis is the limestone and the diagenetic fluids or pore waters. When the distribution coefficient is more than one the trace element is preferentially incorporated into the precipitated material (causing the diagenetic precipitate to be enriched in the trace element), and if the distribution coefficient is less than one, the trace element is preferentially excluded from the precipitate (and thus is depleted) (Dickson 1990). Therefore, understanding the geochemistry of diagenetic fluids (particularly compared to the primary ambient seawater) can help elucidate whether a material has undergone geochemical diagenetic alteration.

In reality, the process is not so simple; the distribution coefficient is also influenced by kinetic factors; for example, with increased temperature the distribution coefficients of Mg, Mn and Fe increases (Mucci 1987) and with increased precipitation rate the Sr substitution rate increased (Lorenz 1981). There are also differences to consider when

dealing with an open system wherein the pore waters and the precipitate may be constantly changing or closed system where nothing is added or taken away (Morse and Mackenzie, 1990). Additionally, the limestone may have undergone multiple phases of diagenetic alteration where the trace element concentration of the starting precipitate and the diagenetic fluids are different during each phases, and there may be changes reflecting whether the system is open or closed.

4.1.2 Identifying geochemical diagenetic alteration

Strontium (Sr), magnesium (Mg), manganese (Mn) and iron (Fe) are most frequently used as indicators of biogenic calcite alteration. These key elements have been shown to provide the most indicative information about preservation (e.g. Brand and Veizer 1980, Grossman et al., 1996, Azmy et al., 2011; Brand, 2004; Brand et al., 2011; Brand et al., 2003; Garbelli et al., 2012; Lee et al., 2004) and potentially environment (e.g. Freitas et al., 2006; Perez-Huerta et al., 2008). Despite their fluctuating abundance during the Phanerozoic Eon (Steuber and Veizer, 2002) both Mg^{2+} and Sr^{2+} have remained major ions in standard seawater and, as they are readily incorporated into the calcite lattice, both are expected to be abundant in the shell of calcifying organisms which have remained well-preserved through geological time. Mn and Fe however, do not occur in abundance in ambient seawater, as both are insoluble in oxic conditions. Given that gigantoproductids required oxygenated waters, it is not expected that Mn and Fe be abundant in their shell calcite if they have remained well-preserved. Where abundance of these key elements differs to what may be expected when compared to modern organisms and previous studies, it must be considered if this is due to environmental factors (and therefore primary), or diagenetic, (and therefore secondary) processes. Alongside this, it is also important to consider the influences which affect the concentrations of these elements within the water column, such as temperature, salinity and pH (Swart, 2015), as these may vary through time causing natural geochemical variability within a single specimen that may be interpreted as diagenetic alteration.

Seawater (both shallow and deep) is typically enriched in Sr and Mg and depleted in Mn and Fe compared with meteoric waters or deep burial fluids which are usually involved in post depositional diagenesis (Swart, 2015). Additionally, shells that are enriched in Sr, and depleted in Mn and Fe compared to modern brachiopods are considered to be

geochemically well-preserved (Grossman et al., 1996). Therefore, comparing the concentration of these elements within the biogenic material to material precipitated from diagenetic fluids can give an indication of the preservation of the original material and if meteoric waters have been present within these rocks.

To help define the geochemical ranges of well-preserved biogenic calcite within the fossil shells, comparisons are made with comparable a) modern materials (in this case, brachiopods) (which are presumed to be well preserved) and b) previously published data from fossil material. In both cases, it is preferable to compare materials from similar environment and for ancient material, it is also materials of a comparable age that is preferred, however the availability of data is often limiting. Data are also compared to other non-shell materials, some of which are expected to have a geochemistry comparable to well-preserved shell calcite if they have been precipitated in, or near equilibrium with seawater (e.g. coeval bulk rock) and others that are not expected to have been precipitated in equilibrium with the original seawater, (e.g. secondary diagenetic calcite), and therefore, may be representative of the chemistry of diagenetic fluids. These materials may show visible evidence of recrystallisation of secondary mineralisation and may be define a diagenetic end member that may be used as a comparison. The chemistry of these secondary materials is expected to be different from that of the well-preserved biogenic calcite if it was precipitated at or near to equilibrium. Although this provides a good second reference, it is also important to consider a recent study by Garcia et al. (2017) that demonstrates that trace element concentrations of the tertiary shell layer in some modern brachiopods (*Liothyrella neozelanica* and *Gryphus vitreus*) may be influenced by metabolic fractionation and therefore, may not be in equilibrium with seawater. A summary of selected literature and their given trace elements and isotope values from well-preserved (usually fabric retentive and non-luminescent) biogenic calcite is provided in Table 4-1. This incorporates well-preserved biogenic calcite from both modern and fossil shells. In addition to Mg, Sr, Mn and Fe, a range of sodium (Na) concentrations are reported by some (e.g. Angiolini et al., 2012; Brand et al., 2003a) as Na can be indicative of alteration; however its incorporation is not fully understood, meaning concentrations are often reported but not discussed.

The range in trace elements assigned/observed by different authors is large with some authors determining Sr values <400 ppm (Korte et al., 2003) while others report Sr values >1178 ppm in non-luminescent calcite (Armendáriz et al., 2008). Similarly, Mn concentrations in non-luminescent biogenic calcite can range from 10 – 47 ppm (Lepzelter et al., 1983) to up to 350 ppm (Bruckschen and Veizer, 1997). This disparity in trace element concentrations across studies however, is not, necessarily unexpected. Ranges in trace elements may be attributed to many differing factors, for example the abundance of certain trace elements (and $\delta^{18}\text{O}$ values) in seawater may vary through geological time (Horita et al., 2002) and in different environmental and geographical conditions (Bowen and Wilkinson, 2002; Brand et al., 2003), e.g. high Mn availability may be observed in poorly oxygenated environments, which in turn is commonly influenced by water depth. Variations in trace element concentrations have been observed within and between fossil groups (Korte and Hesselbo, 2011), for example, *Gigantoproductus* contain higher Sr concentrations than other brachiopod genera (Popp et al., 1986). This could be due to the fact that some organisms may preferentially include or exclude particular elements into their calcite shells (a type of vital effect).

As environmental and biological factors may lead to variations in the trace element composition of shells, identifying a *range* of study-specific geochemical compositions, within which material may be considered to be well preserved, rather than establishing more generic cut-offs in geochemistry, is beneficial. This is because this method accommodates error when predicting the natural heterogeneity observed within brachiopod biogenic calcite derived from different seawaters (Angiolini et al., 2012; Brand et al., 2011; Cusack et al., 2008). Natural heterogeneity can provide information which can help understand the natural environmental variability if other indicators of preservations are used.

$\delta^{18}\text{O}$ from marine calcite can be an indicator of diagenesis, as meteoric waters typically have lower $\delta^{18}\text{O}$ than seawater (Swart, 2015). However, $\delta^{18}\text{O}$ is also controlled by temperature; higher temperatures lead to lower $\delta^{18}\text{O}$ values during calcite precipitation (Epstein et al., 1953), meaning that there is often a degree of natural (seasonal) variation evident within shell calcite and in this study $\delta^{18}\text{O}$ is being used to calculate temperature, It is not appropriate to use these data as a preservation screening mechanism as this

might lead to unwanted bias (selection of data points that calculate 'desired' sea surface temperatures). However, where non-luminescent and fabric retentive material show trace element chemistry suggesting good preservation, its pristineness can be cross checked against the expected range of $\delta^{18}\text{O}$ data. For this, the 'expected range' may be defined by comparing the shell $\delta^{18}\text{O}$ data with the $\delta^{18}\text{O}$ values of diagenetic cements, a reference point of $\delta^{18}\text{O}$ values in diagenetic materials, and therefore what values may be expected from pristine or well-preserved shell calcite (typically higher than those of the diagenetic material). Carbon stable isotopes ($\delta^{13}\text{C}$) are much less frequently used to assess preservation, as there are a wider range of environmental variables, both primary and secondary, that influence their fractionation and distinguishing between these variables is much more difficult. However, where there is a positive correlation between $\delta^{13}\text{C}$ and $\delta^{18}\text{O}$, this has been interpreted as a signal of diagenesis (Swart, 2015), although both can be changed in a correlative way by changes in the environment (e.g. Keith and Weber, 1965).

Publication	Study focus/material analysed	Assigned preservation parameters				Other preservation methods used
		Sr	Mg	Mn	Fe	
Angiolini et al. (2012)	Brigantian <i>Gigantoproductus</i>	793–1338	3154–4719	0–195	0 - 646	CL and Ultrastructure
Korte et al. (2003)	$^{87}\text{Sr}/^{86}\text{Sr}$ of Permian and Triassic brachiopods	>400	Not given	<250	Not given	CL and ultrastructure
Morrison and Brand (1986)	Modern brachiopods	200–1300	Not given	5– 500	Not given	None given
Popp et al. (1986)	Palaeozoic brachiopods	300–3400 (but <i>Gigantoproductus</i> observed higher)	Not given	<250	Not given	CL
Bruckschen and Veizer (1997)	Visean brachiopods	>600	Not given	<350	Not given	CL
Brand et al. (2003)	Modern Mediterranean brachiopods	450 – 1498 But generally ~ 1000	600–7330	9–198.5	<167 but higher values are also observed	Ultrastructure
Armendáriz et al. (2008)	Mississippian <i>Gigantoproductus</i>	>1187	Not given	<60	<300	CL and ultrastructure

van Geldern et al. (2006)	Devonian brachiopods	500	Not given	<100	<400	CL
Angiolini et al. (2009)	Early Permian brachiopods	350–800	Not given	<200	Up to 1600 observed but not used as a parameter	CL and ultrastructure
This study	Brigantian Gigantoproductus	>700	961–5293 observed (>2000 ppm cut-off)	<25	<25	CL and ultrastructure

Table 4-1 Summary of published geochemical parameters of well-preserved biogenic calcite from both modern and fossil shells.

Values from Angiolini et al. (2012) are the ranges observed in non-luminescent shell areas. In some studies (e.g. Bruckschen and Veizer (1997) that no upper boundary of Sr is given when assessing preservation and in all studies listed, where CL was conducted it was used as an ‘initial’ screening mechanism. In this study, Mg itself was not used as a parameter for diagenesis identification due to complications of biological and environmental effects. Mg values indicated in this table for this study are the range in Mg concentration from those data points that are considered well preserved via their Sr, Mn and Fe concentrations.

4.2 Materials and Methods

Following cathodoluminescence and ultrastructure analyses specimens were selected to undergo trace element and stable isotope analyses. A small selection of specimens were analysed using an initial methodology the results were used to adapt the methodologies to generate data at desired resolution to identify any natural variability that may be present within the shells (see section 2.2). These secondary trace element and stable isotope methodologies were then conducted on a second set of selected specimens. Table 4-2 outlines the selected specimens, their species and the analyses that they underwent.

Sample number	Species	CL and SEM	Preliminary trace element	Secondary trace element	Preliminary stable isotope	Secondary stable isotope
OAW 51	<i>G. inflatus</i>					
OAW 50	<i>G. inflatus</i>		4 transects			
RCK 36	<i>G. okensis</i>					
RCK 35	<i>G. inflatus</i>					
RCK 33	<i>G. inflatus</i>					
RCK 28	<i>G. inflatus</i>					
OAW 02	<i>G. elongatus</i>					
RCK 6	<i>G. inflatus</i>			2 transects		
RCK 6bis	<i>G. inflatus</i>		3 transects			
RCK 41	<i>G. inflatus</i>		4 transects			
XG	<i>Unknown</i>					
OAW 05	<i>G. inflatus</i>					
RCK 28bis	<i>G. okensis</i>			2 transects		2 transects
OAW 08	<i>G. inflatus</i>					
OAW 102	<i>G. elongatus</i>					
RCK 100	<i>G. okensis</i>					
OAW 104	<i>G. inflatus</i>					
OAW 105	<i>G. inflatus</i>					
OAW 03	<i>G. inflatus</i>					

Table 4-2 Summary of analyses conducted.

Green cells represent that these analyses were conducted while red indicates they were not. Where multiple analyses of the same methodology were conducted this is indicated.

4.2.1 Preliminary sampling methodology

4.2.1.1 Preliminary Trace element analyses

Five specimens, all *G. inflatus*, were selected (RCK 6bis, RCK 35, RCK 41, RCK 33 and OAW 50), to undergo trace element analysis via laser ablation ICP–MS. These specimens were selected on the basis of good preservation as indicated by the cathodoluminescence and ultrastructure analyses (Chapter 3 Section 3 and Appendix E). The five specimens also

showed areas of alteration and secondary calcite within the matrix. Small areas of the bulk rock surrounding the specimen and other materials, were also analysed in order to provide a chemical signature of the whole rock and secondary calcite materials (Figure 4-1).

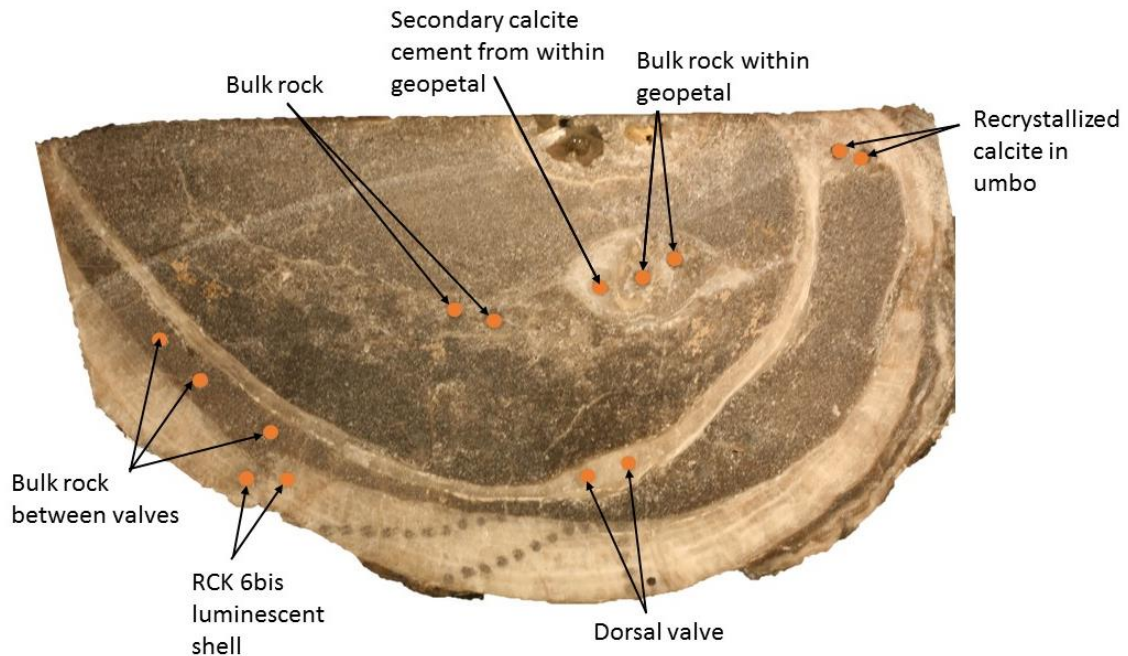


Figure 4-1 Additionally analysed materials analysed alongside specimen RCK 6bis using the preliminary sampling methodology.

Bulk rock samples (including that within the geopetal) appear to contain both primary coeval material and some calcitic cement. These data points were analysed both for trace element and stable isotope data. Additional 'bulk rock between valves' samples were analysed from trace element data from specimens RCK 28bis, RCK 28bis_2, RCK 28 and RCK 33 following the secondary sampling methodology however these were not analysed for isotope data.

On the same sectioned surface that was analysed using the SEM, the specimen was cleaned with alcohol and spot transects through non-luminescent shell material were marked in pencil. These tracks were drawn at different angles (relative to growth). Where possible a ~ 1 mm diameter pencil spot was drawn between two growth lines therefore, each sample spot represents a different time/period of growth during the organism's life span (Figure 4-2). In some instances where growth lines were not visible on the shell surface (i.e. shell RCK 35 and RCK 41) transects were drawn in the same way across the shell thickness with spots spaced ~1 mm apart. On each pencil spot, three 100 µm diameter laser ablation analyses were undertaken. The average concentration of each

element gives the elemental concentration for the pencil spot. This methodology was chosen so that it is possible to directly correlate trace element data with the later collected stable isotope analyses.

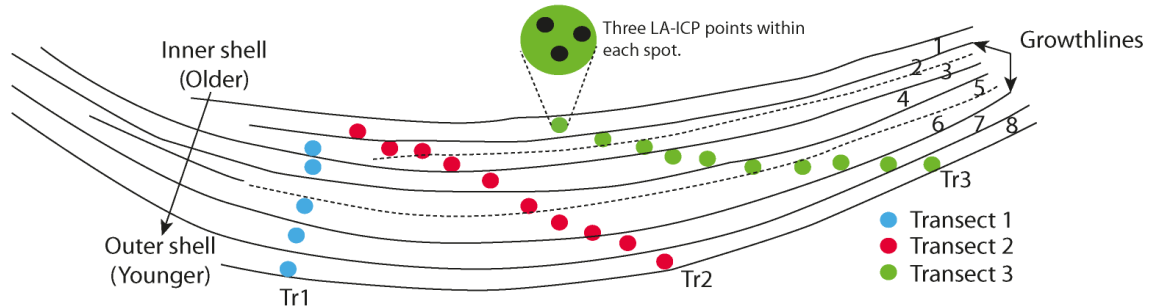


Figure 4-2 Shell RCK 6bis growth lines and sampling technique for trace element analysis.

Analytical procedure

A suite of 15 elements were analysed (Li, Na, Mg, Ca, Si, Zn, Fe, Cu, Sr, Mo, Ba, La, Ce, Pb and U) but data evaluation is concentrated on Sr, Mg, Mn and Fe (all data is provided in Appendix F). Analyses were achieved using a laser system connected to an ICP-MS. The laser output during analysis was 75% with a repetition rate of 10 Hz and spot size of 100 μm . The laser was left for a wash out delay of 20 seconds and was allowed to warm up for 10 seconds before every analysis which has a dwell time of 60 seconds per sample spot. On each pencil marked sample spot, three measurements were taken

When the laser is activated it 'ablates' the surface of the sample, turning the small targeted portion of the specimen into a fine powder. This powder is then sucked up through a tube and is transported via a stream of He gas to the coupled Agilent 7500 series ICP-MS.

For calibration purposes three spots were analysed three times and two standards (NIST 610 and 612- also analysed three times each) were analysed at the start and end of every run. The data were normalised to the NIST 610 glass standard and NIST 612 glass was used as an internal (secondary) standard for quality control. Where a planned sampling run is expected to exceed one hour, additional analyses of the NIST 612 standard were analysed within the run to check quality control.

It is standard practice when analysing calcite to normalise the data to the NIST 610 glass standard, however, there are concerns about whether the laser interaction with the glass and carbonate material may not be comparable. MACS-3 carbonate standard was analysed alongside the unknowns (the shells analysed) and processed in the same way (normalising to NIST 610 glass) the results have acceptable error, between 0.01 and 6% percentage error (accuracy) for all elements of interest, excluding Mg which has percentage errors between 15 and 18.3%. Precision for all elements is between ± 0.1 and ± 6.7 (full results and error for individual elements are provided in the Appendix F). Overall, given the small error observed with the MACS-3 analyses, it was deemed that normalising it was acceptable. It introduces little additional error to normalise the carbonate unknowns to the NIST 610 glass standards.

When processing the data (using IOLITE) all concentrations are calibrated to the Ca concentration within the NIST 610 glass standard and for the unknowns, for calibration purposes, it was assumed that the sample was 100% calcium carbonate (CaCO_3). Corrections were made to the data by subtracting a background reading (gas blanks measured throughout analyses) from all acquired data peaks. For all samples (including standards), when processing the data, the initial peak recorded by the instrument was not used. This peak often displayed high concentrations of elements such as Fe and was thought to represent contamination occurring on the surface, given that it appeared on peaks derived from both unknown and standard samples and concentrations of such elements dramatically decreased after the initial peak. Once this initial peak had subsided, the following plateau of the signal was considered the true signal of the specimen and was manually selected and processed. By discarding the initial part of the signal, it can be confidently concluded that no pencil lead or other contaminants on the surface of the sample are compromising the results. This is further ensured by the delay in beginning the acquisition of data only after the laser has been ablating for ten seconds.

Accuracy of data was calculated from the analysis of the NIST 612 internal glass standard results were compared to the expected concentrations and is between 0.1% – 8.2% (percentage error) for all elements of interest (Sr, Mn and Fe), excluding Mg which is between 14.5 -16.3%. The increased error observed for Mg is likely caused by the interference of two carbon atoms with a mass of 12 (therefore being mistaken by the

instrument as a single Mg atom with a mass of 24) and therefore is somewhat expected and unavoidable given the nature of the materials in question. For almost all data points, the error bars depicting the 95% confidence limits of the data are smaller than the data point itself (typically less than 1) and therefore are not shown.

Elements that are primarily incorporated into the calcite lattice via substitution are better recorded as ratios to Ca as this gives an indication as to whether or not this element is preferentially incorporated or discriminated against (Swart, 2015). However, during the processing of laser ablation ICP-MS data elemental concentrations are normalised to Ca values (assumed 100%) in the unknown. This means that an accurate Ca to element ratio cannot be obtained. Therefore, trace element data within this study are recorded as concentrations (as parts per million, ppm).

4.2.1.2 Preliminary isotope sample collection

Following the preliminary trace element analyses, a single specimen (RCK 6bis) was selected to undergo isotope analyses as this was considered the best-preserved shell.

Firstly, powdered samples of the shell calcite were collected using a hand held micro drill with a 0.3 mm diamond encrusted drill-bit. The surface of the specimen was cleaned using deionised water and the diamond drill bit was cleaned using alcohol. When a powdered sample was drilled, the powder was collected from the sample surface using a scalpel, placed on a small sheet of greaseproof weighing paper and then placed into a brand new mini Eppendorf tube. Between the collections of each powder the surface of the specimen and the drill bit was cleaned with a paintbrush and the scalpel was also cleaned and a new weighing paper was used to collect each sample. The individual sample locations (originally marked by pencil dots) used for trace element analysis were 'excavated' to a depth of ~1 mm. Each sample spot was spaced in individual growth lines visible on the surface of the sectioned shell; where growth lines were not visible sample points were spaced ~1 mm apart and were collected continuously with sample points progressing from the outer to the inner shell margin and therefore each sample point represents a different time. Each isotope sample can be directly correlated to the trace element data.

Analytical procedure

Isotope analyses were undertaken at the NERC Isotope Geoscience Laboratory (NIGL), British Geological Survey (BGS), by Hilary Sloane. Approximately 50-100 micrograms of carbonate are used for isotope analysis using an Isoprime dual inlet mass spectrometer plus Multiprep device. Samples were loaded into glass vials and sealed with septa. The automated system evacuates vials and delivers anhydrous phosphoric acid to the carbonate at 90°C. The evolved CO₂ is collected for 15 minutes, cryogenically cleaned and passed into the mass spectrometer. Isotope values ($\delta^{13}\text{C}$, $\delta^{18}\text{O}$) are reported as per mille (‰) deviations of the isotopic ratios ($^{13}\text{C}/^{12}\text{C}$, $^{18}\text{O}/^{16}\text{O}$) calculated to the VPDB scale using a within-run laboratory standard calibrated against NBS-19 (Friedman and O'Neil, 1977). The calcite-acid fractionation factor applied to the gas values is 1.00798 (McCrea, 1950). Due to the long run time of 21 hours a drift correction was applied across each run, calculated using the standards that bracket the samples. The Craig Correction was also applied to account for ^{17}O (Craig, 1957). The long-term average analytical reproducibility of the in house laboratory standard calcite (KCM) is 0.05‰ for $\delta^{13}\text{C}$ and $\delta^{18}\text{O}$.

4.2.2 Modification of the methodologies

4.2.2.1 The secondary methodology of trace element analyses

Results from both the preliminary trace element and stable isotope analyses revealed geochemical heterogeneity within individual specimens. This heterogeneity was observed across shell transects and between the three laser analyses within individual pencil spots. However, the spatial resolution of the sampling meant it was not possible to identify any patterns of elemental distribution. Therefore, in order to better understand the variability within individual specimens, the spatial resolution of the sampling was increased.

Next, further analyses were run at varying spatial resolutions with the aim of identifying a sampling resolution that captured the scale and nature of variability within the specimen and was also comparable to the expected isotope sampling resolution. The chosen resolution needed to optimise the number of specimens that could be analysed. Experiments at spatial resolutions of 50, 100 and 200 μm resolutions were run.

Figure 4-4 provides an illustrated example of the 200 μm spatial resolution sampling. Additional analyses included: transects across the shell at 45° to growth (See Chapter 1

for explanation of shell growth and Figure 4-1 for orientation of drilled transects) designed to investigate if variability is clearer when the transect angle is changed; analyses along a single growth line designed to investigate how much variability occurs along the same increment of growth; and analyses of a grid of 20 μm laser spots covering the equivalent area of a 100 μm spot in order to investigate how much variability is lost when using a 100 μm spot size.

For these and all subsequent analyses the laser setup was as described previously, however when the spot size was reduced to 50 μm and 20 μm the dwell time was also reduced to 30 and 20 seconds respectively. This ensured that the laser crater does not have a depth larger than its diameter. For all analyses, the laser rep rate was 10 Hz, and the output was 75%. Although no pencil marks were present on the samples, where the initial 'peak' of analysed the signal received from the mass spectrometer was still not used during the data processing, just the plateau, as described previously. This is because the standards are also processed in this way.

These experiments revealed that analysing transects that are perpendicular to growth reduces the analytical time spent on a single specimen whilst ensuring that each sample point represents a different interval of time. When comparing the nature of trace element heterogeneity from analyses conducted at 50, 100 and 200 μm spatial resolutions, the same general 'pattern' of distribution is evident at all these resolutions. This means that although some of the fine scale detail is lost at lower resolutions, the prominent peaks and troughs present in the 50 μm resolution transect remain present in the 200 μm resolution transect. This is illustrated in Figure 4-2, which compares observed peaks and troughs identified at 100 μm spatial resolution most of which are also present within the 200 μm resolution data. The patterns of peak and troughs can also be observed in transects at other resolutions (see Appendix E).

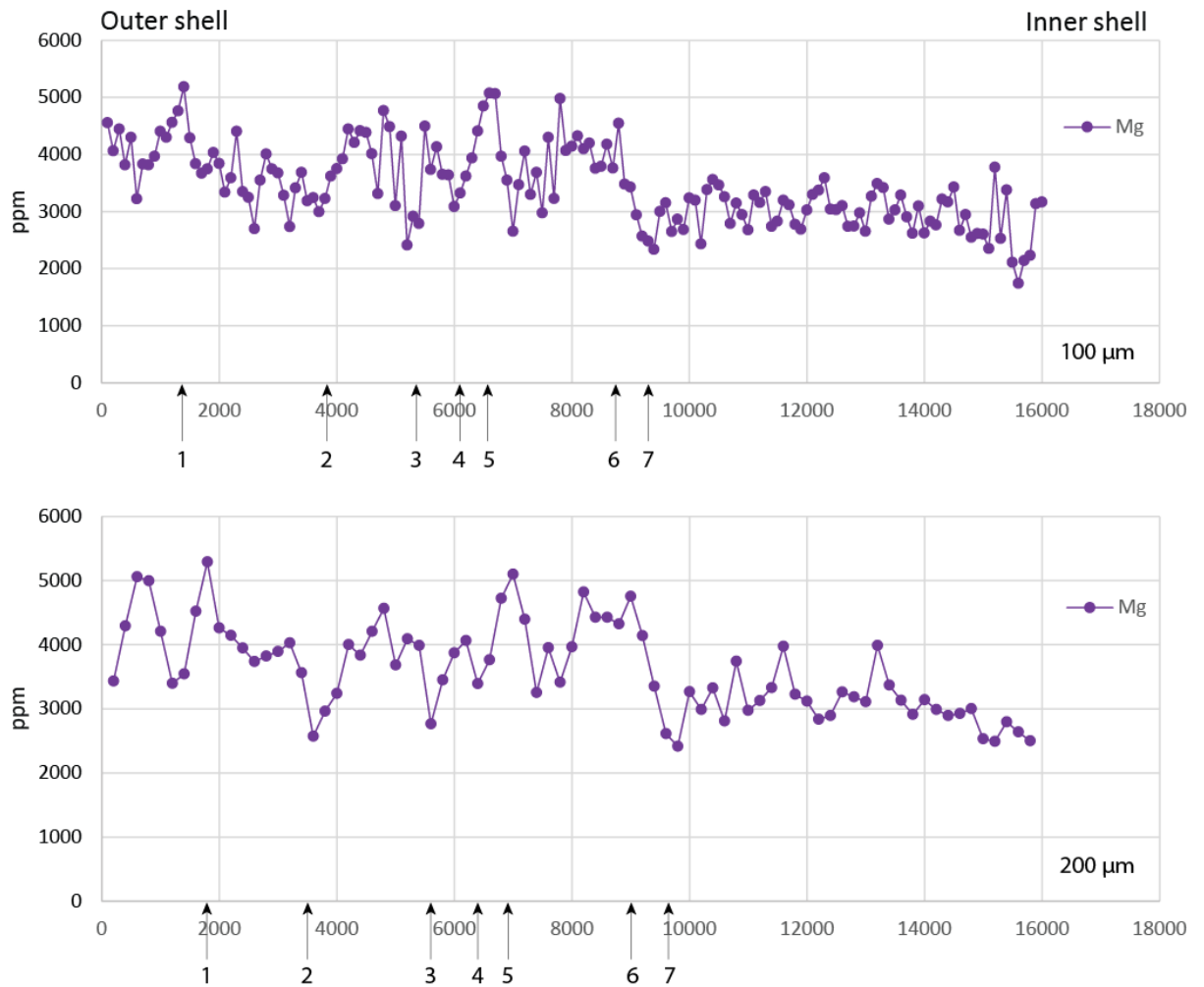


Figure 4-3. Comparing Mg concentrations through the XG shell transect at 100 µm (top) and 200 µm (bottom) spatial resolution.

Key peaks and troughs present in the higher resolution data are also present in the lower resolution and the overall trend (high variability within the first half of the dataset and reduced variability in the latter) is observed within both data sets.

Given the benefits previously described, analysing the shell at 90° to the direction of growth (e.g. following Transect 1 illustrated on Figure 4-2) was thought preferable and was implemented in all further analyses. When sampling at 200 µm spatial resolution the number of sample points required to complete a full transect from the outer to the inner shell margin is great enough to ensure geochemical heterogeneity is observed, and the time it takes to complete a full transect is short meaning multiple specimens can be analysed within the analytical time available. Therefore, the following trace element analyses utilised a ‘secondary methodology’ where analyses were carried out using 100

μm spots, spaced at 90° to the growth vector from the inner to the outer shell margin with laser parameters as previously described.

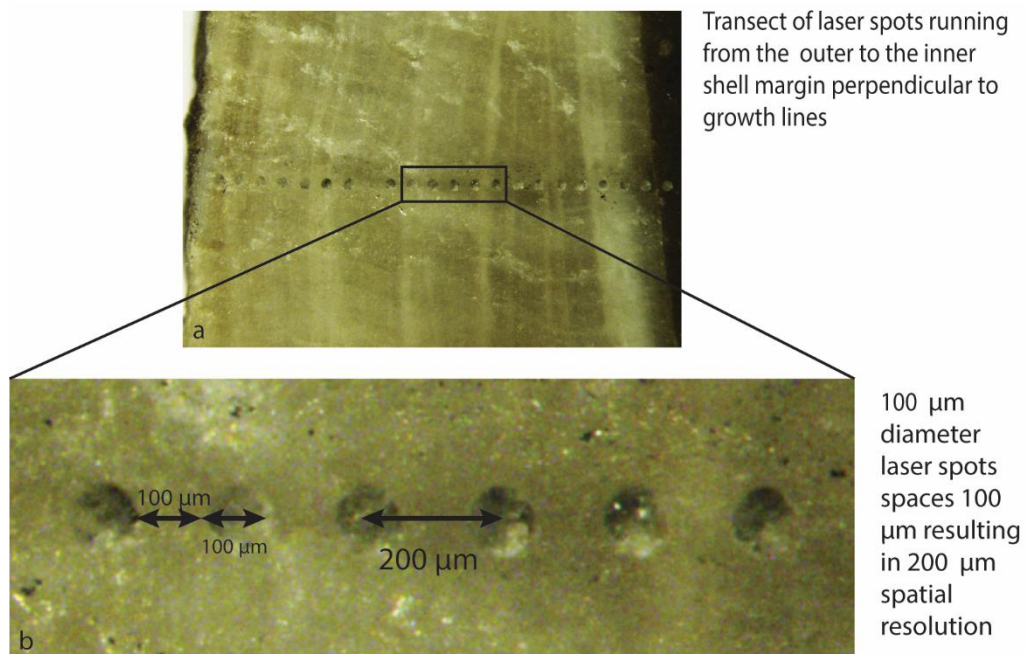


Figure 4-4. Laser ablation craters in *Gigantoproductus* sample with 200 μm spatial resolution.

a) The full transect from the outer to the inner shell margin perpendicular to growth lines. b) An enlarged view zoomed in section demonstrating the sampling resolution: 100 μm diameter laser spots spaced at 200 μm apart results in 200 μm spatial resolution.

4.2.2.2 Secondary isotope sample collection

A secondary set of five specimens consisting of three *G. inflaus* (RCK 33, RCK 28 and OAW 03), one *G. okensis* (RCK 28bis) and one *Gignatoproductus* sp. (XG) were selected to undergo isotope analyses once trace element analyses at 200 μm spatial resolution were completed. These specimens were selected because they passed the ultrastructure and CL tests by large areas of their shells appearing to be non-luminescent and having preserved fine detail within their ultrastructure, although they represent a spectrum of different preservation patterns and features based on the trace element results. Isotope samples were collected from the specimens using a computer-assisted 0.3 mm diamond-headed micro drill using NIGL facilities at the BGS.

Variations in Mg concentrations in brachiopod shells have previously been attributed to variations in environmental influences in a similar way to $\delta^{18}\text{O}$ (e.g. Butler et al., 2015; Freitas et al., 2006; Perez-Huerta et al., 2008). Therefore, Mg variability was used to

identify isotope sampling locations on the specimens. The sampling resolution that can be achieved for isotope analyses is lower than that for the trace element analyses because of the amount of sample required. If the specimen is well preserved, sampling peaks and troughs in Mg concentrations along a transect through an individual specimen should translate into peaks and troughs in the corresponding stable isotope record, although some variability will be lost.

To collect enough material, transects along growth lines were drilled to shallow depths (~200 – 300 μm) because there may be differences in preservation with depth. When transects were drilled growth lines were traced by eye. Subsequent trace element analyses (laser ablation ICP–MS) were carried out within the drilled out transect and illustrate that individual growth lines were followed successfully (see Appendix E).

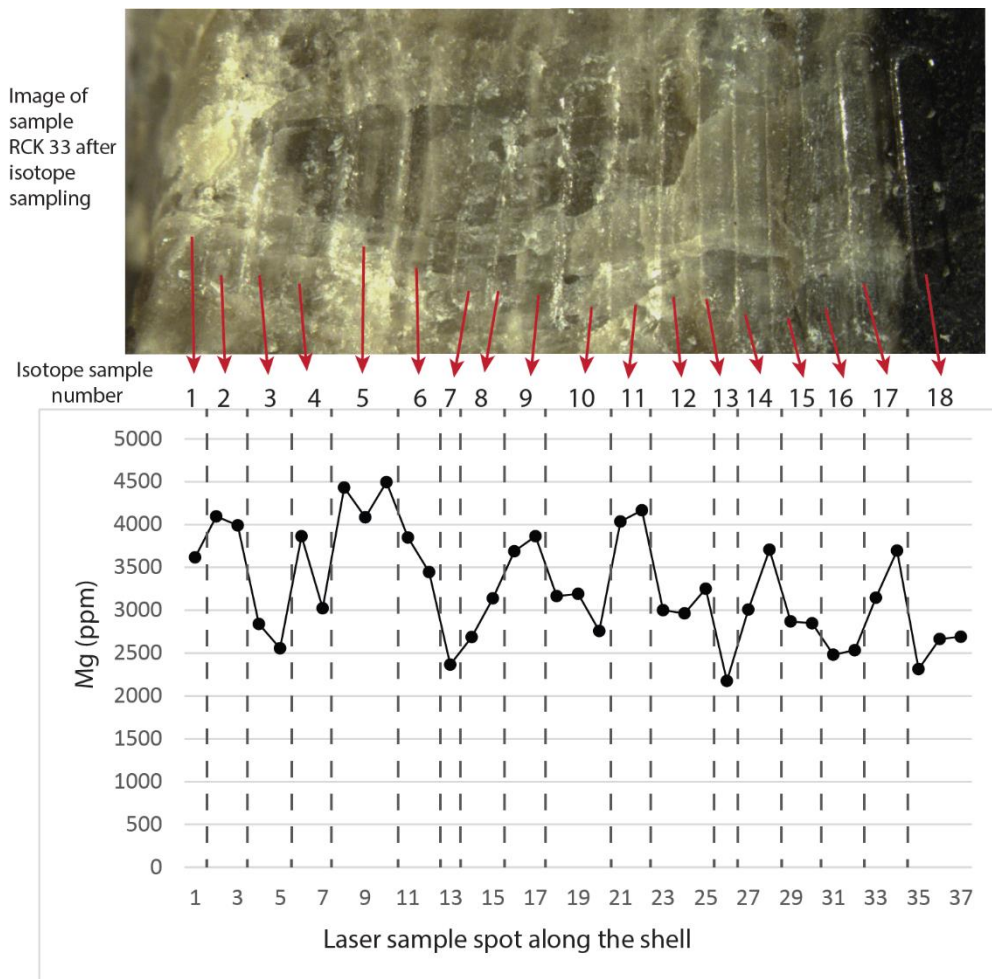


Figure 4-5. The isotope sampling strategy.

The top image shows specimen RCK 33 after isotope sampling where drilled troughs relate to an individual isotope sample. Thicknesses of the troughs are determined by targeting minimum and maximum concentrations of Mg. The isotope sample tracks were correlated to the trace element laser pits during sampling.

4.3 Results

A total of 15 specimens (OAW 51, OAW 50, RCK 36, RCK 35, RCK 33, RCK 28, RCK 6, RCK 6bis, RCK 41, XG, RCK 28bis, OAW 100, OAW 104, OAW 105 and OAW 03) were selected for trace element analyses based on good preservation of fine ultrastructure details being preserved and appearing non-luminescent (Table 4.2). Five specimens, all *G. inflatus* (OAW 50, RCK 35, RCK 33, RCK 6bis and RCK 41) were analysed in accordance with the preliminary methodology. Specimens RCK 35, RCK 33 and RCK 6bis were also analysed in accordance with the secondary trace element methodology alongside ten other specimens, six *G. inflatus* (OAW 51, RCK 35, RCK 28, OAW 104, OAW 105 and OAW 03), three *G. okensis* (RCK 36, RCK 28bis, RCK 100) and one and a single *Gigantoproductus*. Sp (XG). Additionally, two spot analyses of the dorsal valve of specimen RCK 6bis (*G. inflatus*) were also conducted. A single specimen (RCK 6bis, *G. inflatus*) underwent isotope analyses via the preliminary method and five specimens via the secondary method. Of these five specimens, four of these specimens, three *G. inflatus* (RCK 33, RCK 28 and OAW 03) and one unknown species of *Gigantoproductus* (XG), were analysed using a single transect through the shell and for one specimen (RCK 28bis, *G. okensis*) two transects through different areas of the shell were analysed for trace elements and stable isotopes (see Table 4.2 for a summary of specimen, names, species and conducted analyses).

The trace element results are only discussed for those specimens that were subsequently chosen for stable isotope analyses. Full geochemical profiles of the additional specimens which underwent trace element analyses are reported in Appendix E. Samples of non-shell and recrystallized shell materials (i.e. groundmass, matrix, a single sample of luminescent shell calcite and various types of recrystallized calcite) were also analysed for both trace elements and stable isotopes. All key trace element data are summarised in Section 4.3. Where elemental values were measured as 'negative numbers' (e.g. Fe concentration in RCK 33), it was assumed that the concentration was 0 ppm.

4.3.1 Trace element analyses

Three transects through specimen RCK 6bis (*G. inflatus*), were analysed via the preliminary methodology (raw data is provided in Appendix F).

Element of interest	Statistic/specimen	RCK 6bis
Mg (ppm)	n	25
	Min	1860.00
	Max	5820.00
	Mean	3094.37
	SD	1109.18
Sr (ppm)	Min	668.67
	Max	1425.67
	Mean	1016.95
	SD	201.26
Mn (ppm)	Min	1.02
	Max	12.32
	Mean	4.85
	SD	3.25
Fe (ppm)	Min	0.41
	Max	6.96
	Mean	3.13
	SD	1.48

Table 4-3 Summary table of preliminary trace element analyses for specimen RCK 6bis.

Minimum (Min), maximum (Max) and mean (Mean) concentrations and standard deviation of the data (SD) for Mg, Sr, Mn and Fe for trace element analyses collected via the preliminary sampling methodology. All values are recorded as parts per million (ppm). This data includes all the three transects analysed using the preliminary methodology of this specimen.

These preliminary analyses of the ventral valve (Table 4-3) show Mg concentrations between 1860 and 5820 ppm, Sr between 669 and 1426 ppm, Mn between 1 and 12 ppm and Fe between 0.4 and 7 ppm. The mean Fe and Mn concentrations are below 5 ppm and Sr and the mean Mg concentration is above 1000 ppm, which makes all the element data within the range of well-preserved material as outlined in Table 4-1.

Trace element data from specimens which underwent analyses via the secondary methodology are summarised in Table 4-4.

Element of interest	Specimen/Statistic	RCK 33	RCK 28	RCK 28bis	RCK 28bis_2	XG	OAW 03
	n	34	45	20	21	79	72
Mg (ppm)	Min	2174.00	2492.00	1145.00	2510.00	2413.00	788.00
	Max	4496.00	4888.00	4840.00	5580.00	5293.00	3226.00
	Mean	3324.59	3536.96	3009.40	3586.14	3610.04	2197.97
	SD	625.43	454.03	969.56	855.20	702.46	639.33
Sr (ppm)	Min	654.00	761.00	399.00	992.00	404.00	250.50
	Max	1244.00	1234.00	1354.00	1499.00	1592.00	1224.00
	Mean	973.59	1068.24	940.40	1141.60	997.14	878.49
	SD	117.11	103.25	309.22	153.98	245.47	267.42
Mn (ppm)	Min	0.13	0.81	1.60	0.47	0.70	0.08
	Max	26.10	59.00	257.80	4.87	1188.00	100.80
	Mean	3.05	7.24	53.48	2.56	30.13	14.70
	SD	4.67	9.42	70.29	1.25	133.38	15.63
Fe (ppm)	Min	-0.79	6.60	3.40	4.80	3.62	2.04
	Max	9.02	275.00	7.33	9.69	7300.00	78.20
	Mean	2.14	44.60	5.14	6.86	146.86	13.66
	SD	2.59	66.08	1.26	1.29	885.86	12.06

Table 4-4. Summary table of trace element data for shell specimens in ppm.

Minimum (Min), Maximum (Max) and mean concentrations and the standard deviation (SD) of the Mg, Sr, Mn and Fe data for each specimen. All values are recorded as parts per million (ppm).

4.3.1.1 Strontium

The six transects through the five specimens yielded Sr concentrations between 250 ppm and 1592 ppm and mean Sr concentrations ranging from 878 ppm to 1141 ppm. The lowest Sr concentration (250 ppm) occurs within specimen OAW 03. OAW 03 also has the lowest of the maximum measured Sr concentrations. The highest Sr concentration across all specimens (1592 ppm) occurs within specimen XG, which also has the largest range in Sr values (1188 ppm). The maximum Sr concentration within transects RCK 28bis and RCK 28bis_2 are comparable however, their minimum Sr concentrations are not. The mean Sr concentrations of all specimens lie within the range of well-preserved Palaeozoic and modern brachiopods (Table 4-1).

The distribution of Sr through individual transects is heterogeneous. There is no consistent pattern of Sr distribution across specimens with the exception of the lowest Sr concentration typically occurring at the shell margins and the higher concentrations occurring within the shell interior.

4.3.1.2 Magnesium

All specimens contain Mg concentrations between 2197 and 3610 ppm. Typically, Mg concentrations are above 2000 ppm, and are commonly above 3000 ppm (Table 4-4). OAW 03 has the lowest minimum Mg concentration (778 ppm) and the lowest of the maximum concentrations (3226 ppm), which is lower than other maximum Mg concentrations by more than 1000 ppm. The highest concentration occurs within specimen RCK 28bis_2 while the highest average concentration occurs within specimen XG. The largest range (3695 ppm) occurs within transect RCK 28bis, however the data range in all transects is >2000 ppm. All shells yield Mg concentrations within the range of modern brachiopods (Brand et al., 2003b).

The minimum Mg concentrations occur at the inner and outer shell margins whilst the maximum is generally present within the shell interior. Excluding this observation there are no patterns observed within the distribution of Mg through the shell transects.

4.3.1.3 Manganese

Specimens yielded Mn concentrations between 0.1 to 1188 ppm, however concentrations are typically below 260 ppm. Within all specimens the minimum Mn concentrations are comparable across specimens (<1.6 ppm) however the maximum Mn concentrations range from 4.9 ppm (within specimen RCK 28bis_2) to 1188 ppm (measured in specimen XG). Despite this, the average Mn concentrations have a small range (from 2.6 ppm to 53 ppm).

For specimen XG the highest Mn concentration (1188 ppm) occurs at the inner shell margin and the second highest (132 ppm) occurs at the outer shell margin. This is similar to specimens OAW 03 and RCK 28bis where the highest Mn concentration (100 ppm) occurs at the shell margins whilst all other sample points have low concentrations (typically <40ppm).

All average Mn concentrations are below or within the concentration ranges recorded in modern and ancient brachiopods. Several individual samples have concentrations that are higher than those previously reported (see Table 4-1).

4.3.1.4 Iron

Specimens yielded Fe concentrations between 0 and 7300 ppm, although concentrations are mostly below 80 ppm. Minimum Fe concentrations are consistently low (<6.6 ppm) whilst maximum concentrations range from 9.0 ppm, observed in RCK 33, to 7300 ppm, observed in specimen XG. Excluding specimen XG, average Fe concentrations are below 45 ppm. Specimen XG, has two sample points with Fe concentrations above 3000 ppm and a single data point with a concentrations of 178 ppm. Therefore, despite all other data points having Fe concentrations below 25 ppm the average Fe concentration for this specimen is 147 ppm, as it has been skewed by the three data points with elevated concentrations. Within most specimens, the highest Fe concentration occurs at the shell margins whilst the lower occur within the shell interior.

The average concentrations of all specimens within this dataset are within the realms of the Fe concentrations recorded in modern and ancient brachiopods however, there are individual data points that significantly exceed modern values. This highlights the heterogeneity in the distribution of Fe both within the dataset and within individual specimens.

4.3.2 Trace element analysis of non-shell and secondary/recrystallized calcite materials

The trace element data of all non-shell or recrystallized shell samples (e.g. groundmass and diagenetic calcite) are summarised in Table 4-5.

The range in trace element concentrations for these analyses is much greater than that of the shell calcite, which is expected given that some are likely to represent secondary chemistry while others may be coeval and therefore more comparable to primary shell chemistry. All Mg average concentrations are below 3000 ppm and most are below 2000 ppm. Sr concentrations are highly variable with averages ranging from 228 ppm to 937 ppm.

Element of interest	Material/statistic	RCK 6bis luminescent shell	Bulk rock between valves	Bulk rock	Secondary calcite from within geopetal	Bulk rock within geopetal	Recrystallised calcite within umbo
	n	2	13	2	1	2	2
Mg (ppm)	Min	2112.00	2151.00	783.00	N/A	894.67	1075.67
	Max	3193.33	3710.00	1184.33	N/A	1752.00	1397.67
	Mean	2652.67	2948.72	983.67	1091.33	1323.33	1236.67
	SD	N/A	555.84	N/A	N/A	N/A	N/A
Sr (ppm)	Min	576.00	276.73	140.67	N/A	164.37	259.67
	Max	1140.33	1282.00	323.20	N/A	293.00	685.67
	Mean	858.17	632.73	231.93	304.80	228.68	472.67
	SD	N/A	318.87	N/A	N/A	N/A	N/A
Mn (ppm)	Min	6.68	28.00	58.37	N/A	48.60	58.53
	Max	22.31	130.07	101.23	N/A	72.57	66.03
	Mean	14.49	75.96	79.80	53.40	60.58	62.28
	SD	N/A	27.74	N/A	N/A	N/A	N/A
Fe (ppm)	Min	2.46	5.37	4.56	N/A	1.14	1.54
	Max	10.48	409.00	8.32	N/A	6.47	6.13
	Mean	6.47	121.61	6.44	0.85	3.81	3.84
	SD	N/A	156.25	N/A	N/A	N/A	N/A

Table 4-5. Summary of trace element data for end-member sample points. Minimum (Min), maximum (Max) and Average (Av) concentrations for Mg, Sr, Mn and Fe for end-member sample points.

Averages written in italics represent values that were calculated from only two data points. Minimum and maximum values are not calculated for 'secondary calcite cement from within the geopetal' as this is a single data point.

Mn is high in all end-member samples compared to much of the shell calcite however, Fe is only significantly higher in the groundmass within the body cavity between the dorsal and ventral valves. Within the groundmass between the valves, Mg is also significantly lower both compared to non-luminescent shell calcite and other end-member specimens whilst Sr is lower compared to shell-calcite but not compared to other end-member samples. Despite these observations, for many of the materials analysed the range in data observed is within the parameters of well-preserved Palaeozoic and modern biogenic calcite (Table 4-1).

Histograms showing the distribution of the raw data for the elements of interest (Mg, Sr, Mn and Fe) combined across all shell specimens are presented in Figure 4-6. The p values calculated for the Shapiro Wilks test (which tests for normality within a dataset) using

JMP software indicate that there is sufficient evidence to conclude that the underlying distribution of the data across all elements of interest is not normally distributed (with a significance level of 0.05, as ascribed by JMP). This is expected given that this data is likely to contain both poorly preserved and well-preserved data.

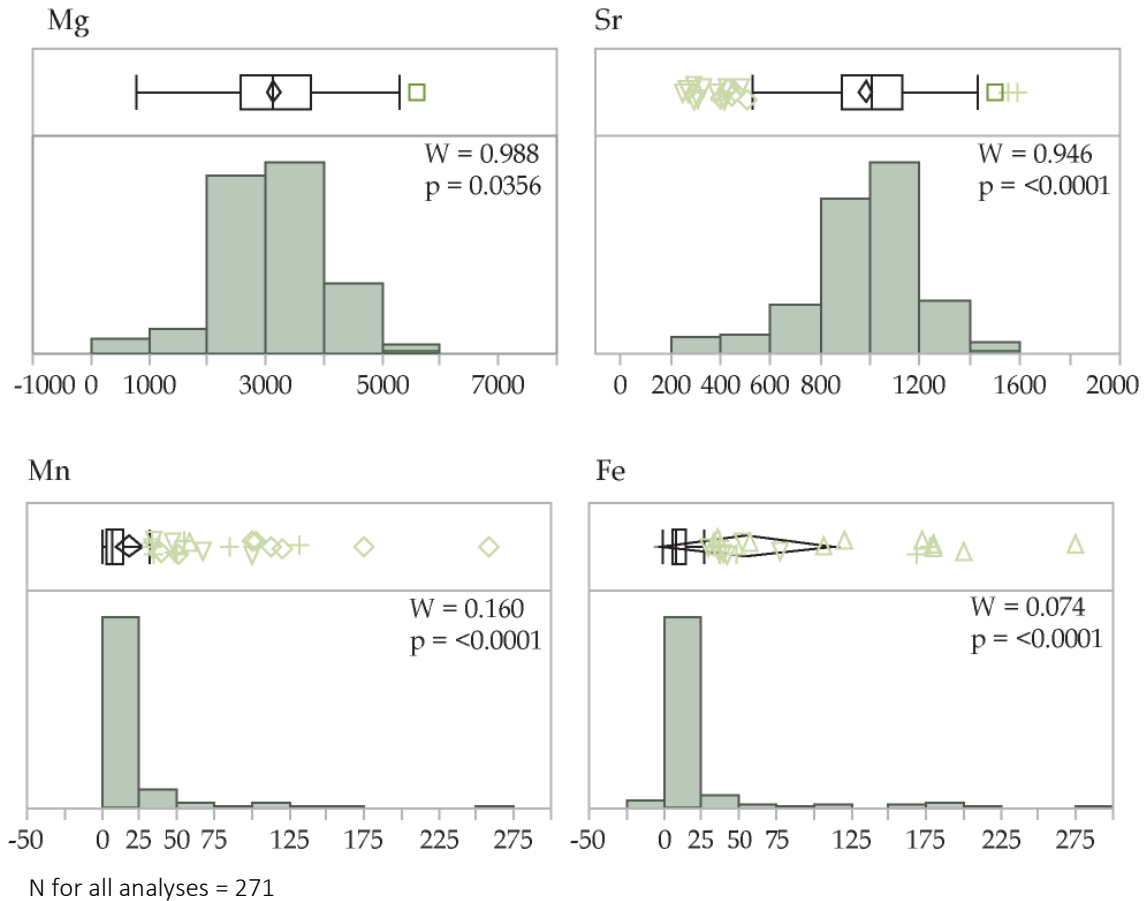


Figure 4-6 shows the distribution of all raw Mg, Sr, Mn and Fe data with results from the Schapiro Wilks test (w) and the associated p value for this test (p).

Outliers within the data are present however at this point are not removed. This is because without understanding the preservation of the material, it cannot be certain whether these outliers represent poorly or well-preserved material.

4.3.3 Stable isotopes

4.3.3.1 Stable isotope data of ventral valve transects

Stable isotope values ($\delta^{13}\text{C}$ and $\delta^{18}\text{O}$) recorded from specimen RCK 6bis are given in Table 4-6 and from specimens RCK 33, RCK 28, RCK 28bis, XG and OAW 03 in Table 4-7.

Element of interest	Statistic/ specimen	RCK 6bis
$\delta^{18}\text{O}$ (‰)	n	25
	Min	-5.26
	Max	-2.52
	Mean	-3.53
	SD	0.66
$\delta^{13}\text{C}$ (‰)	Min	0.93
	Max	2.44
	Mean	2.05
	SD	0.40

Table 4-6. Summary table of stable isotope results collected from the ventral valve of *G. inflatus*, specimen RCK 6bis via the preliminary sampling technique.

Specimen RCK 6bis was analysed using the preliminary sampling method and yielded $\delta^{18}\text{O}$ values between -2.52‰ and -5.26‰ and $\delta^{13}\text{C}$ values between $+0.93\text{‰}$ and $+2.44\text{‰}$. The average values are -3.53‰ and $+2.05\text{‰}$ for $\delta^{18}\text{O}$ and $\delta^{13}\text{C}$ respectively. The data ranges, 2.7‰ for $\delta^{18}\text{O}$ 1.5‰ for $\delta^{13}\text{C}$, show that there is variability within the dataset, although there are no patterns other than the lowest values for both isotopes are observed at both shell margins, though more commonly at the outer shell margin.

Element of interest	Statistic/ specimen	RCK 33	RCK 28	RCK 28bis	RCK 28bis_2	XG	OAW 03
$\delta^{18}\text{O}$ (‰)	n	17	22	10	10	37	33
	Min	-7.10	-4.82	-8.71	-4.46	-5.95	-5.90
	Max	-2.56	-3.07	-3.25	-2.94	-3.18	-3.54
	Mean	-3.98	-3.80	-4.53	-3.70	-4.92	-4.56
	SD	1.06	0.44	1.54	0.51	0.65	0.67
$\delta^{13}\text{C}$ (‰)	Min	-0.06	1.14	0.57	0.94	-0.98	-1.65
	Max	2.31	2.73	2.70	2.71	2.64	1.99
	Mean	1.47	2.15	1.79	2.19	1.50	0.54
	SD	0.67	0.45	0.89	0.53	1.13	1.13

Table 4-7. Summary of all stable isotope data of transects through five specimens that run from the inner to the outer shell margin.

All specimens analysed via the secondary methodology yielded $\delta^{18}\text{O}$ values between -8.71‰ and -2.56‰ and $\delta^{13}\text{C}$ between -1.65‰ and $+2.73\text{‰}$. Average $\delta^{13}\text{C}$ values are between $+0.54\text{‰}$ and $+2.19\text{‰}$ with the lowest average observed in specimen OAW 03 and all other specimens having similar averages. Average $\delta^{18}\text{O}$ values are between -5.02‰ and -3.7‰ with the lowest average values observed within specimen XG and the

highest within RCK 28bis_2 (however, specimens RCK 33, and RCK 28 have average values only slightly lower than RCK 28bis_2).

4.3.3.2 Stable isotope data of non-shell and secondary/recrystallized calcite samples

Stable isotope data from end-member samples yielded $\delta^{18}\text{O}$ values between -10.54‰ and -2.61‰ and $\delta^{13}\text{C}$ values between -0.59‰ and $+2.61\text{‰}$. The average values for $\delta^{18}\text{O}$ and $\delta^{13}\text{C}$ are -10.05‰ to -3.89‰ and -0.37‰ to $+2.46\text{‰}$ respectively. The most negative $\delta^{18}\text{O}$ value was from the recrystallized umbonal shell calcite whereas the lowest $\delta^{13}\text{C}$ was observed in the bulk rock.

Element of interest	Material/statistic	RCK 6bis luminescent shell	Bulk rock between valves	Bulk rock	Secondary calcite from within geopetal	Bulk rock within geopetal	Recrystallised calcite within umbo
	n	2	11	2	1	2	2
$\delta^{18}\text{O}$ (‰)	Min	-4.61	-6.33	-9.45	N/A	-8.25	-10.54
	Max	-3.17	-2.67	-5.71	N/A	-5.37	-9.24
	Mean	-3.89	-4.68	-7.58	-10.50	-6.81	-9.89
	SD	N/A	1.32	N/A	N/A	N/A	N/A
$\delta^{13}\text{C}$ (‰)	Min	2.32	1.30	-0.59	N/A	-0.28	-0.55
	Max	2.61	2.09	0.39	N/A	0.59	0.85
	Mean	2.46	1.64	-0.10	-0.37	0.16	0.15
	SD	N/A	0.29	N/A	N/A	N/A	N/A

Table 4-8. Summary of stable isotope data of non-shell and recrystallized materials.

Some samples (e.g. luminescent shell, groundmass between valves, and one sample of general groundmass) have $\delta^{13}\text{C}$ and $\delta^{18}\text{O}$ values that lie within the range of analysed shell specimens. Some samples (e.g. calcite from within the geopetal, recrystallized calcite in the umbo and one sample of groundmass matrix) have significantly lower $\delta^{18}\text{O}$ values despite $\delta^{13}\text{C}$ remaining comparable to other end-member samples. Two data points (one from specimen RCK 28bis and one from specimen RCK 33) have $\delta^{18}\text{O}$ values that are much lower than many other shell data points and more comparable to the diagenetic calcitic infilling cement of the geopetal and recrystallized umbonal calcite (Figure 4-7).

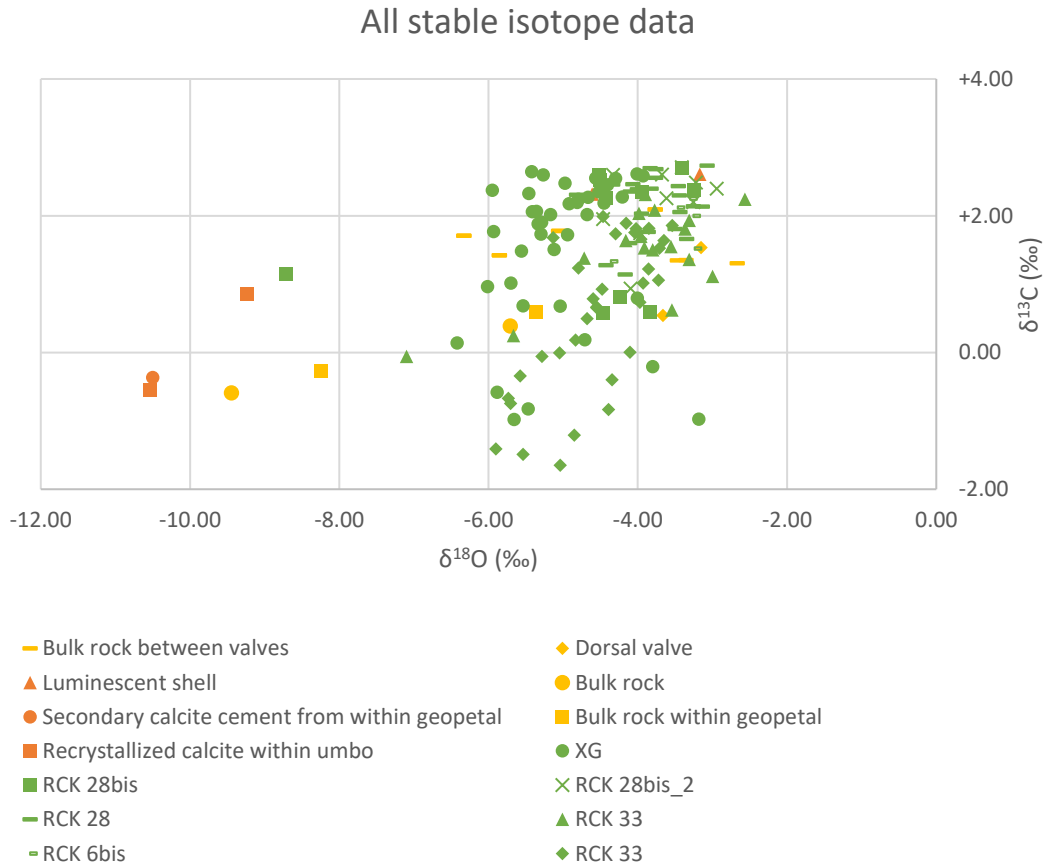


Figure 4-7. Stable isotope values of all samples of all materials.

4.3.4 Correlation of trace element and stable isotope data

Most of the trace element data described here (both shell and end-member data) have Sr, Mn and Mg concentrations that lie within the geochemical ranges exhibited in modern brachiopods, and within the ranges of previously published ‘well-preserved Viséan *Gigantoproductus* species (Figure 4-8 and Table 4-1). Typically, data points that are not within the realms of well-preserved biogenic calcite occur at the shell margins (both the inner and outer within the central shell region) and coincide with areas of the shell that show some luminescence and commonly have poor ultrastructure preservation (Chapter 3).

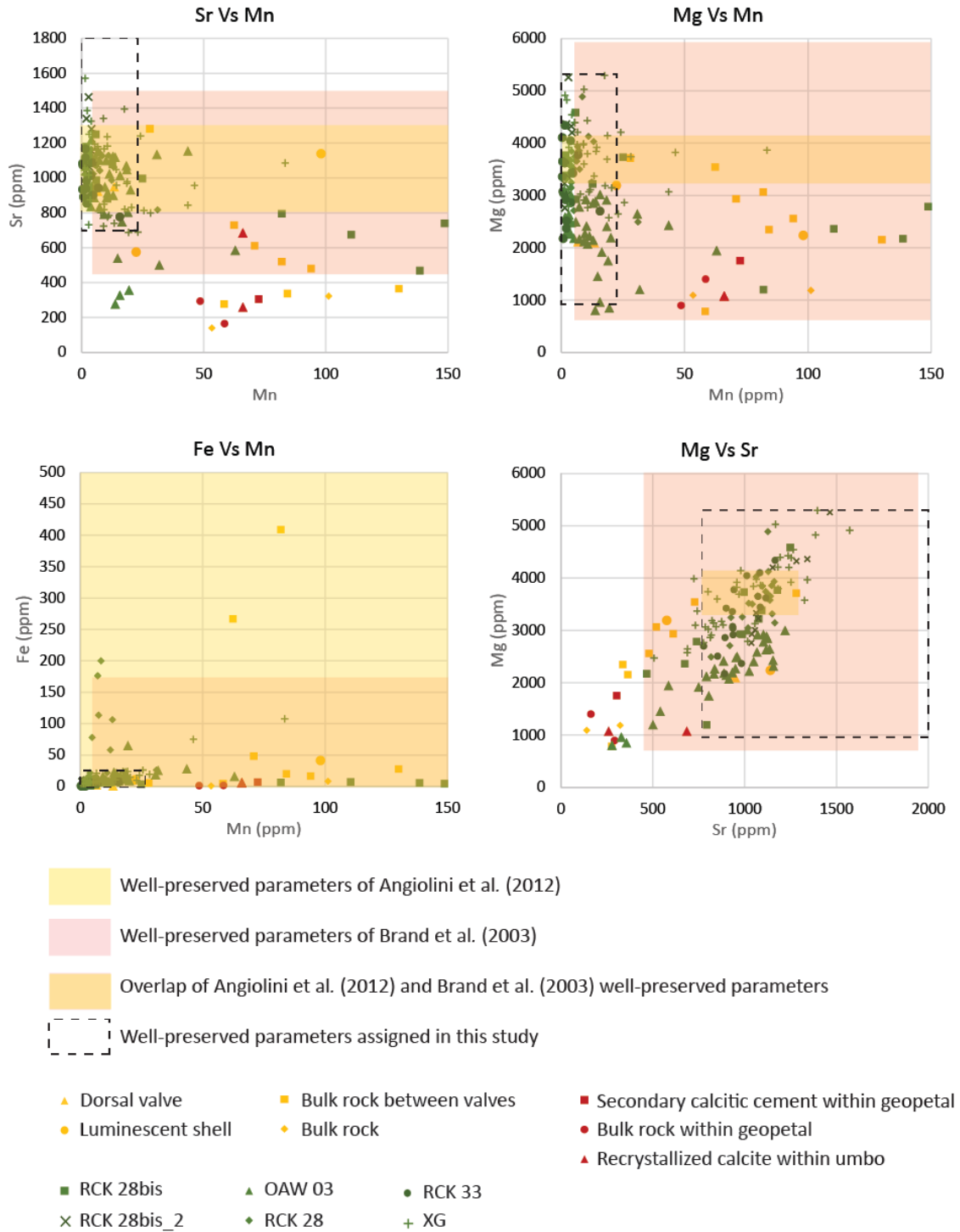


Figure 4-8. Trace element cross plots for Fe, Mn, Sr and Mg of all shell and end-member data.

Cross plots of key elements for the shell and non-shell data (Figure 4-8) demonstrate that within some specimens there appears to be a relationship (i.e. as one element concentration increases another may simultaneously increase or decrease) between

particular element (particularly Sr and Mg). To investigate this further, Spearman’s rank correlation was carried out. Spearman’s rank correlation is a non-parametric test (can be applied to datasets that are not normally distributed) that tests for a directional relationship between two variables. This works by first independently ranking the variables in order (i.e. highest to lowest), then comparing the relationship between the two variants identifying if one increases with the other. The results of these analyses are presented in Table 4-9 and Table 4-10.

Within Figure 4-8 the red shaded areas represent the range of data values observed in modern brachiopods (Brand et al., 2003b), yellow areas are the range of values observed in non-luminescent Visean *G. aff. okensis* (Angiolini et al., 2012) and the outlined black dashed boxes outline the data points considered to be well-preserved shells based on the geochemical parameters assigned in this study (see Section 4.2). For exact values, see Table 4-1. This figure highlights how there is some separation of the shell samples and groundmass, matrix and recrystallized material, however there is some overlap which may be expected given that some shell data may have undergone alteration and some of the non-shell or recrystallized materials may have a geochemistry comparable to well-preserved shell data. Additionally, this figure illustrates that for most elements almost all the material analysed lies within the ranges of well-preserved material outlined by the two example studies given.

OAW 03							
	Mg	Na	Sr	Mn	Fe	$\delta^{13}\text{C}$	$\delta^{18}\text{O}$
Mg	-	0.8743	0.8663	-0.3199	-0.4525	-0.0431	0.1232
Na	0.8743	-	0.9739	-0.2376	-0.3402	-0.2032	0.1553
Sr	0.8663	0.9739	-	-0.2844	-0.4238	-0.1636	0.1947
Mn	-0.3199	-0.2376	-0.2844	-	0.8305	-0.3020	-0.1755
Fe	-0.4525	-0.3402	-0.4238	0.8305	-	-0.4531	-0.4406
$\delta^{13}\text{C}$	-0.0431	-0.2032	-0.1636	-0.3020	-0.4531	-	0.6792
$\delta^{18}\text{O}$	0.1232	0.1553	0.1947	-0.1755	-0.4406	0.6792	-
RCK 28							
	Mg	Na	Sr	Mn	Fe	$\delta^{13}\text{C}$	$\delta^{18}\text{O}$
Mg	-	0.4907	0.5381	0.3721	0.4150	0.4434	-0.2023
Na	0.4907	-	0.7820	-0.2885	0.0130	0.1463	0.1757
Sr	0.5381	0.7820	-	-0.1361	0.1733	0.0847	0.0119
Mn	0.3721	-0.2885	-0.1361	-	0.6691	0.2028	-0.4254
Fe	0.4150	0.0130	0.1733	0.6691	-	0.0887	-0.3921
$\delta^{13}\text{C}$	0.4434	0.1463	0.0847	0.2028	0.0887	-	0.1904
$\delta^{18}\text{O}$	-0.2023	0.1757	0.0119	-0.4254	-0.3921	0.1904	-

RCK 28bis							
	Mg	Na	Sr	Mn	Fe	$\delta^{13}\text{C}$	$\delta^{18}\text{O}$
Mg	-	0.9545	0.8455	-0.7273	-0.6818	0.7818	0.1152
Na	0.9545	-	0.8909	-0.7000	-0.5909	0.7939	0.2000
Sr	0.8455	0.8909	-	-0.7273	-0.4455	0.7939	-0.1758
Mn	-0.7273	-0.7000	-0.7273	-	0.3636	-0.6727	0.2121
Fe	-0.6818	-0.5909	-0.4455	0.3636	-	-0.6606	-0.0303
$\delta^{13}\text{C}$	0.7818	0.7939	0.7939	-0.6727	-0.6606	-	0.1030
$\delta^{18}\text{O}$	0.1152	0.2000	-0.1758	0.2121	-0.0303	0.1030	-
RCK 2bis_2							
	Mg	Na	Sr	Mn	Fe	$\delta^{13}\text{C}$	$\delta^{18}\text{O}$
Mg	-	0.3697	0.9515	0.4182	0.5030	-0.1581	-0.3818
Na	0.3697	-	0.2364	0.1515	-0.2242	-0.5471	-0.5394
Sr	0.9515	0.2364	-	0.2121	0.4061	-0.1337	-0.1879
Mn	0.4182	0.1515	0.2121	-	0.7333	0.2918	-0.6970
Fe	0.5030	-0.2242	0.4061	0.7333	-	0.4985	-0.2000
$\delta^{13}\text{C}$	-0.1581	-0.5471	-0.1337	0.2918	0.4985	-	0.3161
$\delta^{18}\text{O}$	-0.3818	-0.5394	-0.1879	-0.6970	-0.2000	0.3161	-
RCK 33							
	Mg	Na	Sr	Mn	Fe	$\delta^{13}\text{C}$	$\delta^{18}\text{O}$
Mg	-	0.3284	0.7525	-0.1225	-0.0098	-0.3873	-0.1643
Na	0.3284	-	0.1225	-0.3137	-0.1201	-0.5343	0.3029
Sr	0.7525	0.1225	-	-0.2304	-0.2059	-0.2083	-0.4464
Mn	-0.1225	-0.3137	-0.2304	-	0.7623	0.3676	-0.2833
Fe	-0.0098	-0.1201	-0.2059	0.7623	-	0.0221	-0.2894
$\delta^{13}\text{C}$	-0.3873	-0.5343	-0.2083	0.3676	0.0221	-	0.2820
$\delta^{18}\text{O}$	-0.1643	0.3029	-0.4464	-0.2833	-0.2894	0.2820	-
XG							
	Mg	Na	Sr	Mn	Fe	$\delta^{13}\text{C}$	$\delta^{18}\text{O}$
Mg	-	0.7250	0.7814	-0.2853	-0.1634	-0.2099	0.3990
Na	0.7250	-	0.9340	-0.4263	-0.3025	-0.2426	0.4953
Sr	0.7814		-	-0.4518	-0.3607	-0.2900	0.4638
Mn	-0.2853	-0.4263	-0.4518	-	0.8400	0.0853	-0.3237
Fe	-0.1634	-0.3025	-0.3607	0.8400	-	0.3990	-0.1692
$\delta^{13}\text{C}$	-0.2099	-0.2426	-0.2900	0.0853	0.3990	-	0.2225
$\delta^{18}\text{O}$	0.3990	0.4953	0.4638	-0.3237	-0.1692	0.2225	-

Table 4-9. Correlation data calculated as Spearman’s rank correlation of key elements within all shell data (excluding RCK 6bis).

Yellow cells represent data where the calculated correlation is significant. This was calculated in JMP and is an evaluation of the probability of the apparent correlation occurring randomly, where the correlation observed could have occurred randomly it is not deemed significant.

Bulk rock and end-member data							
	Mg	Na	Sr	Mn	Fe	$\delta^{13}\text{C}$	$\delta^{18}\text{O}$
Mg	-	0.7840	0.6327	0.0728	0.6313	0.6952	0.3201
Na	0.7840	-	0.7960	-0.2343	0.2818	0.5705	0.4419
Sr	0.6327	0.7960	-	-0.1474	0.3256	0.6670	0.4386
Mn	0.0728	-0.2343	-0.1474	-	0.6696	0.0258	-0.0898
Fe	0.6313	0.2818	0.3256	0.6696	-	0.5795	0.1446
$\delta^{13}\text{C}$	0.6952	0.5705	0.6670	0.0258	0.5795	-	0.6030
$\delta^{18}\text{O}$	0.3201	0.4419	0.4386	-0.0898	0.1446	0.6030	-

Table 4-10. Correlation data for all non-shell end-member data samples and recrystallized materials. Colour coding following that described for Table 4-9.

Sr and Mg have strong and significant positive directional correlation within all specimens. Sr and Mg also have a strong positive correlation with Na within all specimen transects except RCK 33 and RCK 28bis_2. Fe and Mn are also positively correlated in all specimens except RCK 28bis, while XG and OAW 03 show correlation between Sr and Fe and XG and RCK 28bis show significant negative correlation between Sr and Mn. Through specimen OAW 03 these chemical variations can also be loosely correlated with variability in the visual properties in the specimen (Figure 4-8).

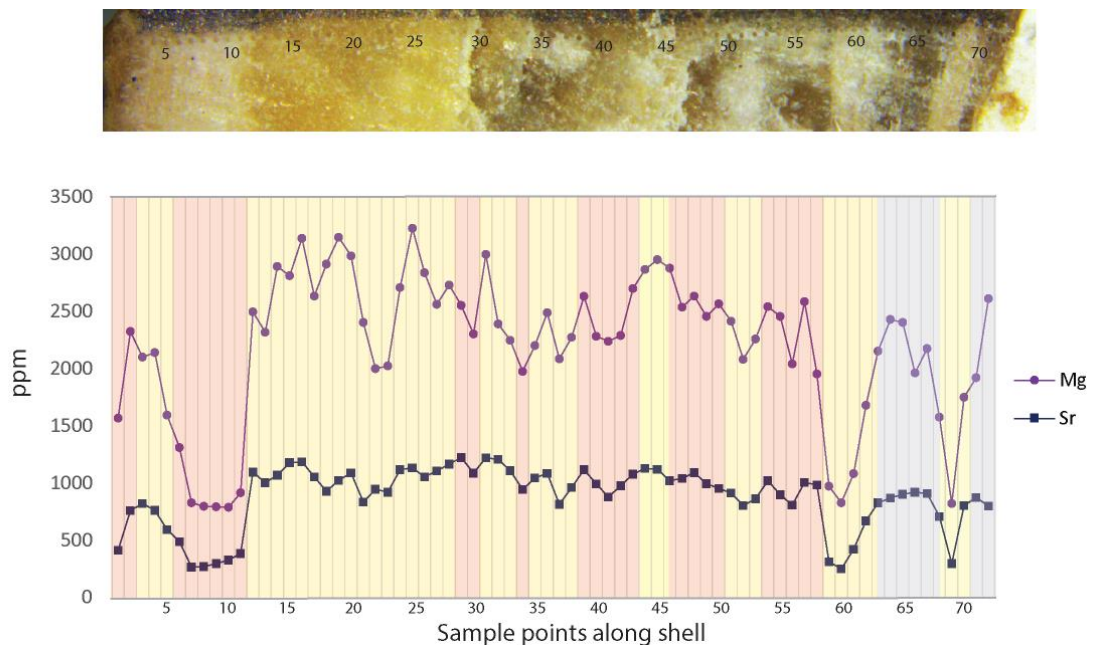


Figure 4-9. Photograph and Mg, Sr concentrations of transect through the central, non-luminescent and generally fabric retentive *G. inflatus* specimen, OAW 03.

Coloured sections of the graph highlight where the shell calcite colours change. Pink and yellow shading simply represent a change in colour and blue shading represents areas of the shell that are a similar colour to calcite of other specimens.

The occurrence of $\delta^{13}\text{C}$ and $\delta^{18}\text{O}$ correlations within shell specimens is more sporadic, with $\delta^{18}\text{O}$ correlating with all trace elements excluding Fe within specimen XG, negatively correlating with Mn in specimens RCK 28 and RCK 28bis_2 and correlating with Fe in specimen OAW 03. $\delta^{13}\text{C}$ and $\delta^{18}\text{O}$ have no significant directional correlation with the exception of specimen OAW 03, where they are positively correlated. $\delta^{13}\text{C}$ correlation with trace elements is similarly sporadic and it significantly correlates with all trace elements in specimen RCK 28bis while in RCK 28bis_2 there is no significant correlation between $\delta^{13}\text{C}$ and any of the trace elements.

Within the non-shell and recrystallized shell data, Mg has a significant positive directional correlation with all elements, excluding Mn, and also correlates with $\delta^{13}\text{C}$. Within these samples Sr does not correlate with Mn or Fe and Mn only correlates significantly with Fe. $\delta^{18}\text{O}$ does not correlate with any trace elements within these samples.

Both Sr and Mg concentrations are highly variable with the lowest values of both elements occurring near (but not at) both the outer and inner shell margins. Fe and Mn are heterogeneously distributed with the highest values of both elements occurring close to the outer shell margin. Values of $\delta^{13}\text{C}$ show a gradual increase from the outer to the inner shell margin. A similar trend of increasing values is also observed in $\delta^{18}\text{O}$ data.

Figures 4-10 through to 4-15 show Mg, Sr, Mn, Fe, $\delta^{13}\text{C}$, $\delta^{18}\text{O}$ variations through the transect of each analysed specimen. Note that varying scales are used both for different elements but also for different specimens.

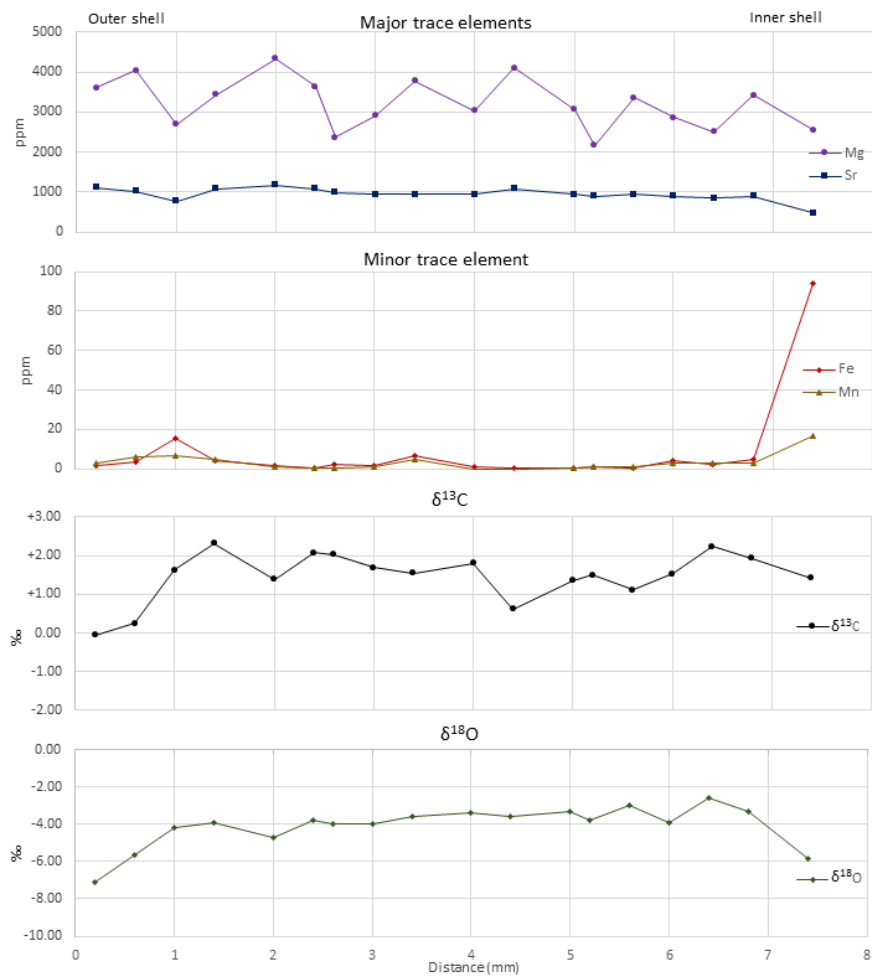


Figure 4-10. Trace element and stable isotope data through the central, non-luminescent region shell region of *G. inflatus*, specimen RCK 33.

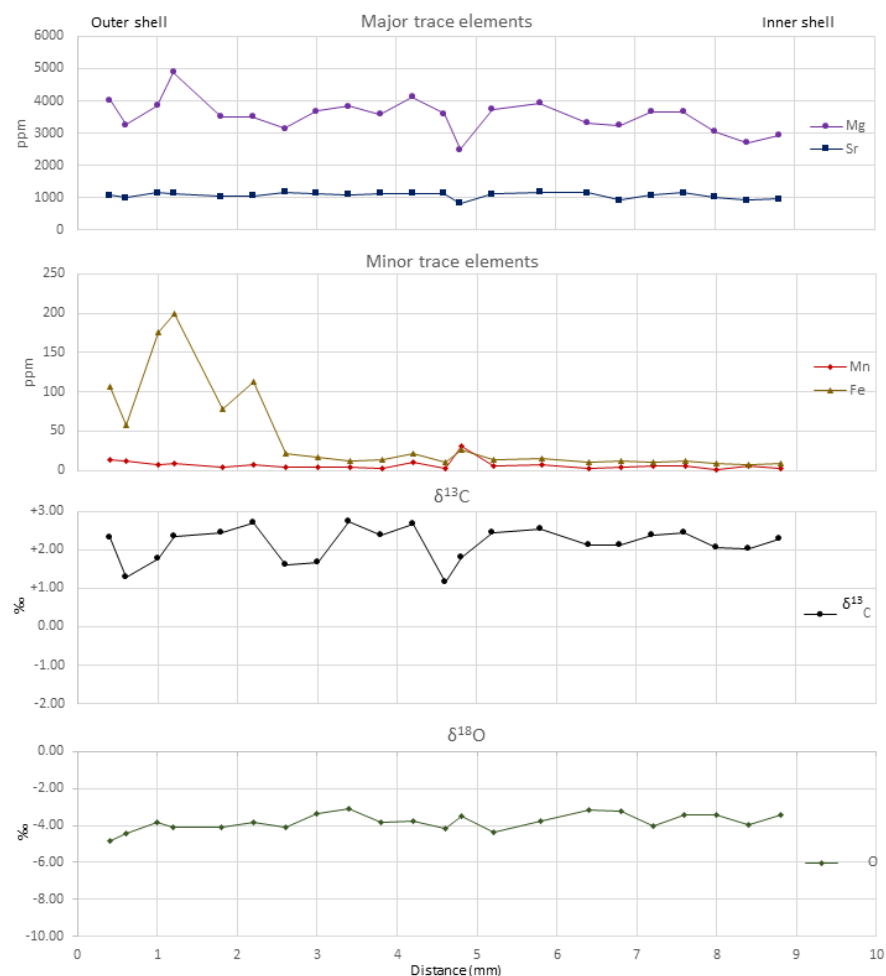


Figure 4-11. Trace element and stable isotope data from a transect through the central, non-luminescent of *G. inflatus*, specimen RCK 28.

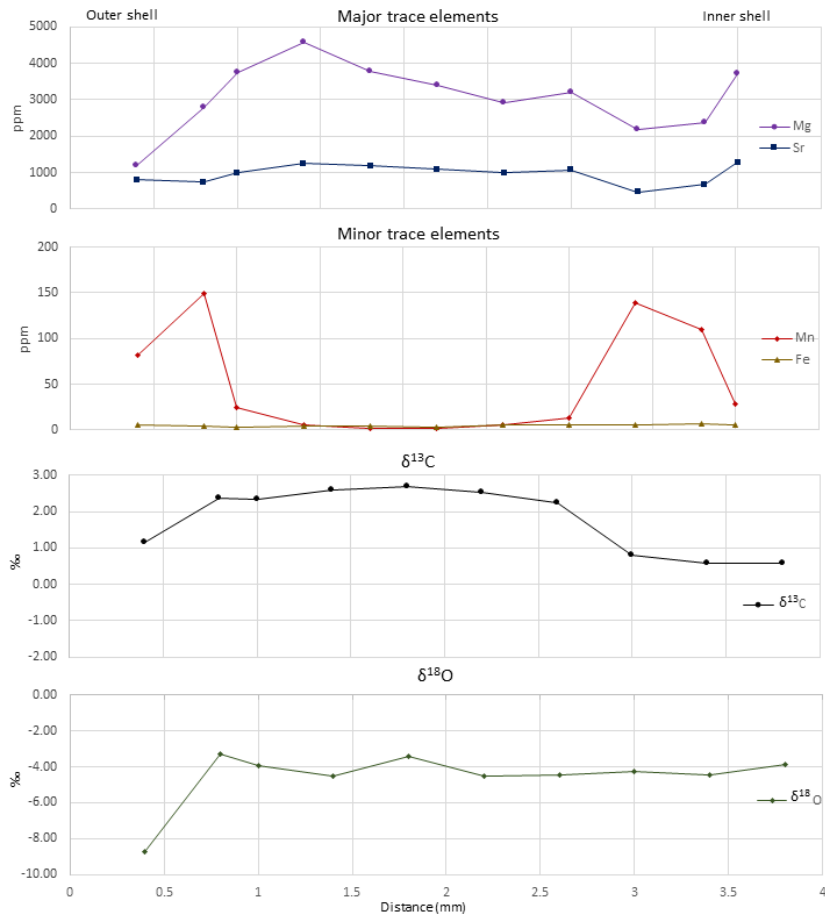


Figure 4-12. Trace element and stable isotope data for transect through the non-luminescent central shell region of *G. okensis*, specimen RCK 28bis.

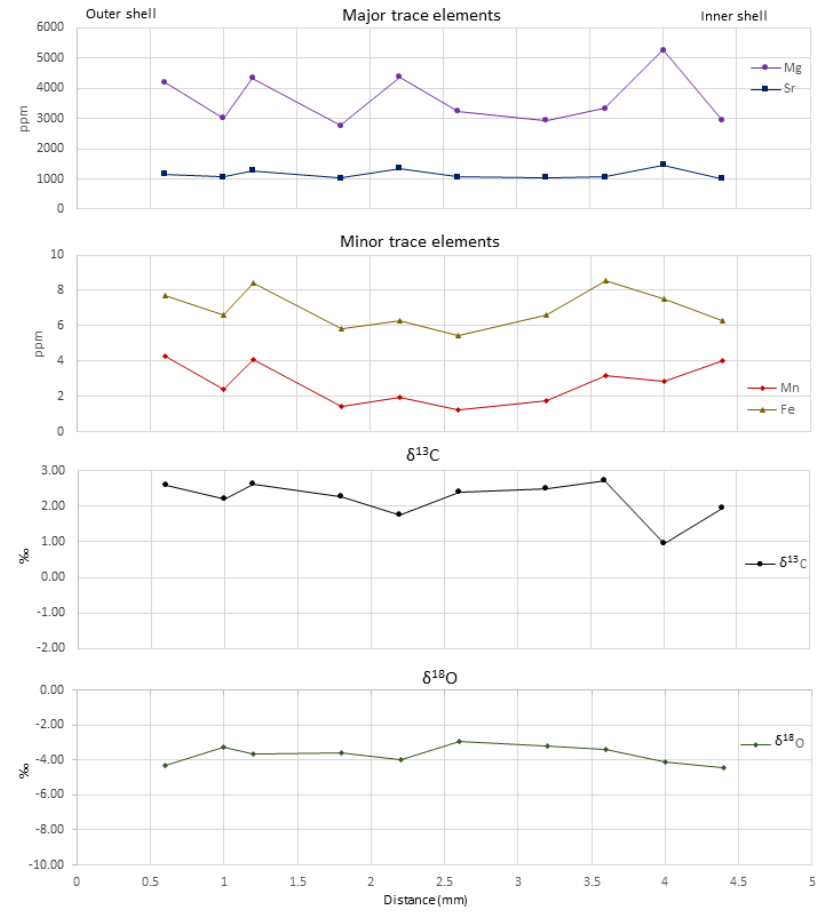


Figure 4-13. Trace element and stable isotope data for transect through non-luminescent area of the shell ~1 cm from the anterior margin of *G. okensis*, specimen RCK 28bis, transect two (RCK 28bis_2).

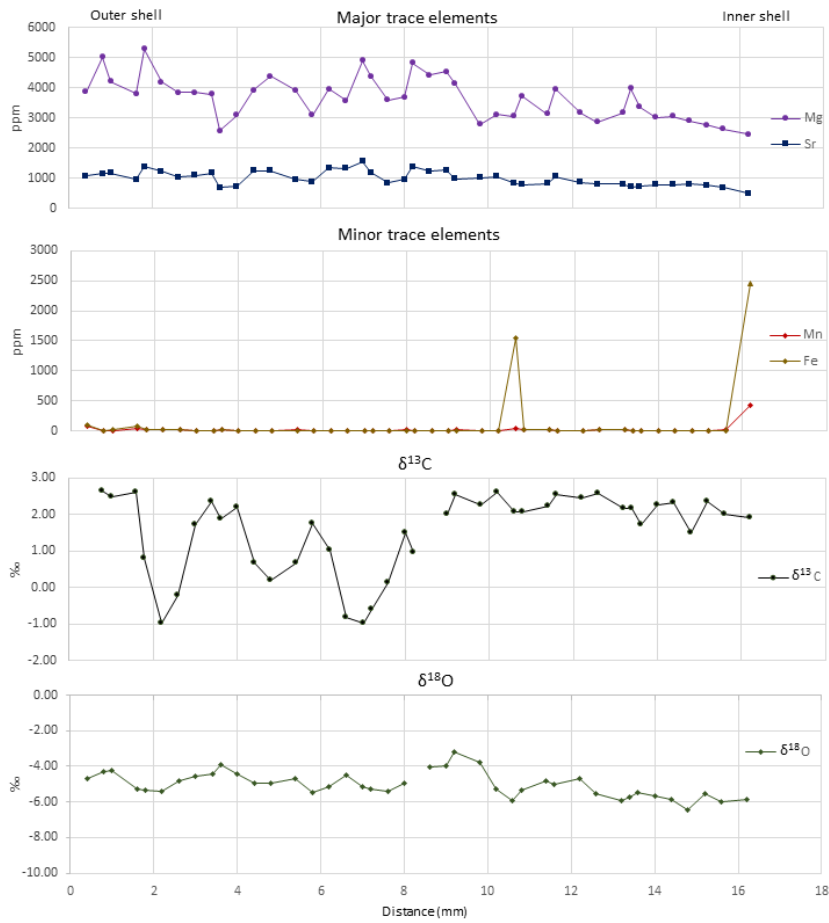


Figure 4-14. Trace element and stable isotope data from a transect through the non-luminescent, central shell region of *Gigantoproductus* sp. specimen XG.

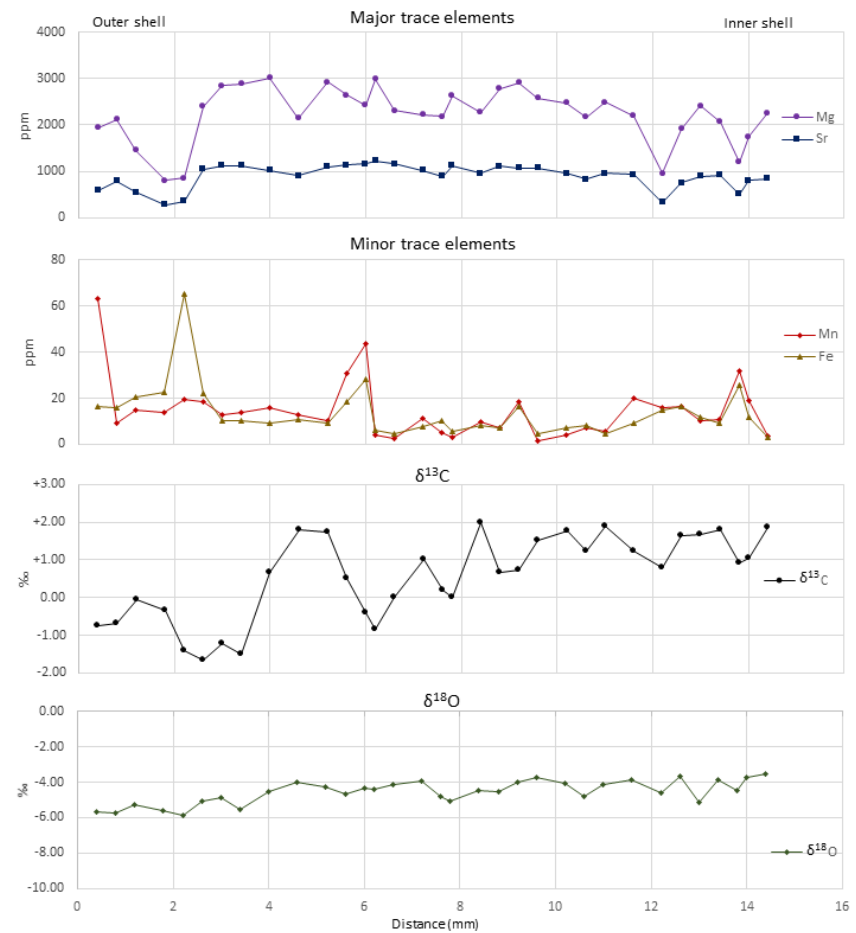


Figure 4-15. Trace element and stable isotope data from a transect through the non-luminescent central shell region of *G. inflatus*, specimen OAW 03.

4.4 Discussion

4.4.1 Comparing the geochemistry of shell and non-shell or recrystallized materials

Comparing the geochemistry of shells analysed in this study to that of well-preserved ancient and modern biogenic calcite provides a good benchmark for preservation. Most shell samples from this study yielded Sr, Mn and Fe concentrations within the expected range of well-preserved modern and fossil Palaeozoic brachiopod calcite (Table 4-1). Additionally, many non-shell materials analysed also fall within these ranges.

For some non-shell materials (i.e. bulk rock samples) it may be expected that they would have a comparable chemistry to that of the shell calcite, given they may have been precipitated in, or close to, equilibrium with seawater and may not have undergone subsequent diagenesis. While some additionally analysed materials are more likely to have a chemistry more representative of diagenetic alteration, such as the recrystallized umbonal shell calcite which appears brightly luminescent, appears milky in colour (compared to the 'clear' grey colour of the non-luminescent shell) and has little or no retention of ultrastructure fabric. Additionally, some materials, such as the bulk rock within the geopetal, may represent a combination of primary and diagenetic chemistry as they contain some recrystallized material, but also possibly some primary groundmass which may not have been altered. These analyses also occur alongside the analysis of some luminescent shell calcite, which typically occurs at the outer and inner shell margins of multiple shell specimens analysed and two samples taken from the luminescent shell calcite, close to a fracture present in specimen RCK 6bis. As these data points are commonly classified as altered based on their bright luminescent and poor ultrastructure retention it may be expected that their chemistry is representation of material which has undergone some degree of diagenetic alteration.

When these additional data are compared to shell data, some materials can be differentiated from the non-luminescent shell data based on differences in their trace element composition. For example, a distinct difference is observed between non-luminescent shell material and the recrystallized umbonal shell calcite, the calcitic geopetal cement, and the recrystallized matrix sample. Meanwhile, there is less differentiation between non-luminescent shell samples and the luminescent shell calcite,

the bulk rock between valves between valves and the general groundmass sample. In all cases, whether geochemical differences are well or poorly pronounced, all of these additional materials are most easily differentiated from shell specimens via their Sr and Mg concentrations. Additionally, the recrystallized umbonal shell calcite, the calcitic geopetal cement, and the recrystallized matrix samples can be differentiated from shell samples based on Mn and Na concentrations. Despite observed and theoretical differences between different types of additional materials, much of this data, including those more likely to represent primary and those more likely to represent diagenetic fluids, are still within the range of well-preserved modern biogenic calcite. Therefore, those data points (shell and non-shell) which lie outside the range of modern brachiopods, are considered poorly preserved, but, for those that lie within this range, it cannot be assumed that they are well preserved. This overlap of values derived from modern material with the material that appears not to be primary, such as recrystallized materials, demonstrates that, for this dataset, the geochemical parameters derived from modern brachiopods are mostly not suitable for detecting diagenetically-altered material and should be coupled with additional analyses and screening processes. This is complementary of the findings outlined by Brand et al., (2011) which demonstrated that for these reasons it is necessary to use a multi-proxy approach to the screening of biogenic specimens. This therefore highlights the importance of prior ultrastructure and cathodoluminescence analyses occurring alongside trace element screening.

Additionally, although not focused on within this study, it is also noted that an offset of $\delta^{18}\text{O}$ values between the dorsal and ventral valves of some brachiopod species has been reported (Curry and Fallick, 2002; Parkinson et al., 2005). This is not observed within this study therefore suggesting that the dorsal valve chemistry is not significantly different from that of the ventral valve within *G. inflatus*, although this should be treated with caution as this interpretation is based on a very limited dataset of only two ventral valve samples from a single *G. inflatus* specimen which is presented in Appendix F.

The different geochemical signals of non-luminescent shell data and non-shell and recrystallized materials was tested using parameters Mn, Fe, Mg, Sr, $\delta^{18}\text{O}$ and $\delta^{13}\text{C}$, via principal component analysis (Figure 4-16). In this statistical test data points are mostly separated into two distributions primarily consisting of shell and many non-biogenic and

recrystallized sample data along principal components 1 and 2. The distribution of data illustrates that end-member samples do have different geochemical signatures to shell data, and therefore comparisons of geochemical data from end-members and shells can be used to identify diagenetic alteration within a shell. Principal component 1 (PC1) appears to be the greatest axis of separation. Parameters Mn, Sr, Mg and $\delta^{18}\text{O}$ show the greatest loading on this axis with the eigenvectors for these elements being 0.478 for Mg, -0.442 for Mn, 0.526 for Sr and 0.401 for $\delta^{18}\text{O}$. There is some overlap between shell and non-biogenic calcite samples, which is to be expected, as some non-luminescent or partly luminescent shell material analysed within the central shell region may be altered and equally, some non-shell samples, such as primary groundmass, may have a geochemistry similar to the primary shell calcite if it was precipitated at or near to chemical equilibrium with seawater.

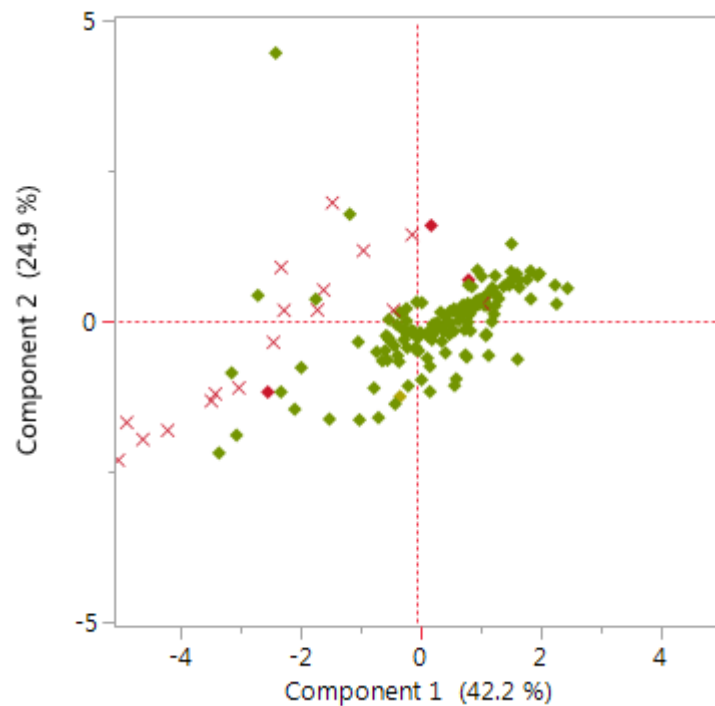


Figure 4-16. Principal component analysis (PCA) of all shell (green) and non-shell and recrystallized materials.

Red with 'X' represents geopetal calcite, recrystallized matrix, recrystallized umbonal shell calcite, matrix between valves, the general groundmass and luminescent shell. Red diamonds represent luminescent shell calcite occurring at the outer or inner shell margin. The data shows distribution of the data along principal components 1 and 2 using parameters Mn, Fe, Mg, Sr, $\delta^{18}\text{O}$ and $\delta^{13}\text{C}$. Parameters Mn, Sr, Mg and $\delta^{18}\text{O}$ show the greatest loading (eigenvectors) on PC1 (Mn = -0.442 , Sr = 0.526, Mg = 0.479 and $\delta^{18}\text{O}$ = 0.401). Parameters (Mn, Fe and $\delta^{13}\text{C}$) show the greatest loading on PC2 (Mn = 0.481, Fe = 0.657 and $\delta^{13}\text{C}$ = 0.456).

4.4.2 Assigning geochemical parameters for identifying well preserved biogenic calcite

Given that variability between and within fossil groups is common (Brand et al., 2003; Korte and Hesselbo, 2011; Popp et al., 1986) and the potential for unknown metabolic effects to have occurred (e.g. with Sr and Mn within *Gigantopproductus* species (Grossman et al., 1993)) some studies have concluded that it is problematic to assign absolute cut-off concentrations for trace elements within well-preserved calcite (Brand et al., 2011). Additionally, during diagenesis, increased Sr depletion occurs with increased diagenetic alteration (Ullmann and Korte, 2015) meaning that depletion may have occurred but may not be large and easily identifiable. For all elements, if the diagenetic fluids are similar to the well-preserved biogenic calcite (i.e. if they have undergone early diagenesis in the marine realm), then differentiating between well-preserved biogenic calcite and altered biogenic calcite is difficult. For these reasons, geochemical parameters are often used as a guidance rather than absolute cut-off values. This concept of a 'non-static approach' (Ullmann and Korte, 2015) is not without its problems and can lead to further ambiguity. However, it has been adopted by other authors (e.g. Brand et al., 2007) as it allows low/high parameters to be assigned whilst also considering natural variability. In this study cut-off parameters are assigned to Mn, Sr and Fe concentrations, however the sample point is discarded only when two or more of the trace element indicators suggest alteration.

In addition to observed natural variability in fossil groups, further complications arise given that it has recently been demonstrated that not all trace elements with the tertiary shell layer are precipitated in equilibrium with seawater (Garcia et al., 2017). This means that anomalous trace element values may be caused by disequilibrium rather than diagenetic alteration, while the corresponding $\delta^{18}\text{O}$ value may in fact still be representative of seawater. Therefore, when cut-off parameters are assigned to identify altered shell material based on trace element concentrations, there is a risk that some material which has well-preserved $\delta^{18}\text{O}$ data that is in equilibrium and therefore may be suitable for use as a palaeothermometer (if it is also fabric retentive and non-luminescent) may be discarded. However, it is considered that in this case, given the large dataset it is preferable to assign strict parameters (e.g. very low Mn or very high Sr) and potentially exclude some well-preserved material, rather than employ generous

limits to account for disequilibrium. When generous limits are adopted, there is a risk that some altered material may be unidentified, potentially leading to altered and inaccurate palaeotemperature calculations and invalid interpretations. Alternatively, it is considered that it is preferable to exclude some data points due to potential alteration as this means subsequent calculated temperature from $\delta^{18}\text{O}$ data can be interpreted with confidence that no (or very little) altered material is causing bias in the dataset.

When identifying alteration based on trace element analyses it is difficult to establish if alteration within the marine realm has occurred, as the diagenetic fluids (marine waters) are likely to be similar to the ambient seawater from which the biogenic calcite was precipitated in equilibrium with, especially given that these carbonates are formed in oxic environments and not on the continental shelf where subsequent shallow marine pore waters may be anoxic (Morse and Mackenzie 1990). When assessing the likelihood of marine alteration, it is perhaps best to consider the heterogeneity in trace elements such as Sr and Mg that are thought to be influenced by environmental factors. If the entirety of a specimen has undergone marine diagenesis it may be expected that the natural variability has been removed and the Sr and Mg content in shell is homogeneous as the marine diagenetic fluids and the shell calcite near equilibrium.

Sr and Mn

Brand and Veizer (1980) demonstrated that Sr and Mn are useful diagenetic indicators as they have very different distribution coefficients and meteoric fluids have very different Sr and Mn concentration than marine waters. Therefore, plotting Sr against Mn can be a good indication of preservation of specimens and has been used by many authors (e.g. Brand and Veizer, 1980; Korte et al., 2003). To date, this is the most common method of identification of diagenetically altered calcite via trace element chemistry (Swart, 2015), although, as demonstrated by Brand et al. (2011) it should not be used as an isolated trace element screening mechanism it can help with identifying alteration. Azmy et al. (2011) also showed that calcite Sr depletion and Mn enrichment can occur by varying degrees depending on the starting geochemistry of the material, and that patterns of alteration can differ between geological time periods

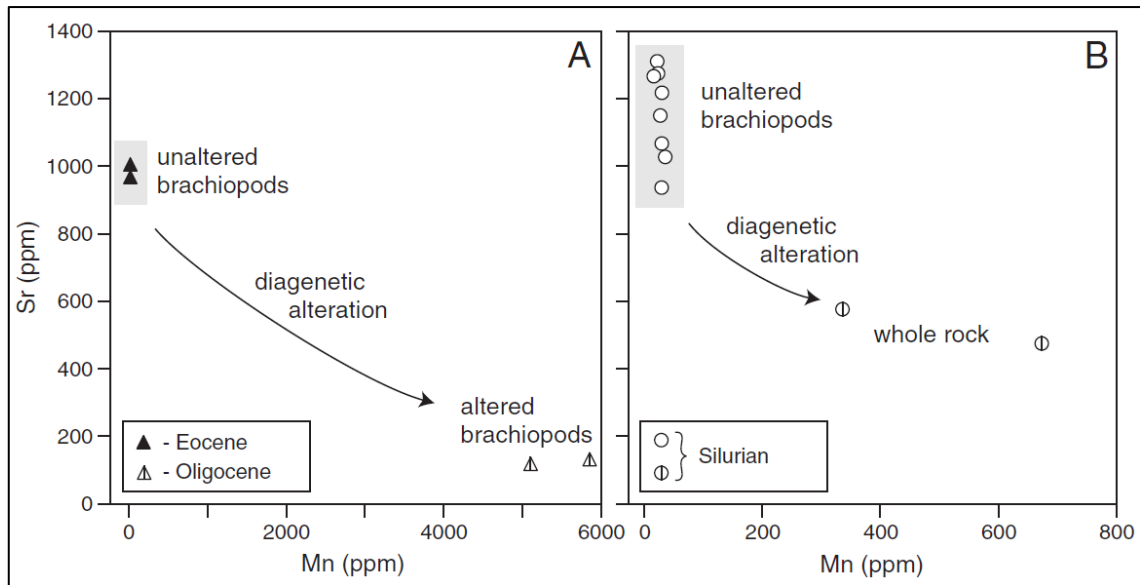


Figure 4-17 Patterns observed in Sr and Mn concentrations within different materials.

Unaltered brachiopods from the Eocene and Silurian have elevated Sr and depleted Mn concentrations compared to their altered counterparts and whole rock material. The shift between these two materials represents a diagenetic trend. Figure taken from (Azmy et al., 2011).

Given that diagenesis occurs on a spectrum, if trace elements were precipitated in equilibrium with seawater, then a correlation between Sr and Mn may be indicative of alteration. In this study, Mn and Sr only correlate within one *G. okensis* specimen, RCK 28bis, and one *Gigantoproductus* sp. specimen, XG. A plot of Mn against Sr for shell and non-shell materials from this study illustrates that some non-shell materials, typically the matrix and groundmass samples and the recrystallized samples are depleted in Sr and enriched in Mn when compared to the non-luminescent shell samples. This suggests that some of the groundmass samples were either not precipitated in equilibrium with ambient seawater and/or they have undergone diagenesis with fluids of depleted Sr and enriched Mn concentrations.

In this dataset where materials are depleted in Sr and enriched in Mn, compared to the non-luminescent shell calcite of the inner shell, Sr concentrations are typically below 700 ppm and Mn concentrations above 25 ppm, whilst most shell data have Mn concentrations below 25 ppm and Sr concentrations above 700 ppm. Therefore, these values are used as a parameter for distinguishing between well and poorly preserved materials within this data set. For samples of all materials that plot outside of these parameters, it is suspected that they may have undergone some diagenetic alteration

(Figure 4-8). This is supported by the fact that many of the samples with Sr concentrations below 700 ppm and Mn concentrations above 25 ppm are from the shell margins and therefore are within the areas where luminescence is commonly seen. However, it should also be considered that some of the outlying shell data points may have trace element chemistry which was not precipitated in equilibrium with seawater and therefore their trace element chemistry indicates alteration, whilst their stable isotope chemistry was precipitated in equilibrium and has remained pristine.

Many authors (Bruckschen et al., 1999; Mii et al., 1999; Popp et al., 1986) have shown that species of *Gigantoproductus* contained significantly lower Mn concentrations and increased Sr concentrations compared to other biogenic calcite materials (including that of other brachiopods) possibly due to biological fractionation (Popp et al., 1986). This may contribute to the significantly lower Mn concentrations observed in these data compared to previous studies of different genus. However, incorporation of Mn can only occur if it is present within the water column and availability of Mn requires the oxygenation levels of ambient water to decrease (Swart, 2015) and the Mn concentrations observed in this study are even lower than those reported in the previously mentioned studies that analyse species of *Gigantoproductus*. The large size of the *Gigantoproductus* and their high abundance at the two localities (Ricklow and Once-A-Week quarries) suggests that these environments were highly oxygenated (Chapter 2) therefore, low availability of Mn due to high oxygenation levels likely resulted in low Mn concentrations within species of *Gigantoproductus* examined in this study. This may account for differences between *Gigantoproductus* species of this study and those studied by the (Bruckschen et al., 1999; Mii et al., 1999; Popp et al., 1986) whilst the disparity between different genera appears to be a biological effect. It is also worth considering that if dissolution of the surrounding matrix during early diagenesis was the main source of diagenetic fluids within this system, then given the low Mn concentrations in the rock matrix (likely due to its high bioclastic content), even shell calcite that has undergone early diagenesis may contain little Mn. Therefore, assigning low Mn concentrations as a preservation parameter is rational.

Fe

Previous authors have observed variable Fe concentrations within modern brachiopods (e.g. Popp et al., 1986) suggesting it is not a reliable indicator of alteration. However, as Fe is known to behave in a similar manner to Mn (Ullmann and Korte, 2015) elevated Fe concentrations may also be indicative of alteration. In well-oxygenated conditions Fe would be less abundant in the water column and therefore also in the shell calcite and coeval matrix. For these reasons, a relatively low upper boundary of 25 ppm for Fe is used as a preservation parameter in this study.

It is noted that low Fe concentrations are observed within many shell and non-biogenic calcite samples (~6 ppm) while samples from the groundmass between the valves often have much higher (up to 400 ppm). This may reflect an anoxic microenvironment within the cavity between the valves as the soft body decays.

Fe concentrations observed in this study are highly variable, both within individual shell specimens and across different materials, perhaps mimicking the finding of Popp et al. (1986) and it is noted that Fe concentrations may not be in equilibrium with primary seawater (Garcia et al., 2017) suggesting that they may not be a reliable indicator of alteration. However, where large ranges in concentration occur within a single specimen (e.g. from 6.6 to 275 ppm as is seen in *G. inflatus*, specimen RCK 28, or from 0 to >2000 ppm, as is observed in *Gigantoproductus* sp., specimen XG), it is reasonable to conclude that the elevated concentrations are caused by secondary processes as this range in concentration is not likely to be caused by natural variation or biogenic fractionation in oxygenation conditions.

Mg

Theoretically, as Mg and Sr behave similarly during diagenesis (Swart, 2015), by plotting Mg against Sr, the concentration of Mg within well-preserved biogenic calcite can be estimated given that an Sr cut-off parameter has been assigned. However, because of the complexity of the environmental influences involved in the incorporation of Mg into the shell (e.g. salinity, temperature, growth rates) (Mii and Grossman, 1994), and potentially disequilibrium of both elements, within these data defining an Mg 'cut-off', whilst ensuring no natural variation is lost is challenging.

A strong positive correlation between Mg and Sr is seen within all shell specimens indicating that they are likely influenced by the same factors. All non-biogenic calcite and recrystallized materials analysed have Mg concentrations below 2000 ppm and all shell samples (excluding one sample from *G. inflatus* OAW 03) that have Mg below 2000 ppm have either Mn concentration above 25 ppm, Sr concentration below 700 ppm, or both and therefore would already be identified as potentially poorly preserved. This means that applying an Mg cut-off parameter to this dataset is not necessary.

Na

Similarly, Na has been shown to correlate with Mg and Mii and Grossman (1994) also demonstrated that Na concentrations negatively correlate with $\delta^{18}\text{O}$, suggesting that Na concentration increases with temperature. However, because of a lack of understanding of the behaviours of Na during diagenesis (Ullmann and Korte, 2015) and the likelihood that it is influenced by environmental factors, Na is not discussed further.

It is noted here that all of those data points that are identified as anomalous in Figure 4-8 have elemental concentrations outside of the well-preserved parameters and are excluded on the basis of poor preservation. This is with the exception of three data points, however these data points do not occur as anomalies for all the elements of interest and therefore cannot be excluded from the dataset (as this would make Spearman's rank correlations invalid). Additional to this, despite being identified as anomalous to this dataset, they illustrate high Mg and Sr values, but are still within the realms of what may be expected of well-preserved Mississippian biogenic calcite. This is seen as further justification that the parameters assigned for poorly preserved and well-preserved materials are suitable for this dataset.

4.4.3 Using $\delta^{18}\text{O}$ and $\delta^{13}\text{C}$ to cross-check preservation

Typically, $\delta^{18}\text{O}$ values should not be used to directly assess preservation. It is possible, however, for these data to be used alongside trace element, CL and ultrastructure assessments as an additional preservation cross-check.

A 'typical' diagenetic $\delta^{18}\text{O}$ component has lower values caused by meteoric water or due to recrystallisation under increased temperatures during burial. If diagenesis has

occurred, it would therefore be expected that $\delta^{18}\text{O}$ is lower in those samples, which have undergone increasing diagenesis (Swart, 2015). The interpretation of $\delta^{13}\text{C}$ during diagenetic processes is less well constrained, however, like $\delta^{18}\text{O}$, lower values are generally thought to indicate diagenesis (Swart, 2015; Ullmann and Korte, 2015). Based on these understandings of the diagenetic trends of $\delta^{18}\text{O}$ and $\delta^{13}\text{C}$, if alteration is pervasive, a correlation between $\delta^{13}\text{C}$ and $\delta^{18}\text{O}$ may be expected.

A significant positive correlation is observed within the $\delta^{18}\text{O}$ and $\delta^{13}\text{C}$ data in the data from the non-biogenic calcite and recrystallized materials and when plotted with shell data there is some separation between different materials. The lowest $\delta^{18}\text{O}$ values are present within samples of the recrystallized umbonal shell calcite and the secondary calcite cement of the geopetal infill, which are both materials that are not likely to have been precipitated in equilibrium with seawater and are likely representative of diagenetic processes. Additionally, low values (significantly lower than the average non-luminescent shell values) are also observed in some groundmass and recrystallized matrix samples; these are samples of material that may contain a mixed signal of primary and diagenetic chemistry. However, given their decreased $\delta^{18}\text{O}$ values compared to much of the non-luminescent and fabric retentive shell calcite, it is suggestive that some of these materials no longer represent the original seawater chemistry and present a $\delta^{18}\text{O}$ signal indicative of *some* diagenetic alteration or secondary mineralisation. Therefore, assigning a parameter to cross check for preservation based on $\delta^{18}\text{O}$ values of these materials is valid. This was done by identifying the highest $\delta^{18}\text{O}$ value from the materials previously discussed, which, in this case, is -5.37‰ . This value is therefore used as a cut-off parameter and any sample points with $\delta^{18}\text{O}$ lower than -5.37‰ are identified as possibly having undergone some diagenetic alteration. Angiolini et al. (2012) determined $\delta^{18}\text{O}$ values between -4.4‰ and -6.4‰ in non-luminescent shell calcite from the inner prismatic shell of Visean *G. aff. okensis*. The cut-off applied in this study is therefore almost exactly in the middle of this range. It is also noted that Angiolini et al. (2012) also determined decreased $\delta^{18}\text{O}$ values (-11.9‰ to -7‰) from shell material to be evidence of diagenetic alteration.

$\delta^{18}\text{O}$ data can then be compared to trace element data as it might be expected that data points with Mn, Sr and/or Fe outside of well-preserved parameters also have $\delta^{18}\text{O}$ below

-5.36‰. However, this is not the case for the non-luminescent shell data (Figure 4-17), suggesting that some trace elements may have been precipitated in disequilibrium with seawater or that the two systems have been influenced by different diagenetic process. ^{13}C and $\delta^{18}\text{O}$ of shell specimens with one or two diagenetic indicators (i.e. Mn, Fe, Sr outside of the cut-off parameter) are highlighted in Figure 4-17. Most shell data points have $\delta^{18}\text{O}$ values above the diagenetic cut-off and these data points include many data points that have two or more trace element values within the diagenetic range. There are also data points that have no trace element values indicative of diagenetic alteration yet have $\delta^{18}\text{O}$ values of less than -5.37‰. However, as previously discussed it is seen as preferable within this study to continue to exclude these data points as there remains some possibility that they have also undergone some diagenetic alteration.

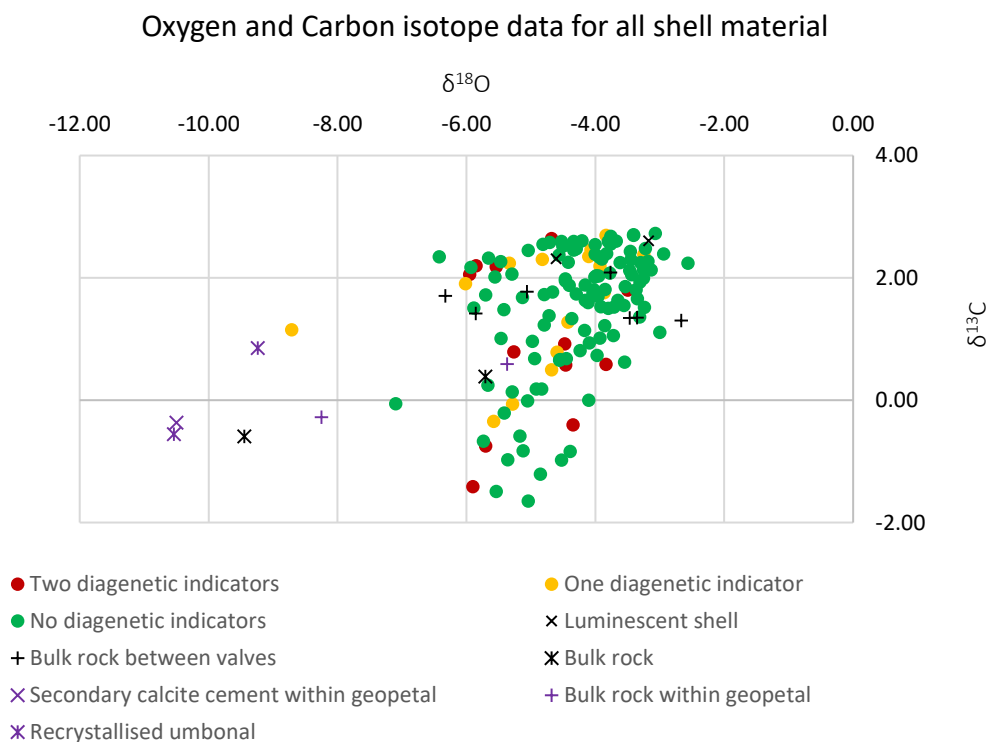


Figure 4-18. Carbon and oxygen isotopes of shell specimens with diagenetic indicators highlighted.

Data points with two diagenetic indicators have a combination of trace element values of Mn or Fe above 25 ppm and Sr below 700 ppm. Of the 138 samples from shell calcite, 19 have $\delta^{18}\text{O}$ values less than -5.36‰. Of these data points, five have two trace element values indicative of alteration and four have one trace element diagenetic indicator. Note that 12 out of the 19 samples are from specimen XG.

Understanding correlations within a dataset is complex as some elemental variations are influenced by preservation, some by environmental factors, and in many cases, they are influenced by a combination of both of these factors as well as possibly not having been precipitated in equilibrium with seawater. It is noted that within all these specimens analysed the combination of elements that correlate are not consistent, suggesting that the influences on individual specimens are likely different, thus highlighting that individual specimens should be analysed separately.

Angiolini et al. (2012) identified several possible types of diagenesis occurring within a single specimen from the Derbyshire carbonate platform. They similarly identified decreased Sr and increased Mn without a notable difference in Mg at the outer shell margin, which was also coupled with decreased $\delta^{18}\text{O}$. Whilst also identifying areas of the shell with elevated Fe concentrations but Mn concentration not considered abnormal as well areas of the shell where Mg and Sr are depleted and both Mn and Fe are enriched. These patterns are also observed in this dataset, although no pattern in the location of each type of signal can be identified.

There are few correlations between trace element and $\delta^{18}\text{O}$ values. There is a significant negative correlation between $\delta^{18}\text{O}$ and Mn within one *G. okensis* specimen, (RCK28bis_2), and one *G. inflatus* specimen, (RCK 28) and between $\delta^{18}\text{O}$ and Fe within a single *G. inflatus* specimen, (OAW 03), and the *Gigantoproductus* sp. specimen analysed (XG) has a significant directional correlation with $\delta^{18}\text{O}$ and all trace elements excluding Fe. $\delta^{13}\text{C}$ correlates positively with Mg in specimen RCK 28, negatively with Fe in specimen OAW 03 and correlates with all trace elements with all trace elements in specimen RCK 28bis (Table 4-9). Whilst there are some correlations observed, there appears to be no pattern or trend in the observed element/isotope correlation and or the species of specimen in which they are observed.

The observed lack of correlation between Mg and $\delta^{18}\text{O}$ is coupled with a significant correlation between Mg and Sr. This suggesting that Mg and Sr are being influenced by the same process, which in turn, appear to be different to those influencing $\delta^{18}\text{O}$ values. This may be different diagenetic processes, or that both Sr and Mg have been similarly offset and have been both been precipitated in disequilibrium, by the same amount.

It is also noted that a significant positive correlation between $\delta^{18}\text{O}$ and $\delta^{13}\text{C}$ is observed in one *G. inflatus* specimen, OAW 03, which, given its trace element concentrations, appears to be mostly well-preserved, yet no correlation between $\delta^{18}\text{O}$ and $\delta^{13}\text{C}$ is observed in specimen XG where $\delta^{18}\text{O}$ correlates with trace element diagenetic indicators (i.e. Sr and Mn). Although, these correlations could be due to environmental or biological effects, given that this specimen (XG) contains multiple (13) data points with trace element values suggesting diagenetic alteration, this is probably not the case.

Within this dataset, it is not possible to confirm whether $\delta^{18}\text{O}$ increased during diagenesis, as there is no end-member sample for comparison. Periods of non-deposition can result in carbonate cementation at or near the sea floor forming hardgrounds. When this cementation occurs in cooler and/or deeper waters than the original sedimentation the $\delta^{18}\text{O}$ can be relatively increased. As no hardgrounds are present within either of the sections through the two study sites it can be assumed that the $\delta^{18}\text{O}$ has not been increased during secondary processes.

4.4.4 Modification of the dataset

Following the assignment of preservation parameters, those data that fall outside of these parameters can be excluded from the dataset. Tables 4-11 and 4-12 outline the minimum, mean, maximum and standard deviation of Mg, Sr, Mn, Fe, $\delta^{18}\text{O}$ and $\delta^{13}\text{C}$ of the well-preserved data points. Because the isotope sampling strategy often involves the combination of multiple laser data points (section 4.2.2.2) a mean of the trace element values incorporated within the single isotope sample is calculated. It is these averaged values that are presented in these data tables. Note that because it is decided that a data point should be excluded only if it has two out of the three (Sr, Mn and Fe) elements of interest outside of the preservation parameters, values for some of elements may be outside of the cut-off for individual elements.

Element of interest	Statistic/specimen	RCK 33	RCK 28	RCK 28bis	RCK 28bis_2	XG	OAW 03	RCK 6bis
	n	15	22	8	9	26	26	22
Mg (ppm)	Min	2174.00	2709.50	2783.50	2760.67	2572.00	961.00	1860.00
	Max	4338.00	4888.00	4580.00	5257.50	5293.00	3015.00	5820.00
	Mean	3180.84	3562.35	3511.25	3570.94	3936.97	2348.83	2999.67
	SD	625.91	474.13	570.06	866.32	690.26	485.36	1100.39
Sr (ppm)	Min	777.00	919.00	740.00	1006.00	688.00	328.57	668.67
	Max	1167.00	1164.00	1282.00	1464.00	1571.50	1220.00	1418.00
	Mean	959.88	1078.71	1075.63	1151.57	1110.33	948.67	1000.24
	SD	102.44	79.82	173.37	165.87	219.21	195.82	194.64
Mn (ppm)	Min	0.41	1.45	1.85	1.23	1.24	1.54	1.02
	Max	15.71	12.29	148.80	4.06	28.20	30.80	12.32
	Mean	3.15	5.42	28.76	2.54	9.49	11.20	4.39
	SD	3.97	2.84	49.53	1.05	7.23	5.81	3.12
Fe (ppm)	Min	0.00	7.73	3.40	5.44	4.41	3.00	0.41
	Max	6.80	200.00	6.30	8.55	24.14	22.08	6.96
	Mean	1.98	41.16	4.66	6.84	10.38	10.34	2.97
	SD	2.11	57.33	1.04	1.09	6.06	4.87	1.49

Table 4-11 Shows the Minimum (min) Maximum (max) mean and standard deviations of the elements of interest within the well-preserved dataset for individual specimens.

Element of interest	Statistic/specimen	All data
	n	128
Mg (ppm)	Min	961.00
	Max	5313.33
	Range	4352.33
	Mean	3219.86
	SD	891.58
Sr (ppm)	Min	328.57
	Max	1571.50
	Range	1242.93
	Mean	1048.77
	SD	184.85
Mn (ppm)	Min	0.41
	Max	148.80
	Range	148.39
	Mean	7.87
	SD	14.17
Fe (ppm)	Min	0.00
	Max	200.00
	Range	200.00
	Mean	7.69
	SD	26.31

Table 4-12 gives the minimum (min), maximum (max), range, mean and standard deviation (SD) of all of the well-preserved data points across all specimens.

Note that although decreased the standard deviation of both Sr and Mg is high which is likely because these elements may also be influenced by varying environmental factors.

Following the removal of all poorly preserved data points based on the previously outlined preservation parameters, distribution of the $\delta^{18}\text{O}$ values from this dataset are normally distributed with no anomalous data points (Figure 4-19). This may be expected if the data is representing seasonal variation.

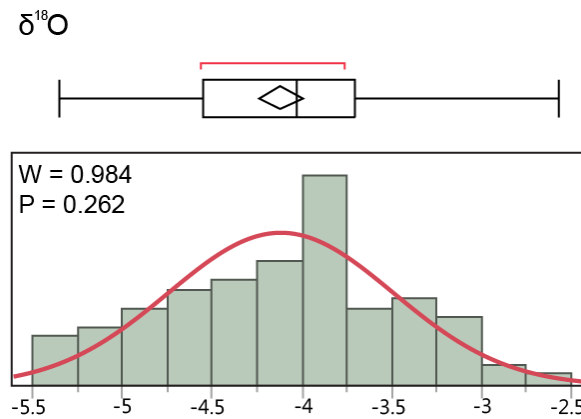


Figure 4-19 presents the distribution of the $\delta^{18}\text{O}$ data from all well-preserved data points.

4.4.5 Identification of diagenetic processes

Although dolomitisation has occurred on the Derbyshire carbonate platform, primarily occurs in two linear 'strips' the southern regions (south of Monyash) (Aitkenhead et al., 1985, Ford, 2002). Dolomitisation is not observed within the Eyam limestone formation and evidence of it was not observed in the field studies or identified within any thin sections analysed in Chapter 2. Therefore, the effects of this diagenetic process occurring within the selected *Gigantoproductus* specimens can be discarded. Similarly, there is no reason to consider the effect of calcitisation (the process of aragonite dissolution and re-precipitation as calcite) or the alteration of high Mg calcite into low Mg calcite as the primary material of the specimens is low Mg calcite.

Multiple studies have analysed the diagenetic history of the Asbian and Brigantian limestones of the Derbyshire carbonate platform (e.g. Walkden and Williams (1991), Walkden and Berry (1984), Hollis and Walkden (2002) and Hollis and Walkden (2012)). These studies identified that the Eyam Limestone Formation, has undergone multiple phases of diagenetic alteration, which include early marine, meteoric and deep burial diagenesis.

Walkden and Williams (1991) identified four zones of cements however, the geochemistry of a single zone of alteration was observed to be heterogeneous. For example, some zone one cements are enriched in Mn and Fe and depleted in Sr by several hundred ppm whilst others show no significant trace element alteration. For Mn and Fe to be enriched anoxic environments must have been present, while these elements remaining unaffected by some modes of alteration suggests some phases of alteration occurred under oxic conditions (Walkden and Williams, 1991) indicating an evolution in diagenetic fluids and environments occurring during a single phase of cement formation.

Syntaxial cementation associated with crinoid ossicles is commonly observed in many thin sections analysed in Chapter 2. This form of cementation was interpreted by Walkden and Berry (1984) as being the product of meteoric phreatic diagenesis and Walkden Williams (1991) also identify it within phases of burial diagenesis.

Burial diagenesis of the Eyam Limestone Formation discussed by Walkden and Williams (1991) identified mean Fe and Mn concentrations as high as 515 ppm and 1534 ppm respectively and a Sr concentration of 183 ppm. This observation is consistent with some of the data points observed in this study and further justifies the removal of these data.

Mg concentrations are commonly not depleted within diagenetic cements of the Eyam Limestone Formation (Walkden and Williams, 1991), possibly due to the presence of volcanic activity, which may have contributed Mg into the system (Macdonald et al., 1984). This form of alteration could account for the lack correlation between Mg and Mn, Fe and demonstrates that trace element data should be treated with caution as specimens that are not depleted or enriched in some elements should not automatically be classified as unaltered.

Although there is some evidence of these diagenetic processes having affected some data points with the specimens such diagenetic signals are not pervasive. This may be a reflection of the specific diagenetic processes occurring locally and the stability of the biogenic LMG calcite.

Stable isotope data are also used to detect diagenetic alteration. Burial diagenesis typically results in depletion of ^{18}O , caused by the temperature increase associated with burial changing the fractionation effect. This decrease in $\delta^{18}\text{O}$ with increased burial was

identified by Dickson and Coleman (1980) who identified a trend of increased $\delta^{18}\text{O}$ depletion from -2.5 to -12.4‰ through different cement zones. Alternatively, if alteration has occurred early, on the sea floor, changes in $\delta^{18}\text{O}$ may not occur or may not be obvious. Within meteoric diagenesis, the signal may be more complex depending on the environment (marine or non-marine) and whether or not the system is open or closed. Higher $\delta^{18}\text{O}$ values can also occur during diagenesis (Sample and Reid, 1998) via early cementation in cold waters, and interaction with evolved hydrothermal fluids. However, the environment from which these samples come suggest that the conditions required for this type of diagenesis were not reached within these gigantoproductids.

Walkden and Williams (1991) identified that all cements and whole rock compositions evolved towards heavier $\delta^{18}\text{O}$ and $\delta^{13}\text{C}$ values through all stages of diagenesis with the exception of the final phase of diagenesis where $\delta^{18}\text{O}$ reversed towards lighter values (as did $\delta^{13}\text{C}$ but to a less extent). More specifically early meteoric diagenesis is associated with $\delta^{18}\text{O}$ values of -9.6 to -6.8‰ (Hollis and Walkden 2002) and burial diagenesis.

Furthermore, the highest $\delta^{18}\text{O}$ value recorded within diagenetic calcite by Hollis and Walkden (2002) is -5.5‰ further demonstrating that the applied cut-off is sensible. Thus, indicates that the preservation parameter of -5.36‰ applied to this dataset would exclude material that has undergone early meteoric diagenesis.

Figure 4-20 compares stable isotope data from Walkden and Williams (1991) and this study. The figure demonstrates that there is little overlap between the isotope values from zone three cements (which Walkden and Williams (1991) consider to be the most pervasive phase of diagenesis within the Brigantian limestones of the Derbyshire carbonate platform) and the better preserved data points from this study. This figure highlights that the parameters assigned in this study appear to exclude most if not all altered material and that much of the shell data appears to be well-preserved.

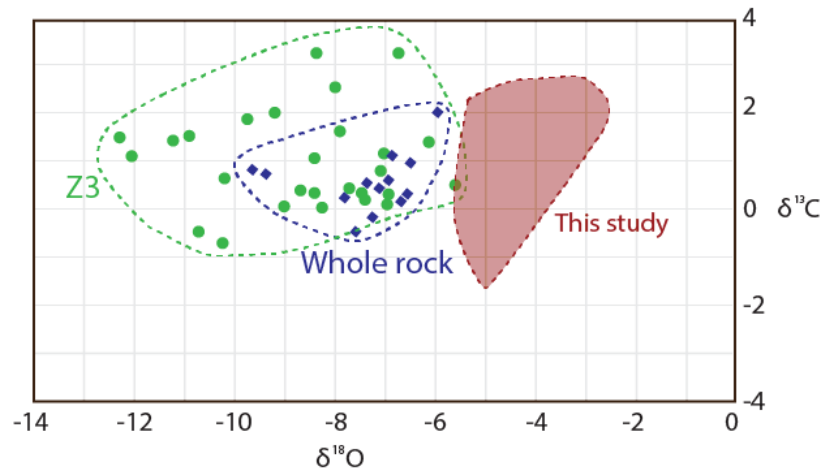


Figure 4-20 Comparisons of stable isotope data from Walkden and Williams (1991) and well-preserved data from this study.

Note minimal overlap between diagenetic cements and well-preserved data from this study. Z3 refers to the Zone three cements identified by Walkden and Williams (1991).

The trace element data appear to have undergone more alteration than the $\delta^{18}\text{O}$ data, suggesting that trace element chemistry may be more sensitive to the diagenetic processes than $\delta^{18}\text{O}$. During loss or incorporation of trace elements within the calcite lattice, single ions can be exchanged (affecting the geochemistry), whilst changing the stable isotope signal requires at least some partial dissolution followed by recrystallisation of the calcite lattice and exchange of the major elements. Additionally, given that most sample points which appear to be altered are identified as so based on their element chemistry or $\delta^{18}\text{O}$ values, but rarely both, it appears that the trace element and stable isotope data could have been influenced by different diagenetic processes. While the diagenetic end-members which show reduced Sr concentrations, increased Mn and lowered $\delta^{18}\text{O}$ values were influenced by both.

End-member materials which overlap with shell samples were likely precipitated from fluids with chemistry similar to those derived from the original environment. These may result in unevolved, early diagenetic fluids subtly altering the trace element chemistry of some shell samples. The very low $\delta^{18}\text{O}$ values seen in the diagenetic end-member samples suggests later freshwater diagenesis or alteration via much later hot marine fluids (that lead to lower $\delta^{18}\text{O}$) as also identified by Angiolini et al., (2012).

Within the Peak Limestone Group, on the Derbyshire carbonate platform, localised Mississippi-Valley-Type mineralisation and late diagenetic cements occur. The relatively

low temperature mineralisation events have a typical geochemistry resulting in galena and fluorite mineralisation alongside barite gangue and sphalerite (Hollis and Walkden, 1996). However, in the specimens analysed in this study a diagenetic signal corresponding to Mississippi-Type mineralisation is not observed. At Ricklow Quarry, there are no Mississippi-Valley-Type mineral deposits within close vicinity, however small amounts of bitumen have been observed at this locality. At Once-a-Week Quarry a large mineral vein containing lead and zinc mineralisation occurs close to the quarry. OAW 03 has four data points within the shell interior with Zn concentrations between 4 and 15 ppm whilst all other specimens have elevated Zn only at the outer shell margin (up to 90 ppm for specimen XG but less than 15 ppm in other specimens and frequently less than 5 ppm). No specimens have data points with Pb concentrations higher than 1 ppm other than a single data point at the outer shell margin of specimen XG. Additionally, given the change in temperature condition required for bitumen emplacement associated with Mississippi-Valley-Type hydrocarbon deposits present in the South Pennine Orefield (Ewbank et al., 1995) it would be expected that this may be demonstrated in the alteration of both the carbon and oxygen isotopes if the inner shell material were affected, which they appear not to be. However, it would be advised that if further work were to be carried out at the locality this issue should be further explored to ensure that shell material analysed have not been locally affected.

Ultrastructure and CL analyses indicate that Ricklow Quarry specimens appear better preserved than those from Once-a-Week Quarry, hence most trace element and stable isotope analyses were conducted on these specimens. Differences in preservation between the two localities may result from localised temperature variations influenced by the proximity of mineral deposits, and the generally higher permeability and porosity in the grainstones of Once-a-Week Quarry compared to the floatstones, packstones and wackestones at Ricklow Quarry (Garbelli et al., 2012).

The lack of correlation between $\delta^{18}\text{O}$ and Mg (both influenced by temperature during primary precipitation) could indicate that both Mg and $\delta^{18}\text{O}$ have been influenced by diagenetic processes, and therefore no longer preserve a primary temperature signal. However, if this were the case, if the entirety of the specimen had been altered it might also be expected that their concentrations and values would be homogenous across an

individual shell or perhaps a systematic pattern in the changing of Mg and $\delta^{18}\text{O}$ resulting in some correlation specimens, with multiple sample points representing the same diagenetic chemistry. Therefore it appears more likely that this lack of correlation is primary, as has been observed in some recent brachiopods (Milner Garcia et al., 2017), and is due to Mg not being precipitated in equilibrium with seawater. This further implies that Mg concentrations within species of *Gigantoproductus* cannot be used as a palaeothermometer, as has been demonstrated by some studies, such as Butler et al. (2015) Brand et al. (2013) Perez-Huerta et al. (2008).

4.5 Summary

By including the results of the cathodoluminescence and ultrastructure analyses, several criteria can be implemented to identify sample points that should, or should not, be used as a palaeotemperature proxy and are listed below.

- All data points at the extreme outer shell margin should be not be used as a palaeotemperature proxy, as these areas commonly show bright luminescence and lack of preservation of the ultrastructure (see Chapter 3 and confirmation in trace element data). It is suspected that these areas have undergone alteration because they are at the interface of the shell surface with the surrounding rock matrix. These shell areas are also commonly depleted in Sr and Mg and enriched in Mn and Fe.
- In material with good ultrastructure preservation that is non or poorly luminescent, data points with two trace elements with Sr <700 ppm, Fe and Mn >25 ppm will not be used as a palaeotemperature proxy in order to reduce the likelihood of including material which has undergone diagenetic alteration. This will likely result in some well-preserved material being excluded by applying this strict cut off due to precipitation in disequilibrium. This is seen as a preferable screening mechanism for this large dataset as it increases reliability of the resultant palaeotemperature data by ensuring as little as possible altered material is included.

- Given the strict parameters assigned above, data points with one trace element parameter (Sr, Fe or Mn) indicating diagenetic alteration may be used as a palaeotemperature proxy, but should be treated with caution.
- Given that the $\delta^{18}\text{O}$ data is used as a palaeotemperature proxy and it is suspected, based on this study, that the $\delta^{18}\text{O}$ system is different to the trace element system, a static cut-off is applied to this data and samples with $\delta^{18}\text{O}$ values below -5.36‰ are not used as a palaeotemperature proxy.

This process of specimen selection is also outlined in Figure 4-21 and Figure 4-22 demonstrates what data is excluded from a transect once the parameters are assigned (using specimen OAW 03 as an example).

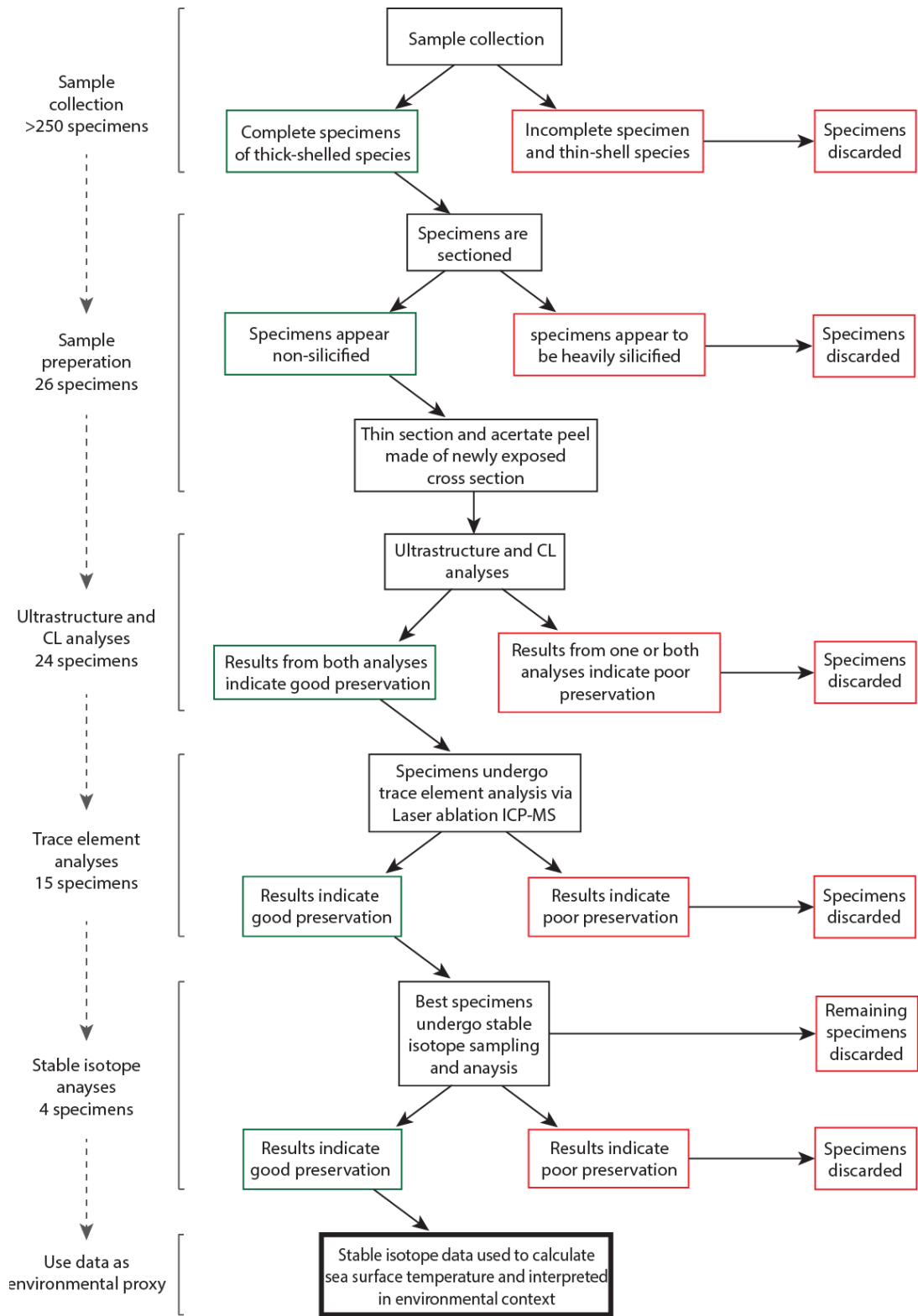


Figure 4-21 flow diagram illustrating the screening process adopted to select specimens.

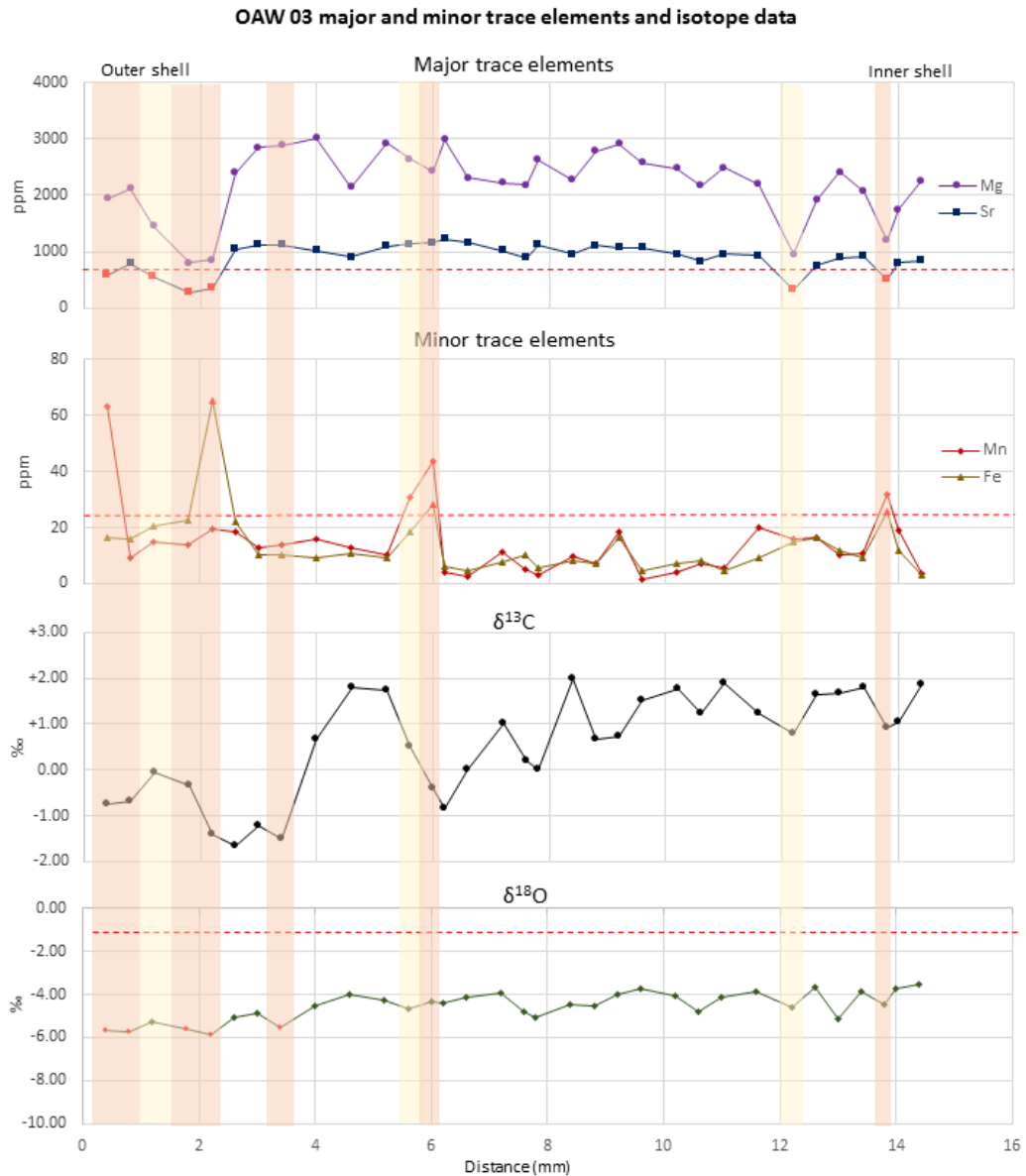


Figure 4-22. Trace element and stable isotope data for *G. inflatus*, specimen OAW 03 following preservation analyses.

Sample points that should not be used as palaeotemperature proxies highlighted by a red strip, and those that should be used with caution highlighted with a yellow strip.

Further to these guidelines, the following observations regarding the preservation of studied specimens are made:

- If published geochemical parameters for modern brachiopods and well-preserved Palaeozoic brachiopods (Table 4-1) were used to differentiate well and poorly preserved data points from this study, much of the non-shell material, which is likely to represent diagenetic chemistry, would be classified as well-preserved and almost all shell data, including that which shows luminescence. This highlights

the necessity of a multi-proxy approach to preservation screening as outlined by Brand et al. (2011).

- In many cases the geochemistry of the end-member samples and the shell samples are different (although not necessarily significantly) and therefore assigning new geochemical parameters for well-preserved biogenic calcite based on the chemistry of the diagenetic end-members is valid and suitable for this study.
- Although some end-members show evidence of meteoric diagenesis, there is no strong meteoric diagenetic signal within shell specimens with only a handful of shell data points having geochemistry suggesting some meteoric diagenesis has occurred.
- Detection of alteration within this dataset is difficult because of the multiple phases which may have occurred, all having slightly different geochemical signatures (see Walkden and Williams, 1991) some of which are not signals typical of common diagenetic environments. However, by applying a multiphase screening approach with multiple geochemical parameters assigned, the likelihood of identifying these atypical signals is enhanced.
- Additionally, it is suspected that detecting diagenesis within shell specimens is difficult as little material, especially that within the inner shell, has undergone significant alteration.
- The most commonly observed form of diagenetic alteration observed during ultrastructure analyses is localised mimetic silicification at the outer shell margin. This form of silicification has been observed at other locations on the Derbyshire carbonate platform as early stage diagenetic alteration (Hollis and Walkden, 1996).
- As the shell is less permeable than the surrounding matrix, it appears that diagenetic fluids are not able to penetrate the shell interior. Therefore, in many specimens whilst the outer shell margin may have undergone some alteration the shell interior remains well preserved. A similar phenomenon may also be the reason why patches of alteration surrounded by well-preserved material can occur within the shell interior. In this case, a point of weakness within the shell

may allow diagenetic fluids to partially penetrate the shell while the surrounding material remains impermeable. This is observed in specimen OAW 03 and may be particularly significant within *Gigantoproductus* species as the more porous laminar layer can contain diagenetic alteration while the thick, prismatic tertiary layer remains impermeable and well preserved. This theory is supported by the observation that luminescence and ultrastructure alteration occurs more commonly along growth lines and within the secondary laminar layer. This highlights the benefits of using a shell with a thick prismatic shell layer for such geochemical studies, as they are more likely to remain well preserved through geological time than shells with only a laminar secondary layer.

This study highlights the need for rigorous high-resolution preservation analyses and trace element analyses, as random spot sampling may not capture the true variability present within a specimen. The resolution of the preservation analyses should be at least as high as the subsequent stable isotope analyses or, if spot analysis is being conducted, the specimen should be analysed at a resolution where the secondary and tertiary shell layer can be differentiated. If high resolution sampling is not possible, then specimens with different 'types' of alteration or perhaps only subtle alteration within their shell interior may not be identified. Care must be taken in sample selection at every stage, beginning with sample collection in the field, through to stable isotope analyses to ensure only the best material is analysed, but, importantly, it is demonstrated that Mississippian species of *Gigantoproductus* can remain well preserved through geological time, and therefore, contain environmental information from the time of growth.

Chapter 5: Using high resolution $\delta^{18}\text{O}$ and $\delta^{13}\text{C}$ data from well-preserved species of *Gigantoproductus* brachiopods to help reconstruct palaeoenvironments of the Brigantian tropics

5.1 Background

The Eyam Limestone Formation of the Derbyshire carbonate platform was deposited in the late Brigantian (Gutteridge, 1987) during a highstand period (Strank, 1987) while the series of basins which form the Brigantian stratigraphy of the UK were connected. The connection of these basins formed an epicontinental seaway with an area comparable to the modern Mediterranean (Wells et al., 2005). During the Brigantian the UK, and this epicontinental seaway, was located close to the equator (Figure 5-1) within tropical regions, meaning that $\delta^{18}\text{O}$ data collected from well-preserved species of *Gigantoproductus* found in these rocks may provide information on the palaeoceanography (e.g. sea surface temperatures and/or $\delta^{18}\text{O}$ of seawater) for palaeoequatorial seas at that time.

The Brigantian stage at the end of the Visean (Chapter 2) is an interesting time in the Earth's climate history as the general consensus is that the onset of the major phase of glaciation associated with the Late Palaeozoic icehouse occurred around the Brigantian stage (Montañez and Poulsen, 2013). However, it is still debated as to whether the Brigantian stage represents a final warm period prior to the onset of the major glacial phase, as is suggested by much of the $\delta^{18}\text{O}$ data from ancient brachiopods (Giles, 2009), or, the glaciation was ongoing during the Brigantian, as is suggested by sedimentological

evidence, including in the UK, where sea level change has been associated with glacioeustasy (Wright and Vanstone, 2001). In either case, rocks of Brigantian age hold important information about the timing of the onset of the Late Palaeozoic icehouse that is yet to be fully understood. Therefore, additional studies into Brigantian climate can help resolve the timing of the onset of the major glacial phase, but the study, particularly of *Gigantoproductus* species, may help elucidate the nature of seasonal change during this time, thereby adding to the understanding of complex climate systems during a time of climatic change.

Seasonal cyclicity in $\delta^{18}\text{O}$ has been observed in multiple studies of both modern and ancient brachiopods and bivalves (e.g. Angiolini et al., 2012; Buening and Carlson, 1992; Ivany and Runnegar, 2010; Mii and Grossman, 1994; Perez-Huerta et al., 2008). Boucot et al. (2013) (Figure 5-1) shows that the UK lay within humid, tropical regions and multiple studies have identified seasonal rainfall in the Mississippian via evidence from tree rings (Falcon-Lang, 1999) and palaeosols (Adams, 1980; Wright, 1990).

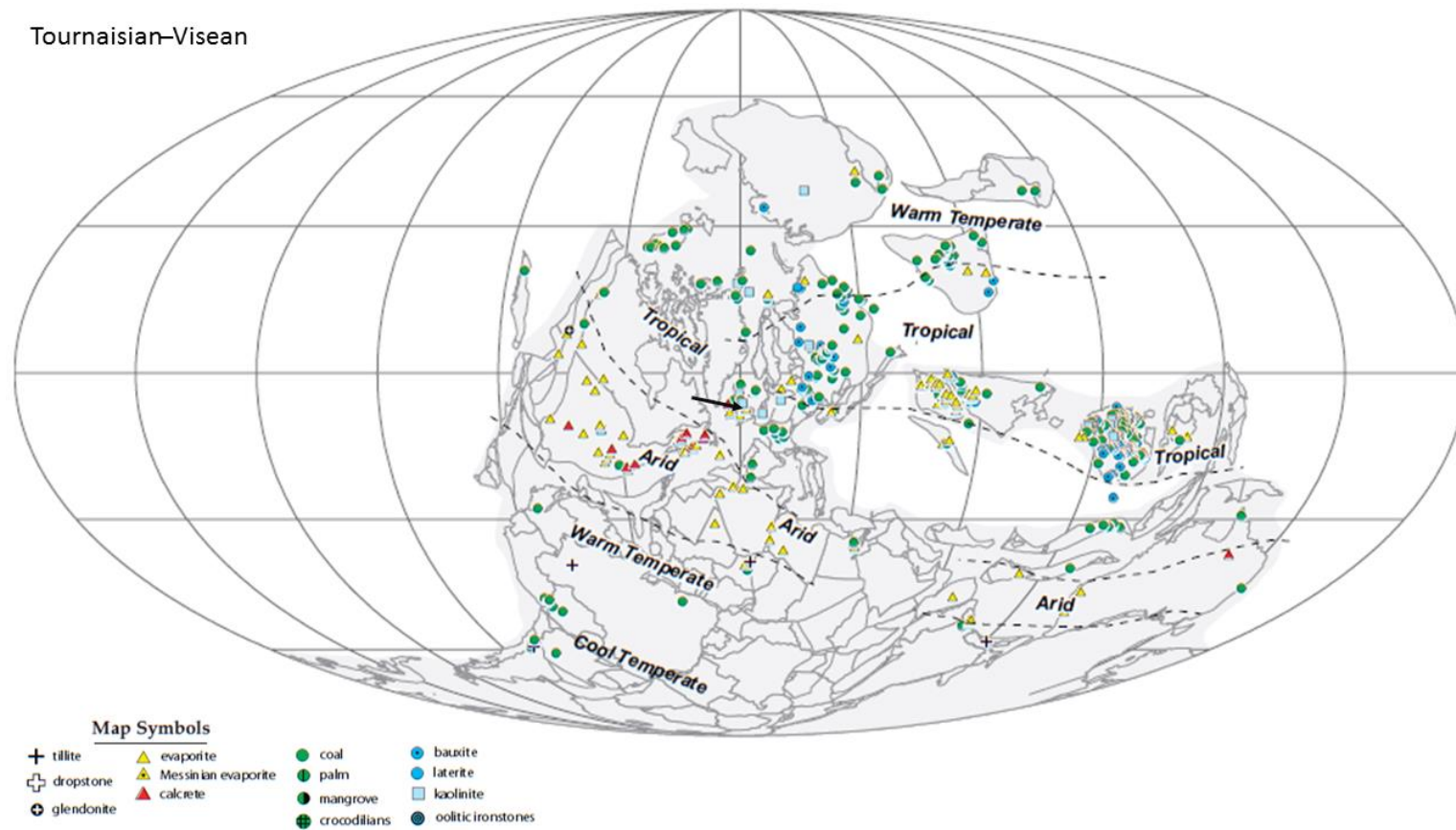


Figure 5-1. Continental configuration during the Tournasian-Visean (Brigantian = latest Visean) with tropical, warm and cold temperate and arid climatic regions shown. Black arrow indicates the location of the Derbyshire carbonate platform location just south of the equator within the tropical climate zone. Figure edited from Boucot et al., (2014).

Angiolini et al., (2012) was one of the first studies to undertake high resolution isotope analyses on a species of *Gigantoproductus* (*G. aff. Okensis*) from the Brigantian. They used a sampling technique whereby samples were taken across the growth episodes of the organism and therefore across time. Fourier transform analyses on the resultant data revealed a cyclical pattern within the dataset. This cyclicity was thought to represent seasonal variation in $\delta^{18}\text{O}$ within both the well and poorly preserved areas of a single specimen. Here the work of Angiolini et al. (2012) is built upon by considering data collected at high resolution from six specimens of *Gigantoproductus* from the Brigantian in order to better understand potentially seasonal variations that may be preserved in the $\delta^{18}\text{O}$ record of the shells and thus contribute to our understanding of the Brigantian tropical seasonality.

$\delta^{13}\text{C}$ and $\delta^{18}\text{O}$ data were collected using the methodologies outlined in Chapter 4. The full data set consists of nine shell transects from the same six specimens which underwent stable isotope analyses via the secondary methodology (Chapter 4). Data from specimen RCK 6bis, (*G. inflatus*) which was the focus of preliminary study, consists of three isotope transects that were sampled at different angles to growth. It is noted that these transects are at a lower resolution (ca. 1 sample every millimetre) than subsequent secondary sampling (~300 – 500 μm spatial resolution).

Although Mg concentrations were also collected and are used as a proxy for sea surface temperature, as $\delta^{18}\text{O}$ values have been shown to preserve seasonality in *Gigantoproductus* species (Angiolini et al., 2012; Mii and Grossman, 1994) only the $\delta^{18}\text{O}$ data are discussed in this chapter. Following the ultrastructure, cathodoluminescence and trace element preservation assessments, only well-preserved data points are used in the calculation of palaeotemperatures. Furthermore, as a species of *Gigantoproductus* has previously been shown to preserve seasonal cyclicity within their $\delta^{18}\text{O}$ data, concerns around the presence of kinetic metabolic fractionation (vital effects) on the isotope data are discarded, this because metabolic fractionation is a biological effect and therefore it is sensible to assume that it will influence all species and individuals in the same way. Additional to this, when kinetic fractionation has been identified it typically affects the primary shell layers or specialised areas of the shell (i.e. the muscle scars; Carpenter and

Lohmann, 1995) neither of which have been analysed in this study. Overall, only well-preserved data are presented ensuring that these data optimise the potential for obtaining palaeo-sea surface temperatures.

The principal of using $\delta^{18}\text{O}$ data as a palaeotemperature proxy relies on the theory that the fractionation of oxygen is temperature dependent (Dickson 1990). Therefore, by knowing that fractionation is dependent on temperature, assuming that the material is precipitated in equilibrium with the surrounding seawater and that after precipitation no secondary alteration of the stable isotope ratio has occurred, the ratio of one isotope to another can be used in a palaeotemperature equation to calculate the temperature of the water in which the material was precipitated. There are multiple version of palaeotemperature equations that utilise the ratio of oxygen stable isotopes (see Grossman 2012 for a summarised review) and they are derived in several different ways. Theoretically, the fractionation coefficient can be calculated using the thermodynamic relationships and bond vibration frequencies (Sharp 2006). However, to improve the accuracy and precision of this proxy further experimental work which includes precipitation mineral in a controlled environment and recording the relationships between oxygen isotope fractionation and temperature has been conducted. Generally there are two types of experimental work that have been conducted with the aim of refining the original Palaeotemperature equation derived by Epstein et al., (1951); 1. As explained previously, synthetic minerals are grown in a controlled environment at a controlled temperature and the oxygen isotope ratio is then measured, this is known as experimentally derived equations and 2. Natural mineral are collected from various global locations the temperature and other environmental conditions from where they are collected are recorded and the oxygen isotope ratio in the material is measured, this is known as a empirically derived equation. There are pros and cons to the equations derived by both the empirical and experimental methods. The pros associated with the experimentally derived equations is that when conducted properly all variables can be controlled, however, they do not account for the large time frames that these minerals are generally given to precipitate when they form naturally, they are difficult to conduct and may be impede by kinetic limitations (Sharp 2006). When deriving empirical equations, it is advantageous that the materials already exist and formed in their natural

environment, however, despite the efforts in measuring the constraints of their natural environments accurately, there is always likely to be error introduced due to natural variations within the environment that may have occurred through time and not have been recorded when the specimens were being collected.

Since the original palaeotemperature equation derived by Epstein (1953) many authors have been recalibrating the equation and creating new variations of the equations based on new experimental and empirical data (see Grossman 2012 for a summarised review). This means that for modern scientists there are many palaeotemperature equations available and it is important to select an appropriate equation as the outputted temperatures can vary by up to 3°C (Figure 5-2)

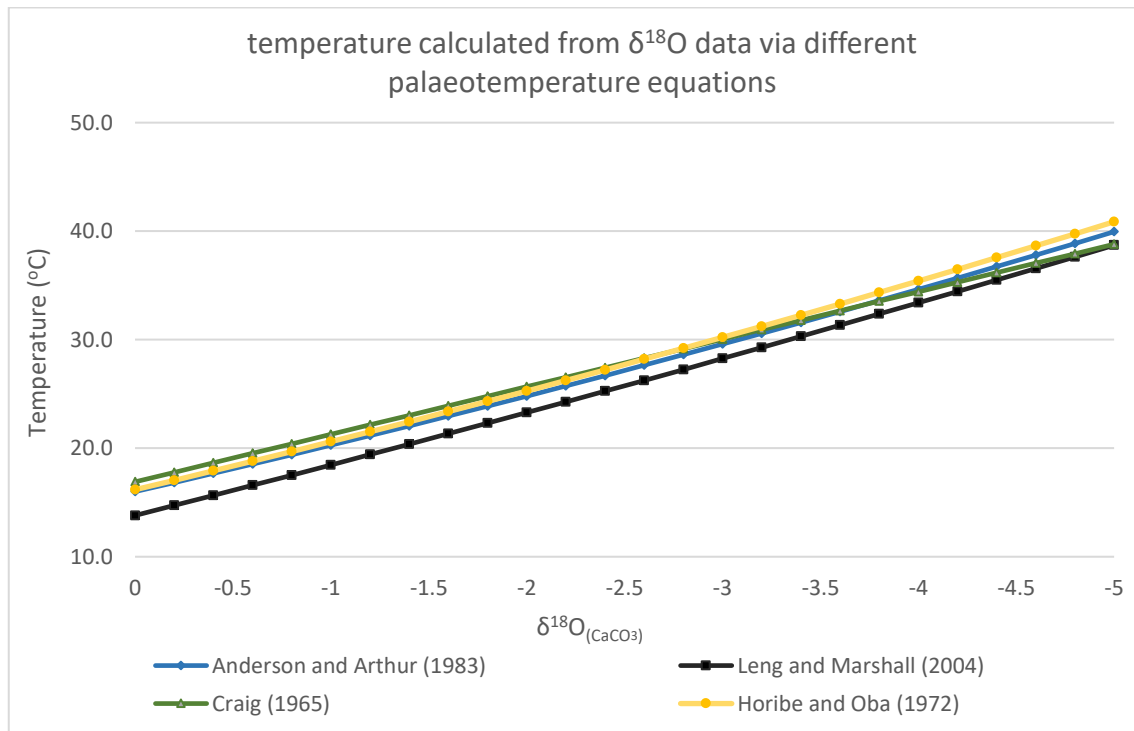


Figure 5-2 Demonstrates the variations in calculated temperature when using differing palaeotemperature equations.

All temperatures are calculated using a seawater $\delta^{18}\text{O}$ value of 0. The equations used are as followed: Anderson and Arthur (1983): $T (^{\circ}\text{C}) = 16.0 - 4.14 (\delta^{18}\text{O}_{\text{CaCO}_3} - \delta^{18}\text{O}_w) + 0.13 (\delta^{18}\text{O}_{\text{CaCO}_3} - \delta^{18}\text{O}_w)^2$. Craig (1965): $T (^{\circ}\text{C}) = 16.9 - 4.38 (\delta^{18}\text{O}_{\text{CaCO}_3} - \delta^{18}\text{O}_w) + 0.1 (\delta^{18}\text{O}_{\text{CaCO}_3} - \delta^{18}\text{O}_w)^2$. Leng and Marshall (1983): $T (^{\circ}\text{C}) = 13.8 - 4.58 (\delta^{18}\text{O}_{\text{CaCO}_3} - \delta^{18}\text{O}_w) + 0.08 (\delta^{18}\text{O}_{\text{CaCO}_3} - \delta^{18}\text{O}_w)^2$. Horibe and Oba (1972): $T (^{\circ}\text{C}) = 17.0 - 4.34 (\delta^{18}\text{O}_{\text{CaCO}_3} - \delta^{18}\text{O}_w + 0.2) + 0.12 (\delta^{18}\text{O}_{\text{CaCO}_3} - \delta^{18}\text{O}_w + 0.2)^2$.

In this study sea surface temperatures are calculated from $\delta^{18}\text{O}$ via the Anderson and Arthur (1983) equation (equation 1) (revised from the original equation (Epstein et al., 1953)):

$$T (^{\circ}\text{C}) = 16.0 - 4.14 (\delta^{18}\text{O}_{\text{CaCO}_3} - \delta^{18}\text{O}_w) + 0.13 (\delta^{18}\text{O}_{\text{CaCO}_3} - \delta^{18}\text{O}_w)^2 \text{ Equation 1.}$$

In Equation 1 $\delta^{18}\text{O}_{\text{CaCO}_3}$, the $\delta^{18}\text{O}$ value measured in the biogenic calcite, and $\delta^{18}\text{O}_w$, the estimated value of seawater, are input into the equation to calculate sea surface temperatures in degrees Celsius ($^{\circ}\text{C}$). The standard deviation of the calculated temperatures from the original Epstein et al., (1953) equations is $\pm 0.6^{\circ}\text{C}$, therefore this error also applies to the Anderson and Arthur equations used herein.

Some researchers choose to calculate temperature using Mg concentrations as in some organisms this is seen to be influenced by temperature. However, the lack of correlation between Mg and $\delta^{18}\text{O}$ data outlined in Chapter 4 suggests that Mg in these specimens is not precipitated in equilibrium with seawater (as was also observed by Garcia et al., 2017) and therefore cannot be used as a palaeotemperature proxy. Additionally, it can be argued that it is best to use either the most up to date equation, or the one derived from material most comparable to that you are working with or the most reliable up-to-date equation. If considering this theory then the Leng and Marshall (2004) equation, which is a re-expression of the Kim and O'Neil (1997) is more recent and has been used by multiple authors (e.g. Garbelli et al, 2016). However, this equation is derived from synthetic rather than biogenic calcite, and Leng and Marshall (2004) recognise that simply due to the mathematical re-expression of the equation cooler temperatures are produced when compared to the original Kim and O'Neil (1997) equation. This suggests that the use of either of these equations could introduce unnecessary mathematical error (or, in the case of Leng and Marshall (2004), bias towards cooler temperatures). Other equations include Hays and Grossman (1991), however, this is also derived from synthetic calcite and not commonly used, and Horibe and Oba (1971) which is derived from cultured brachiopods, but is not commonly used and is now dated. Anderson and Arthur is the only equation derived from biogenic calcite, perhaps making it more reliable, and is therefore favoured in this study, however it should also be noted that it is

dated as it is a variation of the original Epstein et al. equation. Therefore, temperatures are also calculated using the Leng and Marshal (2004) equation and are provided in Appendix G.

Temperatures were calculated on both the original and the detrended data. The 'detrended data' is the original $\delta^{18}\text{O}$ values with 3.65‰ subtracted in order to account for the proposed evolution of seawater $\delta^{18}\text{O}$ values through geological time as is theorised by multiple authors such and summarised by Jaffres et al. (2007). This area of research is still very much a topic of debate and therefore a full discussion of why this step in processing the data should/should not occur is presented in Section 5.3.1. Estimations relating to potential regional variation in $\delta^{18}\text{O}_w$ of -0.375% , $+0.125\%$, $+0.625\%$, $+1\%$, 1.5% and $+2\%$ are made and are input in the temperature equation. Similarly, the process and considered factors behind the selection of appropriate seawater $\delta^{18}\text{O}$ estimations is complex and presents a significant point of discussion within studies of this type. Consequently, a full discussion explaining the logic and reasoning behind these estimated values is presented in Section 5.3.1.

5.1.1 Estimating $\delta^{18}\text{O}$ of seawater

When using oxygen isotope data as a sea surface temperature proxy an estimation of the $\delta^{18}\text{O}$ composition of the local seawater ($\delta^{18}\text{O}_w$) is required for the palaeotemperature equation. This estimation is a large unquantifiable error that is unavoidably inherited in the calculation of palaeotemperature.

The $\delta^{18}\text{O}$ of seawater is influenced by both global and local factors such as salinity, water depth, evaporation, precipitation and global ice volume. Some of these parameters (such as global ice volume) can be estimated based on comparisons to modern day analogues, however others, typically those which are more localised effects, are more difficult to estimate when working with material from the geological record. Estimating the $\delta^{18}\text{O}_w$ value to be used within the palaeotemperature equation is perhaps the source of the greatest uncertainty associated with studies of this type.

5.1.1.1 The evaporation and salinity effect

The baseline of modern oceans average $\delta^{18}\text{O}$ value is $\sim 0\%$ (Grossman, 2012) but LeGrande and Schmidt (2006) illustrate that the $\delta^{18}\text{O}$ values in modern oceans varies

globally. Figure 5-3 shows that the $\delta^{18}\text{O}$ of the Atlantic equatorial waters is $\sim +1\text{‰}$ and equivalent latitude in the Pacific is $\sim +0.25\text{‰}$. These positive values are most likely due to increased evaporation acting in equatorial regions, whilst the reason for the difference between the two oceans is unknown it is probably an accumulated effect of oceanic mixing, differential evaporation and the $\delta^{18}\text{O}$ of local precipitation (LeGrande and Schmidt, 2006). Understanding the interaction of these additional effects and quantifying their influence at different localities and across time within the geological record is difficult. Therefore, an average $\delta^{18}\text{O}$ value from the two oceans, $+0.625\text{‰}$, is used to represent modern global equatorial regions that is an equivalent latitude to the study sites from which the studied gigantoproductids were collected. However, this estimation assumes that the environment in question is well connected to open ocean waters.

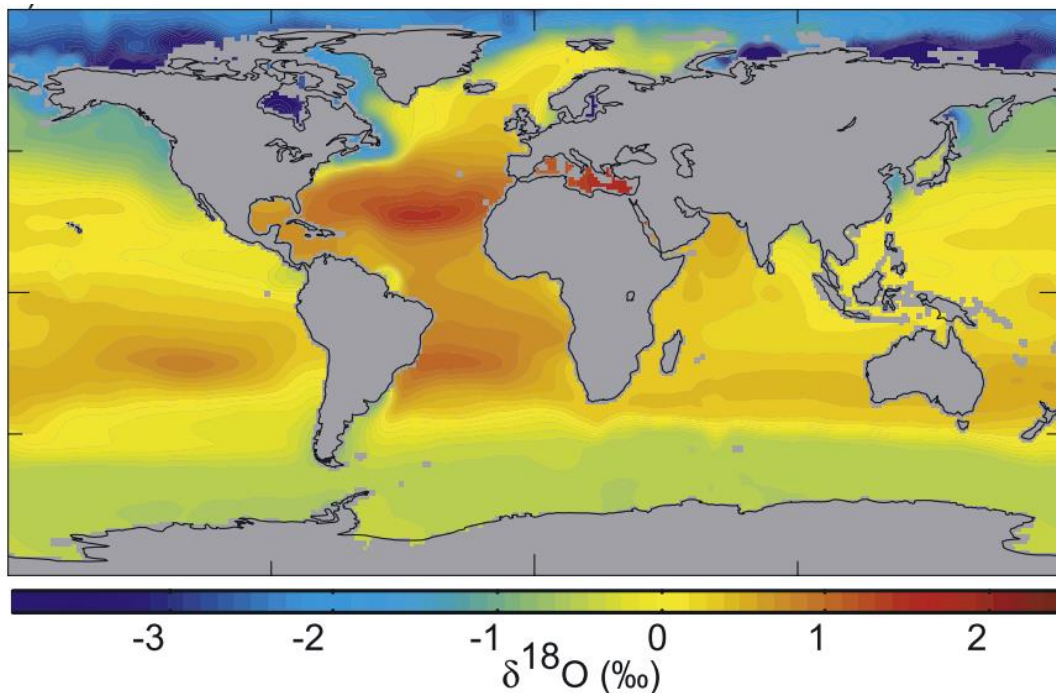


Figure 5-3. Variations in global $\delta^{18}\text{O}$ values in modern oceans, taken from LeGrande and Schmidt (2006).

The small, interconnected basins forming the Brigantian palaeotropical epicontinental seaway in which species of *Gigantoproductus* grew has been compared to the modern Mediterranean Sea in terms of its connection to the open ocean and its surface area (Wells et al., 2005). Modern Mediterranean waters have an average $\delta^{18}\text{O}$ value of $\sim +2\text{‰}$ (LeGrande and Schmidt, 2006) (Figure 5-3), this relatively high value is likely caused by both the evaporation effect and lack of mixing with open oceanic waters (Gat et al.,

1996). Therefore, +2‰ is used as a second estimation the seawater $\delta^{18}\text{O}$ value to account for a possible elevated evaporation effect due to the lack of connectivity to open oceans.

Global ice volume influences seawater $\delta^{18}\text{O}$ as it affects the overall salinity of the oceans. Although extensively studied, the timing of the onset of the Late Palaeozoic icehouse is not yet fully understood and therefore the global ice volume present during the Brigantian is also disputed. If no or very little ice was present at the poles as thought by Fielding et al. (2008) the effect of the incorporation of these additional water masses on global seawater $\delta^{18}\text{O}$ needs to be considered. If the current ice volume were to be incorporated into the modern oceans, then the $\delta^{18}\text{O}$ ocean value would be $\sim -1\%$ lower than it is currently (Grossman, 2012; Joachimski et al., 2004; Savin, 1977) and therefore this value can be incorporated into the estimation of Brigantian seawater $\delta^{18}\text{O}$.

Other studies have suggested that the Late Palaeozoic icehouse was underway by the end of the Brigantian (e.g. Barham et al., 2012). Therefore, temperature calculations were also undertaken based on the presence of ice volumes equivalent to those present today (therefore no change), and with the presence of half the volume of ice than is currently present (-0.5%) to account for those estimations which, suggest an Alpine type glaciation began at the end of the Brigantian (Isbell et al., 2003). Additional calculation however, are provided in Appendix G.

In modern environments it has been shown that fresh water runoff from fluvial systems can affect regional environments. The Amazon delta, for example, produces a $\sim 1.0\%$ negative localised seawater $\delta^{18}\text{O}$ anomaly (see Figure 5-3 **Error! Reference source not found.**) while some 150 km off the coast in the Gulf of Mexico the influence of the Mississippian-Atchafalaya river systems lowers the regional $\delta^{18}\text{O}$ values by 0.6% (Gentry et al., 2008). This system also influences the salinity of the region (by 4 psu) (Gentry et al., 2008). Given that during the Brigantian it has been suggested that monsoon-like seasonal rainfall occurred (Falcon-Lang, 1999), it may be that the effect of seasonal freshwater runoff may influence the seasonal environmental variability. However, it is unlikely that this had a profound effect on the seawater salinity in the environment in which these organisms were living during the Brigantian, as there is no evidence of freshwater input within the sedimentology at either locality (see Chapter 2). The main

fluvial systems present at the time, which were to the north of the Derbyshire carbonate platform, are evident on the northern margin of the platform (Gutteridge, 1991), however were likely too far to effect the local environment during the Brigantian. Additionally, both brachiopods and crinoids live in waters of *normal* salinity (i.e. 35‰ \pm 2‰) (Rudwick, 1959). Modern brachiopods are found in waters with salinity ranges from 29 to 39 (Brand et al., 2009) psu meaning there may be salinity differences between localities, however the salinity variability at a single location are generally significantly smaller (Brand et al., 2003) suggesting that localised salinity variations do not need to be considered, and neither does seasonal salinity change.

These various estimations of the evaporation and salinity effects are combined giving estimations of seawater $\delta^{18}\text{O}$ for Brigantian palaeoequatorial epicontinental seaway for use within the palaeotemperature equation (Table 5-1).

Total seawater $\delta^{18}\text{O}$ value	+2‰	+1.5‰	+1‰	+0.625‰	+0.125‰	-0.375‰
Estimation of ice volume/salinity effect	0	-0.5	-1	0	-0.5	-1
Estimation of evaporation effect	+2	+2	+2	+0.625	+0.625	+0.625

Table 5-1. Seawater $\delta^{18}\text{O}$ values based on estimation for the salinity and evaporation effect of the Brigantian palaeoequatorial epicontinental seaways.

Although these estimations are based on practical analogues, there are inevitably some estimates that are thought to be more accurate than others. When considering the influence of evaporation at the study sites, the palaeogeography maps (which are not generally disputed) place the UK in a location that strongly indicate that the epicontinental seaway would not have been connected to open oceans (Figure 5-1). Given this, it is considered that an estimation of the evaporation effect of +2‰ is likely more accurate than +0.625‰. It could be further argued that the evaporation effect on a poorly connected ocean basin at the equator may have been greater than that currently occurring in the Mediterranean that is situated \sim 35°N. However, estimating this possible

increased effect is not possible given the uncertainties surrounding the state of Late Brigantian climate.

Isbell et al. (2003) focused on the timing of the onset of the Late Palaeozoic glaciation based on sedimentological evidence, and concluded that the major phase of glaciation began at the end of the Visean (and therefore the end of the Brigantian). However, cyclical deposits within Asbian and Brigantian sediments in the UK are thought to be the result of glacio-eustasy (Wright and Vanstone, 2001), therefore suggesting that some ice may have been present and influencing global oceans and environments. It is for these reasons that a range of estimations of the salinity effect are used to account for differing theories on the global ice volume and therefore the onset of the glaciation. Given the convincing cyclical sedimentological sequences present in the Asbian and Brigantian rocks of the UK (Wright and Vanstone, 2001) it is fair to conclude that some ice was present in Gondwana during the Brigantian, and that the discontinuity between the brachiopod $\delta^{18}\text{O}$ records equally suggests that the climate was not cold enough to support large glacial masses. The preferred interpretation is therefore that glacial masses were likely to be present in order to produce sea level changes likely caused by glacio-eustasy from the mid Visean, however the climate was likely not cool enough to support permanent glacial masses as is indicated from the brachiopod stable isotope data. Therefore, 0.5‰ is the preferred estimated value of the salinity effect.

Following the evaluation of the quality of the seawater $\delta^{18}\text{O}$ estimations with the calculated sea surface temperatures it is thought that those temperatures calculated from the detrended data using a seawater $\delta^{18}\text{O}$ value of +1.5‰ are the most representative of Brigantian palaeotropical epicontinental seaways.

5.2 Results

5.2.1 $\delta^{18}\text{O}$ and $\delta^{13}\text{C}$ data summary

$\delta^{18}\text{O}$ and $\delta^{13}\text{C}$ data from well preserved shell transects are given in Table 5.2.

Isotope	Statistic/ specimen	RCK 33	RCK 28	RCK	RCK	XG	OAW	RCK
				28bis	28bis_2		03	6bis
$\delta^{18}\text{O}$	n	15	20	7	9	25	26	22
	Min	-4.72	-4.43	-4.52	-4.46	-5.36	-5.28	-4.62
	Max	-2.56	-3.07	-3.25	-2.94	-3.18	-3.54	-2.52
	Mean	-3.66	-3.77	-4.04	-3.63	-4.63	-4.35	-3.42
	SD	0.51	0.40	1.51	0.48	0.65	0.52	0.53
$\delta^{13}\text{C}$	Min	0.62	1.14	0.81	0.94	-0.98	-1.65	1.33
	Max	2.31	2.73	2.70	2.71	2.61	1.99	2.44
	Mean	1.65	2.16	2.23	2.14	1.43	0.85	2.13
	SD	0.45	0.46	0.99	0.55	1.13	1.03	0.27

Table 5-2 minimum, maximum, mean and standard deviation of well-preserved shell isotope data.

The full range of $\delta^{13}\text{C}$ values across all specimens is 4.38‰ with the highest value of +2.73‰ observed in RCK 28 and the lowest, -1.65‰, in specimen OAW 03. The largest range within an individual specimen is 3.59‰ and is present within specimen XG. Ranges in values within individual specimens are typically ~1.75‰ except XG and OAW 03, which both have ranges above 3.5‰. Average values of all specimens are positive with the highest, +2.23‰, from specimen RCK 28bis and the lowest, +0.85‰, in specimen OAW 03. The $\delta^{13}\text{C}$ values from the non or slightly luminescent material analysed by Angiolini et al. (2012) are between -2.6‰ and +1.3‰. Data from the current study are typically within this range or have slightly lower values.

The range of $\delta^{18}\text{O}$ values across all specimen transects before detrending (Table 5-2) is +2.8‰ and all average values are below -3.5‰. The highest value, -2.56‰, is from specimen RCK 33 whilst the lowest (-5.36‰) is from specimen XG. Average values are all within 1‰ (between -3.63‰ and -4.63‰) with the lowest average value from specimen

XG and highest from RCK 28bis_2. Many of these $\delta^{18}\text{O}$ values are within the range of those observed in Tournasian and Late Visean *Gigantoproductus* species from the Russian Platform by Mii et al. (2001), (-3‰ to -4‰). Some values are lower however, Mii et al. (2001) state that their dataset of has error margins of $\pm 1\text{‰}$, suggesting that the datasets are essentially comparable. The data from Angiolini et al. (2012) from *Gignatoproductus* of the Derbyshire carbonate platform has $\delta^{18}\text{O}$ values from non or slightly-luminescent brachiopods between -4.4‰ to -6.4‰ with the $\delta^{13}\text{C}$ data set, although there is some overlap, the values observed by Angiolini et al. (2012) are generally lower than those observed within this study.

Isotope	Statistic/ specimen	RCK 33	RCK 28	RCK 28bis	RCK 28bis_2	XG	OAW 03	RCK 6bis
$\delta^{18}\text{O}$	n	15	20	7	9	25	26	22
	Min	-4.72	-4.43	-4.52	-4.46	-5.36	-5.28	-4.62
	Max	-2.56	-3.07	-3.25	-2.94	-3.18	-3.54	-2.52
	Mean	-3.66	-3.77	-4.04	-3.63	-4.63	-4.35	-3.42
	SD	0.51	0.40	1.51	0.48	0.65	0.52	0.53
$\delta^{13}\text{C}$	Min	0.62	1.14	0.81	0.94	-0.98	-1.65	1.33
	Max	2.31	2.73	2.70	2.71	2.61	1.99	2.44
	Mean	1.65	2.16	2.23	2.14	1.43	0.85	2.13
	SD	0.45	0.46	0.99	0.55	1.13	1.03	0.27

Table 5-2. Minimum (min), maximum (max) data mean and standard deviation (SD) of $\delta^{13}\text{C}$ and $\delta^{18}\text{O}$ of all shell transects of well-preserved data points.

Data from the three transects through specimen RCK 6bis are combined when calculating statistics. All data is given in per mil (‰). Values for the detrended $\delta^{18}\text{O}$ data are presented in Table 5-3.

Isotope	Statistic/ specimen	RCK 33	RCK 28	RCK 28bis	RCK 28bis_2	XG	OAW 03	RCK 6bis
$\delta^{18}\text{O}$	n	15	20	7	9	25	26	22
	Min	-1.07	-0.78	-0.87	-0.81	-1.71	-1.63	-0.97
	Max	1.09	0.58	0.40	0.71	0.47	0.11	1.13
	Mean	-0.01	-0.12	-0.39	0.02	-0.98	-0.70	0.23

Table 5-3. Minimum (min) Maximum (max) data mean of $\delta^{18}\text{O}$ of all shell transects of well-preserved data points after the data has been detrended (subtracted -3.65‰).

Data from the three transects through specimen RCK 6bis are combined when calculating statistics. All data is given in per mil (‰). Note that the standard deviation of this data is identical to that of $\delta^{18}\text{O}$ in table 5-2.

The correlation between $\delta^{13}\text{C}$ and $\delta^{18}\text{O}$ for data indicate that there is a significant (p value of <0.0001) positive correlation between the two isotopes with a value of 0.43.

5.2.2 Temperature calculations from $\delta^{18}\text{O}$ data

When temperatures are calculated, by changing the seawater $\delta^{18}\text{O}$ value the temperatures are systematically offset by a standard amount related to the seawater $\delta^{18}\text{O}$ value. This means that the relative temperatures are calculated from the same specimen are consistent no matter what the seawater $\delta^{18}\text{O}$ value is. Therefore, the highest overall average temperature is recorded in specimen XG, the lowest overall average temperature is within RCK 6bis. The largest range in temperatures is within XG whilst the smallest temperature range is within RCK 28. Temperatures calculated from individual specimens are summarised in Table 5-4 and Table 5-5 and all calculated temperatures are provided in Appendix G.

Temperatures calculated with a seawater $\delta^{18}\text{O}$ value of +1.5‰ from the standard dataset have an overall range of 15°C from +50.5°C to +34.8°C and the average range of temperatures within individual specimens is 10°C. Average temperatures range between +46.3°C and +39.5°C. All temperatures calculated using a $\delta^{18}\text{O}$ value of +2‰ are systematically 2.8°C higher, those calculated using a seawater value of +1‰ are 2.7°C lower, +0.625‰ are 4.7°C lower, +0.125‰ 7.2°C lower and -0.375‰ are 9.7°C lower than those calculated using a $\delta^{18}\text{O}$ seawater value of +1.5‰ (all calculated temperature are provided in Appendix G).

As expected, temperatures calculated from the detrended data give temperatures that are systematically lower than those calculated from standard data. This means that temperatures calculated using a $\delta^{18}\text{O}$ value of +1.5‰ have temperatures ranging between +17.6°C and +30.6°C with an average temperature of +23.8°C. With the exception of this initial offset (which applies to all the detrended data vales the relative temperature offset caused by changing the seawater $\delta^{18}\text{O}$ value is the same as the standard dataset.

Temperature	Statistic/ specimen	RCK 33	RCK 28	RCK 28bis	RCK 28bis_ 2	XG	OAW 03	RCK 6bis
°C	n	15	20	7	9	25	26	22
	Min	34.97	37.63	38.60	36.95	38.25	-5.28	34.75
	Max	46.76	45.11	45.66	45.31	50.51	26.00	46.21
	Range	11.78	7.47	7.06	8.37	12.27	31.28	11.45
	Mean	40.84	41.43	42.96	40.67	46.31	2.85	39.54

Table 5-4. Summary of calculated temperatures from the standard dataset. All temperatures are given as °C and are calculated using a seawater $\delta^{18}\text{O}$ value of +1.5‰ from equation $T (^{\circ}\text{C}) = 16.0 - 4.14 (\delta^{18}\text{O}_{\text{CaCO}_3} - \delta^{18}\text{O}_w) + 0.13 (\delta^{18}\text{O}_{\text{CaCO}_3} - \delta^{18}\text{O}_w)^2$.

Temperatures above 38°C are outside of brachiopod lethal limits (Lee et al., 2009) (see Section 3.3 for further discussion). Note all temperatures are positive.

Temperature	Statistic/ specimen	RCK 33	RCK 28	RCK 28bis	RCK 28bis_ 2	XG	OAW 03	RCK 6bis
°C	n	15	20	7	9	25	26	22
	Min	17.74	19.92	20.71	19.35	20.42	22.00	17.56
	Max	27.48	26.10	26.56	26.28	30.63	30.25	27.02
	Range	9.74	6.18	5.85	6.92	10.20	8.25	9.46
	Mean	22.57	23.06	24.32	22.42	27.11	25.76	21.49

Table 5-5. Summary of calculated temperatures from the detrended data values with a seawater $\delta^{18}\text{O}$ value of +1.5‰. All temperatures are given as °C from equation $T (^{\circ}\text{C}) = 16.0 - 4.14 (\delta^{18}\text{O}_{\text{CaCO}_3} - \delta^{18}\text{O}_w) + 0.13 (\delta^{18}\text{O}_{\text{CaCO}_3} - \delta^{18}\text{O}_w)^2$.

Note that all temperatures are positive and there are none outside of brachiopod lethal limits.

When the data from all the specimens are combined the average temperature across all the shells for the standard data from the four calculated seawater values are +45°C, +39°C, +38°C and +32°C all with standard deviations $\sim 3^{\circ}\text{C}$. The average range of temperatures within individual specimens is typically 10°C . For the detrended dataset, average temperatures across all specimens are 26°C, 21°C, 20°C and 16°C with a typical standard deviation of $\sim 2.3^{\circ}\text{C}$.

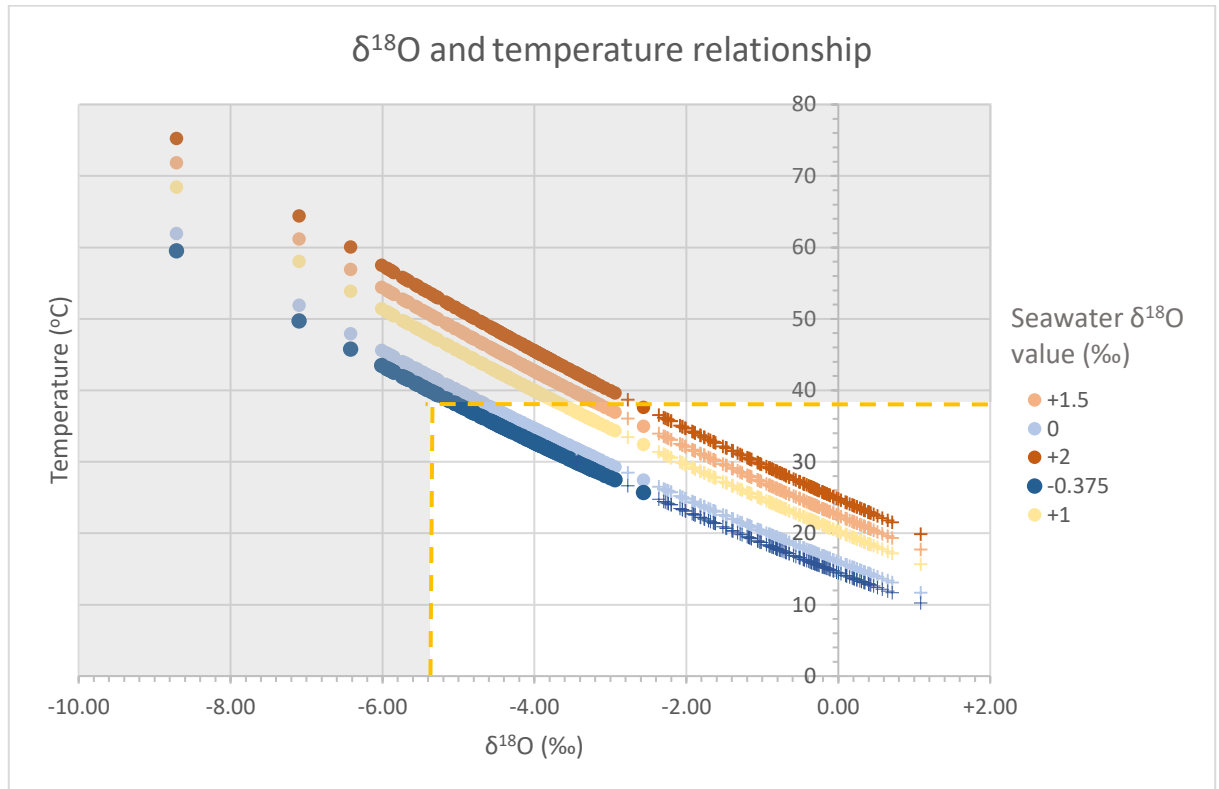


Figure 5-4 plots temperature against $\delta^{18}\text{O}$ showing the relationship between the two with different seawater $\delta^{18}\text{O}$ values when calculating temperature.

Filled circles represent the standard dataset and the crosses the detrended. All data is plotted (including poorly preserved). Grey shaded area indicates data points that are either have a calculated temperature above brachiopod lethal limits (38°C) or $\delta^{18}\text{O}$ value that is considered poorly preserved (below -5.36‰).

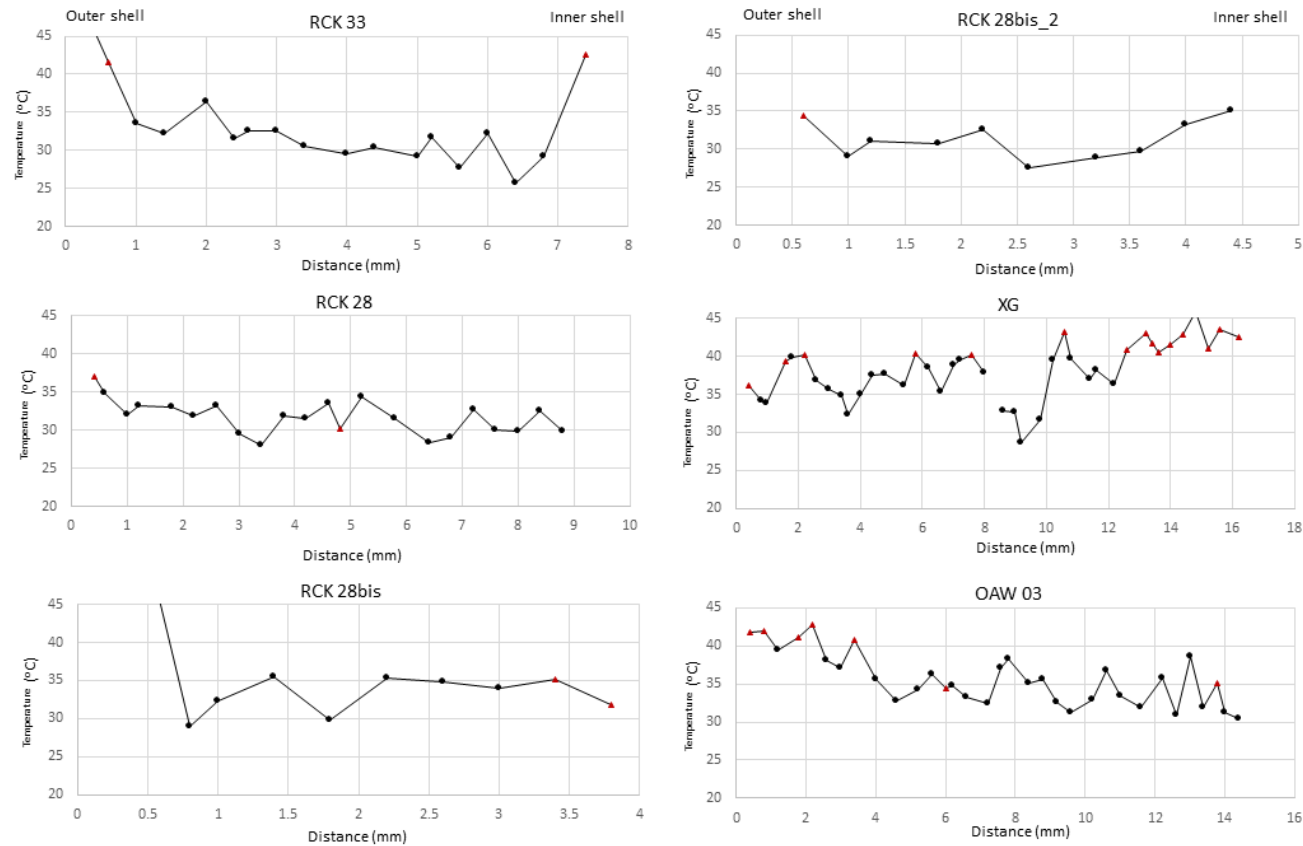


Figure 5-5. Calculated temperatures through all specimen transects.

Temperatures were calculated using the Anderson and Arthur (1983) equation and a $\delta^{18}\text{O}$ water value of -0.375‰ . Red triangle data points represent those which are suspected to be altered based on the parameters outlined in Chapter 4. Data points that are not visible have $\delta^{18}\text{O}$ values less than -5.37‰ and therefore are considered to have undergone diagenetic alteration.

5.3 Discussion

5.3.1 Detrending the dataset

Although its cause is still debated, consideration should also be given to the observed trend of increased seawater $\delta^{18}\text{O}$ through the geological record (Jaffrés et al., 2007). It is argued by some (e.g. Gregory, 1991, Gregory and Taylor, 1981, Muehlenbachs and Clayton, 1976) that this general trend is not caused by a change in the overall ocean $\delta^{18}\text{O}$ value, but that it is caused by changes in the amount of $\delta^{18}\text{O}$ fractionation occurring within the oceans. Changes in fractionation may be caused by a general temperature increase or pH change through time. It is argued that the observed $\delta^{18}\text{O}$ increase through time cannot be caused by an overall evolution in seawater chemistry as changes in ocean $\delta^{18}\text{O}$ are buffered by a balance of seafloor spreading and continental weathering (Gregory and Taylor, 1981). Those who argue that the observed trend is a primary representation of the evolution of seawater $\delta^{18}\text{O}$ (e.g. Popp., et al., 1986, Veizer et al., 1997, Kasting et al., 2006) suggest that this change cannot be caused solely by environmental influences but may be caused by the salinity stratification of oceans through time. Jaffrés et al. (2007) reviewed all arguments and present their own modelling, concluding that the observed $\delta^{18}\text{O}$ change through time is in fact a primary reflection of changing seawater chemistry due to tectonic processes, and that the variability of ocean $\delta^{18}\text{O}$ is larger than just the global ice volume influence. Due to this debate, it is necessary to consider the effects on the dataset presented here, however, there is a complication in estimating the amount by which a dataset should be detrended to account for this trend.

Giles (2012) stated that Jaffrés et al. (2007) had reported a $-0.015\text{‰}/\text{Ma}$ change in seawater $\delta^{18}\text{O}$ through the Palaeozoic to recent. If correct, then the $\delta^{18}\text{O}$ baseline of Brigantian seawater (330 Ma) would be -4.95‰ . However, it is unclear how this $-0.015\text{‰}/\text{Ma}$ gradient was obtained (presumably by calculating a gradient of a straight line drawn from the youngest to the oldest data points). Figure 5-6 shows the seawater trend modelled by Jaffrés et al. (2007), which gives a baseline Brigantian seawater $\delta^{18}\text{O}$ value of -3.65‰ . This 1.3‰ difference between the Giles (2012) and the Jaffrés et al. (2007) estimations would result in a $\sim 16^\circ\text{C}$ temperature difference; a significant error.

Additionally, in Figure 5-6 **Error! Reference source not found.** it is clear that a value of -4.95% for Brigantian seawater is not accurate. When considering the Veizer et al. (1999) dataset, which also looks at the evolution of seawater through the Phanerozoic, a value of -3.9% is given for the Brigantian. Data from Veizer et al. (1999) was plotted with a 5 Ma moving average, with the aim of smoothing out natural variability caused by 'real' climatic changes rather than seawater evolution. Although the smoothing of natural variability is important, for the Brigantian, given its small time span (~ 5 Ma), this is likely inadequate, particularly as it is noted as a global warm period, preceding a prolonged glacial phase, simply averaging the measured calcite $\delta^{18}\text{O}$ data produced from this time slice is not sufficient to remove environmental bias towards warmer conditions. Additional complications are introduced when sampling bias is considered as six out of the eight data points from within the Brigantian are from the tropics and therefore the mean seawater $\delta^{18}\text{O}$ value calculated from these eight data points is not representative of whole ocean condition and provide an average $\delta^{18}\text{O}$ value that is skewed towards warmer conditions. This is further proven when additional averages were calculated considering larger time spans (considering those either side of the Brigantian) was shown to not be normally distributed (Appendix H). This illustrates that the entirety of the dataset (and not just those data points from the Brigantian) is skewed and is likely biased by sampling or data/materials available and therefore is not suitable to calculate average seawater $\delta^{18}\text{O}$ for a given time span which can then be used as a detrending value. In comparison, Jaffrés et al. (2007) takes data available for multiple proxies and models both a calcite evolution curve and a seawater curve. Therefore, it is the value obtained from Jaffrés et al. (2007) (-3.65%) which is preferred and utilised herein.

Chapter 5: Using high resolution $\delta^{18}\text{O}$ and $\delta^{13}\text{C}$ data from well-preserved *Gigantoproductus* brachiopods to help reconstruct palaeoenvironments of the Brigantian tropics

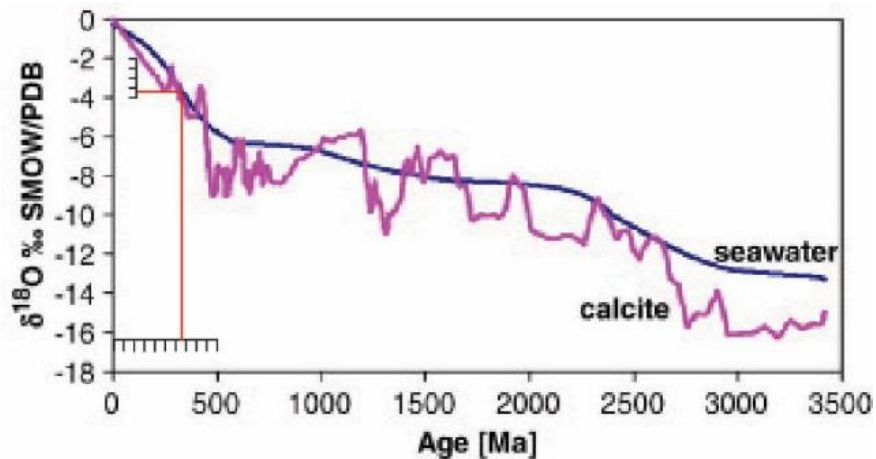


Figure 5-6. Seawater $\delta^{18}\text{O}$ trend after Jaffrés et al. (2007) with the reading of the Brigantian seawater $\delta^{18}\text{O}$ value shown by the red lines.

Following the rationale outlined above, detrended $\delta^{18}\text{O}$ data is also provided here alongside standard $\delta^{18}\text{O}$ data as it is noted that not all accept that evolution of seawater should be considered in temperature calculations; ‘Standard data’ therefore refers to the original $\delta^{18}\text{O}$ values obtained from the analyses while ‘detrended data’ refers to the bulk correction of the dataset wherein 3.65‰ is subtracted from the original $\delta^{18}\text{O}$ values, thus theoretically removing the effect of seawater $\delta^{18}\text{O}$ evolution through geological time from the dataset. An alternative way of accounting for this correction is to include the correction within the temperature equation. If the Anderson and Arthur equation were to be modified in order to account for this correction it would be as is demonstrated in Equation 2.

$$T (^{\circ}\text{C}) = 16.0 - 4.14 (\delta^{18}\text{O}_{\text{CaCO}_3} - (\delta^{18}\text{O}_{\text{w}} - 3.65)) + 0.13 (\delta^{18}\text{O}_{\text{CaCO}_3} - (\delta^{18}\text{O}_{\text{w}} - 3.65))^2 \text{ Equation 2.}$$

Following detrending, the same estimated seawater $\delta^{18}\text{O}$ values based on more variable effects, such as evaporation or salinity, can be applied to both datasets.

5.3.2 Evaluating calculated temperatures

Many of the temperatures calculated from the standard dataset are above 38°C which thought to be the lethal thermal limit of most modern brachiopods (Peck et al., 2009) although some collected from the Red Sea have been shown to be able to withstand temperature of up to 40°C (Nguyen et al., 2011). Given that there are no modern analogues for gigantoproductids, it should also be considered that they may have been

able to tolerate higher temperatures. Garbelli et al. (2016) calculated temperatures from well-preserved ancient brachiopod calcite which exceed 40°C , suggesting that some ancient organisms may have been able to tolerate such temperatures, however; it should be considered that these studies, like this one, inherit error with the calculation of temperature from ancient biogenic calcite and have opted not to de-trend their dataset. Given this, and the fact that the majority of organisms appear to have a lethal limit of 38°C , this temperature limit was applied, with the understanding that all calculated palaeotemperatures have an error margin. Additionally, to produce temperatures of 38°C from a $\delta^{18}\text{O}$ shell value of -5.37‰ (which is the lowest $\delta^{18}\text{O}$ value in this dataset used as a palaeotemperature proxy) a seawater $\delta^{18}\text{O}$ value of $\sim -0.73\text{‰}$ is needed, which for a suspected poorly connected seaway is unrealistic. Therefore, the brachiopod data suggests that detrending of the data to account for evolution of seawater chemistry is necessary. This remains the case even if the Leng and Marshall (2004) equation is used to calculate temperature (Appendix G). By using this alternative equation temperature are systematically 2°C cooler. Despite this, many temperatures calculated using the preferred $+1.5\text{‰}$ seawater value would still be above the proposed brachiopod lethal limits. It is noted that understanding the evolution of seawater through geological time is a developing area of science and therefore the dataset presented here contributes to the developing literature that evaluates this theory, hence both detrended and standard data are presented. However, as the temperatures calculated from the standard dataset appear to be unrealistic, especially given the rigorous screening techniques used in this project, they are not discussed further. All discussion on calculated temperatures from here on refer to those calculated from the detrended dataset. However, as discussed in section 5.3.1, our understanding of seawater evolution through time is limited meaning that estimating by how much a dataset should be detrended come with inherent associated uncertainties. Because of these complications, and despite best efforts, absolute temperatures should be treated with caution. Despite this, given that all data was collected in the same way and that detrending is consistent across all data points, temperature variations that occur within and across specimens can be evaluated with more confidence that they are representative of Brigantian temperature changes.

5.3.2.1 Comparisons with other data sets

If the data produced from this study are deemed reliable, which, given the rigorous preservation screening undertaken and the tight cut-off parameters applied, it is believed to be, then it should be considered that the calculated temperatures are also reliable.

Temperatures calculated from the detrended dataset with this seawater $\delta^{18}\text{O}$ value of +1.5‰ range from 17.6°C to 30.6°C across the analysed specimens, with an average temperature of 23.8°C. Crowley et al. (1996) modelled Carboniferous tropical oceans and proposed that the Visean tropics had a mean sea surface temperature of 25°C to 30°C, and Bruckschen et al. (1999) estimated European Visean oceans to have average sea surface temperatures of 25°C \pm 5°C. The average of the best-estimated temperatures calculated in this study lie within the temperature ranges produced by Bruckschen et al. (1999). However, it should be noted that Bruckschen et al. (1999) classified the Visean as warm climate (therefore indicating their idea that the glaciation was not onset by this time) whilst the temperature estimations of mean sea surface temperatures for the Late Carboniferous, during the glaciation is 20°C \pm 5°C, which also encompasses the mean sea surface temperature calculated in this study.

Modern equatorial open oceans have mean sea surface temperatures of \sim 30°C (see Figure 5-7) which, given that our current climate is cool enough to support permanent ice, suggests that the specimens analysed within this study lived in an icehouse climate. Further to this, temperatures calculated from a seawater $\delta^{18}\text{O}$ value of +2‰ (which assumes modern ice masses present) are also cooler (mean sea surface temperature of 26.2°C) than modern day equatorial ocean sea surface temperatures. For comparison, temperatures during the Palaeocene-Eocene Thermal Maximum, which is a warm period within Earth's geological history, at localities \sim 40°N reached a peak temperature of 33°C (Zachos et al., 2006). Although this was, an extreme pronounced warm period it demonstrates the scale of warm climate periods and illustrates that even the maximum temperatures calculated within this study is below the peak mean temperatures reached at 40°N during this period. This further suggests that it is unlikely that the Brigantian was a global warm period.

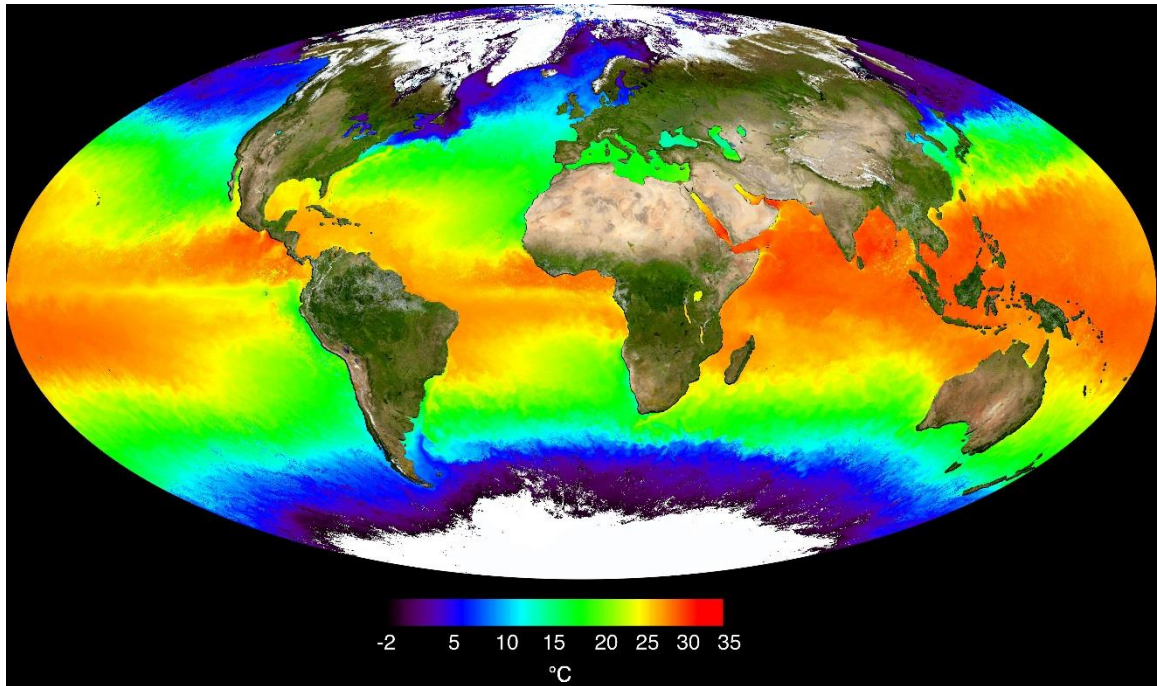


Figure 5-7. Modern sea surface temperature of global oceans (Descloitres, 2001) (data collected in May 2001).

Despite estimations that the Brigantian may have been a cool climatic period rather than a warm one as has previously been suggested, it does not mean that it was not a warmer climatic phase surrounded by cooler climates, and thus terrestrial evidence of climatic variation through the Late Mississippian stratigraphy are still representative. Only the estimated temperatures for these tropical late Brigantian oceans are perhaps too warm.

Giles (2012) synthesises brachiopods $\delta^{18}\text{O}$ data from a large range of environments and localities available in the literature and identified the coolest temperatures recorded in the Brigantian to be cooler than the tropical oceans during the Last Glacial Maximum, and the warmest being warmer than almost all warm climate excursions identified during the Palaeozoic. This large range in climatic conditions identified during the Brigantian suggests that although specifically the late Brigantian appears to represent cooler climates, this may not be the case for the entirety of the Brigantian stage. Thus, highlighting that during this time climate was likely highly dynamic and unstable as is expected during in period of climatic change.

Temperature ranges observed across individuals are somewhat comparable (if also considering inherent error) and range from $\sim 6^\circ\text{C}$ to $\sim 10^\circ\text{C}$. The mean temperatures

observed across the specimens are more spread, ranging from 21.5°C in specimen RCK 6bis to 27°C in specimen XG. A biological fractionation factor can be ruled out as multiple specimens of the same species analysed also present different mean temperatures and it is expected that if biological fractionation is occurring then it will likely be consistent within a single species. A possible cause for the variability between same species but different specimens is a difference in sampling resolution due to different growth rates between individuals, data were collected at as high a resolution possible given the equipment and methods available. However, it is possible that that sampling was not consistent in sampling the true variability and spread of values across each specimen. This issue is likely amplified by lack of understanding of growth rates for species of *Gigantoproductus* and the fine scale of growth lines means that often multiple growth lines are incorporated into a single isotope sample. This sampling issue also likely contributes to not being able to successfully apply Fourier transforms to the data (see section 5.3.2.2). There may also be true temporal differences between the months/years that are represented by the shells leading to the variability on the data.

5.3.2.2 Identifying seasonal variation

Fourier transform analyses were performed on the Mg and $\delta^{18}\text{O}$ data from shells XG and OAW 03 (the largest sample numbers across individual transects) but no significant frequencies depicting cyclicity were detected. Some peaks were detectable however, they were deemed insignificant when error margins of the Fourier transforms were considered. It is likely that this is, in part, because of the small sample size and uneven spacing of $\delta^{18}\text{O}$ data points which is preferred in such analyses.

Within stable isotope datasets seasonality has also been identified as regular fluctuations within the $\delta^{18}\text{O}$ data (Ivany and Runnegar, 2010). Within this dataset there is 'repetitive' variability in both trace elements and $\delta^{18}\text{O}$ data within multiple specimens and the data range within these fluctuations is comparable to that which has previously been identified as seasonal variability (e.g. Angiolini et al., 2012). Therefore, because similar variability is observed within other *Gigantoproductus* species and have been attributed to seasonal variability it is reasonable to tentatively interpret the minimum (presumably winter) and maximum (presumably summer) temperature recorded across specimens

represents the seasonal temperature variations. It is important to consider the range of temperatures across the specimens rather than within individuals because the sampling method cannot ensure that the material within an individual with the minimum and maximum $\delta^{18}\text{O}$ values was analysed. This issue is further amplified when considering that there is limited understanding of the rate of *Gigantoproductus* species growth. Furthermore, it should be noted that it is possible that during times of extreme environmental pressures the organisms stop growing (and stop precipitating the calcitic shell). If this were to be the case then the full range of temperature experienced through the organism's lifetime may not be recorded in the biomineralized shell. Ideally individual growth lines, calcite prisms and lamina would be analysed (both for stable isotopes and trace elements) however, currently this is not possible with the technology available. The likelihood of observing the true variability the specimens within the shell beds experienced is increased when considering multiple specimens.

Modern seasonal temperature ranges in the Santa Barbara Channel are $5^{\circ}\text{C} - 6^{\circ}\text{C}$ (Pak et al., 2004), which is the same as those observed by Mii and Grossman (1994) in Late Pennsylvanian brachiopods from shallow seas suspected tropical climate zone with a $0 - 10^{\circ}\text{N}$ palaeolatitude. The Aegean Sea has seasonal temperature variations of $\sim 11^{\circ}\text{C}$ (Poulos et al., 1997) whilst the southern Bahamas have sea surface temperatures of 25°C in the winter months and 29°C in the summer (Gaudain and Medley, 2000). Temperature ranges within individual specimens of this study are between $\sim 11^{\circ}\text{C}$ and 6°C , which is both comparable to those observed in modern oceans and to those calculated in comparable studies.

Evaluating and quantifying the extent of seasonal variation in mixing of ocean waters in deep time is not possible, however, given the shallow water environment of the epicontinental seaway considered in this study, seasonal changes in ocean currents are likely to have had no effect on seasonal temperature changes. In fact, the relatively large seasonal range observed in this study is likely due to the shallow water environment in which these organisms were living. The difference in the temperature ranges which is observed between individuals may be due to their location within the stratigraphy from which they were collected. All specimens were collected from the two shell beds

discussed in Chapter 3, however, given the thickness of these beds and the potential long life span of these organisms (Angiolini et al., 2012) (particularly the gigantoproductids floatstone at Ricklow Quarry) observed difference in temperature ranges observed within specimens collected from the bottom and the top may not be considered anomalous. This may be particularly true for the late Brigantian as it is expected for systems to be dynamic during periods of climatic instability.

5.3.3 Understanding $\delta^{13}\text{C}$ data

The $\delta^{13}\text{C}$ data of mollusc and brachiopod shells is analysed alongside $\delta^{18}\text{O}$ during IRMS of shell carbonates and have the potential to be important recorders of environmental conditions. $\delta^{13}\text{C}$ recorded within carbonate shells has been shown to be strongly linked to dissolved inorganic carbon in the water column and therefore can be used as proxy for palaeo-ocean productivity (Donner and Nord, 1986; Goodwin et al., 2013; Mook, 1971; Mook and Vogel, 1968). However, interpreting $\delta^{13}\text{C}$ is often complex and often confounded as internal sources of C (from respiration and digestion) may be included in the shell, which can cause signals to be mixed or overprinted (Borchardt, 1985; Gillikin et al., 2006; Klein et al., 1996; Tanaka et al., 1986). This effect has been demonstrated in modern calcifying scallops (*Pecten maximus*) shell that appeared to be incorporating metabolic CO_2 into the shell calcite (Owen et al., 2002) and modern corals which show metabolic fractionation of $\delta^{13}\text{C}$ which is influenced by rates of respiration and photosynthesis (McConnaughey, 1989).

For these reasons, the interpretation of $\delta^{13}\text{C}$ within biogenic calcite is often approached with caution and is generally viewed more as a speculative estimation of the variability of productivity occurring through the organism's lifetime. A further complication occurs with *Gigantoproductus* species as a metabolic effect on the fractionation of $\delta^{13}\text{C}$ was suspected by Popp et al. (1986) as other coeval brachiopods showed *Gigantoproductus* had $\delta^{13}\text{C}$ 1 to 2‰ heavier. Garbelli et al. (2014) demonstrated a similar offset of $\delta^{13}\text{C}$ between Stophomenata (which are typically more negative) and Rhynchonellata and contributed this to differences in their fabric and their respective organic content, indicating that $\delta^{13}\text{C}$ values are strongly affected by metabolic effects.

Despite these complications, it is observed that all data points are within the ranges that suggest they are of ocean settings with minimal terrestrial input. The data from this study is also generally within range of that produced by other that analysed comparable material and environments (Angiolini et al., 2012; Mii et al., 1999; Mii et al., 2001) although generally may be considered to be slightly lower.

5.4 Summary

Using $\delta^{18}\text{O}$ data to calculate sea surface temperatures is difficult given the complexity of estimating a seawater $\delta^{18}\text{O}$ and the application of using modern analogues to understand environmental settings within the geological record. Despite these complications, it is a technique commonly used within palaeoclimate research and gives us the best estimations of sea surface temperatures through geological time. Given the understanding of the application of these techniques and limitations, the following conclusions can be made about the sea surface temperatures of the Brigantian palaeoequatorial epicontinental seaway:

- Temperatures calculated from the standard data set are frequently above the lethal limits for brachiopods. Given that it is likely not caused by material being altered and that the seawater $\delta^{18}\text{O}$ estimations are sensible, it is concluded that seawater $\delta^{18}\text{O}$ have changed over time and it is therefore necessary to detrended $\delta^{18}\text{O}$ before it is used as a sea surface temperature proxy.
- Despite this observation, it is noted that the current resources available to estimate the amount at which individual datasets collected at specific time intervals should be detrended is limited. However, and given the likely biased nature of specimen sampling, it is thought that modelled estimations are better than averaging values from available dataset.
- Average sea surface temperatures are thought to have been $\sim 23^\circ\text{C}$, which is within previously estimated ranges (Bruckschen et al., 1999).
- Disparity between results and between time slices within the Brigantian highlights the likelihood of this time being one with a dynamic climate system.
- Cyclicity could not be statistically identified within this dataset. However, the variability of calculated temperature within individual specimens can be

attributed to seasonal temperature variations. Seasonal temperature ranges of $\sim 6^\circ\text{C}$ to 11°C are therefore thought to have occurred in the Brigantian palaeotropical epicontinental seaways with the difference in temperature ranges between individuals attributed to a dynamic climate.

- Therefore, well-preserved Brigantian *Gigantoproductus* species biogenic calcite can be used to identify seasonal sea surface temperatures. However, if cyclicity is to be proved mathematically then the sampling resolution needs to be increased in order to generate more data points, and they should be evenly spaced, and may require laser sampling to get the high resolution. Although this is possible, generating this much data is costly and timely.

Chapter 6: Conclusions and further work

6.1 Conclusions

Species of *Gigantoproductus* of the Eyam Limestone Formation colonised habitats on the inner to middle ramp. Although there are noted differences in the two studied localities, the palaeoenvironment of both represent shallow waters of normal salinity. At both localities, the shell beds are preceded by a period of decreased energy; it is proposed that these allowed time for the brachiopod larval stages to settle. After colonisation, at Ricklow Quarry, a highly variable community was rapidly established which did not reach a stable climax. Baffling of mud and fine bioclasts aided by the large *Gigantoproductus* shell, may have provided localised shelter for other nearby individuals and larvae resulting in a positive feedback mechanism that encouraged further colonisation. This was also enhanced by the relict mud mound topography that provided shelter on its lee (east) side where the brachiopods colonised. A south-directed palaeoflow indicated by shell alignment contradicts that of the overall easterly palaeoflow of the platform but was likely caused by the relict mud mound topography influencing localised currents. With no mud mound present at Once-a-Week Quarry smaller communities of lower diversity occur, yet species of *Gigantoproductus* remain dominant, as their thick shells are able to withstand the elevated energy levels of the inner ramp which are thought to have occurred at this locality.

At both localities specimens with pristine ultrastructure can be found, although fossils from Ricklow Quarry are more commonly well-preserved. This is thought to be due to the floatstone shell bed at Ricklow Quarry being less porous than the grainstone shell bed at Once-a-Week Quarry and the presence of some minor faulting at Once-a-Week Quarry. The description of well-preserved ultrastructure (Chapter 3) can be used as a benchmark for future studies that wish to use ultrastructure as a means of preservation testing of *Gigantoproductus* species. The *Gigantoproductus* shell typically comprises a

thick prismatic layer often with regular stepped growth lines on prism surfaces, and a laminar secondary shell layer that comprises individual calcite laminae.

Identifying detailed structures, such as stepped growth lines or individual laminae, has been the focus for assessing preservation, as the large size of *Gigantoproductus* species makes it difficult to determine the ultrastructure of the entire shell length or thickness in detail. Following ultrastructure analysis, an overall assessment of preservation can be made by CL analyses that can identify heterogeneous preservation within a specimen.

These analyses indicated that the outer shell margin, the umbonal and anterior region are commonly brightly luminescent and/or not fabric retentive while the inner tertiary prismatic layer, where it remains well preserved, is the preferred material for further preservation and isotope analyses. This pattern of preservation is also seen within the trace element analyses. The heterogeneity of ultrastructure preservation and luminescence properties within a shell further highlights the need for specimens to be considered individually when determining which should be subject to further analyses.

It is concluded that the combined techniques of ultrastructure petrology and CL analyses facilitate targeting of individual specimens, as well as specific areas within the individuals, that are suitably well preserved enough to undergo further preservation assessment via trace element analyses. After preliminary analyses and method development, trace element analyses were conducted at a 200 μm spatial resolution and subsequent stable isotope samples targeted peaks and troughs in the variable Mg data in attempt to maximise the potential of establishing seasonal variation within the $\delta^{18}\text{O}$, if present.

In summary, overall good preservation is identified by the presence of detailed ultrastructure features, none or poor luminescence, trace element concentrations of Sr >700 ppm, Fe and Mn <25 ppm and a $\delta^{18}\text{O}$ value above -5.36‰ . Although ultrastructure and CL criteria, together with the methods of high-resolution trace element analyses, can be applied to future studies, the geochemical parameters outlined here are specific to this study. Published geochemical parameters for modern brachiopods would classify material from this study, which is likely to be diagenetic, as well-preserved and as such, highlights the need for future similar studies to analyse different material from their

study sites to establish acceptance criteria for preservation and ultimately palaeothermometry.

Geochemical alteration is more common at the outer shell margin suggesting that diagenetic fluids are not able to penetrate the shell interior. Similarly, patches of alteration surrounded by well-preserved material can occur within the shell interior likely occurring as growth lines, which are more permeable than the surrounding prismatic tertiary shell, provide a pathway for diagenetic fluids.

All the observations of this study highlight the need for rigorous high-resolution preservation analyses and trace element analyses, as random spot sampling may not capture the true variability of preservation present within a specimen. The resolution of the preservation analysis should be at least as high as the subsequent stable isotope analysis.

Following the identification of well-preserved material, the $\delta^{18}\text{O}$ data is used to calculate sea surface temperatures. The resultant temperatures calculated from this study illustrate that $\delta^{18}\text{O}$ data should be detrended to account for the evolution of seawater before temperatures are calculated. Currently, the means of quantifying the amount of detrending that appears to be necessary is poor. Despite this, average sea surface temperatures for the Brigantian epicontinental seaway are thought to have been $\sim 23^\circ\text{C}$ suggesting that the onset of the transition into the late Palaeozoic icehouse had begun prior to the Late Brigantian given that these temperatures are within the realms of modern tropical seas and we currently have permanent arctic ice masses. Additionally, although cyclicity could not be proved via mathematical means, the systematic variability within the data is attributed to seasonal temperature highs and lows and shows large temperature ranges, highlighting the instability of the climate during this time.

In conclusion, the $\delta^{18}\text{O}$ data from well-preserved biogenic calcite of some species of *Gigantoptoductus* is a good palaeotemperature proxy. Because of the heterogeneous nature of the preservation of the fossils, rigorous and detailed preservation analyses should be conducted, but typically, the thick prismatic shell layer of the inner shell provides the most suitable material. Minimum and maximum temperatures can be calculated and attributed to seasonal temperature variation when data is collected at

~200 μm resolution however, mathematically identifying a seasonal cyclical pattern is limited by sampling techniques and a lack of understanding of shell growth rates and mechanisms.

The significance of this research and the key findings are that both the palaeoecology study (Chapter 2) and the detailed description of species of *Gigantoproductus* ultrastructure (Chapter 3) represent the first studies of their kind for these organisms and therefore provide a good starting point for future studies. Additionally, the identification of variable preservation levels within individual specimens highlights the need for preservation analyses to be conducted at a comparable resolution to subsequent stable isotope analyses. This conclusion should be considered in future palaeoclimate studies of this type. Having conducted such rigorous geochemical preservation analyses, conclusions drawn from the interpretation of stable isotope data can be treated with a high degree of confidence. The recognition of the need to detrend data could prove to be highly significant to future studies that wish to calculate sea surface temperatures from $\delta^{18}\text{O}$ data. Furthermore, this study contributes to the growing literature dealing with the timing of the onset of the late Palaeozoic icehouse, supporting recent suggestions that its onset occurred before the end of the Brigantian.

6.2 Further work

Nolan et al. 2017, presented the first palaeoecological study of *Gigantoproductus* shell beds, this proposes a preferred environment and colonisation mechanism for two localities on the Derbyshire carbonate platform. However, if the links of habitat change with species of *Gigantoproductus* abundance are to be considered furthermore, studies of this type are required in order to see if colonisation mechanisms differ or if preferred environments are less common.

Ultrastructure analysis is a well-established method. However, there is a potential to enhance the benefits through a study of more individuals, measuring metrics of individual growth lines and shell thickness in order to further understand the growth rate and mechanisms of these organisms. If a better understanding of growth is established then it will be easier to tailor a sampling strategy, which optimises the potential of identifying seasonality within $\delta^{18}\text{O}$, and possibly trace element data. Additionally, as with

all studies of this type, more data is always beneficial in refining mean, minimum and maximum palaeotemperature ranges. The preservation profiles provided in Appendix E describe the preservation of all analysed specimens. These profiles may be used to select suitable specimens, should further research opportunities become available. If such research were to be conducted there is also potential to include additional methodologies such as clumped isotope analyses, continuous sampling of the shell via destructive micro drilling or including other palaeotemperature proxies such as Mg from foraminifera or $\delta^{18}\text{O}$ from other organisms such as well-preserved corals which are present within the Ricklow Quarry section. Clumped isotope analyses were not used in this study, as the amount of material required for these analyses is too great to allow sampling on the scale desired. However, if continuous micro drilling were to be used it may be possible to increase the volume of material available whilst maintaining an adequate sampling resolution to investigate seasonality. Using Mg concentrations from well-preserved foraminifera may provide a suitable secondary proxy to mean sea surface temperature (providing the appropriate species are present) however; this proxy cannot help elucidate seasonality. The $\delta^{18}\text{O}$ data from well-preserved coral, however, may provide insight to seasonality; however, there are considerably fewer corals available within the studied sections so finding suitable materials may prove difficult.

Although well beyond the scope of this research project, it is noted that there is still extensive work to be done on understanding if the baseline seawater $\delta^{18}\text{O}$ value has changed through time and developing a more accurate means of quantifying the amount by which data should be detrended before calculating sea surface temperature. Furthermore, if this is deemed the case, then a comprehensive timeline with estimated values through geological time needs to be produced which would provide researchers with values to be used when calculating temperatures. For the Carboniferous alone, this could account for a 16°C difference in calculated temperatures, which is a substantial temperature difference that may change our current understanding of past climates, even more so for those climate scientists working further back in the geological record.

Appendices

Appendix A. Thin section images (provided digitally)

Images of thin section from samples collected from Ricklow and Once-a-Week Quarry. A figure title 'Ricklow sampling' is also present and

Appendix B: Palaeoecology data (provided digitally)

Digitalised palaeoecological data collected from Ricklow and One-a-Week Quarry. This data is used in Chapter 2.

Appendix C: Scanning electron microscope images (provided digitally)

Additional SEM images collected at various magnification of all the species of *Gigantoproductus* that were analysed. These are the original raw images with no interpretation or labelling of features.

Appendix D. Cathodoluminescent images (provided digitally)

Additional CL images of all analyses specimens. These are the additional raw images and do not contain any interpretation. In the folder titled 'CL Mosaics' images of all CL images of individual specimens are stitched together to provide a complete image of each specimen in CL.

Appendix E: Preservation reports (provided digitally)

Here reports detailing the results and some interpretation of all preservation analyses conducted on each specimen are presented. An example is provided between p. 172 – 192.

Appendix F. Trace element and stable isotope data (provided digitally)

This includes all data collected from the preliminary and the secondary methodology and all experimental data that was collected to refine methodologies. Images of the specimens after laser ablation analyses are also provided and allow the analysed transect to be seen.

Appendices

Analyses that were conducted to inform the method development and include the following data sets:

1. Trace element data collected from the MACS carbonate standard which was then used to justify the use of a glass standard when analysing carbonate materials.
2. Trace element data from transects through specimens that were ran on selected specimens at various resolutions which were used to inform the decision of sampling resolution.
3. Trace element data from transects ran at various angles (relative to growth) through the shell.
4. Trace element data collected from a 'grid' of analyses covering an area of a 100 μm^2 which was conducted with the aim of quantifying the variability that may be lost if the 100 μm laser spot sized was used.
5. Trace element data from transects of laser analyses that were ran along the track produced from the microdrilling for collecting material for stable isotope analyses. The aim of these analyses was to cross check that there is minimal lateral variation in trace elements with growth lines.

Data from specimens that were not selected for stable isotope analyses is also present and includes specimens that were analysed via both the primary and secondary methodology. For those specimens discussed in this thesis both the trace element and stable isotope data is provided in the same spreadsheet along with details on how those two datasets correlate for each individual specimen.

Data from end-member and bulk rock samples is also present in this folder, both trace element and stable isotope as well as a single spreadsheet with all samples trace element and stable isotope data compiled. All spreadsheets containing raw data also include error calculations for each element and each specimen and documents produced from JMP that outline details of distribution analyses and Spearman's Rank correlations are present.

Appendix G. Palaeotemperature calculations (provided digitally)

from all stable isotope data using multiple palaeotemperature equations and additional seawater $\delta^{18}\text{O}$ values. Temperatures are calculated for seawater $\delta^{18}\text{O}$ values of 2‰, 1.5‰, 1‰, 0.625‰, 0.125‰, 0‰, -1‰, -2‰, -2.5‰, -3.25‰ and -3.5‰ of the standard

Appendices

and detrended data and are calculated using the Leng and Marshall (2004) and the Anderson and Arthur (1883) equations.

Appendix H. Supplementary data from Veizer et al., (1999)

The data set discussed in Veizer et al., (1999) is publicly available and contains $\delta^{18}\text{O}$ and $\delta^{13}\text{C}$ data from present through to 553Ma from low magnesium calcite sample as well as a $\delta^{18}\text{O}$ and $\delta^{13}\text{C}$ data set collected from benthic forams, however this does not span into the carboniferous and therefore was not used within this thesis.

Appendix E

Ultrastructure analysis

Sample name: RCK6bis

Species: *Gigantoproductus inflatus*

Collection Location: Ricklow Quarry

Results

Ultrastructure analysis was conducted on the gold coated surface of the shell via scanning electron microscopy at the Dipartimento di Scienze della Terra “A. Desio” University of Milano. Shell fabric can be recognised within this specimen and the secondary laminar and tertiary prismatic layers easily identified. No primary shell layer is present.

Transects through the shell (from the inner to outer margin – Figure 1) indicate a high variability within the ultrastructure. This frequently includes multiple changes between the secondary and tertiary fabrics and occasional overprinting of primary features via secondary mineralisation.

Frequently detailed primary structures such as individual laminae within the secondary layer, individual calcitic prisms within the tertiary layer and the transition between these two layers can be recognised at high resolution (x 750 magnification). Within the tertiary prisms apparent ‘stepped growth’ can also be seen. This appears as small, often faint but frequent, lines on the surface of individual prisms (Figures 1 and 2).

Small areas of the shells ultrastructure are disturbed by diagenetic recrystallisation (mainly silicification). This mineralisation is seen to overprint small areas of the shell and either mimic the form of the biogenic calcite which lies below or forms a crystal which crosscut and disrupt the shell fabric. Secondary mineralisation also appears as microcrystals protruding out of the surface of the shell (Figure 3b and c). Both features

Appendices

occur on the shell surface meaning the ultrastructure below is either no longer present or cannot be seen. The silicification present within this sample occurs at the transition zone between the secondary and tertiary shell layers. There is only one occurrence of this type seen within this sample. The isolated micro crystals appear to have no preferable position within the ultrastructure. They occur around the mimetic mineralisation and in isolated areas around the shell.

Pseudopunctae are present within the secondary laminae layer however, within this sample they are rare with only two examples recognised. Punctae are recognised as areas of the secondary layer where the lateral direction of the laminae changes. The spines which would have been present are no longer attached to the shell.

Fractures within this sample occur at boundaries of significant changes of growth, for example between the secondary and tertiary layers. However, none of these fractures continue along the entire length of the shell and they do not occur at every boundary.

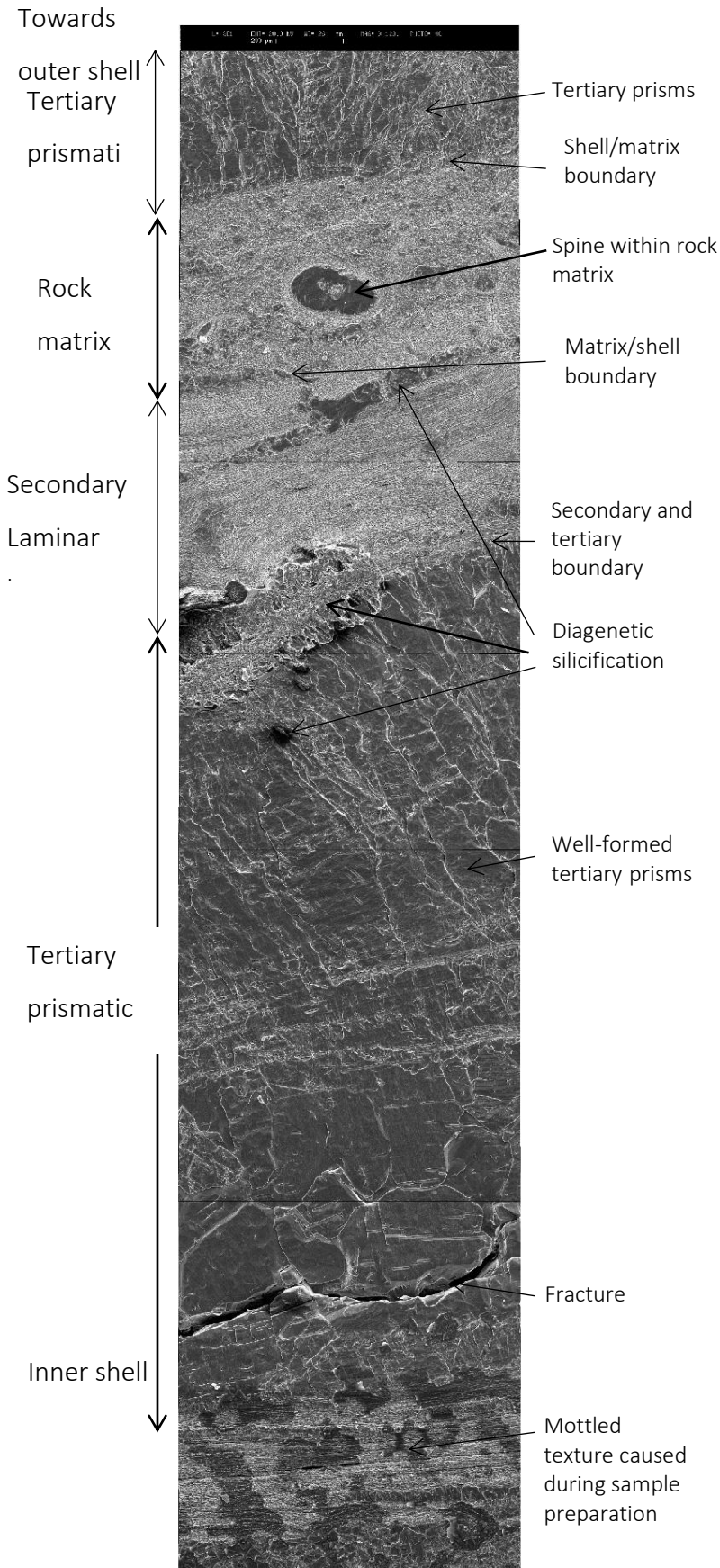


Figure 1. Transect from the inner shell (bottom) towards the outer shell boundary (indicated by the first occurrence of secondary laminar layer below the rock matrix) indicating changes in texture between the secondary and tertiary shell layers. A significant fracture occurs in the innermost part of the tertiary layer, toward the bottom of the image.

Progressing into the secondary layer the ultrastructure is formed of secondary laminae. These are well-formed laminae and organized into layers with cross bladed units (details in Fig. 2a). In some areas the secondary laminae have been overprinted by secondary mineralisation. Secondary mineralisation is also present at the secondary - tertiary boundary here there is further overprinting of the original shell ultrastructure which stands proud of the shell surface with additional secondary microcrystals also surrounding the region. The prismatic layer is formed of tertiary prisms which, when they first occur are small, and although individual prisms can be recognised they are less well-formed than those at the base of the layer which are well-formed, large and easily identified.

Appendices

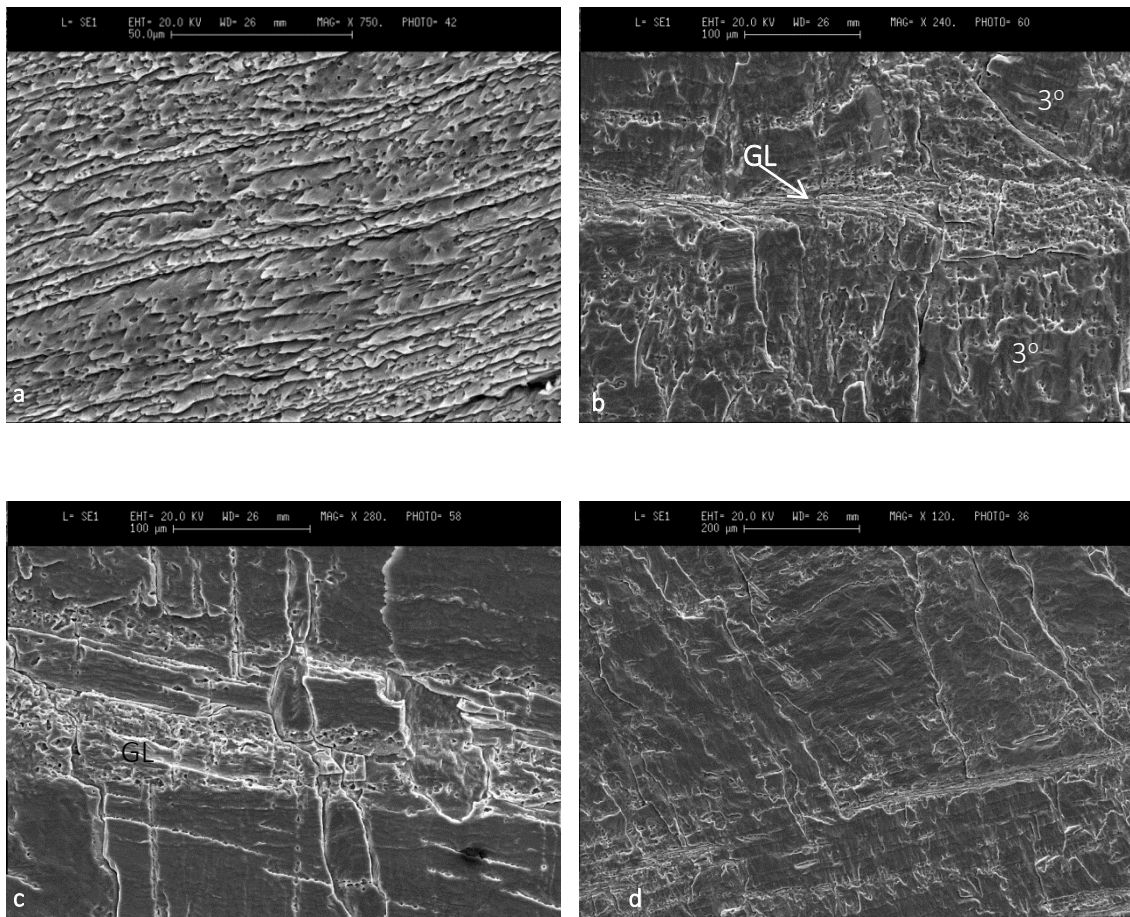


Figure 2. Detailed SEM imagery of sample RCK6bis. Image a) shows individual laminae within the secondary laminar layer which throughout the imaged section of the shell average at $\sim 0.9 - 1.0 \mu\text{m}$ thickness. b) Shows a growth line between $1\mu\text{m}$ and $2.25\mu\text{m}$ thickness within the tertiary prisms into the tertiary prism (3°). Image c) shows a growth line (GL) within the ultrastructure with a thickness ranging between $43 \mu\text{m}$ and $63 \mu\text{m}$. These growth lines have an average spacing of 0.47 mm d) Shows the stepped growth visible within the tertiary prisms. These stepped growths are spaced between $0.41 \mu\text{m}$ and $1.22 \mu\text{m}$.

Generally, the ultrastructure within this sample appears to be well preserved as primary features such as secondary laminae and tertiary prisms can easily be identified. Cathodoluminescent microscopy (CL) was conducted on a thin section made of this sample and indicated that there is a substantial area of the shell ($\sim 2.3 \text{ cm}$ length) which appears nonluminescent and therefore is interpreted as consisting of primary calcite. This is consistent with the ultrastructure data as this also indicates that there are large areas

Appendices

of shell which consist of seemingly pristine calcite. However, within the CL data there are several large areas of heavily fractured material which has been in filled with luminescent secondary material. This is not apparent from the ultrastructure images as although microfractures are identified it is difficult to identify what material, if any, these fractured have been in filled with. Furthermore, within the ultrastructure images there are no large areas of heavily fractured material seen. This could be that at high magnifications, such as those needed.

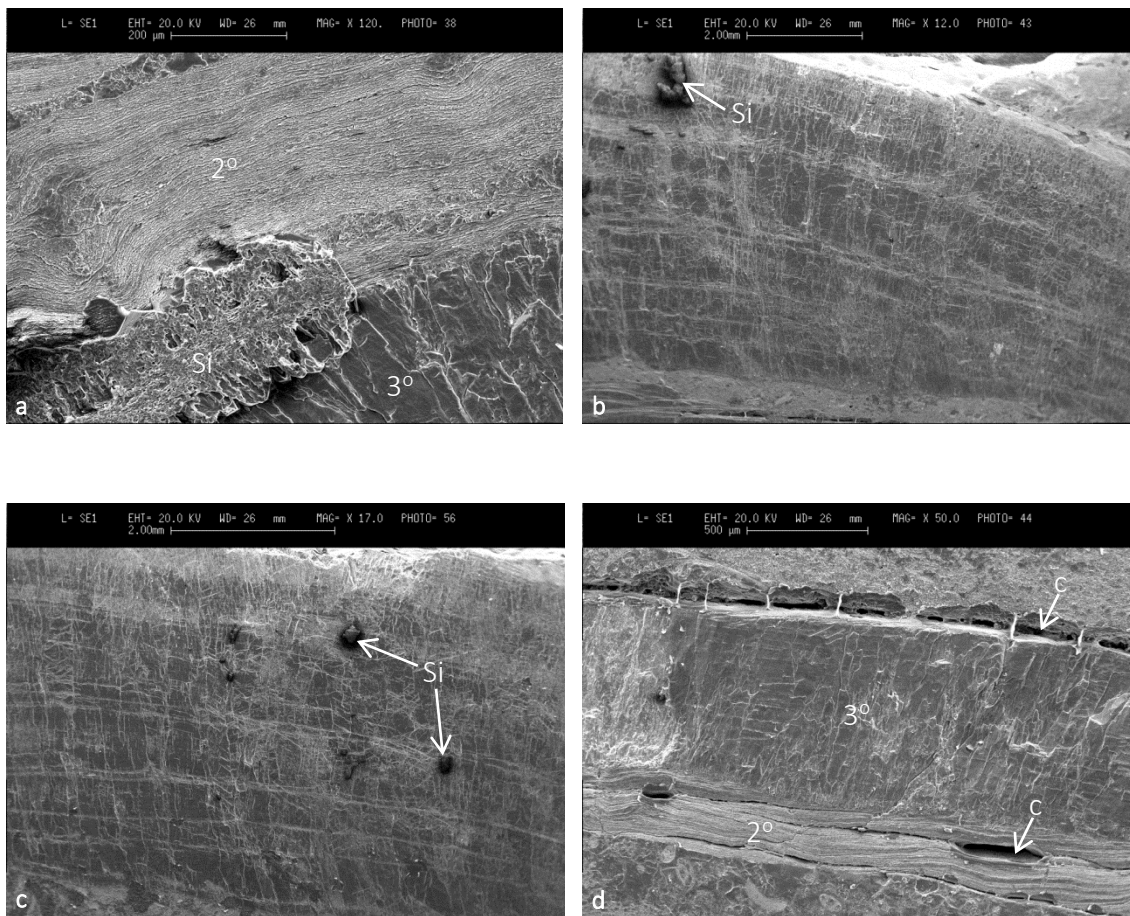


Figure 3. Image a shows the diagenetic silicification (Si) occurring at the transition zone between the secondary and tertiary shell layers. Figures b and c show secondary mineralisation (likely to be micro quartz) occurring as small isolated crystals and protruding from the surface of the shell. Image in c you see several growth lines which are spaced between 0.2 mm and 1.2 mm apart. d) Shows small cavities less than 1 μ m wide (c) between the matrix and the tertiary layer of the dorsal valve and between the secondary and tertiary layers of this valve.

CL analysis

Results

Thin sections were made of the sectioned surface of the sample and were analysed, at the university of Milan, under stable conditions (10 KV voltage and between 3-6 MA current) using a cathodoluminescence luminoscope (CL) (Nuclide mod ELM2B) mounted on a Letz Ortolux II microscope. Images of the (thin section) microfacies were taken in cathodoluminescence (CL) and replica images were also taken under parallel and/or cross polarised light to allow comparison of the same microfacies detail. The images were taken in a systematic manner where they overlap. This allows the images to be stitched together to produce a single image of the shell under CL light enabling the identification and comparison of luminescent and non-luminescent areas (Figure 1).

Within the sample RCK6bis there are three sections of varying degrees of luminescence which can be defined (Figure 1). Roughly 1 third of the shell, towards the umbo, has a moderate degree of luminescence however, contains an open fracture/cavity which has a thin, first high luminescent (orange) calcitic rim around the fracture/clast boundaries (Figure 2a). Within the open fracture and on either side, the calcitic matrix is highly luminescent and contains other small fractures. Progressing away from this crack, on both sides, the calcite is partially luminescent and then it gradually becomes less luminescent as you progress further from the fractured material. The second and central third of the shell contains only some minor fracturing (luminescent microfractures) and is generally non-luminescent or has very little luminescence. The final third towards the anterior margin is heavily fractured. This consists of small scale fractures which penetrate small areas of shell as well as large major fractures which continue through the entire thickness of the shell. Additionally, this shell material appears highly luminescent.

In addition to comparing sections of the shell via the degree of luminescence, comparisons can also be drawn when relating the colour of the luminescence. For example, in this sample in the third section of this sample the partially luminescent material (i.e., the shell material, not the secondary in filled microfracture) luminesce a dull purple/violet colour but the secondary veins which run through this section and still

Appendices

luminesce a bright orange colour, the same as that in other sections of the shell. Where the shell material does not luminesce, purple and is luminescent it appears as a dull orange colour, where it is not luminescent or purple it appears as a dark brown/grey. The secondary material which is highly luminescent, such as the matrix or material infilling fractures is a bright orange/red colour.

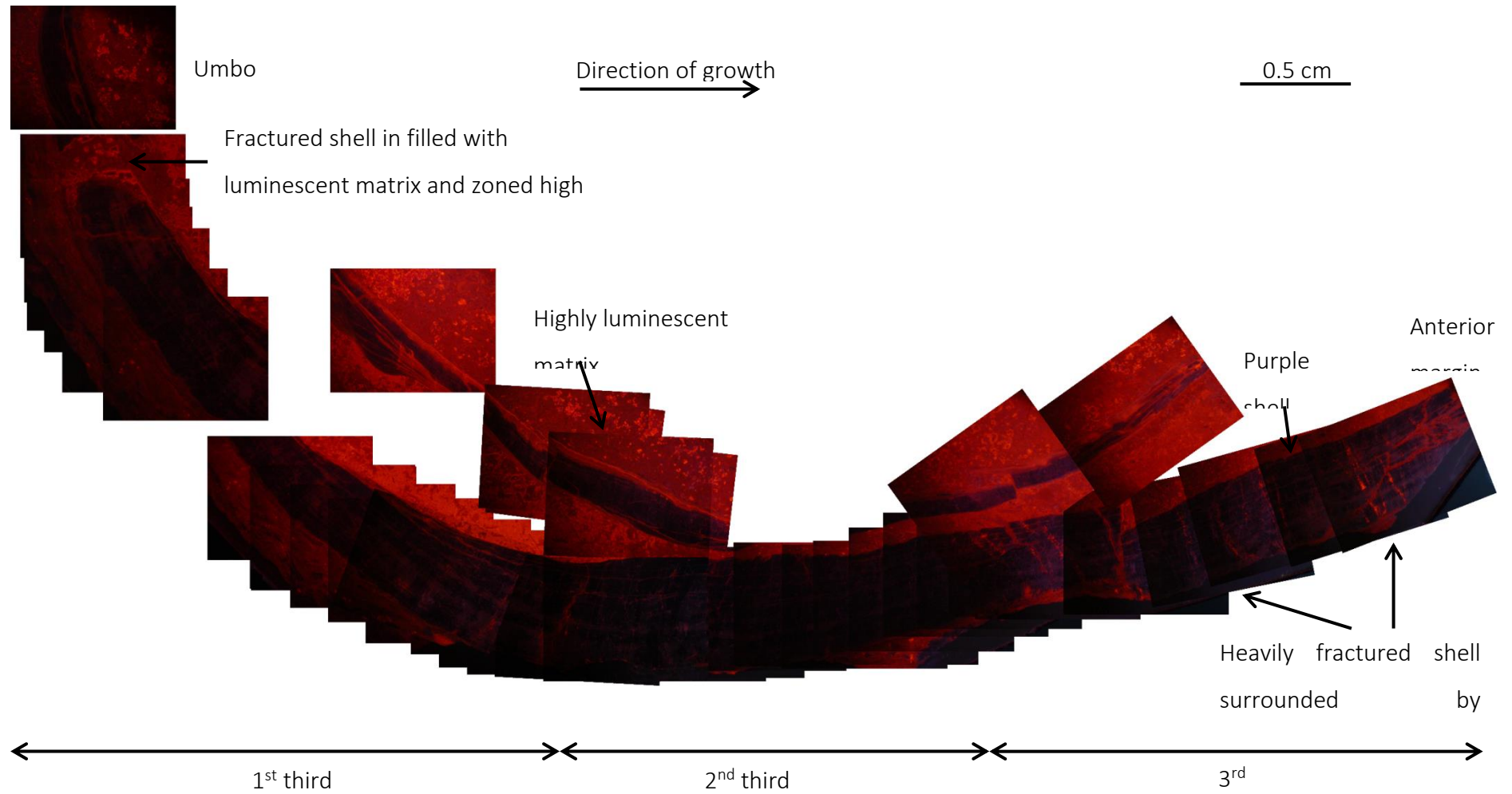


Figure 1, An overview of the luminescent qualities of the sample via stitched together individual CL images. The figure indicates how the luminescent properties of the shell allow it to be divided into three sections.

Appendices

Detailed images of significance areas are shown in figure 2. These images highlight the variety of differing degrees of luminescence within sections of one single shell.

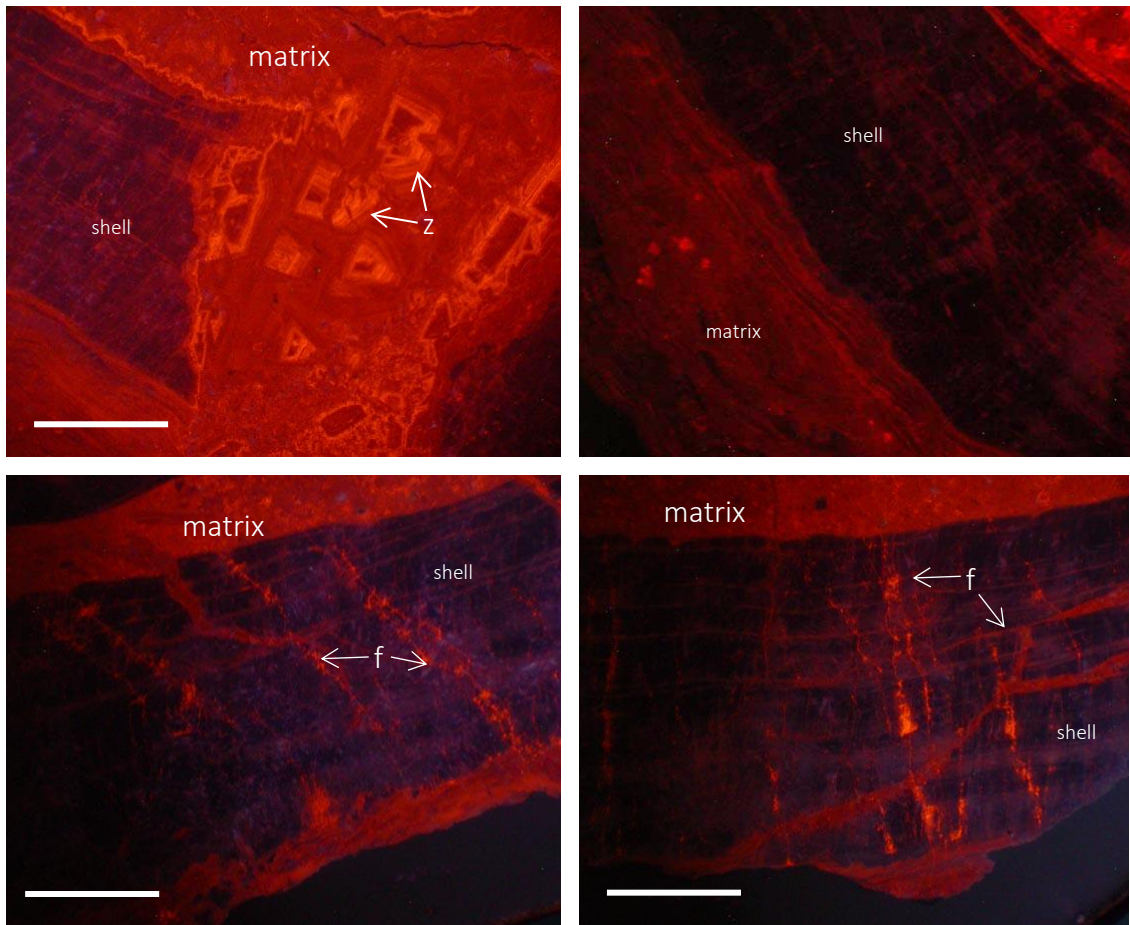


Figure 2. a) Image a shows the large crack in the 1st third of the shell. The open fracture is firstly in filled with homogenous luminescent matrix. Later rims around diagenetic material made forming a zoned high luminescent (orange) diagenetic calcite (z) illustrating a different chemical phase during its formation. b) shows a non-luminescent section of the 2nd third of the shell indicating good preservation within this region. c and d) show what is likely to be two different generations of luminescent microfractures which may be caused by diagenetic packing and or tectonic affects indicated (f) within the 3rd third of the sample. Note that in all images the matrix is more luminescent that the shell material but in some cases not as luminescent as the secondary calcite present within fractures. All scale bars are 5 mm.

Although there are areas of the shell which have undergone secondary diagenetic processes which are likely to have affected the geochemistry of the calcite these areas can be defined and are frequently constrained meaning in many cases they can be avoided. Within the non-luminescent section, the degree of luminescence is generally homogenous this in theory suggests that any trace element data obtained from this

Appendices

region should also be generally homogenous. This is a means of cross examination between varying methods of preservation testing.

If further analysis such as trace element and isotope data is to be obtained from this sample is advised that the centre non-luminescent section of the shell is analysed as this region is more likely to contain primary calcite, unaffected by diagenetic affects.

Ultrastructure analysis

Sample name: RCK36

Species: *Gigantoproductus okensis*

Collection Location: Ricklow Quarry

Results

Transects through this shell (from the inner to outer margin – Figures 1 and 2) show that it is dominated by the prismatic tertiary layer. There are areas of the shell which consist of the laminar secondary layer which occur predominantly at the outer shell margin. The passage from the secondary to the tertiary layer is transitional with frequent intercalations of the two layers. No primary layer is preserved.

Detailed primary structures, such as individual lamina within the secondary shell layer, can be seen at magnifications of X 400 and individual prisms can be seen at magnifications of X 70 within the tertiary prismatic shell layer. In areas where high detail is preserved stepped growth patterns on the surface of these prisms can be seen at magnifications of X 800. Growth lines can also be seen, often have well-defined edges and can be traced along images.

Localised silicification commonly occurs at the outer shell margin and occasionally at the inner shell margin. This silicification occurs externally and overprints the underlying original shell texture, however it is noted that this occurs both within the secondary and tertiary shell layer.

Pseudopunctae are present within the secondary laminae layer these are recognised as structures within the secondary shell layer where the direction of the laminae is deflected inwards. In some cases, within this specimen the taleolae are also visible.

Fractures are present within this specimen and are frequently seen to occur within the shell and follow growth lines.

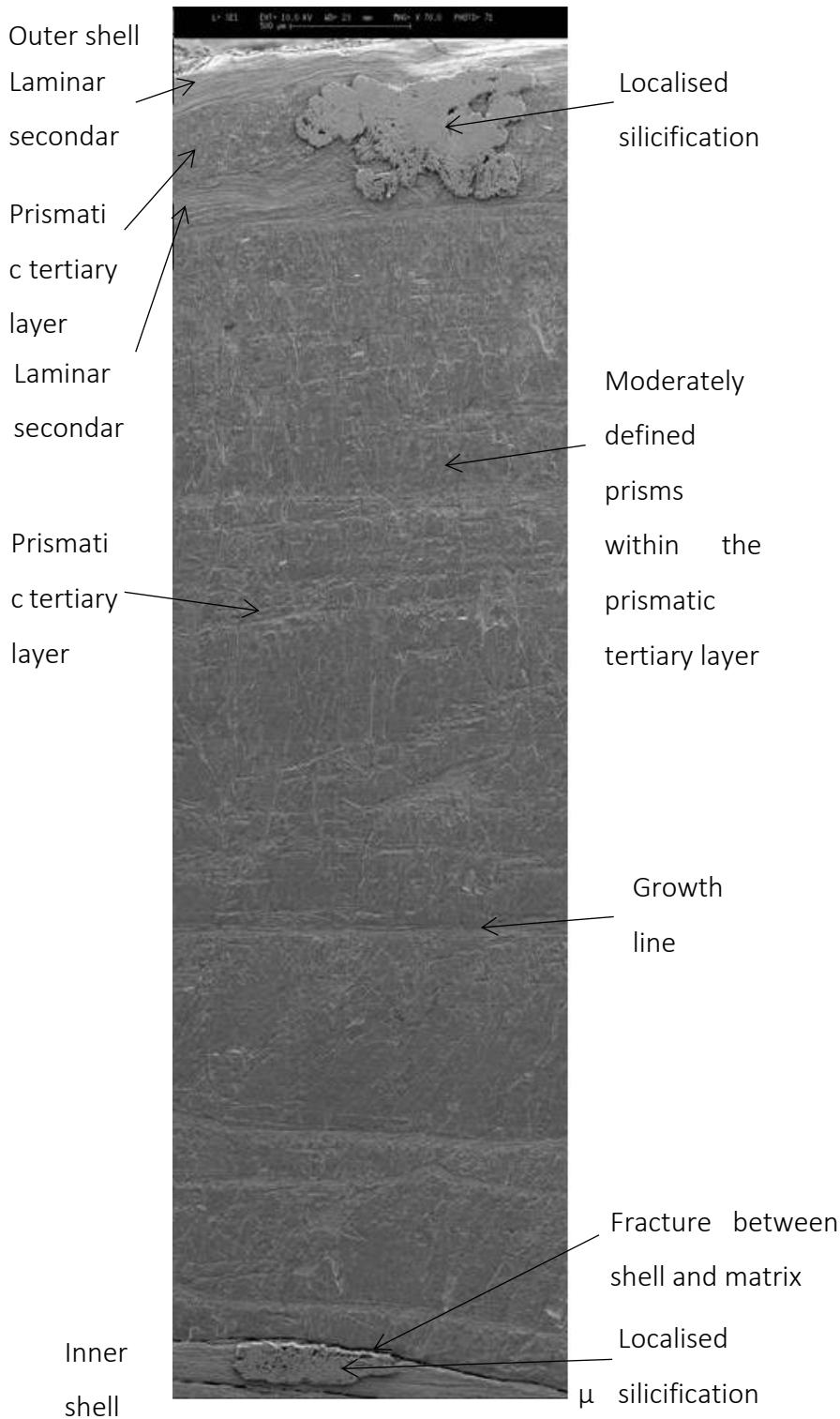


Figure 1 Transect from the inner (bottom) towards the outer shell boundary (top) indicating changes in texture.

The outer shell margin remains intact with a thin layer of the laminar secondary shell layer present. The passage between the underlying tertiary layer is transitional with intercalation of the two layers. There is a large patch of localised silicification overprinting the original shell texture (both tertiary and secondary layers). The prismatic layer appears well preserved with some individual prisms identified at this magnification (X 70).

Through the section, 1 third of the way down, within the tertiary layer there are several traceable growth lines.

The well preserved tertiary layer continues through the section until the inner shell margin is reached. Here there is a fracture between the matrix and shell material as well as more localised silicification.

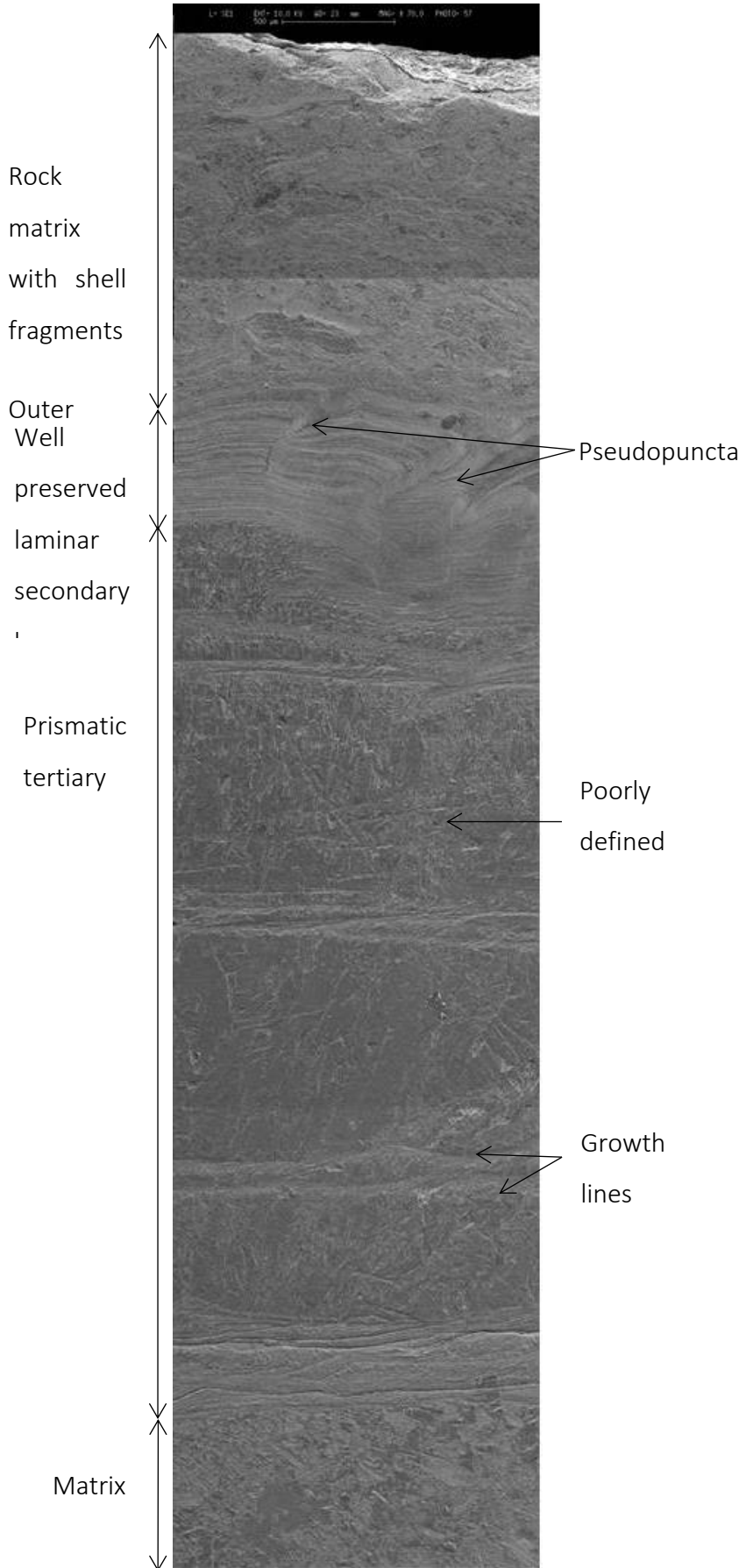


Figure 2 Transect from the inner (bottom) towards the outer shell boundary (top) indicating changes in texture.

The outer shell comprises of a thin layer (~500 μm) of the laminar secondary layer with pseudopunctae visible.

The remaining shell thickness consist of the tertiary prismatic layer with some individual prisms recognisable however generally poorly defined. Running across the tertiary layer are several moderately defined but traceable growth lines.

Towards the inner shell margin there are two fractures which can be traced across the image however the matrix – shell boundary appears well defined within the matrix recognisable from the difference of texture between the two materials.

Appendices

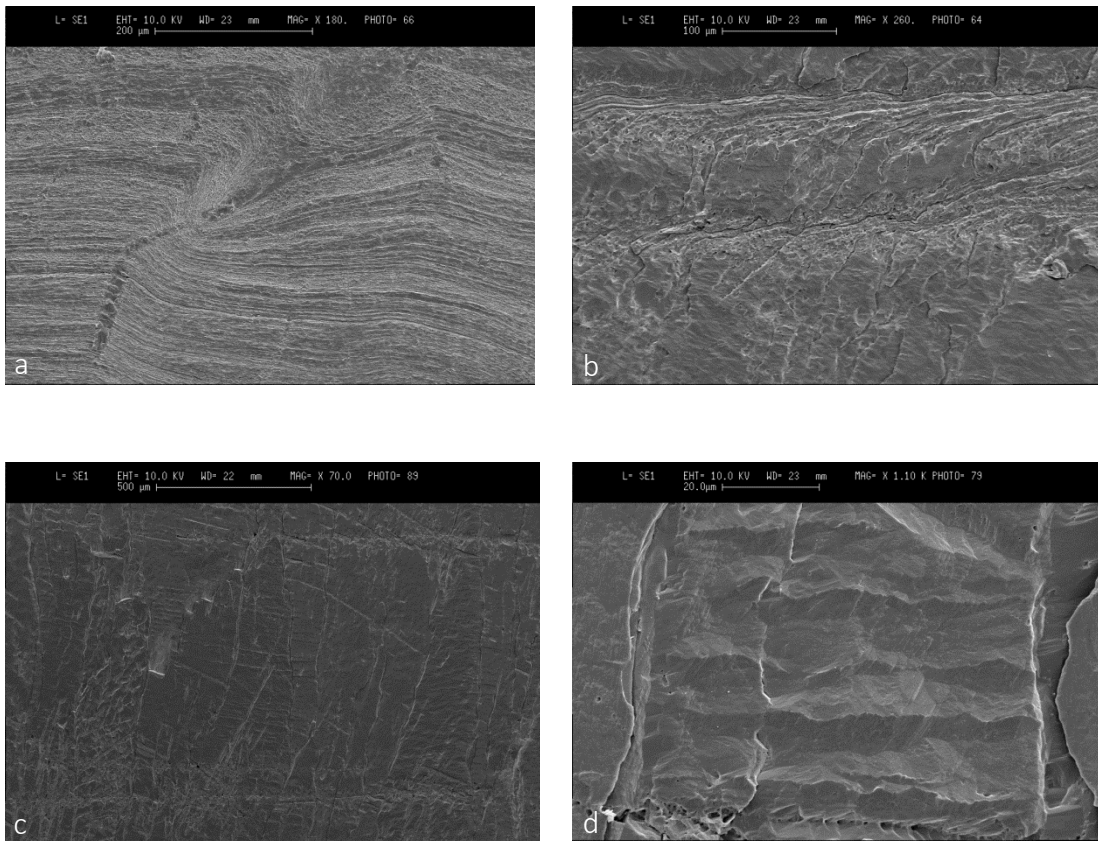


Figure 3 image a) shows the well-formed laminar and pseudopunctae within the secondary shell layer. Image b) shows the formation of individual prisms within the tertiary shell layer. Image c) shows the well-formed tertiary prisms and image d) shows the stepped growth lines on the prism surfaces. Stepped growth lines are spaced between 2.1 μm and 6 μm.

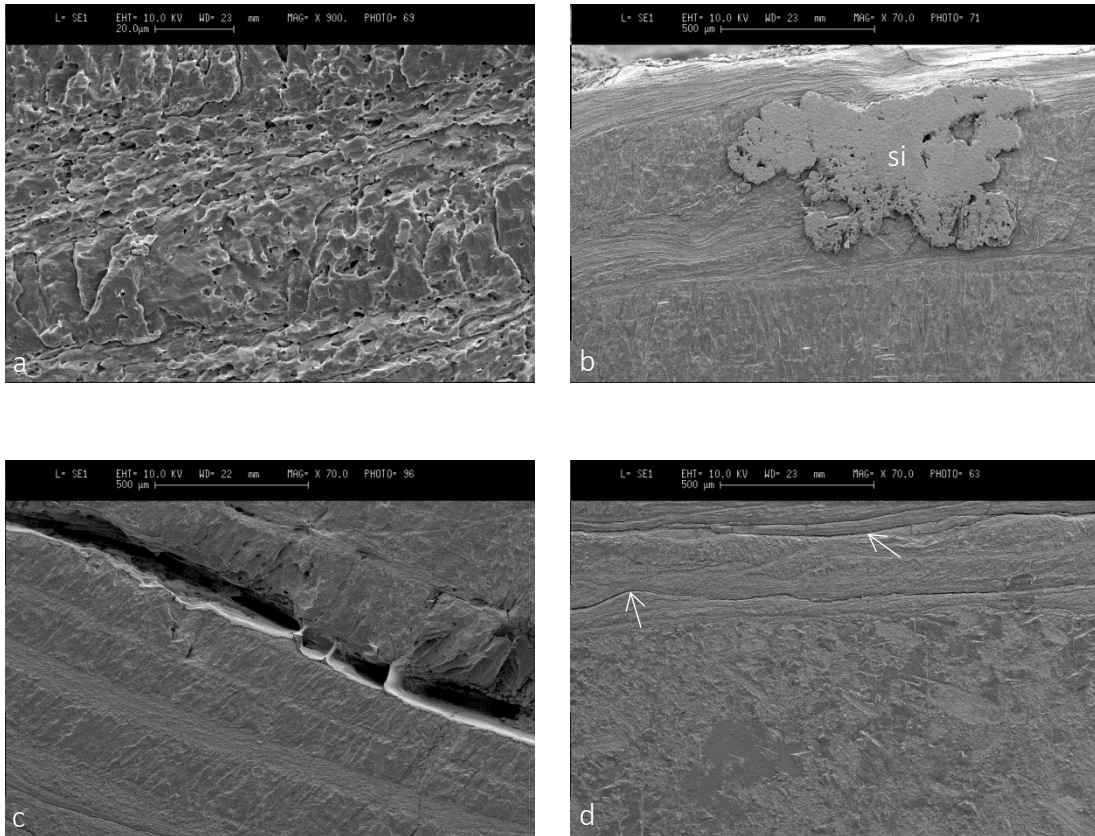


Figure 4. a) Amalgamation of the shell fabrics leading to poorly defined original textures in this case this is the formation of tertiary prisms. Image b) shows localised silicification at the outer shell margin. Here the silica completely replaces the shell fabric. Image c) shows a large fracture running through the shell interior. Image d) shows two fractures running parallel with the inner shell margin.

Diagenetic mineralisation within this specimen is rare with only localised silicification present in isolated areas and at the shell margins. There is some evidence of amalgamation of shell fabrics but again, this appears to be localised and rare. Cathodoluminescent analysis also shows that the preservation of this specimen is good.

CL analysis

Results

Cathodoluminescence analysis of this specimen shows generally poor luminescence indicating a well preserved shell with some small areas of alteration indicated by brightly luminescent calcite.

The outer shell margin of this specimen is consistently highly luminescent showing that it is poorly preserved. Although the brightness and colour of the luminescent calcite remains consistent the thickness of this luminescent band varies. Within the umbonal region this band forms only a small slither whereas within the central shell region a larger band, more than 1 mm thick is orange and luminescent. This luminescent band reflects the altered secondary laminar layer.

Within the umbonal region the shell thickness decreases and at the inner shell margin there are several closely spaced moderately luminescent bands. These are growth lines and can be traced some way along the length of the shell into the central shell region remaining at the inner shell margin.

The internal shell appears generally poorly to non-luminescent and is a dark blue to violet colour. Within this region growth lines appear faint, poorly luminescent and violet in colour and follow the shell contours. Similar luminescent lines can also be running obliquely to the shell contours. These show a similar amount and colour of luminescent but only occur within the shell interior and within the central shell region and are due to the growth of a median ridge inside the ventral valve. They are not present towards the anterior margin or. These lines are also visible within the PPL scan of the specimen. Because of the nature and colour of these two types of luminescent lines it is thought that these are primary feature of the shell texture.

There are additional brightly luminescent orange colour lines which cross cut at 90°, therefore running from the external to internal shell margin although these lines do not always cut through the entire shell thickness. Because of the brightness and colour (similar to matrix material) it is thought that these are diagenetic features.

Anterior
margin

Umbo



Figure 5. scan of the whole section of the specimen. This image highlights the thickness changes in the shell and visible growth lines.

Appendices

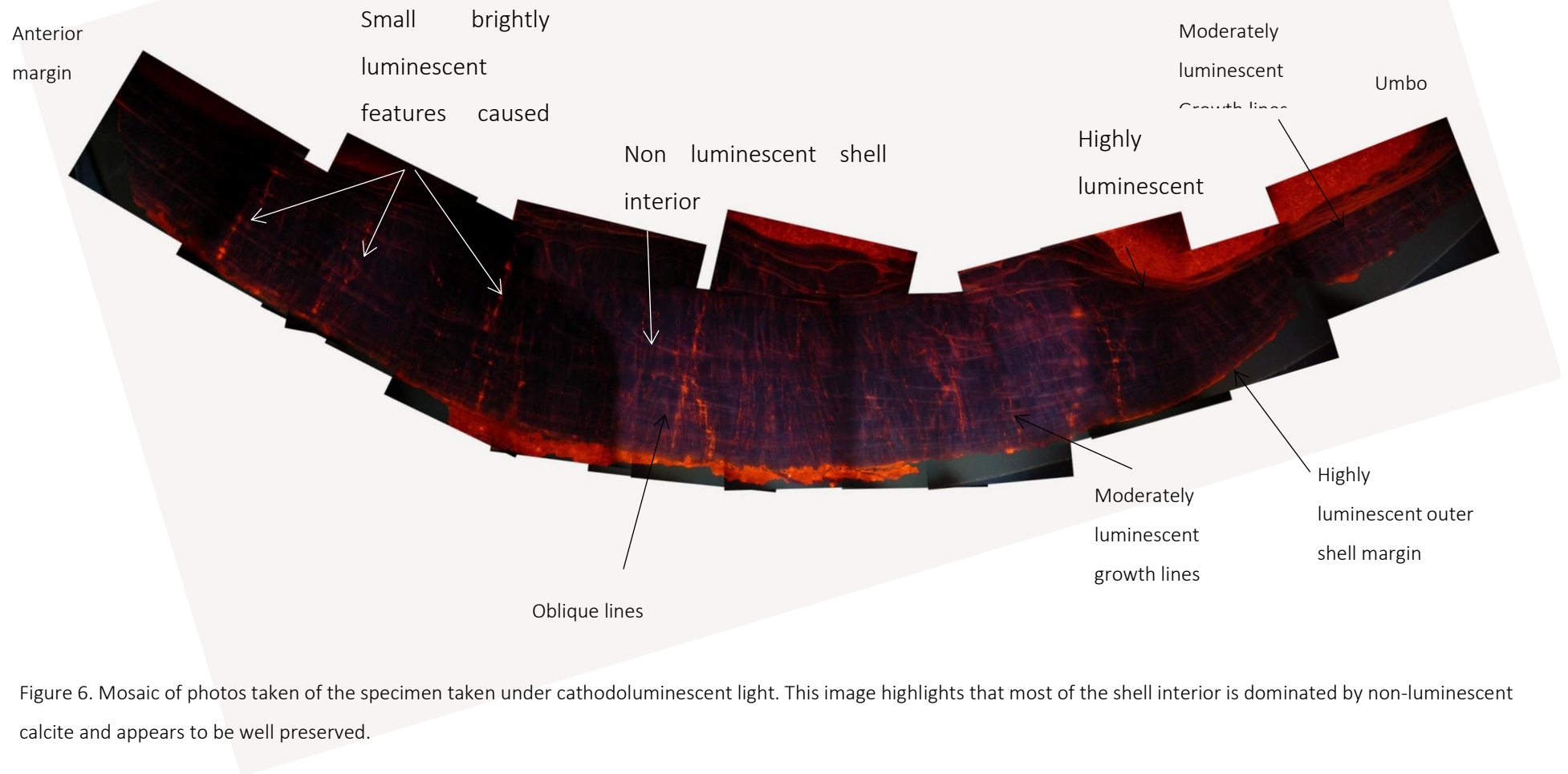


Figure 6. Mosaic of photos taken of the specimen taken under cathodoluminescent light. This image highlights that most of the shell interior is dominated by non-luminescent calcite and appears to be well preserved.

Appendices

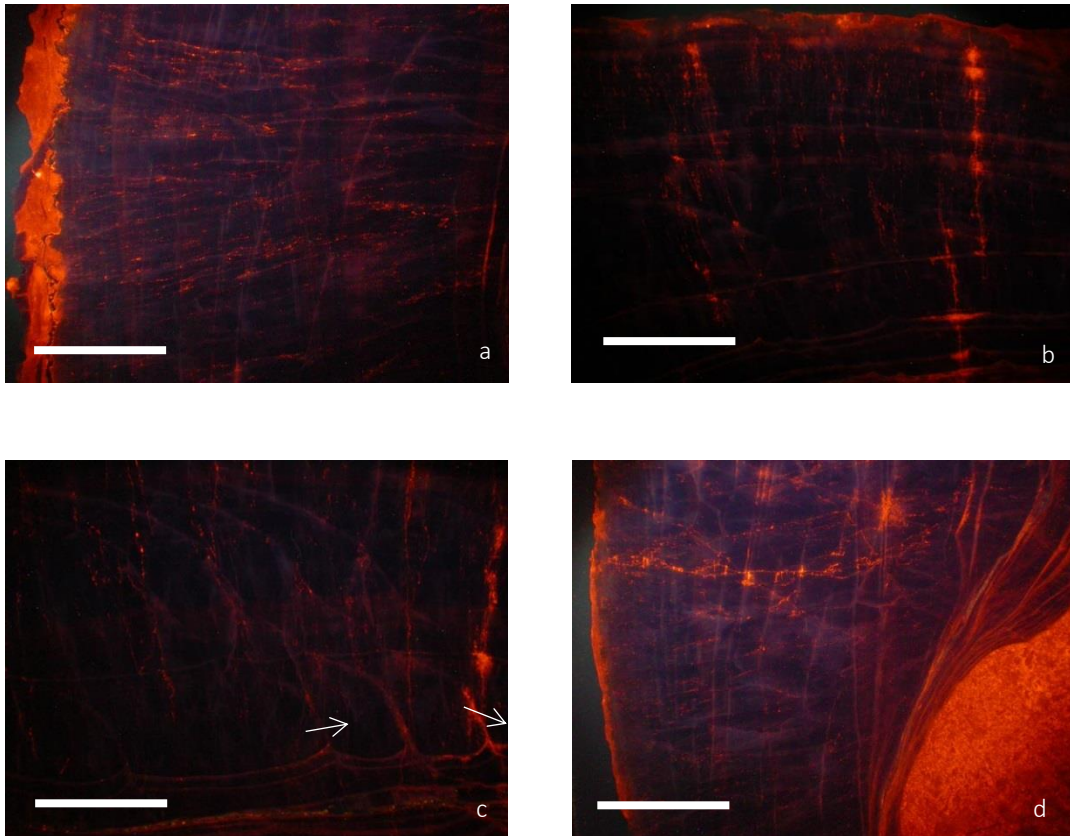


Figure 7. Details seen within Figure 2. Image a) shows the luminescent outer shell margin with non-luminescent shell interior. Image b) shows the vertical luminescent lines cutting through the non-luminescent shell interior. Image c) shows poorly luminescent lines following shell contours, running vertical and oblique (indicated) to shell growth. Image d) shows the umbonal region with a thin strip of brightly luminescent shell at the outer margin and concentrated luminescent growth lines at the inner shell margin. All scale bars are approximately 5 mm.

Both ultrastructure and cathodoluminescent analysis of this specimen reveals that it is well-preserved. Few areas appear to consist of diagenetic material and all images localised silicification is concentrated at the outer shell margin. Therefore, it is suggested that this specimen is suitable for further sampling and could be used in isotope analysis if the outer margin is avoided.

Geochemical analyses

Results

A summary of the results of geochemical analyses of a transect of this specimen are given in Table 1 and then shown in Figure 8a and b.

	Na (ppm)	Mg (ppm)	Mn (ppm)	Fe (ppm)	Sr (ppm)
Min	0	1032	0	3	70
Max	1401	5827	585	7100	1361
Range	1401	4795	585	7097	1291
Mean	877	3008.	22	113	1067

Table 1. Minimum (min), Maximum (max), overall data range (range) and means of key trace element data through the specimen.

Mn concentrations are between 0 ppm and 585 ppm and Fe concentrations are between 3 ppm and 7000 ppm with average concentrations for 22 ppm and 113 ppm respectively. Sr concentrations are between ~600 ppm and ~1500 ppm with an average concentration of ~1000 ppm. Mg concentrations are between 1728 ppm and 7160 ppm with an average concentration of 3248 ppm.

Figure 8 illustrates the heterogeneous distribution of Sr and Mg through the shell transect whilst Mn and Fe remain low throughout except for the data point at the outer shell margin. It is suspected that this data point also skews the average data value to be high, particularly the Fe concentration. Mn and Sr average concentrations are within the parameters of well-preserved material and the shell interior appears well preserved.

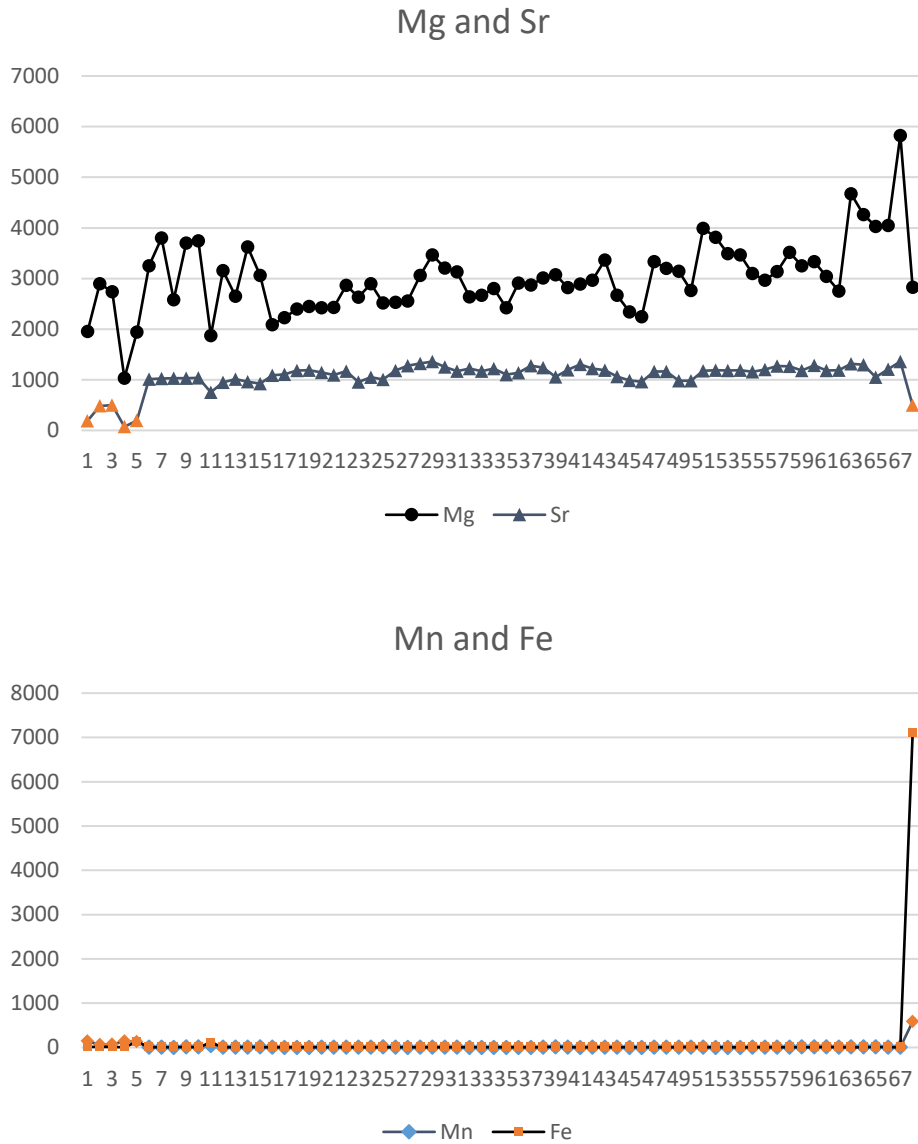


Figure 8. Mg, Sr, Fe and Mn concentrations through specimen RCK 36 running from the inner to the outer shell margins.

Preservation analyses of this specimen suggest that it is well preserved and is a suitable candidate for further analyses. However, if such analyses should go ahead then both shell margins should be avoided.

References

- Adams, A.E., 1980, Calcrete profiles in the Eyam Limestones (Carboniferous) of the Derbyshire Dome: petrology and regional significance: *Sedimentology*, v. 27, p. 651–660.
- Aitkenhead, N., and Chisholm, J.I., 1982, A standard nomenclature for the Dinantian formations of the Peak District of Derbyshire and Staffordshire: London, Institute of Geological Sciences.
- Aitkenhead, N., Chisholm, J.I. and Stevenson, I.P., 1985, Geology of the country around Buxton, Leek and Bakewell. Memoir for 1:50 000 geological sheet 111 (England and Wales): London, HMSO Publications, 4 p.
- Al-Aasm, I., and Viezer, J., 1982, Chemical stabilization of Low-Mg Calcite: An example of brachiopods: *Journal of Sedimentary Research*, v. 52, no. 4, p. 1101–1109.
- Anderson, T.F., and Arthur, M.A., 1983, Stable isotopes of oxygen and carbon and their application to sedimentological and paleoenvironmental problems: *Stable Isotopes in Sedimentary Geology SEPM Short Course*, v. 10, no. 10, p. 1–151.
- Angiolini, L., 2007, Quantitative palaeoecology in the *Pachycyrtella* Bed, Early Permian of Interior Oman: *Palaeoworld*, v. 16, p. 233–245.
- Angiolini, L., Balini, M., Garzanti, E., Nicora, A. and Tintori, A., 2003, Gondwana deglaciation and opening of Neothethys: the Al Khlata and Saiwan Formations of Interior Oman. *Palaeogeography, Palaeoclimatology, Palaeoecology*, v. 196, p. 99–123.
- Angiolini, L., Darbyshire, D.P.F., Stephenson, M.H., Leng, M.J., Brewer, T.S., Berra, F., and Jadoul, F., 2007, Lower Permian brachiopods from Oman: their potential as climatic proxies: *Earth and Environmental Science Transactions of the Royal Society of Edinburgh*, v. 98, no. 3–4. p. 327–344.
- Angiolini, L., Jadoul, F., Leng, M.J., Stephenson, M.H., Rushton, J., Chenery, S., and Crippa, G., 2009, How cold were the Early Permian glacial tropics? Testing sea-surface temperature using the oxygen isotope composition of rigorously screened brachiopod shells: *Journal of the Geological Society*, v. 166, no. 5, p. 933–945.
- Angiolini, L., Stephenson, M., Leng, M.J., Jadoul, F., Millward, D., Aldridge, A., Andrews, J., Chenery, S., and Williams, G., 2012, Heterogeneity, cyclicity and diagenesis in a Mississippian brachiopod shell of palaeoequatorial Britain: *Terra Nova*, v. 24, no. 1, p. 16–26.

References

- Armendáriz, M., Rosales, I., and Quesada, C., 2008, Oxygen isotope and Mg/Ca composition of Late Viséan (Mississippian) brachiopod shells from SW Iberia: Palaeoclimatic and palaeogeographic implications in northern Gondwana: *Palaeogeography, Palaeoclimatology, Palaeoecology*, v. 268, no. 1–2, p. 65–79.
- Ausich, W.I., Kammer, T.W. and Lane, N.G., 1979, Fossil communities of the Borden (Mississippian) Delta in Indiana and northern Kentucky: *Journal of Paleontology*, v. 53, no. 5, p. 1182–1196.
- Azmy, K., Brand, U., Sylvester, P., Gleeson, S.A., Logan, A., and Bitner, M.A., 2011, Biogenic and abiogenic low-Mg calcite (bLMC and aLMC): Evaluation of seawater-REE composition, water masses and carbonate diagenesis: *Chemical Geology*, v. 280, no. 1-2, p. 180–190.
- Barbin, V., and Gaspard, D., 1995, Cathodoluminescence of recent articulate brachiopod shells. Implications for growth stages and diagenesis evaluation: *Geobios*, v. 18, p. 39–45.
- Barham, M., Murray, J., Joachimski, M.M., and Williams, D.M., 2012, The onset of the Permo-Carboniferous glaciation: reconciling global stratigraphic evidence with biogenic apatite ^{18}O records in the late Viséan: *Journal of the Geological Society*, v. 169, no. 2, p. 119–122.
- Baumiller, T.K. and Ausich, W.I., 1992, The broken-stick model as a null hypothesis for crinoid stalk taphonomy and as a guide to the distribution of connective tissue on fossils: *Paleobiology*, v. 18, p. 288–298.
- Boggs, S., and Krinsley, D., 2006, *Application of Cathodoluminescence imaging to the study of Sedimentary rocks*, New York, Cambridge university press.
- Borchardt, T., 1985, Relationships between carbon and cadmium uptake in *Mytilus edulis*: *Marine Biology*, v. 85, no. 3, p. 233–244.
- Boucot, A. J., Xu, C., Scotese, C.R., and Morley, S.A., 2013, Phanerozoic paleoclimate: An atlas of lithological indicators of climate, SEPM Concepts in Sedimentology and Paleontology No. 11: *Map Folio: Society for Sedimentary Geology*, 12 p.
- Bowen, G.J., and Wilkinson, B., 2002, Spatial distribution of $\delta^{18}\text{O}$ in meteoric precipitation: *Geology*, v. 30, no. 4, p. 315–318.
- Brand, U., 2004, Carbon, oxygen and strontium isotopes in Paleozoic carbonate components: an evaluation of original seawater-chemistry proxies: *Chemical Geology*, v. 204, no. 1-2, p. 23–44.
- Brand, U., and Veizer, J., 1980, Chemical diagenesis of a multicomponent carbonate system - 1: Trace elements: *Journal of Sedimentary Petrology*, v. 50, no. 4, p. 1219–1236.

References

- Brand, U., Logan, A., Binter, M.A., Griesshaber, E., Azmy, K., and Buhl, D., 2011, What is the ideal proxy of Palaeozoic seawater chemistry?: *Memoirs of the Association of Australasian palaeontologists*, v. 41, p. 9–24.
- Brand, U., Logan, A., Hiller, N., and Richardson, J., 2003, Geochemistry of modern brachiopods: applications and implications for oceanography and paleoceanography: *Chemical Geology*, v. 198, no. 3-4, p. 305–334.
- Brand, U., Tazawa, J.I., Sano, H., Azmy, K., and Lee, X., 2009, Is mid-late Paleozoic ocean-water chemistry coupled with epeiric seawater isotope records?: *Geology*, v. 37, no. 9, p. 823–826.
- Brand, U., Webster, G.D., Azmy, K., and Logan, A., 2007, Bathymetry and productivity of the southern Great Basin seaway, Nevada, USA: An evaluation of isotope and trace element chemistry in mid-Carboniferous and modern brachiopods: *Palaeogeography, Palaeoclimatology, Palaeoecology*, v. 256, no. 3–4, p. 273–297.
- Brenchley, P.J. and Harper, D.A.T., 1998., *Palaeoecology: Ecosystems, environments and evolution*: Chapman and Hall, London.
- Brezinski, D.K. and Kollar, A.D., 2012. Paleoclimatically induced size increase in the early Carboniferous brachiopod clade *Gigantoproductus*. *Geological Society of America Abstracts with Programs*, v. 44, n. 7, p. 83.
- Bridges, P.H. and Chapman, A.J., 1988, The anatomy of a deep water mud-mound complex to the southwest of the Dinantian platform in Derbyshire, UK: *Sedimentology*, v. 35, p. 139–162.
- Bridges, P.H., 1982, The origin of cyclothems in the late Dinantian platform carbonates at Crich, Derbyshire: *Proceedings of the Yorkshire Geological Society*, v. 44, p. 159–180.
- Bridges, P.H., Gutteridge, P. and Pickard, N.A.H., 1995, The environmental setting of the Early Carboniferous mud-mounds *in* Monty, C.L.V., Bosence, D.W.J., Bridges, P.H. and Pratt, B.R., eds., *Carbonate mud-mounds; their origin and evolution*: International Association of Sedimentologists, Special Publications, v. 23, p. 171–190.
- Bruckschen, P., and Veizer, J., 1997, Oxygen and carbon isotopic composition of Dinantian brachiopods: Paleoenvironmental implications for the Lower Carboniferous of western Europe: *Palaeogeography, Palaeoclimatology, Palaeoecology*, v. 132, p. 243–264.
- Bruckschen, P., Oesmann, S., and Veizer, J., 1999, Isotope stratigraphy of the European Carboniferous, proxy signals for ocean chemistry, climate and tectonics: *Chemical Geology*, v. 161, p. 127–163.

References

- Buening, N., and Carlson, S.J., 1992, Geochemical investigation of growth in selected Recent articulate brachiopods: *Lethaia*, v. 25, p. 331–345.
- Butler, S., Bailey, T.R., Lear, C.H., Curry, G.B., Cherns, L., and McDonald, I., 2015, The Mg/Ca–temperature relationship in brachiopod shells: Calibrating a potential palaeoseasonality proxy: *Chemical Geology*, v. 397, p. 106–117.
- Cain, J.D.B., 1968, Aspects of the depositional environment and palaeoecology of crinoidal limestones: *Scottish Journal of Geology*, v. 4, p. 191–210.
- Carpenter, S.J., and Lohmann, K.C., 1995, ^{18}O and ^{13}C values of modern brachiopod shells: *Geochemica et Cosmochimica*, v. 59, no. 18, p. 3749–3764.
- Chave, K. E., 1954, Aspects of the biogeochemistry of Magnesium 1. Calcareous Marine Organisms: *Journal of Geology*, v. 62, p. 266–283.
- Chisholm, J.I. 1971– 1972. 1:10,000 Geological Map of SK 16 NE [-] (Composite). Ordnance Survey, Southampton, Provisional edition.
- Cohen, K.M., Finney, S.C., Gibbard, P.L. and Fan, J.-X., 2013, The ICS International Chronostratigraphic Chart. *Episodes*, v. 36, p. 199–204.
- Copper, P., 1988, Ecological succession in Phanerozoic reef ecosystems: is it real?: *Palaios*, v. 3, p. 136– 151.
- Cox, F.C., Bridge, D. McC., Chisholm, J.I. and Aitkenhead, N., 1977, The limestone and dolomite resources of the country around Monyash, Derbyshire. Description of 1:25 00 resource sheet SK 16. Institute of Geological Sciences, London.
- Craig, H., 1965, The measurement of oxygen isotope palaeotemperatures *in* Tongiorgi, E., eds., *Oceanographic studies and Palaeotemperatures: Consiglio Nazionale delle Ricerche, Laboratorio di geologia Nucleare, Pisa*, 1-24.
- Craig, H., 1957, Isotopic standards for carbon and oxygen and correction factors for mass-spectrometric analysis of carbon dioxide: *Geochimica et Cosmochimica Acta*, v. 12, no. 1, p. 133-149.
- Crowley, J.L., Yip, K.-J., Baum, S.K., and Moore, S.B., 1996, Modelling Carboniferous coal formation: *Palaeoclimates*, v. 2, p. 159–177.
- Curry, G.B., and Fallick, A.E., 2002, Use of stable oxygen isotope determinations from brachiopods in palaeoenvironmental reconstruction: *Palaeogeography, Palaeoclimatology, Palaeoecology*, v. 182, p. 133–143.

References

- Cusack, M., Pérez-Huerta, A., Chung, P., Parkinson, D., Dauphin, Y., and Cuif, J.P., 2008, Oxygen isotope equilibrium in brachiopod shell fibres in the context of biological control: *Mineralogical Magazine*, v. 72, no. 1, p. 239–242.
- Davies, S.J., 2008, The record of Carboniferous sea-level in low-latitude sedimentary successions from Britain and Ireland during the onset of the late Paleozoic ice age: *The Geological Society of America Special Papers*, v. 441, p. 187–204.
- Descloitres, D., 2001, Surface reflectance and ocean temperature, in MODIS land Rapid Response Team, N. G., ed., *Visible Earth, Volume 2017*: <https://visibleearth.nasa.gov/view.php?id=55878>, NASA.
- Dickson, T. 1990, Carbonate mineralogy and chemistry, *in* Tucker, M. E. and Wright, P. V., *carbonate sedimentology*: Blackwell Scientific Publications, Oxford, p. 284-313.
- Dickson, J. A. D. and Coleman, M. L., 1980, Changes in carbon and oxygen isotope composition during limestones diagenesis: *sedimentology*, v. 27, p. 107-118.
- Donner, J., and Nord, A.G., 1986, Carbon and oxygen stable isotope values in shells of *Mytilus edulis* and *Modiolus modiolus* from holocene raised beaches at the outer coast of the varanger Peninsula, North Norway: *Palaeogeography, Palaeoclimatology, Palaeoecology*, v. 56, no. 1, p. 35–50.
- Dunham, R.J., 1962, Classification of carbonate rocks according to depositional texture: *American Association of Petroleum Geologists Memoir*, v. 1, p. 108–121.
- Embry, A.F. and Klovan, E.J., 1971, A Late Devonian reef tract on northeastern Banks Island, N.W.T: *Bulletin of Canadian Petroleum Geology*, v. 19, p. 730–781.
- Epstein, S., Ruchsbaum, R., Lowenstam, H.A., and Urey, H.C., 1953, Revised carbonate-water isotopic temperature scale: *Bulletin of the geological society of America*, v. 64, p. 1315–1328.
- Ewbank, G., Manning, D.A.C., and Abbott, G.D., 1995, The relationship between bitumens and mineralization in the South Pennine Orefield, central England: *Journal of the Geological Society*, v. 152, p. 751–765.
- Falcon-Lang, H.J., 1999, Early Carboniferous (Asbian-Brigantian) Seasonal Tropical Climate of Northern Britain: *Society for Sedimentary Geology*, v. 14, p. 116–126.
- Ferguson, J. 1978. Some aspects of the ecology and growth of the Carboniferous gigantoproductids: *Proceedings of the Yorkshire Geological Society*, v. 42, p. 41–54.

References

- Fielding, C.R., Frank, T.D., and Isbell, J.L., 2008, The late Paleozoic ice age - A review of current understanding and synthesis of global climate patterns: Special Paper of the Geological Society of America, v. 441, p. 343–354.
- Folk, R. L., 1965, Some aspects of recrystallization in ancient limestones. In: Pray, L. C., and Murray, R.C. eds., Dolomitization and Limestone diagenesis: Special publication society of economic palaeontologists and mineralogists, v. 13, p. 14-48.
- Ford, T. D., 2002, Dolomitization of the Carboniferous Limestone of the Peak District: a Review: *Mercian Geologist*, v. 15, no. 3, p. 163-170.
- Freitas, P.S., Clarke, L.J., Kennedy, H., Richardson, C.A., and Abrantes, F., 2006, Environmental and biological controls on elemental (Mg/Ca, Sr/Ca and Mn/Ca) ratios in shells of the king scallop *Pecten maximus*: *Geochimica et Cosmochimica Acta*, v. 70, no. 20, p. 5119–5133.
- Friedman, I., and O'Neil, J.R., 1977, Data of geochemistry: Compilation of stable isotope fractionation factors of geochemical interest, Washington, US Government Printing Office, v. 44.
- Fürsich, F.T., 1993, Palaeoecology and evolution of Mesozoic salinity-controlled benthic macroinvertebrate associations: *Lethaia*, v. 26, p. 327–346.
- Gamito, S., 2010, Caution is needed when applying Margalef diversity index: *Ecological Indicators*, v. 10, p. 550–551.
- Garbelli, C., 2010, Brachiopodi del Permiano superiore (260-251 Ma) Ultrastruttura e diagenesi della conchiglia [Ph.D. thesis]: Milano, University of Milano, 141 p.
- Garbelli, C., Angiolini, L., Brand, U., and Jadoul, F., 2014, Brachiopod fabric, classes and biogeochemistry: Implications for the reconstruction and interpretation of seawater carbon-isotope curves and records: *Chemical Geology*, v. 371, p. 60-67.
- Garbelli, C., Angiolini, L., Brand, U., Shen, S., Jadoul, F., Posenato, R., Azmy, K., and Cao, C., 2016, Neotethys seawater chemistry and temperature at the dawn of the end Permian mass extinction: *Gondwana Research*, v. 35, p. 272–285.
- Garbelli, C., Angiolini, L., Jadoul, F., and Brand, U., 2012. Micromorphology and differential preservation of Upper Permian brachiopod low-Mg calcite: *Chemical Geology*, v. 298-299, p. 1–10.
- Gat, J.R., Shemesh, A., Tziperman, E., Hecht, A., Georgopoulos, D., and Basturk, O., 1996, The stable isotope composition of waters of the eastern Mediterranean Sea: *Journal of Geophysical Research*, v. 101, p. 6441–6451.

References

- Gaudain, G., and Medley, P., 2000, The Turks and Caicos Islands, *in* Sheppard, C., ed., *Seas at the Millennium: An Environmental Evaluation*: Amsterdam, Pergamon, p. 587-594.
- Gawthorpe, R.L. and Gutteridge, P., 1990, Geometry and evolution of platform-margin bioclastic shoals, late Dinantian (Mississippian), Derbyshire, UK: *Special Publications of the International Association of Sedimentologists*, v. 9, p. 39–54.
- Gentry, D.K., Sosdian, S., Grossman, E.L., Rosenthal, Y., Hicks, D., and Lear, C.H., 2008, Stable Isotope and Sr/Ca Profiles From the Marine Gastropod *Conus ermineus*: Testing a Multiproxy Approach For Inferring Paleotemperature and Paleosalinity: *PALAIOS*, v. 23, no. 4, p. 195–209.
- Giles, P.S., 2009, Orbital forcing and Mississippian sea level change: time series analysis of marine flooding events in the Visean Windsor Group of eastern Canada and implications for Gondwana glaciation: *Bulletin of Canadian petroleum geology*, v. 57, n. 4, p. 449–471
- Gillikin, D.P., Lorrain, A., Bouillon, S., Willenz, P., and Dehairs, F., 2006, Stable carbon isotopic composition of *Mytilus edulis* shells: relation to metabolism, salinity, $\delta^{13}\text{C}$ and phytoplankton: *Organic Geochemistry*, v. 37, no. 10, p. 1371–1382.
- Goodwin, D.H., Gillikin, D.P., and Roopnarine, P.D., 2013, Preliminary evaluation of potential stable isotope and trace element productivity proxies in the oyster *Crassostrea gigas*: *Palaeogeography, Palaeoclimatology, palaeoecology*, v. 373, p. 88-97.
- Gradstein, F. M., Ogg, J. G., Schmitz, M. D., and Ogg, G. M., 2012, *The geological time scale*, London, Elsevier.
- Graham, J.B., Aguilar, N.M., Dudley, R. and Gans, C., 1995, Implications of the late Palaeozoic oxygen pulse for physiology and evolution: *Nature*, v. 375, p. 117–120.
- Gregory, R. T., 1991, Oxygen isotope history of seawater revisited: timescales for boundary event changes in oxygen isotope composition of seawater, *in* Taylor, H. P., O'Neil, J. R., Kaplan, I. R., eds. *Stable Isotope Geochemistry: A tribute to Samuel Epstein*: Geochemical Society Special Publications, v. 3, p. 65-76. St Louis.
- Gregory, R. T., and Taylor, H. P., 1981, An oxygen isotope profile in a section of Cretaceous oceanic crust, Samail ophiolite, Oman: evidence for $\delta^{18}\text{O}$ buffering of the oceans by deep (>5 km) seawater-hydrothermal circulations at mid-ocean ridges: *Journal of Geophysical Research*, v. 86, p. 2737-2755.
- Grinnell, J.R.S. 1974. Vertical orientation of shells on some Florida oyster reefs. *Journal of Sedimentary Petrology*, v. 44, p. 116–122.

References

- Grossman, E.L., 2012, Applying oxygen isotope paleothermometry in deep time, in Ivany, L., Huber, B., eds. *Reconstructing Earth's Deep-Time Climate: The Paleontological Society Papers*, v. 18, p.39–67
- Grossman, E.L., Mii, H.-S., and Yancey, T.E., 1993, Stable isotopes in Late Pennsylvanian brachiopods from the United States: Implications for Carboniferous paleoceanography: *Geological Society of America Bulletin*, v. 105, no. 10, p. 1284–1296.
- Guion, P., and Fielding, C., 1988, Westphalian A and B sedimentation, in Besly, B.M. and Kelling, G., eds., *Sedimentation in a synorogenic basin complex; the Upper Carboniferous of NW Europe*. Blackie, Glasgow, p. 153–177.
- Gutteridge, P., 1983, Sedimentological study of the Eyam Limestone formation of the east-central part of the Derbyshire Dome. [Ph.D. thesis], Manchester, University of Manchester.
- Gutteridge, P., 1987, Dinantian sedimentation and the basement structure of the Derbyshire Dome: *Geological Journal*, v. 22, p. 25–41.
- Gutteridge, P., 1990, The origin and significance of the distribution of shelly macrofauna in late Dinantian carbonate mud mounds of Derbyshire: *Proceedings of the Yorkshire Geological Society*, v. 48, p. 23–32.
- Gutteridge, P., 1991, Aspects of Dinantian sedimentation in the Edale Basin, Northern Derbyshire: *Geological Journal*, v. 26, p. 245–269.
- Gutteridge, P., 1991b, Revision of the Monsal Dale/Eyam Limestone boundary (Dinantian) in Derbyshire: *Mercian Geologist*, v. 12, p. 71–78.
- Gutteridge, P., 1995, Late Dinantian (Brigantian) carbonate mud-mounds of the Derbyshire carbonate platform, in Monty, C.L.V., Bosence, D.W.J., Bridges, P.H. and Pratt, B.R. eds., *Carbonate mud-mounds: their origin and evolution: International Association of Sedimentologists Special Publications*, v. 23, p. 289–307.
- Gutteridge, P., 2003, A record of the Brigantian limestone succession in the partly infilled dale quarry, Wirksworth: *Mercian Geologist*, v. 15, p. 219 - 224.
- Gutteridge, P., Nolan, S., and McMahon, A., 1987, The role of tectonics in Devonian and Carboniferous sedimentation in the British Isles, in *Proceedings of the Yorkshire Geological Society*, Leeds University, 1987, v. 47, The geological Society of London, p. 91-92.
- Hammer, Ø., Harper, D. A.T., and Ryan, P.D., 2001, PAST: Palaeontologia statistics software package for education and data analysis: *Paleontological Electronica*, v. 4.

References

- Harper, D.A.T., and Jeffrey, A.L., 1996, Mid-Dinantian brachiopod biofacies from western Ireland, *in* Strogon, P., Somerville, I.D. and Jone, G.L.I. eds., Recent advances in Lower Carboniferous geology: Geological Society, Special Publications, p. 427–436.
- Hays, P.D., and Grossman, E.L., 1991, Oxygen isotopes in meteoric calcite cements as indicators of continental paleoclimate: *Geology*, v. 19, p. 441–444.
- Hiller, N., 1988, The development of growth lines on articulate brachiopods: *Lethaia*, v. 21, p. 177–188.
- Hollis, C., 1998, reconstructing fluid history: an intergrated approach to timing fluid expulsion and migration an the Carboniferous Derbyshire Platform, England: Geological Society, London, Special Publications v. 144, n. 1, p. 153–159.
- Hollis, C., and Walkden, G., 1996, The use of burial diagenetic calcite cements to determine the controls upon hydrocarbon emplacement and mineralization on the carbonate platform, Derbyshire, England: Geological society, London, Special Plublications, v. 107, p. 35–49.
- Hollis, C., and Walkden, G., 2002, Reconstructing fluid expulsion and migration north of the Variscan Orogen, Northern england: *Journal of Sedimentary research*, v.7, n. 5, p. 700–710.
- Horibe, Y., and Oba, T., 1972, Temperature scales of aragonite-water and calcite-water systems: *Fossils*, v. 23–24, p. 69–78.
- Horita, J., Zimmermann, H., and Holland, H.D., 2002, Chemical evolution of seawater during the Phanerozoic: Implications from the record of marine evaporites: *Geochimica et Cosmochimica Acta*, v. 66, no. 21, p. 3733–3756.
- Immenhauser, A., Schöne, B.R., Hoffmann, R., and Niedermayr, A., 2016, Mollusc and brachiopod skeletal hard parts: Intricate archives of their marine environment: *Sedimentology*, v. 63, no. 1, p. 1–59.
- Isbell, J.L., Miller, M.F., Wolfe, K.L., and Lenaker, P.A., 2003, Timing of late Paleozoic glaciation in Gondwana: Was glaciation responsible for the development of Northern Hemisphere cyclothems?: *Geological Society of America Special Papers*, v. 370, p. 5–24.
- Ivany, L.C., and Runnegar, B., 2010, Early Permian seasonality from bivalve $\delta^{18}\text{O}$ and implications for the oxygen isotopic composition of seawater: *Geology*, v. 38, no. 11, p. 1027–1030.
- Ixer, R.A., and Vaughan, D.J., 1993, Lead-zinc-flourite-barite deposits of the Pennine, North Wales and the Mendips, *in*, Mineralization in the British Isles, 355–418, p.

References

- Jaffrés, J.B.D., Shields, G.A., and Wallmann, K., 2007, The oxygen isotope evolution of seawater: A critical review of a long-standing controversy and an improved geological water cycle model for the past 3.4 billion years: *Earth-Science Reviews*, v. 83, no. 1–2, p. 83–122.
- Joachimski, M.M., Van Geldren, R., Breisig, S., Buggisch, W., and Day, J., 2004, Oxygen isotope evolution of biogenic calcite and apatite during the Middle and Late Devonian: *International journal of Earth Science*, v. 93, p. 542–553.
- Kammer, T.W. and Ausich, W.I., 2006, The "Age of the Crinoids": A Mississippian biodiversity spike coincident with widespread carbonate ramps: *Palaios*, v. 21, p. 238–248.
- Kasting, J. F., Howard, M. T., wallmann, K., Veizer, J., Shields, G., and Jaffrés, J., 2006, Paleoclimates, ocean depth, and the oxygen isotopic composition of seawater: *Earth and Planetary Science Letters*, v. 252, no. 1-2, p. 82–93.
- Keith, M. L., and Weber, J. N., 1965, Systematic Relationships between Carbon and Oxygen Isotopes in Carbonates Deposited by Modern Corals and Algae: *Science*, v. 150, no. 3695, p. 498–501.
- Kim, S.T., and O'Neil, J.R., 1997, Equilibrium and nonequilibrium oxygen isotope effects in synthetic carbonates: *Geochimica et Cosmochimica Acta*, v. 61, p. 3461–3475.
- Klein, R.T., Lohmann, K.C., and Thayer, C.W., 1996, Sr/Ca and $^{13}\text{C}/^{12}\text{C}$ ratios in skeletal calcite of *Mytilus trossulus*: Covariation with metabolic rate, salinity, and carbon isotopic composition of seawater: *Geochimica et Cosmochimica Acta*, v. 60, no. 21, p. 4207–4221.
- Korte, C., and Hesselbo, S.P., 2011, Shallow marine carbon and oxygen isotope and elemental records indicate icehouse-greenhouse cycles during the Early Jurassic: *Paleoceanography*, v. 26, n. 4, PA4291
- Korte, C., Kozur, H. W., Bruckschen, P., and Veizer, J., 2003, Strontium isotope evolution of Late Permian and Triassic seawater: *Geochimica et Cosmochimica Acta*, v. 67, no. 1, p. 47–62.
- Lane, N.G., 1973, Paleontology and paleoecology of the Crawfordsville fossil site (Upper Osagian: Indiana): *University of California Publications in Geoscience*, v. 99, p. 1–141
- Lee, X., Hu, R., Brand, U., Zhou, H., Liu, X., Yuan, H., Yan, C., and Cheng, H., 2004, Ontogenetic trace element distribution in brachiopod shells: an indicator of original seawater chemistry: *Chemical Geology*, v. 209, no. 1–2, p. 49–65.
- LeGrande, A.N., and Schmidt, G.A., 2006, Global gridded data set of the oxygen isotopic composition in seawater: *Geophysical Research Letters*, v. 33, no. 12, p. L12604.

References

- Leng, M.J., and Marshall, J.D., 2004, Palaeoclimate interpretation of stable isotope data from lake sediment archives: *Quaternary Science Reviews*, v. 23, no. 7, p. 811-831.
- Lepzelter, C.G., Anderson, T.F., and Sandberg, P.A., 1983, Stable isotope variations in modern articulate brachiopods: *American Association of Petroleum Geologists Bulletin*, v. 67, p. 500–501.
- Lorens, R. B., 1981, Sr, Cd, Mn, and Co distribution coefficients in calcite as a function of calcite precipitation rate: *geochemica et Cosmochimica Acta*, v. 44, p. 1265-1278.
- Lowenstam, H.A., 1961, Mineralogy, O^{18}/O^{16} ratios and strontium and magnesium contents of recent and fossil brachiopods and their bearing on the history of oceans: *The Journal of Geology*, v. 69, no. 3, p. 241-260.
- Macdonald, K., 1976, Paleocommunities: Toward some confidence limits, *in* Scott, R.W, West, R.R., eds., *Structure and classification of paleocommunities*. Dowden, Hutchinson and Ross, Stroudsburg, Pennsylvania, 87–106 p.
- Macdonald, R., Gass, K.N., Thorpe, R.S., and Gass, I.G., 1984, Geochemistry and petrogenesis of the Derbyshire Carboniferous basalts: *Journal of the Geological Society of London*, v. 141, p. 147–159.
- MacKinnon, D.I., and Williams, A., 1974, Shell structure of terebratulid brachiopods: *Palaentology*, v. 17, no. 1, p. 179-202.
- Madi, A., Bourque, P.-A. and Mamet, B.L., 1996, Depth-related ecological zonation of a carboniferous carbonate ramp: Upper Viséan of Béchar Basin, Western Algeria: *Facies*, v. 35, p. 59-79.
- McConnaughey, T., 1989, ^{13}C and ^{18}O isotopic disequilibrium in biological carbonates: I. Patterns: *Geochimica et Cosmochimica Acta*, v. 53, no. 1, p. 151-162.
- McCrea, J.M., 1950, On the Isotopic Chemistry of Carbonates and a Paleotemperature Scale: *The Journal of Chemical Physics*, v. 18, no. 6, p. 849–857.
- McIntire, W.L., 1963, Trace element partition coefficients—a review of theory and applications to geology: *Geochimica et Cosmochimica Acta*, v. 27, no. 12, p. 1209–1264.
- Mii, H.S., and Grossman, E.L., 1994, Late Pennsylvanian seasonality reflected in the ^{18}O and element composition of a brachiopod shell: *Geology*, v. 22, p. 661–664.
- Mii, H.S., Grossman, E.L., and Yancey, T.E., 1999, Carboniferous isotope stratigraphies of North America: Implications for Carboniferous paleoceanography and Mississippian glaciation: *Geological Society of America Bulletin*, v. 111, no. 7, p. 960–973.

References

- Mii, H.S., Grossman, E.L., Yancey, T.E., and Egorov, A.C., 2001, Isotopic records of brachiopod shells from the Russian Platform — evidence for the onset of mid-Carboniferous glaciation: *Chemical Geology*, v. 175, p. 133–147.
- Milner Garcia, S.A.M., Rollion-Bard, C., Burckel, P., Tomasovych, A., Angiolini, L., and Henkel, D., 2017, Assessing the biomineralization processes in the shell microstructure of modern brachiopods: variations in the oxygen isotope composition and minor element ratios: *Proceedings EGU General Assembly, Vienna*, v.19.
- Montañez, I.P., and Poulsen, C.J., 2013, The Late Paleozoic Ice Age: An Evolving Paradigm: *Annual Review of Earth and Planetary Sciences*, v. 41, no. 1, p. 629–656.
- Mook, W.G., 1971, Paleotemperatures and chlorinities from stable carbon and oxygen isotopes in shell carbonate: *Palaeogeography, Palaeoclimatology, Palaeoecology*, v. 9, no. 4, p. 245–263.
- Mook, W.G., and Vogel, J. C., 1968, Isotopic Equilibrium between Shells and Their Environment: *Science*, v. 159, no. 3817, p. 874–875.
- Morrison, O.J., and Brand, U., 1986, Geochemistry of recent marine invertebrates: *Geoscience*, v. 13, p. 237-254.
- Morse, J. W. and Mackenzie, F. T., 1990, *Geochemistry of Sedimentary Carbonates: Developments in Sedimentology*. v. 48, Amsterdam.
- Mucci, A., 1987, Influence of temperature on the composition of magnesian calcite overgrowths precipitated from seawater: *Geochimica et Cosmochimica Acta*, v. 51, p. 1977-1984.
- Muehlenbachs, K., and Clayton, R. N., 1976, Oxygen Isotope Composition of the Oceanic Crust and Its Bearing on Seawater: *Journal of Geophysical Research*, v. 81, no. 23, p. 4365-4369.
- Muir-Wood, H.M., and Cooper, G.A., 1960, Morphology, classification and life habits of the Productoidea (Brachiopoda): *Memoirs of the Geological Society of America*, v. 81, p. 1–567.
- Nguyen, K.D.T., Morley, S.A., Lai, C-H., Clark, M.S., Tan, K.S., Bates, A.E., and Peck, L.S., 2011, Upper temperature limits of tropical marine ectotherms: Global warming implications: *PLoS ONE*, e29340.
- Nolan, L.S.P., Angiolini, L., Jadoul, F., Della Porta, G., Davies, S., Banks, V.J., Stephenson, M.H., and Leng, M.J., 2017, Sedimentary context and palaeoecology of *Gigantoproductus* shell beds in the Mississippian Eyam Limestone Formation, Derbyshire carbonate platform, central England: *Proceedings of the Yorkshire Geological Society*.

References

- Owen, R., Kennedy, H., and Richardson, C., 2002, Experimental investigation into partitioning of stable isotopes between scallop (*Pecten maximus*) shell calcite and sea water: *Palaeogeography, Palaeoclimatology, Palaeoecology*, v. 185, no. 1–2, p. 163–174.
- Pak, D.K., Lea, D.W., and Kennett, J.P., 2004, Seasonal and interannual variation in Santa Barbara Basin water temperatures observed in sediment trap foraminiferal Mg/Ca: *Geochemistry, Geophysics, Geosystems*, v. 5, no. 12, Q12008.
- Parkinson, D., Curry, G.B., Cusack, M., and Fallick, A.E., 2005, Shell structure, patterns and trends of oxygen and carbon stable isotopes in modern brachiopod shells: *Chemical Geology*, v. 219, no. 1–4, p. 193–235.
- Pattison, J., 1981, The stratigraphical distribution of gigantoproductid brachiopods in the Viséan and Namurian rocks of some areas in northern England. Institute of Geological Sciences, London.
- Peck, L.S., Clark, M.S., Morley, S.A., Massey, A., and Rossetti, H., 2009, Animal temperature limits and ecological relevance: effects of size, activity and rates of change: *Functional Ecology*, v. 23, no. 2, p. 248–256.
- Perez-Huerta, A., Cusack, M., Jeffries, T., and Williams, C., 2008, High resolution distribution of magnesium and strontium and the evaluation of Mg/Ca thermometry in Recent brachiopod shells: *Chemical Geology*, v. 247, no. 1-2, p. 229–241.
- Popp, B.N., Anderson, T.F., and Sandberg, P.A., 1986, Brachiopods as indicators of original isotopic compositions in some Paleozoic limestones: *Geological Society of America Bulletin*, v. 97, no. 10, p. 1262.
- Poulos, S.E., Drakopoulos, P.G., and Collins, M.B., 1997, Seasonal variability in sea surface oceanographic conditions in the Aegean Sea (Eastern Mediterranean): an overview: *Journal of Marine Systems*, v. 13, no. 1, p. 225–244.
- Qiao, L., and Shen, S.-Z., 2015, A global review of the Late Mississippian (Carboniferous) *Gigantoproductus* (Brachiopoda) faunas and their paleogeographical, paleoecological, and paleoclimatic implications: *Palaeogeography, Palaeoclimatology, Palaeoecology*, v. 420, p. 128–137.
- Ruban, D.A., 2015, Comment on "A global review of the Late Mississippian (Carboniferous) *Gigantoproductus* (Brachiopoda) faunas and the palaeogeographical, palaeoecological, and palaeoclimatic implications" by L. Qiao and S. Shen [*Palaeogeography, Palaeoclimatology, Palaeoecology* 420 (2015) 128-137]: *Palaeogeography, Palaeoclimatology, Palaeoecology*, v. 433, p. 259 - 261.

References

- Rudwick, M.J.S., 1959, The Growth and Form of Brachiopod Shells: Geological Magazine, v. 96, no. 1.
- Sample, J.C., and Reid, M.R., 1998, Contrasting hydrogeologic regimes along strike-slip and thrust faults in the Oregon convergent margin: Evidence from the chemistry of syntectonic carbonate cements and veins: Geological Society of America Bulletin, v. 110, no. 1, p. 48-59.
- Sarytcheva, T.G., 1928, The Productidae of the group *Productus giganteus* Mart. from the Visean of Moscow: Memorandum of the Geological Science Research Institute; Physics and Maths Faculty; 1st Moscow State University, v. 1, p. 71.
- Savin, S.M., 1977, The history of the earth's surface temperature during the past 100 million years: Annual review of Earth and Planetary Sciences, v. 5, p. 319–355.
- Schmahl, W.W., Griesshaber, E., Kelm, K., Goetz, A., Jordan, G., Ball, A., Xu, D., Merkel, C., and Brand, U., 2012, Hierarchical structure of marine shell biomaterials: biomechanical functionalization of calcite by brachiopods: Zeitschrift für Kristallographie - Crystalline Materials, v. 227, no. 11, p. 793–804.
- Schofield, K., and Adams, A.E., 1985, Stratigraphy and depositional environments of the Woo Dale Limestones Formation (Dinantian), Derbyshire. Proceedings of the Yorkshire Geological Society, v. 45, p. 225–233.
- Schofield, K., and Adams, A.E., 1986, Burial dolomitization of the Woo Dale Limestone Formation (Lower Carboniferous), Derbyshire, England: Sedimentology, v. 33, p. 207–219.
- Scotese, C.R., and McKerrow, W.S., 1990, Revised world maps and introduction, *in* Scotese, C.R., and McKerrow, W.S., eds., Palaeozoic palaeogeography and biogeography: Geological Society, Memoirs, London, v. 12, p. 1–21.
- Sharp, Z., 2006, Principals of Stable Isotope Geochemistry, Prentice-Hall, Upper saddle river.
- Shino, Y., and Suzuki, Y., 2011, The ideal hydrodynamic form of the concavo-convex productide brachiopod shell: Lethaia, v. 44, p. 329–343
- Smith, K., Smith, N.J.P., and Holliday, D.W., 1985, The deep structure of Derbyshire: Geological Journal, v. 20, p. 215–225.
- Steuber, T., and Veizer, J., 2002, Phanerozoic record of plate tectonic control of seawater chemistry and carbonate sedimentation: Geological Society of America, V. 30, n, 12, P. 1123–1126.

References

- Strank, A.R.E., 1987, The stratigraphy and structure of Dinantian strata in the East Midlands, UK, *in* Miller, J., Adams, A.E., and Wright, V.,P., eds., *European Dinantian Environments: Geological Journal Special Issues*, Chichester, UK, v. 12:, p. 157–175.
- Swart, P.K., 2015, The geochemistry of carbonate diagenesis: The past, present and future: *Sedimentology*, v. 62, no. 5, p. 1233-1304.
- Tanaka, N., Monaghan, M.C., and Rye, D.M., 1986, Contribution of metabolic carbon to mollusc and barnacle shell carbonate: *Nature*, v. 320, no. 6062, p. 520-523.
- Tomasovych, A., and Farkas, J., 2005, Cathodoluminescence of Late triassic terebratulid brachiopods: implications for growth patterns: palaeogeography, Palaeoclimatology, Palaeoecology, v. 216, p. 215-233.
- Tucker, M. E. and Wright, P. V., *carbonate sedimentology*: Blackwell Scientific Publications, Oxford.
- Tudhope, A.W., Chilcott, C.P., McCulloch, M.T., Cook, E.R., Chappell, J., Ellam, R.M., Lea, D.W., Lough, J.M., Shimmield, G.B., 2001, Variability in the El Nina-Southern Oscillations Through a Glacial-Interglacial Cycle: *Science*, v. 291, n. 5508, p. 1511-1517.
- Ullmann, C.V., and Korte, C., 2015, Diagenetic alteration in low-Mg calcite from macrofossils: a review: *Geological Quarterly*, v. 59, no. 1, p. 3–20.
- Urey, H.C., 1947, *The Thermodynamic Properties of Isotopic Substances*: Chemical Society, p. 562-581.
- Van Geldern, R., Joachimski, M.M., Day, J., Jansen, U., Alvarez, F., Yolkin, E.A., and Ma, X.P., 2006, Carbon, oxygen and strontium isotope records of Devonian brachiopod shell calcite: *Palaeogeography, Palaeoclimatology, Palaeoecology*, v. 240, no. 1–2, p. 47–67.
- Veizer, J., 1983, trace elements and isotopes in sedimentary carbonates, *in* Reeder, R.J., eds., *carbonates:Mineralogy and chemistry: Mineralogical societies of America*, reviews in Mineralogy, v. 11, p. 265-300.
- Veizer, J., Ala, D., Azmy, K., Bruckschen, P., Buhl, D., Bruhn, F., Carden, G.A.F., Diener, A., Ebner, S., Godderis, Y., Jasper, T., Korte, C., Pawellek, F., Podlaha, O.G., and Strauss, H., 1999, $^{87}\text{Sr}/^{86}\text{Sr}$, $\delta^{13}\text{C}$ and $\delta^{18}\text{O}$ evolution of Phanerozoic seawater: *Chemical geology*, v. 161, p. 59–88.
- Veizer, J., Bruckschen, P., Pawellek, F., Diener, A., Podlaha, O.G., Carden, G.A.F., Jasper, T., Korte, C., Strauss, H., Azmy, K., and Ala, D., 1997, Oxygen isotope evolution of Phanerozoic seawater: *Palaeogeography, Palaeoclimatology, Palaeoecology*, v. 132, p. 159–172.

References

- Walkden, G.M., and Berry, J.R., 1984, Natural calcite in cathodoluminescence: crystal growth during diagenesis: *Nature*, v. 308, no. 5959, p. 525-527.
- Walkden, G.M., 1987, Sedimentary and diagenetic styles in late Dinantian carbonates of Britain, *in* Miller, J., Adams, A.E. and Wright, Q.P. eds., *European Dinantian environments*: Chichester, p. 131–155.
- Waters, C.N., Waters, R.A., Barclay, W.J., and Davies, J.R., 2009., *A lithostratigraphical framework for the Carboniferous successions of southern Great Britain (Onshore)*: British Geological Survey, Keyworth.
- Walkden, G.M., and Williams, D.O., 1991, The diagenesis of the later Dinantian Derbyshire-East Midland carbonate shelf, central England: *Sedimentology*, v. 38, P. 643–670.
- Wells, M., R., Allison, P.A., Piggott, M.D., Pain, C.C., Hampson, G.J., and De Oliveira, C.R.E., 2005, Large sea, small tides: the Late Carboniferous seaway of NW Europe: *Journal of the Geological Society*, v. 162, no. 3, p. 417–420.
- Williams A., Brunton C.H.C., and Carlson S.J., Alvarez F., Baker P.G., Bassett M.G., Boucot A.J., Carter J.L., Cocks L.R.M., Cohen B.L., Curry G.B., Cusack M., Emig C.C., Gourvenec R., Harper D. A. T., Holmer L.E., Lee D.E., Logan A., Luter D., MacKinnon D.I., Mancenido M.O., and Mergl M., 2007. *In* Selden P.A. eds., *Treatise on Invertebrate Paleontology, Part H, Revised, Brachiopoda v. 6, Supplement*, p. 2321–3226.
- Williams, A., and Wright, A. D., 1970, Shell structure of the Craniacea and other calcareous inarticulate brachiopods: *Special papers in palaeontology*, v. 7, p.1–51.
- Wright, V.P., and Vanstone, S.D., 2001, Onset of late palaeozoic glacio-eustasy and the evolving climates of low latitude areas: a synthesis of current understanding: *Geological Society*, v. 158, p. 579–882.
- Yao, L., Aretz, M., Li, Y. and Wang, Y., 2016, Gigantoproductid brachiopod storm shell beds in the Mississippian of South China: implications for their palaeoenvironmental and palaeogeographical significances. *Geologica Belgica*, v. 19, p. 57–67.
- Zachara, J.M., Cowan, C.E., and Resch, C.T., 1991, Sorption of divalent metals on calcite: *Geochimica et Cosmochimica Acta*, v. 55, no. 6, p. 1549-1562.
- Zachos, J.C., Schouten, S., Bohaty, S., Quattlebaum, T., Sluijs, A., Brinkhuis, H., Gibbs, S. J., and Bralower, T.J., 2006, Extreme warming of mid-latitude coastal ocean during the Paleocene-ocene Thermal Maximum: Inferences from TEX86 and isotope data: *Geology*, v. 34, no. 9, p. 737–740.